Rough Version

BULLETIN

MATHEMATICAL MODELLING OF SEDIMENT TRANSPORT AND DEPOSITION IN RESERVOIRS

Guidelines and case studies

CIGB ICOLD

2007

TABLE OF CONTENTS

LIST OF FIGURES

LIST OF TABLES

LIST OF SYMBOLS

a	adaptation coefficient representing mean settling depth
α	dimensionless exponent
α	coefficient
A	coefficient used in *Ackers and White (1973)* equation
A	integration constant
A	channel cross-section area
b	constant
B	bed width of flushing channel
B	top width of flow
B_o	buoyancy flux
β	constant
βi	% of i-th sediment fraction in the bed
c	integration constant
c_{-}	coefficient used in *Ackers and White (1973)* equation
C_{eq}	equilibrium concentration
C	sediment concentration
C_{vy}	average sediment concentration at a distance y above the bed (in percent by volume)
$C^{*}_{\tilde{e}\tilde{q}}$	relative equilibrium concentration
C_{v}	average sediment concentration
C_t	sediment concentration by weight
C_s	suspended sediment concentration
C_o	initial sediment concentration
C_{fo}	resistance coefficient
C_d	drag coefficient
C_i	actual sediment transport per fraction
C_{ci}	transport capacity of the i-th class
C_1	near bed sediment concentration
C_a	reference concentration
C^{*}	equilibrium sediment concentration
C_H	Chezy coefficient
C_b	bed load concentration
C^{-}	Chezy type coefficient for density current
C_o	sediment concentration at the bed where
Δz	depth of recent deposits
d	sediment particle diameter
d_{90}	sediment size for which 90 % of particles is finer

d_{50}	median sediment particle size
d_{gr}	sediment particle size
d_s	representative particle size
δ_b	saltation height
D	flow depth
D	dispersion coefficient
D_*	dimensionless particle diameter
D1..4	density current layer depths
e_b	efficiency coefficient
ε	coefficient of turbulence exchange
η	parameter as function of sediment particle size, settling velocity and water viscosity
E	erosion rate
E	applied stream power
E	specific energy
E_o	empirical erosion rate coefficient
f	Lacey's silt factor
f	Darcy Weisbach resistance coefficient
f_k	resistance coefficient with equilibrium sediment transport
f_o	Darcy Weisbach resistance coefficient where
F	mean shear force
Fr	Froude number
Fr_D	densimetric Froude number
F_{gr}	mobility number
F_o	inflow Froude number
F_{V_a}	shear box power
g	gravitational acceleration
g'	gravitational acceleration adjusted for density difference ratio
γ'	specific weight of density current
γ	specific weight of water
γ_d	specific weight of deposits
γ_s	specific weight of sediment
G_{gr}	sediment transport function
h	depth of uniform density current flow
h	depth of water above density current
h'	density current depth
h_p	density current depth at plunge point
h_L	maximum climbing height of a density current
h_5	density current layer depth
h_o	density current depth at plunge point

h_n	depth of density current head
H	bed form height
H	depth of flushing channel
H	water depth
I	moment of inertia of element around axis 0
J_n	water surface slope
J_i	density current interface slope
J_o	density current bed slope
k	roughness coefficient
k_s	roughness coefficient
k_1	dimensionless coefficient
κ	Von Kármán coefficient
K_1, K_2	constants
K_T	reservoir capacity - sediment inflow ratio
K_3	constant related to sediment concentration
K, K_1, K_2	coefficient
K_W	reservoir capacity - inflow ratio
ℓ	Prandtl's mixing length
ℓ_o	mixing length
λ	rate of erosion
λ_m	mean friction coefficient of the underflow
$\lambda_o ; \lambda_i$	coefficients of friction at bed and interface
L_i^*	adaptation length for each fraction
m	coefficient used in *Ackers and White (1973)* equation
m	coefficient related to sediment concentration
m	morphological channel stability coefficient
m_c	stable bank slope
μ	dynamic viscosity
η	coefficient of rigidity
M	constant
M	erosion rate
M	mass of element
υ	kinematic viscosity
n	coefficient used in *Ackers and White (1973)* equation
N	coefficient
p	total pressure
p_c, p_m, p_s	percentages of clay, silt and sand
ψ	suspension parameter correction coefficient
$\propto$	angle

$\propto$	empirical erosion rate coefficient
$\propto$	erosion constant
$\propto$	coefficient for non-equilibrium density current sediment transport
$\propto_1 ; \propto_2$	coefficients
$\propto_3 ; \propto_4$	constant and coefficient
$\propto_5 ; \propto_6$	constant and coefficient
P	wetted perimeter
P	applied power
q	discharge per unit width
q_{so}	sediment inflow per unit width
q_{st}	suspended load transport rate
q_t	total load transport rate
q_{bw}	bed load transport rate
q_T	total sediment load
q_{st}	sediment transport capacity
q_d , q_e	fluxes of deposition and erosion of sediment
q_s	sediment discharge per unit width
Q	flow rate
Q_s	total sediment discharge
r	ratio of predicted to observed sediment transport rate
r^2	correlation coefficient
$\rho g s \mathrm{v}$	unit input stream power
ρ_c , ρ_m , ρ_s	densities of clay, silt and sand fractions
ρ_T	sediment density after T years
ρ_s	sediment density
ρ_m	density of sediment-laden water
ρ_2	density in density current
ρ_∞	long-term sediment density
ρ_o	initial sediment density
R_o	radius of eddies near bed
R	hydraulic radius
R_ρ	hydraulic radius at plunge point
s	slope
ss	sediment source/sink term
s_f	energy slope
s^*	sediment transport capacity
S_2	energy slope for sediment-laden water
S_1	energy slope for clear-water
s_o	bed slope

s_s	water surface slope
$\tan\alpha$	ratio of tangential shear to normal force
θ	coefficient used in Engelund Hansen equation
τ_{ce}	critical shear stress for surface erosion
τ	bed shear stress
τ_{cme}	critical bed shear stress for mass erosion
τ_o	bed shear stress
τ_*	shear velocity to the power 2
τ_o	shear stress at bed
$\tau \frac{d\,\mathrm{v}}{\mathrm{dy}}$	applied stream power
τ_i	shear resistance at the interface
τ_B	yield shear stress
τ_o	mean bed shear stress
τ_c	critical shear stress
$\tau\,\mathrm{v}$	stream power
τ_{oc}	critical shear stress for incipient motion *(Shields, 1936)*
$\tau_{\bar{o}}$	grain shear stress
T	time scale in non-equilibrium sediment transport
T	transport stage parameter
T	width
u_{bs}	particle velocity
$u_{\bar{g}}$	bed shear velocity
u_a	effective particle velocity at reference level a
$u_{\bar{g}}$	effective bed shear
$u_{\bar{f}\ xcr}$	Shields critical bed shear velocity
$\bar{\mathrm{u}}$	average velocity in direction
u_, u__	first and second derivations of velocity
U_x, U_y	fluctuating components of velocity in and transverse directions
U_x	mean shear velocity
$u_$,v_	fluctuating part of velocities in the and directions
v	flow velocity
$\mathrm{v_y}$	flow velocity at distance y above the bed
$\mathrm{v_{max}}$	maximum flow velocity
$\mathrm{v_p}$	velocity at plunge point
$\mathrm{v_f}$	front velocity of a laminar density current
$\mathrm{v_*}$	shear velocity
$\mathrm{v_o}$	rotation centre point velocity
$\mathrm{v_n}$	density current head (nose) velocity

$\bar{v}$	average flow velocity
vs_{cr}	critical input stream power for incipient motion
$\bar{v}s$	average input unit stream power
V	reservoir capacity
V_t	reservoir capacity after t years of operation
V_o	density current flow velocity at plunge point
w	particle settling velocity
w	distance from centre point of a sphere
w_{50}	settling velocity of median particle diameter
x	Einstein correction coefficient
y_1	distance from bed where laminar velocity distribution equals that of turbulent flow
y_o	mathematical distance from bed where flow velocity is zero
z	suspension theory coefficient
z_d	depth of previously deposited sediment
z_1	suspension theory coefficient as revised by *Rooseboom (1975)*
ζ	non-equilibrium sediment transport parameter

FOREWORD

These guidelines have been written by Gerrit Basson, professor in hydraulic engineering and his predecessor, Albert Rooseboom, both of the University of Stellenbosch, South Africa, with inputs from members of the ICOLD sedimentation committee.

As reservoir sedimentation has proven to be a serious problem in South Africa, research in this field has been ongoing for more than 70 years. This publication emanates from extensive research which has been undertaken over the past 30 years with the support of the South African Department of Water Affairs and Forestry as well as the South African Water Research Commission.

A great deal of information has fortunately also been obtained from China, the country with the most extensive experience in this field.

Given the universal nature of hydraulic formulae it is not surprising, yet gratifying, that Chinese and South African data generally conform to the same mathematical relationships. This indicates that these relationships should be applicable in other countries as well. Much of the information contained here has been condensed from a more comprehensive publication (Basson and Rooseboom, 1997).

This ICOLD Bulletin follows on Bulletin 115 (ICOLD, 2000): "Dealing with reservoir sedimentation," which gave guidelines for management of reservoirs to limit sedimentation. The guidelines on mathematical modelling of sediment transport dynamics in reservoirs in this document can be used during the planning and design of new dams, and management of existing dams.

1. INTRODUCTION

Although there are reservoirs where sedimentation has proven to be a problem within 10 years after construction, sedimentation typically only becomes a significant problem 50 more years after construction of a dam. With only about 7% of the existing storage capacity in reservoirs world-wide having been created before 1950 (see **figure 1-1**), and with the average annual sedimentation rate now being estimated at 0,8% of the original storage capacities, it is expected that sedimentation will become a serious problem in many reservoirs during the next 50 years. The average age of reservoirs is now about 35 years (based on storage capacity) and since many reservoirs have been designed with a dead storage for sedimentation of about 50 years, serious sedimentation problems are going to develop with about 50 percent of the live storage capacity in reservoirs affected within the next 20 years. The effect of loss of the live storage at hydropower dams is however less of an impact than at storage/irrigation dams. Most of the existing reservoirs in the world will be completely silted up in 200 to 300 years from now, with large reaches of river system permanently modified. The ecological functioning would be completely different and only run-of-river water diversion or hydropower schemes can be implemented.

In 2006, 21 % of the total storage capacity was filled with sediment, increasing to 42% by the year 2050.

There has been a dramatic increase in the number and size of the dams being built after the Second World War, peaking during the 1970's worldwide (**Figure 1-1**). Damming created by a dam results in reduced sediment transport capacity upstream of the dam and sediment deposition, with the loss of live storage capacity. In many cases sediment deposition also occurs above the full supply level of the reservoir, sometimes constituting more than 10 % of the deposited sediment. As sediment deposition continues, the sediment delta grows higher and eventually flood levels start to rise. Not only flood levels are affected, but also drainage from agricultural land, bridge discharge capacity, pump station and hydropower operation and navigation. In semi-arid climates, the primary effect of reservoir sedimentation is however the loss in storage capacity for domestic or industrial supply and irrigation.

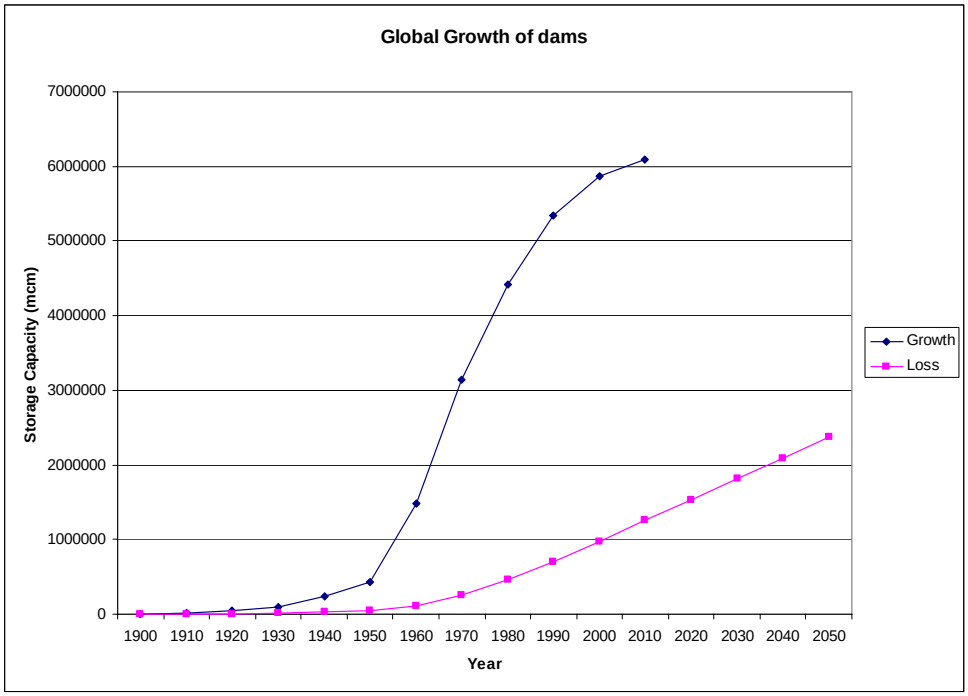

Figure 1-1: Global growth of reservoir storage capacity and reservoir sedimentation

Reservoir sedimentation occurs worldwide at a rate of about 0.8 percent per year, but the sedimentation rate in many regions such as Asia is much higher. Using an average rate, Palmieri (2003) estimated the loss to be approximately 45 km^3 per year. The cost of replacing the lost storage is significant; nearly US$ 13 billion per year would be needed, even without counting the environmental and social costs associated with new dams (Palmieri, 2003).

Sediment deposition occurs as a river enters a reservoir and its sediment transport capacity decreases in the backwater created by a dam. Coarse sediment is typically deposited first while finer clay and silt fractions are transported much deeper into the reservoir.

Apart from the obvious fact that sediment build-up within a reservoir leads to decreasing storage capacity, sediment build-up in specific areas can lead to local problems. Sediment build-up in a storage reservoir without facilities for preventing sedimentation typically only approaches equilibrium when the remaining storage capacity is a few percent of the original storage capacity.

Within the reservoir sediment build-up can have serious impacts on diversion and extraction facilities including turbine penstock inlets and pump station intakes.

In the context of reservoirs sedimentation distinction can be drawn between “small reservoirs” and”large reservoirs”. Small reservoirs, with capacities in the order of a few present of their MAR’s (Mean Annual Runoffs), can be designed and operated in such ways that they retain large proportions of their original capacities over long periods of time. In the case of small reservoirs the required calculations concentrate on the shapes and volumes of the equilibrium sediment deposits as well as the sizes of gates that may be required to sluice (pass incoming sediments through) ant to flush (scour sediments out). In addition, these calculations serve to predict the associated sediment concentrations so as to ensure that environmental standards are met with regard to the releases downstream.

Reservoir sedimentation and the corresponding loss of storage capacity is a common problem, which has attracted more and more attention in recent years. A number of different hydraulic measures can contribute to the management of the sedimentation problem, such as:

- Minimizing deposition in reservoirs through sluicing or venting of density currents
- Removing accumulated sediment from the reservoir through flood flushing
- Diverting sediment-laden flow to bypass the reservoir
- Controlling the location of sediment deposits in the reservoir for later dry excavation.

The first two mentioned measures above are costly in terms of water, hence effective reservoir management requires tools such as detailed prediction mathematical models, which can predict and monitor the effectiveness of such hydraulic measures.

Sediment sluicing and flushing have proven effective in a number of cases, provided excess water and adequately sized outlets are available or can be installed. Flood flushing are practiced based on availability of excess water, in two ways: (a) water level drawdown during the flood season, or (b) in semi-arid climates flushing during

single flood events with drawdown to free outflow conditions and filling with clear water after the flood.

It is generally not practicable to sluice or to flush sediments in the case of storage reservoirs with capacities well in excess of a few percent of their MAR's, except in the case of reservoirs with steep bed slopes where sediment induced density currents occur. Sediment modelling in the case of large reservoirs therefore concentrates on predicting the shapes and volumes of sediment deposits as functions of time, and establishing whether density currents could be sluiced or vented through special gates in order to limit sediment build-up.

These guidelines serve to provide assistance in performing the calculations which are necessary for calculating the volumes and shapes of sediment deposits in reservoirs. More sophisticated models however also consider bed erosion in order to simulate flushing/sluicing operation.

As it proves to be extremely difficult and costly to get rid of sediment-filled reservoirs, the impacts of long-term equilibrium sediment build-up should be considered seriously. Off-channel storage, whereby water is diverted from rivers by very small weir structures via canals, tunnels or pipelines to reservoirs, created high up in catchments, should be seriously considered wherever possible as it constitutes one of a few long-term sustainable development options. Given the complex nature of sediment transport mechanisms within reservoirs it is not possible to provide simply recipes for modelling transport within reservoirs. Such modelling should be undertaken only by persons who have become familiar with the theories in order to establish which relationships are the most appropriate for their situations.
These guidelines thus contain a number of selected formulae which may be considered for use. It is recommended that different formulae be used in order to obtain a feeling for the range of answers that are possible and that as much local field calibration data be obtained as possible. No specific model is prescribed but it is recommended that models which have been calibrated with reservoir data, rather than river data, be preferred.

2. RESERVOIR OPERATION AND SEDIMENT TRANSPORT PROCESSES

2.1 Introduction

When a river enters a reservoir, the sediment transport capacity is reduced and the sediment load is no longer dependent on sediment availability but can be related directly to hydraulic conditions in the reservoir. While coarser sediment is generally deposited in the upstream part of a storage reservoir, fine sediments (silt and clay fractions, d<60 μm), are transported further towards the dam through turbulent suspension, density currents or colloidal suspension. Deposition occurs in the main (original river) channel and overbank areas of the reservoir. Typical flow and deposition patterns within large reservoirs are indicated in **Figure 2.1-1** *(Graf, 1983)*.

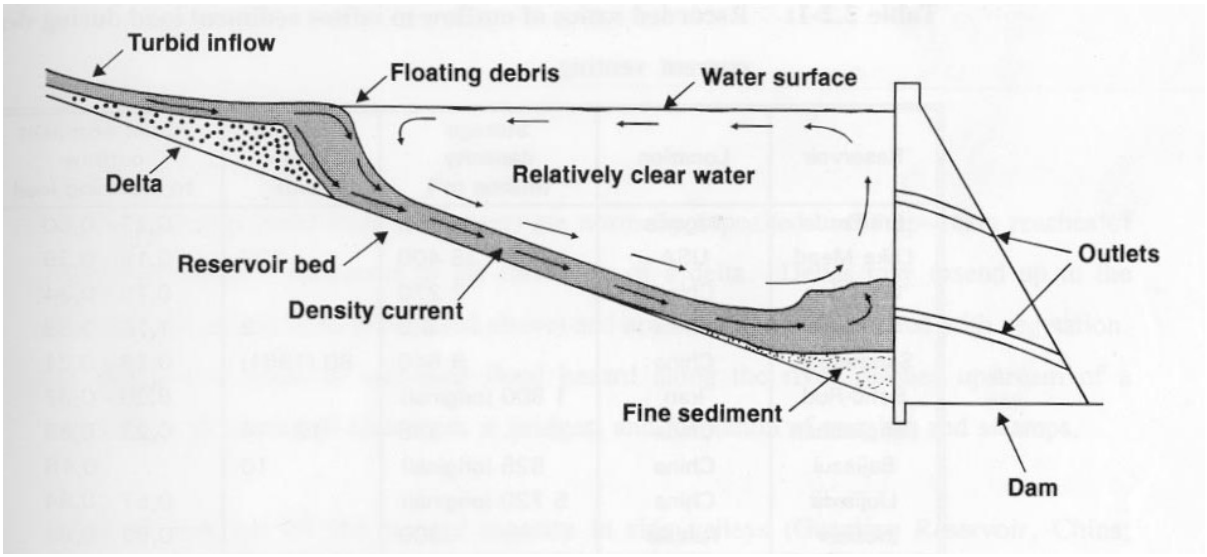

Figure 2.1-1: Schematic diagram of reservoir sedimentation processes (Graf, 1983)

2.2 Sediment transport mechanisms

Three separate mechanisms of sediment transport can be identified within reservoirs, namely turbulent suspended sediment transport, density currents and colloidal suspension.

- Turbulent suspension is the dominant mechanism of sediment transport through most reservoirs (as in rivers), and is discussed in detail in **Chapter 3**.

- A density current may be defined as the movement under gravity of a stream of fluid under, through, or over another fluid, the density of which differs by a small amount from that of the primary fluid. Differences in temperature, salinity or suspended sediment concentration can provide the mechanism by which a denser fluid "dives" below the upper fluid. Different types of density currents have been observed, such as overflow, interflow and underflow, and while the first two are often more related to temperature or salinity density difference systems, the latter is the means of sediment transport sometimes found in reservoirs.

Field data on the ratios of outflowing sediment load to incoming load during density current venting for different reservoirs are presented in **Table 2.2-1** *(Bruk, 1985; Delft Hydraulics, 1992; Tan, 1994; Mahmood, 1987).*

Table 2.2-1: Recorded ratios of outflow to inflow sediment load during density current venting

Reservoir	Location	Storage capacity (million m^3)	Reservoir length (km)	Ratio: sediment outflow to incoming load
Eril Emda	Algeria	160		0,25 - 0,60
Lake Mead	USA	38 400	128	0,18 - 0,39
Guanting	China	2 270		0,19 - 0,34
Heisonlin	China	8,6	2	1,16 - 0,59
Sanmenxia	China	9 640	80 (1961)	0,18 - 0,21
Sefid-Rud	Iran	1 800 (original)		0,20 - 0,37
Fengjiashan	China	398	12 - 14	0,23 - 0,65
Bajiazui	China	525 (original)	10	0,46
Liujiaxia	China	5 720 (original)		0,57 - 0,84
Nebeur	Tunisia	300		0,59 - 0,64

Density currents have been observed in several reservoirs such as Lake Mead, USA, Sautet Reservoir in France, Metha and Groshnitza Reservoirs in the former Yugoslavia, and the Nulele Reservoir in the former USSR *(Wu, 1994)*.

The hydraulics of density currents are discussed in **Chapter 4.**

- Colloidal suspensions are due to electrostatic forces which keep small particles in suspension, and their transport is therefore not related to the effect of gravity. Such suspensions not only depend on particle size, but are largely influenced by water quality. Colloidal sediments fall in the size range of approximately 10^{-3} to 1 micron, between dissolved particles on the one hand and sediments suspended by turbulent/laminar flow conditions on the other.

  The so-called wash load (normally not considered in laboratory calibrated standard sediment transport equations), should not be mistaken for colloidal suspension. The research conducted for this study has shown that the transport of silt and clay sediment fractions as found in many reservoirs can be described by relationships which are also valid for coarse sediments.

  Colloidal suspensions normally would be present in reservoirs at concentrations of less than 100 ppm. Due to their estimated low contribution to total sediment transport through a reservoir (normally less than 3 percent), such suspensions will not be considered further in this study. Even though they are important from a water quality perspective.

2.3 Modes of reservoir operation and impacts on the sediment balance

In order to understand how efficiently the above hydraulic measures can deal with reservoir sedimentation, their respective impacts on sediment loads and on trapping of sediment need to be considered. Over the long term, a sediment load-discharge relationship as indicated in **Figure 2.3-1** is obtained for a "natural" river, indicated by data points for the flood season (Sep to Dec) and the low flow season (Jan to Aug).

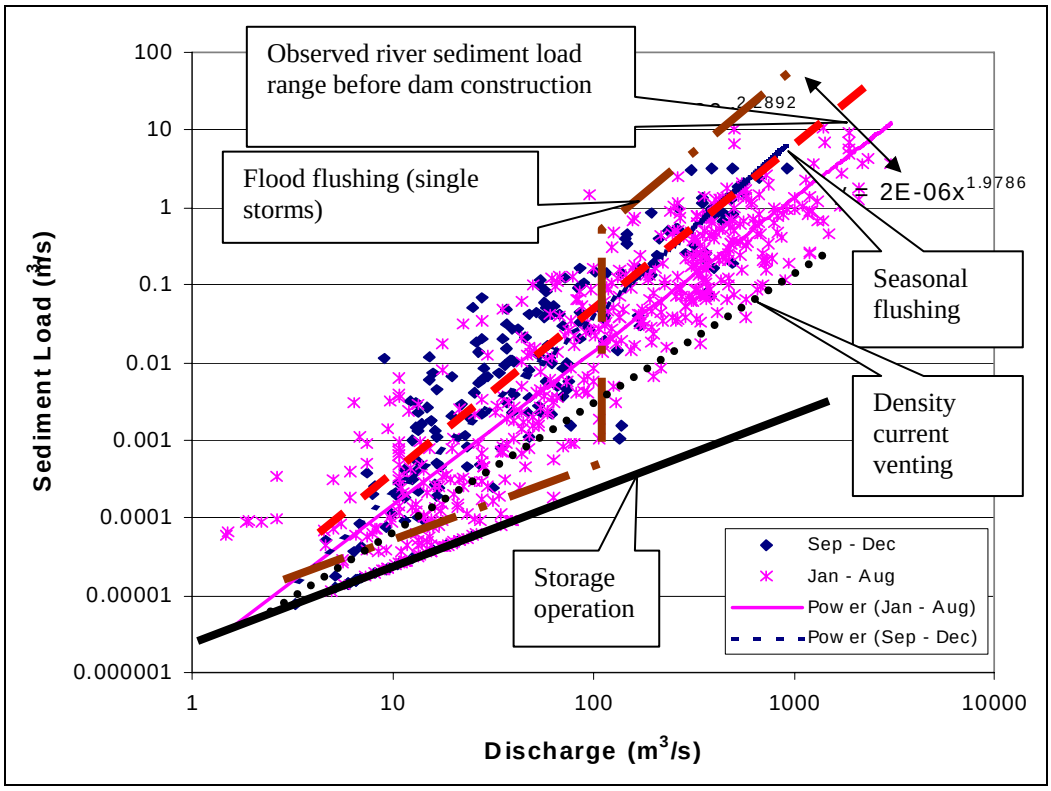

Figure 2.3-1 Reservoir operation and possible changes in the reservoir outflow sediment load-discharge relationship

One typical management option but extreme in terms of sediment transport is storage operation, allowing almost no through-flow of suspended sediment. Almost clear water will be released from storage operated reservoirs, typically resulting in channel degradation downstream of the dam. With regular flood hydrograph flushing (normally practised in semi-arid regions), the operational method is only efficient above a certain discharge. At high discharges, sediment loads higher than the mean seasonal sediment observed for the pre-dam scenario can be expected, but sediment equilibrium can be established. Regular flushing with suitable bottom outlets will ensure that flushed sediment approach the mean background level of sediment concentrations as for the pre-dam conditions. Sluicing (passing through) is another method of operation (partial water level drawdown during high inflows) which can limit the outflowing sediment loads to those for typical natural conditions, but a long-term equilibrium in sediment inflow and outflow cannot be established, since low inflow conditions will normally not be sluiced especially in arid conditions in order to avoid risking failure in water supply. Under such conditions sluicing only delays the rate of reservoir sedimentation and it needs to be used in conjunction with flood flushing to maintain substantial long-term reservoir capacity.

Figure 2.3-1 shows that reservoir operation with combined sluicing and flushing operation should in the long term impact least on the sediment balance if practised regularly, coinciding with high inflow conditions. Rapid changes in water quality with low concentrations of dissolved oxygen and high suspended sediment loads during flood flushing/sluicing (uncharacteristic of the natural river) need to be considered, however, in order to protect the aquatic ecosystem downstream of the dam.

Density current venting of sediment laden flows can also limit the rate of sedimentation, but very specific boundary conditions are required and therefore the general efficiency is less than with flushing/sluicing. This is because of a number of reasons such as: only fine sediment is transported through the reservoir with coarse sediment deposition where the density current forms, as well as the judicious opening of suitable outlets to vent the density current. It also requires excess water, but its key benefit is that the reservoir water level does not have to be lowered.

For flushing/sluicing operation the major constraint is excess water availability, which means that the reservoir has to be small in relation to the runoff if the water is used consumptively. In practice, the most efficient passing through of sediment is obtained when the reservoir capacity is less than 5 % of the mean annual runoff, although larger reservoirs are also sluiced successfully. The Churchill (1948) and Brune (1953) empirical trap efficiency curves indicate why reservoirs need to be so small.

The experience gained at Sanmenxia Reservoir, China, (Delft Hydraulics, 1992) with different reservoir operating rules is further illustrated in **Table 2.3-1**. It was only after reconstruction of the outlets that sediment sluicing could be optimized, with much reduced operating water levels, but with the advantage of maintaining long-term reservoir capacity. **Figure 2.3-1** shows Sanmenxia Dam flushing after reconstruction of the outlets.

Table 2.3-1. Reservoir operation and sediment trapping in Sanmenxia Reservoir

Period	Operation*	Maximum water level (m)	Minimum water level (m)	Sediment outflow as % inflow
9/60 – 3/62	A	332.58	324.04	6.8
4/62 – 7/66	B	325.90	312.81	58
7/66 – 6/70	C	320.13	310.00	83
7/70 – 10/73	D	313.31	298.03	105
11/73 – 10/78	D	317.18	305.60	100

Note* A: Storing water

B: Flood detention and sluicing through 2 tunnels and 4 penstocks

C: Flushing by opening 2 tunnels and 4 penstocks

D: Flushing: 2 tunnels, 4 penstocks and 8 diversion outlets

Figure 2.3-2. Sanmenxia Reservoir flushing after reconstruction of the outlets

When the storage capacity-mean annual runoff (MAR) ratios of reservoirs in the world are plotted against the capacity-sediment yield ratio, the data plot as shown in **Figure 2.3-3**. Most reservoirs have a capacity-MAR ratio of between 0.2 to 3, and a lifespan of 50 to 2000 years when considering reservoir sedimentation.

When the capacity-MAR ratio is less than 0.03 especially in semi-arid regions, sediment sluicing or flushing should be carried out during floods and through large bottom outlets, preferably with free outflow conditions. Flushing is a sustainable operation and a long-term equilibrium storage capacity can be reached. Seasonal flushing for say 2 months per year could be used in regions where the hydrology is less variable with capacity-MAR ratios up to 0.2. Seasonal flushing can also be practised at these relatively high capacity-MAR ratios when water demands and high sediment loads in the river are out of phase.

When capacity-MAR ratios are however larger than 0.2, not enough excess water is available for flushing and the typical operational model is storage operation. Density current venting can be practised at these reservoirs, as well as dredging to recover lost storage capacity.

The operating rules for a reservoir need not be inflexible, but can change with different stages of storage loss. Storage operation may be continued in reservoirs with large capacities relative to the sediment loads, while sluicing/flushing operation can be introduced once the loss of storage capacity reaches a certain stage. These transition zones can be found between the zones represented in **Figure 2.3-3.**

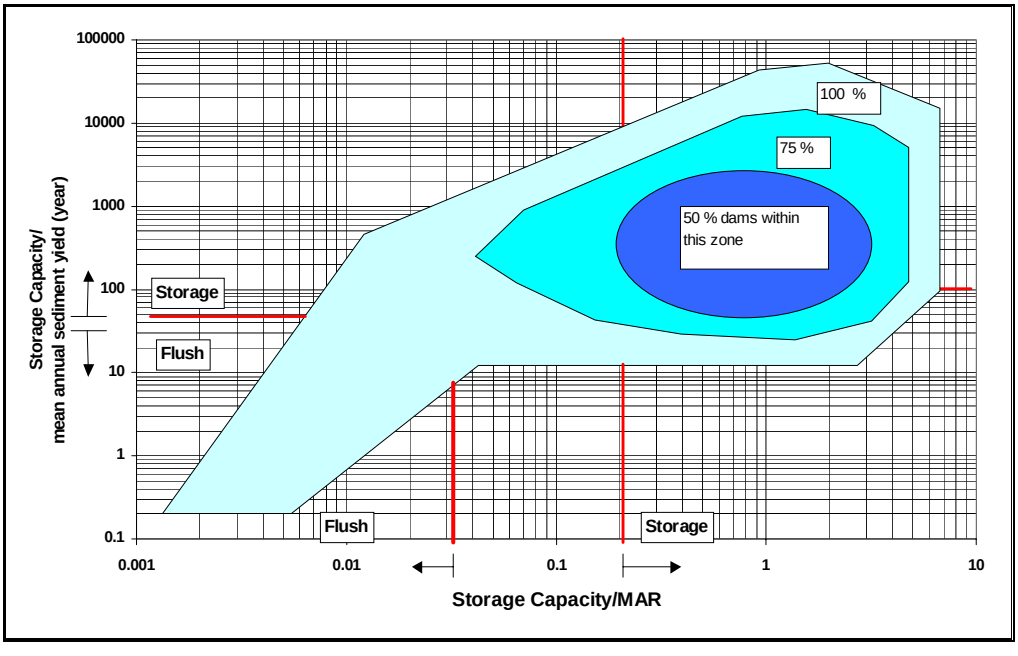

Figure 2.3-3. Empirical reservoir classification system in terms of storage, runoff and sediment yield

3 TURBULENT SEDIMENT TRANSPORT

3.1 Introduction

Experience in semi-arid climates indicates that in most rivers, the transport rate of fine sediments is not limited by the hydraulic conditions, but rather by sediment availability in the catchment. Within a reservoir this changes, however, and it is possible to quantify sediment transport in terms of hydraulic transporting capacity.

A large number of sediment transport equations have been derived during the past century. In most cases the equations were "calibrated" by means of coefficients with laboratory, and in some cases, field data. There are basically two groups of equation formats: those that predict bed load and suspended load transport separately, and those that predict a total sediment load without the distinction between bed load and suspended load. Most equations have been tested and calibrated for sand transport only, and the so-called "wash load" (fine sediments) is not included.

For practical application, specific transport equations are favoured in certain parts of the world. A number of recent studies have compared the accuracy of these equations to predict sediment transport. Quite often, though, these comparisons are biased towards those equations which incorporate some of the verification data in their calibration. Nevertheless, what is important to note (as is shown in **Table 3.1-1**), is the wide range of results which are obtained with these equations, even under controlled laboratory conditions.

The reason for this is that the understanding of sediment transport processes has not been developed well enough, even after many years of research in this field. To name just a few of the complications, neither the interrelationship between bedforms, associated roughness, hydraulic and sediment transport capacities, nor the change in velocity profile when sediment are being transported have been adequately modelled.

Due to the abovementioned, the approach in a number of countries is to calibrate sediment transport equations for site-specific conditions. When "bed load" is the main component or under other conditions where the sediment transport capacity is the limiting factor, such an approach can be used successfully. One set of such relationships is shown in **Figure 3.1-1**

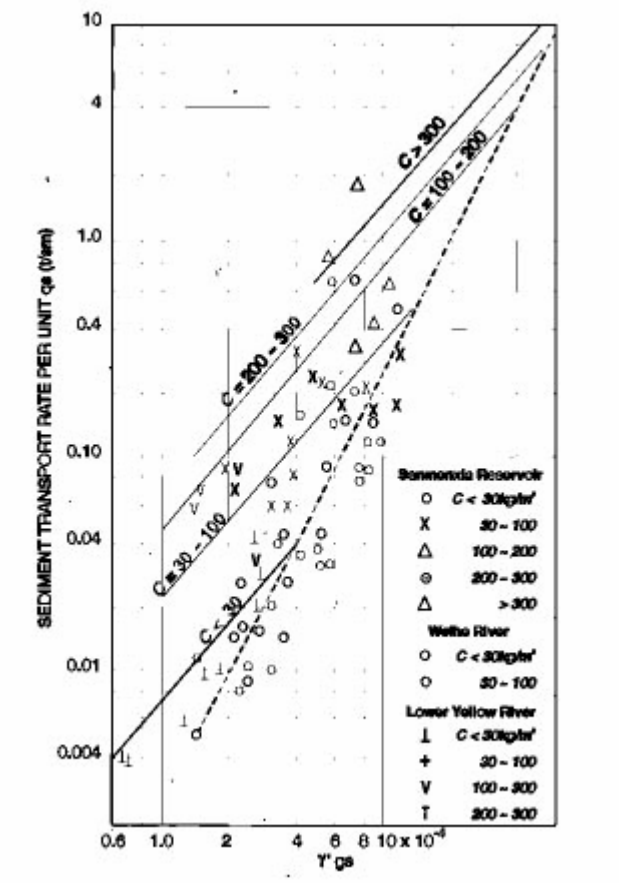

Figure 3.1 - 1 Sediment transport relationships for various Chinese rivers

(Delft Hydraulics, 1992)

Table 3.1-1 Accuracy ranges of commonly used sediment transport equations

White et al., (1975) compared eight formulae using 1 000 flume and 260 field measurements. The discrepancy ratio X_{calc} / X_{obs} was plotted against the dimensionless grain size $(\rho_s q_s / \rho q)$ and the percentages within the 0,5 to 2 range were as follows:

Formula	$\%\ in\ 0{,}5 \le X_{calc} / X_{obs} \le 2\ ranges$
Ackers and White (1973)	68
Engelund and Hansen (1967)	63
Rottner (1959)	56
Einstein (1950) (total load)	46
Bishop et al., (1965)	39
Toffaletti (1968)	37
Bagnold (1966) (total load)	22
Meyer-Peter and Müller (1948)	10

The laboratory data include particle sizes from 0,04 to 4,94 mm and field data from 0,095 to 68 mm.
The comparison of formulae by *Yang and Molinas (1982)* also used laboratory and river data encompassing mean grain sizes from 0,15 to 1,71 mm, channel widths 0,134 to 532 m, flow depths 0,01 to 15,2 m, temperature 0° to 34,3°C, average velocity 0,23 to 1,97 m/s and slopes from 4,3 x 10^{-5} to 2,79 x 10^{-2}. The range of data is the same as given by *Yang (1973)* for the data from which the formula was derived. The discrepancy ratio, defined as the ratio between computed and measured values, is given as follows:

Formula	**Data**		
	Lab.	**River**	**All data**
Colby (1964)	0,31	0,61	0,34
Yang (1973)	1,01	1,31	1,03
Yang (1979)	1,02	1,12	1,03
Shen and Hung (1971)	0,91	1,18	0,95
Engelund and Hansen (1967)	0,88	1,51	0,96
Ackers and White (1973)	1,28	1,50	1,31
Maddock (1976)	0,99	0,49	0,92

A different picture is painted by the comparative study carried out by *Van Rijn (1984b)*, also using field and laboratory data. The discrepancy ratio, r, defined as the ratio of predicted to observed transport rates in per cent were as follows:

Data	$0{,}75 \le r \le 1{,}5$				$0{,}5 \le r \le 2$				$0{,}33 \le r \le 3$			
	1	**2**	**3**	**4**	**1**	**2**	**3**	**4**	**1**	**2**	**3**	**4**
US Rivers Corps Engrs	53	39	32	6	79	67	61	24	94	87	78	44
Middle Loop River	39	13	37	63	78	37	74	94	96	80	98	100
Indian Canals	30	15	27	3	60	45	48	6	90	73	70	24
Pakistan Canals	23	37	34	13	56	71	71	29	91	94	91	48
Niobrara River	55	13	29	86	95	67	58	98	98	95	98	98
Average of field data	45	32	32	22	76	64	63	39	94	88	84	55
Flumes												
Guy et al., (1966)	40	67	56	68	70	89	85	90	91	98	99	98
Oxford	37	20	31	45	84	38	59	89	96	70	81	96
Stein (1973)	54	73	81	56	70	95	97	97	97	97	100	100
Southampton A	64	49	46	49	85	73	79	82	97	91	94	94
Southampton B	18	12	82	91	81	82	96	97	94	97	100	100
Barton-Lin (1955)	35	60	30	40	65	100	50	65	100	100	100	100
Average of laboratory data	41	46	52	59	77	74	77	89	95	89	94	98
Average of all data	43	37	40	36	76	68	68	58	94	88	88	71

In the above table, column 1 lists values obtained by the method of *Van Rijn (1984 a & b)*; 2 by the *Engelund-Hansen* formula *(1967)*; 3 by the *Ackers-White (1973)* formula and 4 by the *Yang (1973)* formula. The result is poor accuracy by the Yang formula for canals in India and Pakistan, which have the deepest flows of the above data. Since the other formulae produce reasonable results Van Rijn concludes that "the method of Yang must have serious systematic errors at large flow depth. On the average the predicted values are much too small".

Most sediment transport equations incorporate only parameters which describe the basic hydraulics and reflect how they are influenced by bedforms and transported sediment in an indirect way. This is often done by determination of the bed roughness independently from the sediment transport calculations. Some equations, like those of *Yang (1973)*, do not contain rules for calculating the velocity.

Instead of comparing the prediction accuracy of sediment transport equations based on observed data, a more appropriate comparison would be to calculate the main hydraulic variables from raw data, as was recommended by *Van Rijn (1984b)*. A new approach based on the interrelationship between hydraulic variables is included here. For reservoir conditions, it is also important to be able to forecast the transport of fine sediments (silt and clay), since in many impoundments they form the main sediment body. The accurate prediction of sediment transport as well as sediment concentrations is important since deposit shape, resuspension, flushing channel deformation, cohesion, flocculation, etc., are all dependent on the sediment transporting capacities and particle size sorting processes.

In practice, the prediction of the transport of fine sediments within reservoirs has been based on different approaches:

a) Use of the diffusion equation.

b) Use of sediment transport equations which were calibrated originally for sand fractions adopted to include fine sediments by recalibration with fine sediment transport data.

c) Combinations of sediment transport equations for sand fractions and diffusion equations for fine sediments.

Two further complicating matters in sediment transport are:

a) Non-uniform sediment particles. "Real" sediments are not nearly as homogeneous in size as the sediments used in laboratories. The normal

approach is to assume a representative sediment particle size or to model different size groups, each with its own sediment transport. Non-uniformity further leads to hiding/shielding and armouring phenomena involved in the re-entrainment of sediment.

b) Non-equilibrium sediment transport. Sediment transport equations as derived from theory and laboratory conditions are valid under steady, uniform flow, equilibrium conditions only. With fine sediments being transported, however, due to the low settling velocities, reaction to changing hydraulic conditions is not immediate.

3.2 Review of selected equilibrium sediment transport equations

Where locally calibrated transport equations exist for reservoirs, they should obviously receive precedence above formula which have been calibrated elsewhere.

In order to be able to express the sediment transporting capacity of a stream, a formula needs to contain all the variables what play roles in determining transporting capacity, particularly as far as hydraulic resistance is concerned.
Comprehensive analysis of variation in hydraulic resistance (Rooseboom & Le Grange, 1999) proves that a number of variables play important roles in determining flow resistance, which in turn determines sediment transporting capacity.

These variables are:

D	=	flow depth
g	=	gravitational acceleration
w	=	particle settling velocity
d	=	particle diameter
s	=	energy gradient
$\sqrt{gDs}$	=	shear velocity or;
ρgsD	=	shear stress
ρ	=	fluid density
ρ_s	=	sediment density

k_s = absolute roughness

ν = kinematic viscosity

As a stream deforms its bed the value of k_s can vary widely. Viscosity surprisingly plays an important role through the development of laminar boundary layer conditions when equilibrium transport conditions prevail.

Six existing transport equations, which are used for riverine transport calculations and which are deemed to have merit for application on reservoirs have been selected. They are discussed below, together with a new formula which includes all the important variables and has been calibrated with reservoir data.

(i) ***Engelund and Hansen (1967) equations***

By using dimensional analysis, *Engelund and Hansen (1967)* related input power per unit area of channel boundary to sediment discharge and proposed the following relationship:.

$$\frac{2GdS}{V^2}\phi = 0{,}10^{\frac{5}{2}} \qquad (3.2\text{-}1)$$

where

$$\phi = \frac{Q_s}{\sqrt{\left(\frac{\gamma_s - \gamma}{\gamma}\right) g d^3}\ ;} \qquad (3.2\text{-}2)$$

$$\theta = \frac{\rho g D s}{(\gamma_s - \gamma) d}\ ; \quad \text{and} \qquad (3.2\text{-}3)$$

D = flow depth

g = gravitational acceleration

v = flow velocity

s = slope

Q_s = total sediment discharge

Υ = specific weight of water

Υ_s = specific weight of sediment

d = sediment particle size

The total sediment discharge can therefore be calculated directly by writing **Equation (3.2-1)** as

$$Q_s = \frac{v^2}{20gDs}\sqrt{\left(\frac{\gamma_s - \gamma}{\gamma}\right)gd^3}\left(\frac{\rho gDs}{(\gamma_s - \gamma)d}\right)^{5/2} \quad (3.2\text{-}4)$$

(ii) ***Ackers and White (1973)***

Ackers and White (1973) used dimensional analysis to derive an equation representing total sediment discharge in terms of three dimensionless numbers, viz. a sediment transport function $G_{gr,}$ a mobility number F_{gr} and dimensionless sediment particle size d_{gr}. The parameters are expressed as

$$G_{gr} = c'\left(\frac{F_{gr}}{A} - 1\right)^m = \frac{c'D}{\gamma_{,} d/\gamma}\left(\frac{\sqrt{gDs}}{\mathrm{v}}\right)^n \quad (3.2\text{-}5)$$

$$F_{gr} = \frac{(\sqrt{gDs})^n}{\sqrt{gd\,(\gamma_s/\gamma - 1)}}\left(\frac{\mathrm{v}}{\sqrt{32}\log 10\,\mathrm{D/d}}\right)^{1\text{-}n} \quad (3.2\text{-}6)$$

$$d_{gr} = d\left(\frac{g(\gamma_s/\gamma - 1)}{v^2}\right)^{\frac{1}{3}} \quad (3.2\text{-}7)$$

where ν = kinematic viscosity.

The coefficients c' , A, m and n are functions of sediment particle size and have the following values:

For coarse sediment $\left(d_{gr} > 60\right)$: $n = 0{,}0$; $A = 0{,}170$; $m = 1{,}50$; $c' = 0{,}025$

whereas for smaller sizes ($60 \geq d_{gr} \geq 1$) their values are given by:

$$n = 1 - 0{,}56 \log d_{gr} \qquad (3.2\text{-}8)$$

$$A = \frac{0{,}23}{\sqrt{d_{gr}}} + 0{,}14 \qquad (3.2\text{-}9)$$

$$m = \frac{9{,}66}{d_{gr}} + 1{,}34 \qquad (3.2\text{-}10)$$

$$\log c' = 2{,}86 \log d_{gr} - (\log d_{gr})^2 - 3{,}53 \qquad (3.2\text{-}11)$$

(iii) **Unit (input) stream power** ***(Yang, 1973, Rooseboom, 1975)***

The basic principles of this approach were proven in South Africa in 1974 and subsequently calibrated with field data from Gariep and Welbedacht Reservoirs. The stream power principle has been used extensively in South Africa, USA and China during the past 35 years in the planning and design of reservoirs.

The suspension theory *(Rouse, 1937)* can be extended to describe both bed load and suspended load (the case of suspended transport with a relatively large z-value is equivalent to the bed load condition) as well as the incipient motion criteria, and is therefore well suited to the analysis of total carrying capacity *(Rooseboom, 1975)*.

Sediment transporting capacity per unit width in terms of flow parameters can be calculated if it is assumed that sediment particles are transported at the same velocity as the fluid:

$$q_s = \int_{y_o}^{D} C \, v \, dy \text{ with } C \propto \left(\tau \frac{dv}{dy} \right)^z \qquad \text{and } \tau \frac{dv}{dy} \text{ the applied power,} \qquad (3.2\text{-}12)$$

with C = sediment concentration

τ = bed shear stress

z = suspension theory coefficient, $= \frac{w}{\kappa\sqrt{gDs}}$

w = settling velocity

κ = Von Kármán coefficient

and y_0 the distance from the bed where v = 0 mathematically, which after integration leads to an equation of the form *(Rooseboom, 1975)*:

$$\log \frac{q_s}{q} = \alpha_1 \log \bar{v}s + \log \left[\frac{\frac{\alpha_1 \alpha_2 C_0}{(sD\sqrt{2\pi\, gDs})^{z_1}}}{y_0} \right] \qquad (3.2\text{-}13)$$

with $\alpha_1; \alpha_2$ = coefficients

z_1 = suspension theory coefficient as derived by *Rooseboom (1975)*

C_0 = sediment concentration at the bed where

$\bar{v}$ = average flow velocity

Yang (1972) found through statistical analysis of available data that **Equation 3.2-13** describes sediment transporting capacity particularly well. The analysis by *Van Rijn (1984b)* later contradicted this finding, as shown in Table 3.1-1. The equation by *Yang (1972)* was, however, only calibrated on laboratory data and as mentioned before, the study by Van Rijn may have been biased. Yang used a slightly different approach by including a critical stream power value for incipient motion in this equation (1972):

$$\log \frac{q_s}{q} = \alpha_3 + \alpha_4 \log(\bar{v}s - vs_{cr}) \qquad (3.2\text{-}14)$$

with α_3, α_4 = constant and coefficient,

vs_{cr} = critical input stream power for incipient motion

and later *(Yang, 1973)*

$$\log \frac{q_s}{q} = \propto_5 + \propto_6 \log\left(\frac{\bar{v}s - v s_{cr}}{w}\right) \qquad (3.2\text{-}15)$$

with $\propto_5 \propto_6$ = constant and coefficient

w = settling velocity

The last term in **Equation 3.2-13** was found *(Rooseboom, 1975)* not to vary much and can be equated to the $\propto_5$ coefficient of Yang. *Yang (1973, 1979)* produced two dimensionless unit stream power equations for sand transport, with and without incipient motion. In 1984, *Yang* proposed a gravel transport equation with an incipient motion term.

The maximum sediment transport capacity of a stream can therefore be determined by an equation of the type:

$$\log \frac{q_s}{q} = \propto \log \bar{v}s + \beta \qquad (3.2\text{-}16)$$

where $\bar{v}s$ represents the average input unit stream power at a cross-section in a reservoir or river, and $\propto$ = coefficient and β = constant.

(iv) **Stream power theory *(Bagnold, 1966)***

Bagnold used the stream power per unit bed area, based on general concepts in physics, to relate the rate of energy dissipation used in transporting materials to the sediment transport:

$$\left(\frac{\gamma_s - \gamma}{\gamma}\right) q_{bw} \tan \propto = \tau \, v \, e_b \qquad (3.2\text{-}17)$$

with q_{bw} = bed load transport rate

$\tan\propto$ = ratio of tangential shear to normal force

v = average flow velocity

e_b = efficiency coefficient

τv = stream power

and for suspended load:

$$\left(\frac{\gamma_s - \gamma}{\gamma}\right) q_{st} = 0{,}01\left(\frac{\tau v^2}{w}\right) \tag{3.2-18}$$

with the total load (q_t)

$$= q_{bw} + q_{st} = \frac{(\gamma_s - \gamma)}{\gamma} \tau v \left(\frac{e_b}{\tan \propto} + 0{,}01\frac{v}{w}\right) \tag{3.2-19}$$

Based on field data (rivers and reservoirs in China), the sediment carrying capacity = $e_b(\tau v) = f(\Upsilon_s\ qs)$ has been indicated in **Figure 3.2-1** for conditions of deposition and erosion.

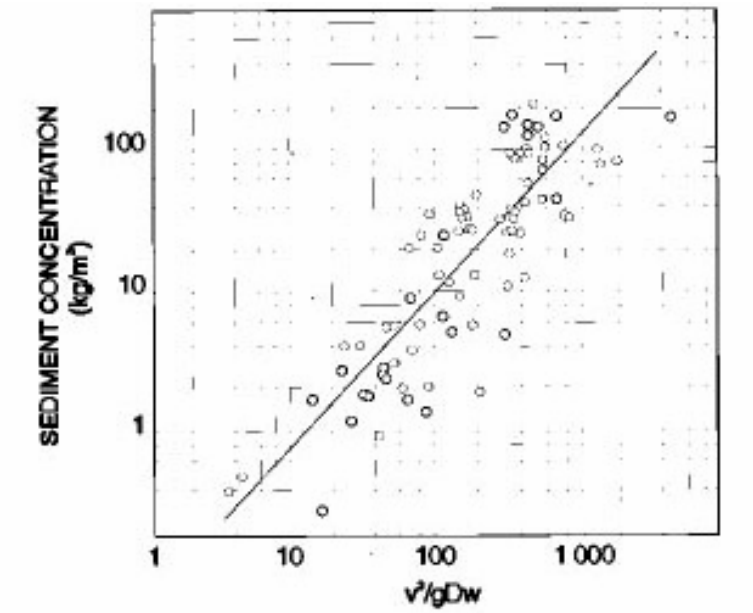

Figure 3.2 - 1 Stream power sediment transport relationship at Fenhe Reservoir, China (*Gaun et al., 1991*)

(v) **Gravitational power theory** ***(Velikanov, 1954; Dou, 1974; Zhang, 1959)***

Velikanov (1954) divided the rate of energy dissipation for sediment transport into two parts: the power required to overcome flow resistance and the power required to keep sediment particles in suspension against the gravitational force:

$$\underset{\text{(i)}}{\rho g(1 - C_{vy})\, v_y s} = \underset{\text{(ii)}}{\rho v_y \frac{d[(1 - C_{vy})\overline{U_x U_y}]}{dy}} + \underset{\text{(iii)}}{g(\rho_s - \rho) C_{vy} (1 - C_{vy}) w} \qquad (3.2\text{-}20)$$

with C_{vy} = time-averaged sediment concentration at a distance y above the bed in percent by volume

v_Y = time-averaged flow velocity at distance y above bed

U_x, U_y = fluctuating part of velocities in the x and y directions

Integration over depth of flow yields

$$g\, vSD = \frac{f_o v^3}{8} + \frac{\rho_s - \rho}{\rho} (gDw\, C_v) \qquad (3.2\text{-}21)$$

The Darcy Weisbach resistance coefficients are given by:

$$f = \frac{8gDs}{v^2}, (C_v \neq o) \qquad (3.2\text{-}22)$$

and $$f_o = \frac{8gD s_0}{v^2}, (C_v = o) \qquad (3.2\text{-}23)$$

with s, s_o = energy slope with and without sediment.

Assuming that $f / f_k = a$ constant, (with f_k = resistance coefficient for a saturated sediment concentration), it follows that

$$\frac{(\rho_s - \rho)}{\rho}\frac{wC_v}{vs} = \text{a constant.} \qquad (3.2\text{-}24)$$

From the above, Velikanov's equation can be expressed in the form:

$$C_v = K\left(\frac{v^3}{gDw}\right) \qquad (3.2\text{-}25)$$

with $K = a$ coefficient to be determined from measured data. Sediment transport equations of this format have been used extensively by Chinese engineers. *Dou (1974)* proposed that the rate of energy dissipation to keep sediment particles suspended should be equal to that used by sediment particles in suspension:

$$C_t = K_1\left(\frac{\gamma_s}{\gamma_s - \gamma}\right)\frac{vs}{w} \qquad (3.2\text{-}26)$$

with C_t = sediment concentration by weight

K_1 = coefficient

and from Chezy : $s = \dfrac{v^2}{C^2 D}$ (3.2-27)

gives $: C_t = K_2\left(\dfrac{v^3}{gDw}\right)$ (3.2-28)

with K_2 = coefficient

Zhang (1959) assumed that the energy being dissipated in keeping sediment particles suspended should come from turbulence instead of from the effective power available from the flow:

Total rate of energy dissipation of clear-water - rate of energy dissipation due to sediment laden flow = total rate of energy reduction due to the damping effect (reduction in turbulence due to suspended sediment).

$$\gamma A v_{s_1} - [\gamma(1 - C_v) A v_{s_2} + \gamma_s C_v A v_{s_2}] = k_1(\gamma_s - \gamma) A w C_v^{\propto} \quad (3.2\text{-}29)$$

with S_2, S_1 = energy slope of sediment-laden water and clear-water

$\propto$ = dimensionless exponent

A = channel cross-sectional area

k_1 = dimensionless coefficient

When C_v is small:

$$C_v^{\propto} = \left[\frac{\gamma}{k_1(\gamma_s - \gamma)}\right]\left[\frac{v}{w}(s_1 - s_2)\right] \quad (3.2\text{-}30)$$

which can be further reduced to:

$$C_t = K_3\left(\frac{v^3}{gRw}\right)^m \quad (3.2\text{-}31)$$

with K_3, m = parameters related to sediment concentration, and

$R \alpha D$ = hydraulic radius

Field data plotted according to this relationship are shown in **Figure 3.2-2.**

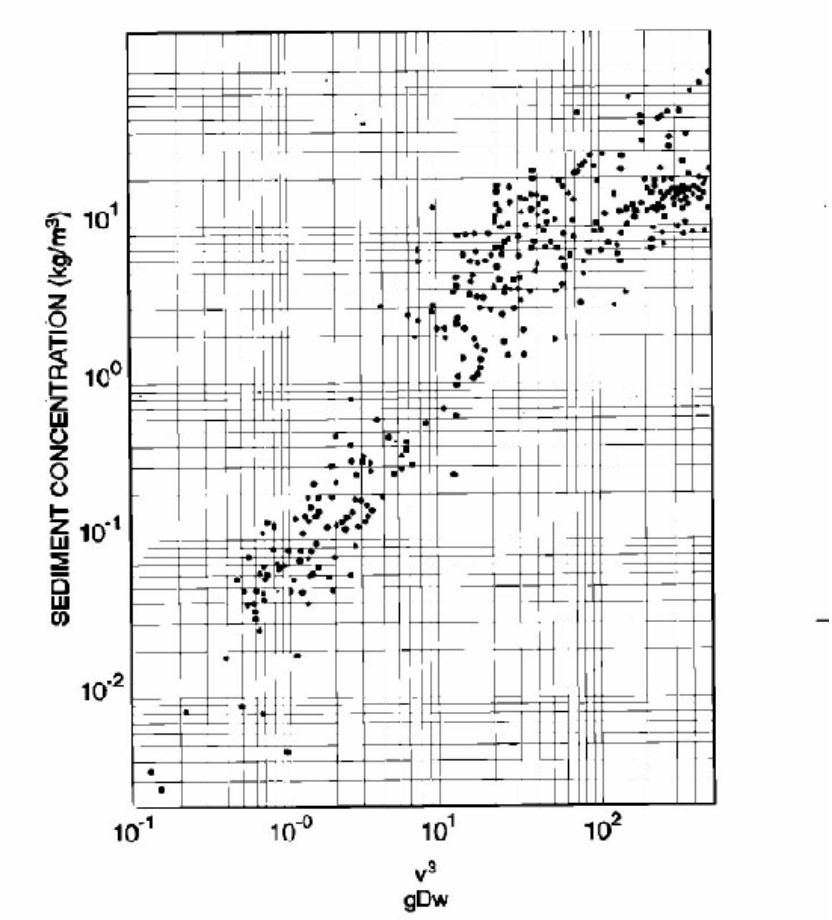

Figure 3.2 - 2 Gravitational power theory calibrated with Chinese data (*Wu, 1994b*)

The use of the stream power theory has been well researched and verified with field data. Three different approaches in the study of sediment transport, based on the concept that the rate of energy dissipation of flowing water should be related to the rate of sediment transport, are generally used.

Yang and Kong, (1991) carried out an analysis and comparison of the three stream power parameters

$$\frac{vs}{w}\,;\tau v\;;\;and\;\frac{v^3}{gDw}$$

The dimensionless unit stream power correlated best with concentration data by *Stein (1965)*, indicated in **Figure 3.2-3**. Velikanov's equation fitted with an S-curve instead of a straight line on a log-log plot as is required by **Equation 3.2-25**. Bagnold's

equation is based on general concepts in physics without using fluid mechanics theory and it is not generally used, and was not reviewed further by *Yang and Kong (1991).*

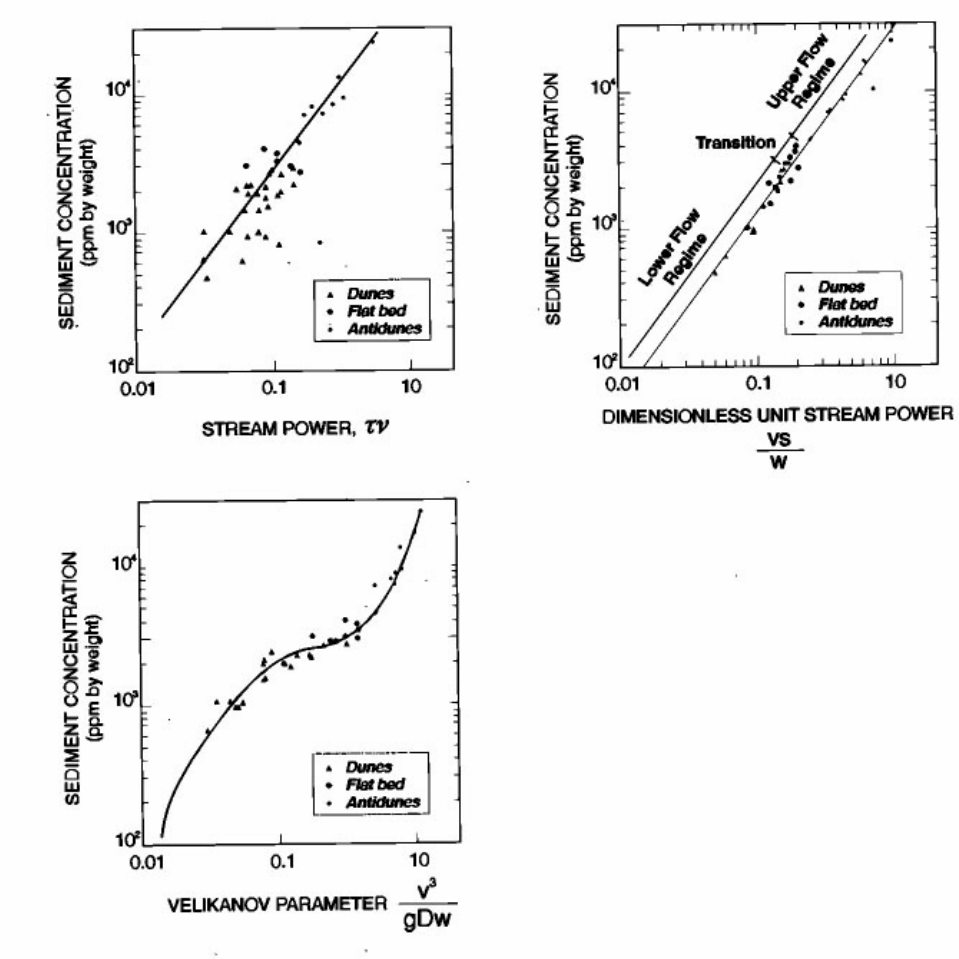

Figure 3.2 - 3 Comparison between stream power equations *(Yang and Kong, 1991)*

Yang and Molinas (1982) showed that bed load, suspended load and total bed-sediment concentrations can all be expressed by the general form of **Equation 3.2-15**. *Yang and Kong (1991)* illustrated that the three equations based on the gravitational theory can all be converted to or derived from the basic form of the unit stream power equation, with differences in coefficients and assumptions to derive coefficients. The assumptions of Dou, Velikanov and Zhang to obtain v^3 / gRw cannot be supported by laboratory or field data used by *Yang and Kong (1991)*. The unit stream power theory is therefore best to use and based on a sound theoretical basis *(Yang and Kong, 1991).*

(vi) ***Van Rijn (1984a and b)***

In the Van Rijn transport model the sediment load is divided between bed load and suspended load according to the relative magnitudes of the bed shear velocity, and the particle fall velocity. When the bed shear velocity exceeds the fall velocity, sediment is transported as both suspended and bed load. Bed load is considered to be transported by rolling and saltation and the rate is described as a function of saltation height. The suspended load is determined from the depth-integration of the product of the local concentration and flow velocity. The reference concentration is determined from the bed load transport.

The bed load transport rate is computed as the product of particle velocity, u_{bs}, saltation height, δ_b and the bed load concentration, C_b:

$$q_b = u_{bs}.\delta_b.C_b \tag{3.2-32}$$

Expressions for the particle velocity and saltation height were obtained by numerically solving the equations of motion applied to a solitary particle. These expressions are given in terms of two dimensionless parameters which are considered to adequately describe bed load transport; a dimensionless particle diameter, D_*, and a transport stage parameter, T as defined below:

$$D_* = d_{50}\left[\frac{(s-1)}{v^2}g\right]^{1/3} \tag{3.2-33}$$

$$T = \frac{(u_{\bar{g}})^2 - (u_{\bar{f},cr})^2}{(u_{\bar{f},cr})^2} \tag{3.2-34}$$

in which u'_g is the bed shear velocity, related to grains, u is the mean flow velocity and $u'_{f,cr}$ is Shields critical bed shear velocity. u'_g is the effective bed shear and is so defined

in order to eliminate the influence of bed forms since form drag was not considered to contribute to bed load transport.

Extensive analysis of flume measurements of bed load transport yielded the following expression for the bed load concentration:

$$\frac{C_b}{C_o} = 0.18 \frac{T}{D_*} \tag{3.2-35}$$

in which C_o is the maximum bed concentration.

Combining equations for particle mobility, saltation height and **Equation 3.2-35** gives the following expression for bed load transport, valid for particles in the range 0.2 to 2.0 mm:

$$\frac{q_b}{\sqrt{(s-1)gd_{50}^3}} = \frac{0.053T^{2.1}}{D_*^{0.3}} \tag{3.2-36}$$

The Van Rijn suspended sediment load method is based on the computation of a reference concentration determined from the bed load transport. Thus the reference concentration, C_a, is described as a function of the dimensionless particle diameter, D_*, and transport stage parameter, T.

$$C_a = 0.015 \frac{d_{50} T^{1.5}}{a D_*^{0.3}} \tag{3.2-37}$$

The representative particle size of suspended load is generally finer than that of bed load. Van Rijn relates this particle size, d_s to the d_{50} and geometric standard deviation, σ_s of the bed material:

$$\frac{d_s}{d_{50}} = 1 + 0.011(\sigma_s - 1)(T - 25) \quad for\ T < 25 \tag{3.2-38}$$

Many factors affect the suspension parameter z, e.g. volume occupied by particles, reduction of fall velocity and damping of turbulence. These effects are grouped into a single correction factor, ψ which is used to define a modified suspension number, Z'

$$Z' = z + \psi \tag{3.2-39}$$

ψ was found to be a function of the main hydraulic parameters:

$$\psi = 2.5\left[\frac{w}{u_f}\right]^{0.8}\left[\frac{C_a}{C_o}\right]^{0.4} \quad for\ 0.1 \preceq 1 \tag{3.2-40}$$

where C_o is the maximum bed concentration.

By combining the expression describing the velocity and concentration profiles with the expressions for z and ψ, *Van Rijn (1984b)* derived the following expression:

$$q_s = FuDC_a \tag{3.2-41}$$

in which F is given by:

$$F = \frac{\left[\frac{a}{D}\right]^{z'} - \left[\frac{a}{D}\right]^{1/2}}{\left[1-\frac{a}{D}\right]^{z'}\left[1.2 - z'\right]} \tag{3.2-42}$$

- It is recommended that at least three different formulae be used for simulation of coarse sediment fractions in reservoir sedimentation calculations so as to obtain a feel for the variability of the results.

- The stream power concept is powerful in describing the sediment transport process. Most equations are, however, based on dimensional analysis and not derived from sound theoretical principles.

- The unit input stream power equation *(Yang, 1973)*, is the only stream

power relationship which can be derived theoretically *(Rooseboom, 1975)*, although some averaging assumptions had to be made. The proven success of this formulae can be particially attributed to the fact that it is based on pure hydraulic principles and that it contains a term representing absolute roughness (y_o) in its derived form (equation 3.2-13).

- The Van Rijn equations are based on several empirical relationships and is based on separate bed load and suspended transport which cannot be justified from fundamental theory. The equations do, however, provide for changes in bed roughness and energy dissipation for different flow regimes and sediment transport.

- The prediction accuracy of most riverine sediment transport equations seems to depend on calibration with as extensive a sediment transport data base as possible (including laboratory and river data). Equations which have been calibrated with reservoir data are obviously to be preferred for reservoir modelling.

Sediment transport through reservoirs has traditionally only been described under conditions of deposition. When management options such as flushing are incorporated, flow through the reservoir reverts back to river conditions, but with high sediment transport. A very wide range of sediment transport, hydraulic, bed roughness and other conditions are therefore encountered.

Basson (1997) has developed a new sediment equation which contains all the important variables involved in the analysis of sediment transport in rivers and reservoirs and which could be calibrated for field as well as laboratory data and which was eventually to be used for calibration with reservoir transport data.

The calibrated new sediment transport equation based on the non-cohesive sediment river data of Gilbert, Guy et al. and Bagnold is given by:

$$C = \left(\left(\frac{\rho}{\rho_s - \rho} \right) (gsD)^{1,5} \right)^{1,969} .(0,4\, k_s)^{-1,146} . w^{-3,286} . \left(\frac{ks}{D} \right)^{0,856} . \left(\frac{w}{0,4\sqrt{gsD}} \right)^{2,560} \qquad (3.2\text{-}43)$$

with C = sediment concentration in % (weight).

The accuracy of the proposed new equation is shown in **Table 3.2-4**.

Table 3.2-4: Accuracy of new sediment transport equation in prediction ranges (for C>0,01%)

Calibration based on	**Percentage of data within accuracy range**		
	$0,67 < \frac{Ccalc}{Cobs} < 1,5$	$0,5 < \frac{Ccalc}{Cobs} < 2,0$	$0,33 < \frac{Ccalc}{Cobs} < 3$
Gilbert and Guy flume data	86 %	97 %	99 %
Bagnold USA river data	48 %	68 %	89 %
Gilbert, Guy and Bagnold data	77 %	92 %	98 %

Although calibration data have been used in the above verification, the results compared with other sediment transport relationships are good and even river data are predicted with relatively good accuracy. *Basson (1997)* provides comprehensive details on the verification of the new sediment transport equation against river and field data. Observed versus calculated sediment transport based on **equation 3.2-43** are shown graphically in **figures 3.2-4 and 3.2-5**.

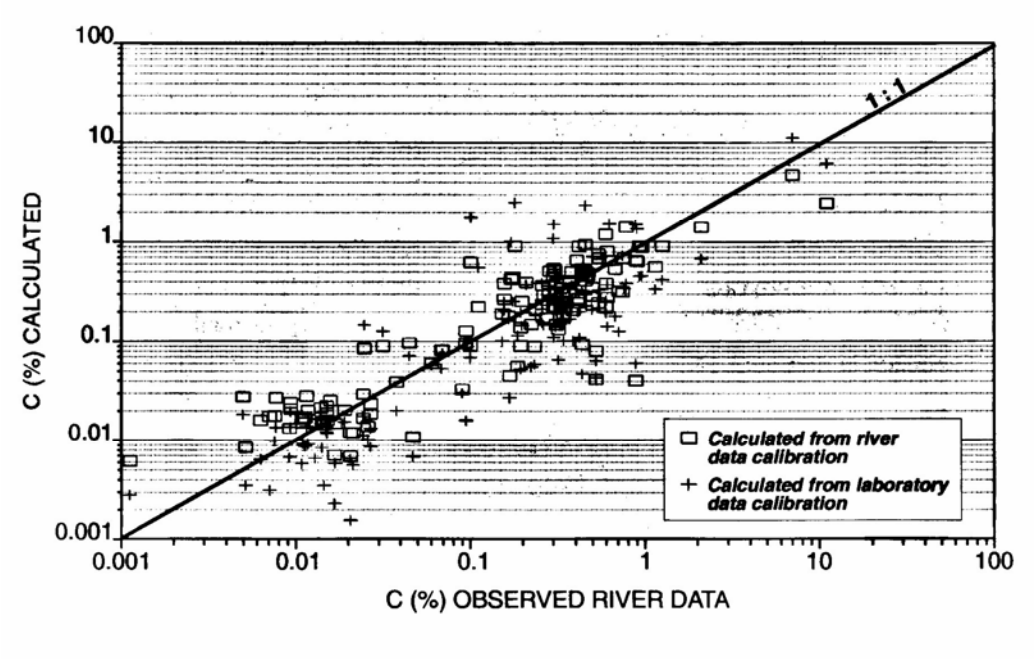

Figure 3.3 - 4 Verification (with river data) of calibrated new sediment transport equation (based on flume data)

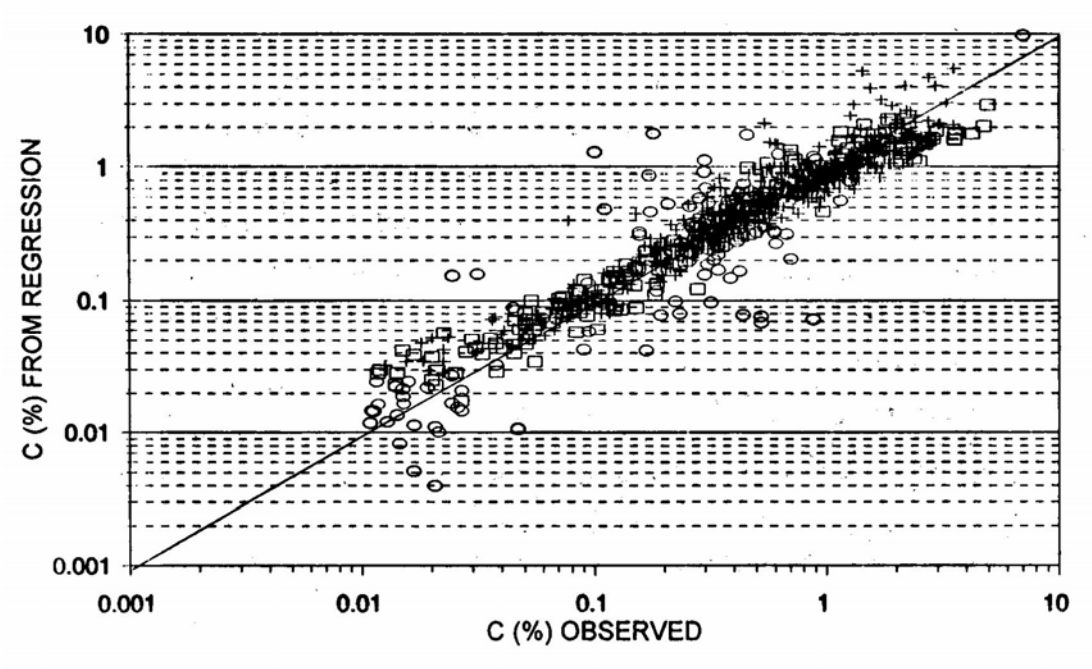

Figure 3.3 - 5 Calibration of new sediment transport equation based on flume and river data

It has been established that good correlations can be obtained with the new sediment transport equation using flume and river data. The question remains, however, whether

this relationship can also be applied to reservoir data. The reservoir data obtained from field sampling at selected South African reservoirs, will be analysed here.

3.3 Calibration with reservoir data

There are a number of important differences between reservoir, laboratory and river data. The latter two sets are normally obtained under uniform and steady (or nearly steady) flow conditions, and with sediment transport and bed deformation equilibrium. In a reservoir the two extreme operational situations are full storage operation with non-uniform, but often near steady conditions in large reservoirs, and drawdown flushing, normally with highly unsteady and non-uniform flow conditions during the retrogressive erosion phase.

The particle sizes of sediments being transported through a reservoir furthermore also differ drastically from the river and flume cases. Along the upper reaches of a reservoir, coarse sediment is still being transported, representing river conditions, but further downstream the sorting process soon causes only fine sediment to be transported. This fine sediment (under storage operation with a large reservoir) can be in the order of d_{50} = 2 micron, which is 10 times smaller than the finest sediments typically encountered in flumes and rivers.

The slope to be used in the sediment transport equation should actually fall somewhere between the energy slope and bed slope for a full reservoir, while during flushing the energy slope should approach the bed slope and uniform flow conditions are approached when equilibrium scour is being reached.

Unsteady flow conditions during flushing can cause over saturation, especially if erosion takes place close to the dam and suspended sediment samples are taken immediately downstream of the dam. On the other hand, non-equilibrium sediment transport also occurs due to the time lag during which fine sediment loads adjust to changing hydraulic conditions (see discussion in **Section 3.5**).

Obtaining field data during flushing is problematic. With complete drawdown, it is impossible and dangerous to obtain concentration samples from the flushing channel, and hydraulic variables are difficult to monitor within the reservoir.

Other processes that can play a role in reservoirs are different mechanisms of sediment transport and flocculation at high sediment concentrations, which may influence settling velocities.

All in all, reservoir data should be analysed and selected with great care. It is doubtful that a relationship which has been calibrated for coarse sediments under uniform, steady flow conditions can be used at all to predict sediment transport through a reservoir. Therefore, the approach followed here was to calibrate the proposed sediment transport relationship with reservoir data and to compare it with the other relationships as calibrated with river and laboratory data. Under high inflow flushing conditions it is expected that the reservoir flows will approach river conditions and that the river and reservoir sediment transport relationships should agree. A sediment transport relationship based on unit input stream power and storage operation for two reservoirs of very different sizes as shown in **Figure 3.3-1** has been used for many years in South Africa.

To interpret the reservoir data sediment concentration was plotted against input stream power (vs) in **Figures 3.3-2** and **3.3-3**. (Note that settling velocity still needs to be taken into account to form a comprehensive picture of the observed sediment transport). After each flushing and closure of the gates at Welbedacht Dam, the stream power decreases rapidly, although sediment concentrations remain high for some time and only then drop back to the "normal" vs against C relationship. It was found that the sediments being transported immediately after closure of the dam outlets were much finer than with free flow.

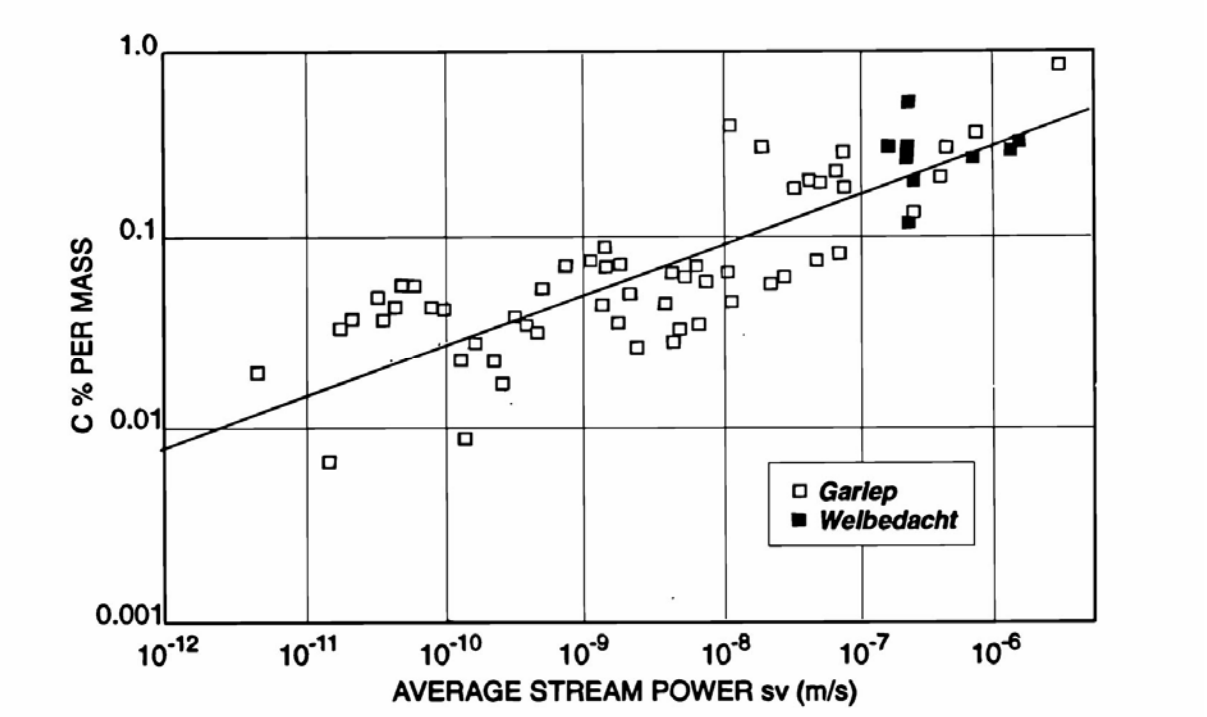

Figure 3.3 - 1 Sediment concentration versus stream power for two South African reservoirs (*Rooseboom et al., 1986*)

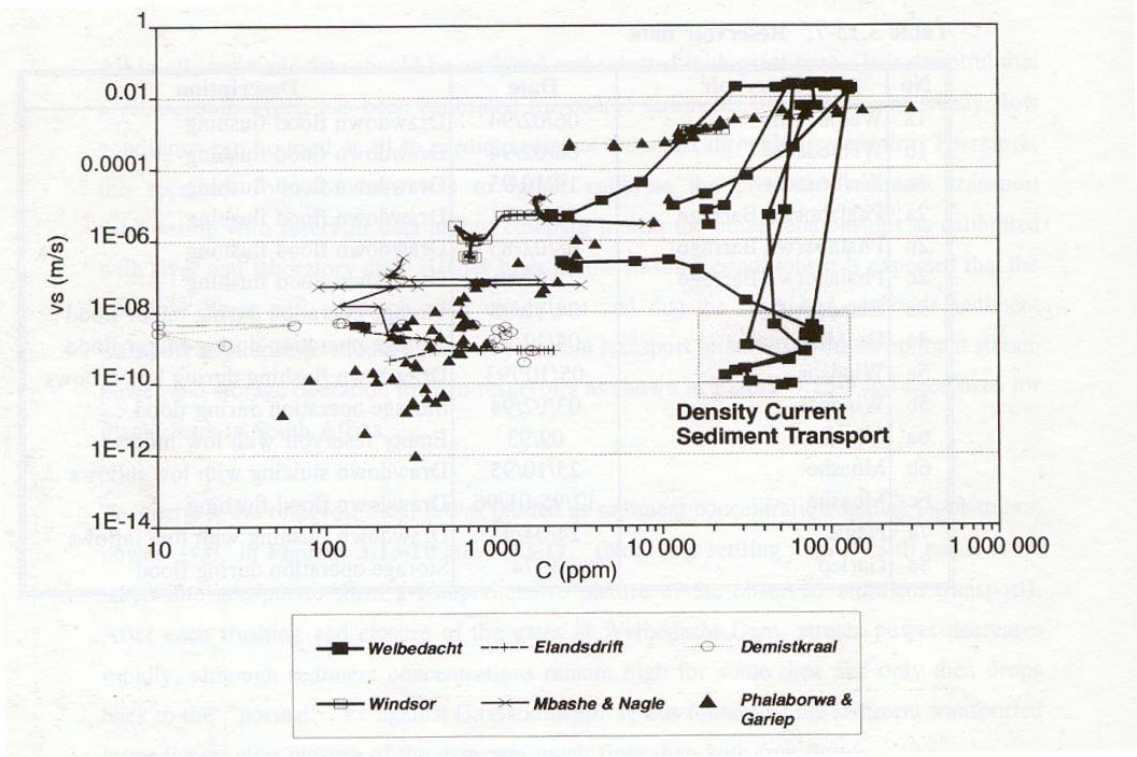

Figure 3.3 - 2 Input stream power versus observed suspended sediment concentration for South African reservoirs

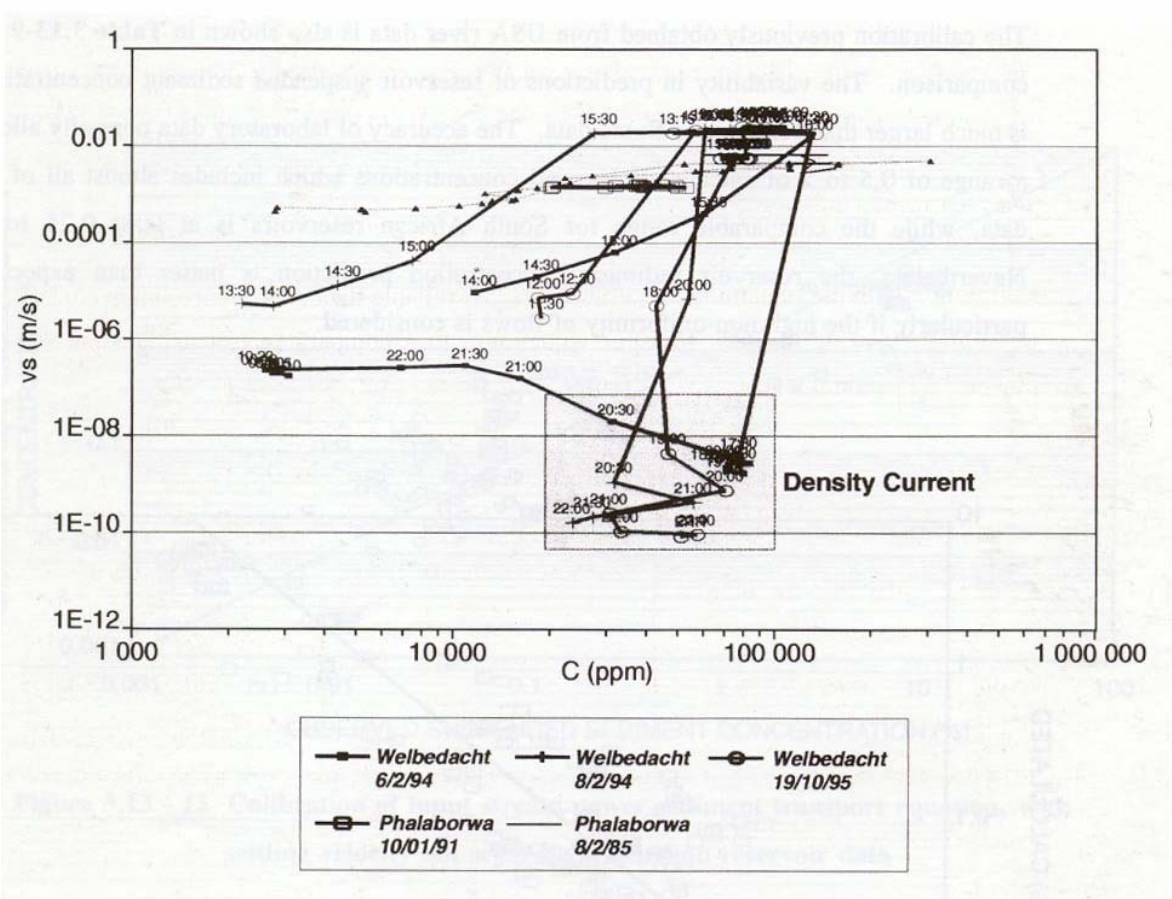

Figure 3.3 - 3 Density current data at Welbedacht Dam

Reservoir data have been obtained at a number of reservoirs under variable operational and flood conditions, as indicated in **Table 3.3-1**

A check whether plotting $\frac{vs}{w}$ versus C would not "correct" the relationship as indicated by vs versus C for part of the data proved to be unsuccessful, and everything pointed to the fact that density currents and not turbulent sediment transport had been present. This data set was therefore removed from the data used for calibration of the new transport equation and is discussed and analysed further in **Chapter 4**.

Table 3.3-1: Reservoir data

No	Reservoir	Date	Description
1a	Welbedacht	06/02/94	Drawdown flood flushing
1b	Welbedacht	08/02/94	Drawdown flood flushing
1c	Welbedacht	19/10/95	Drawdown flood flushing
2a	Phalaborwa Barrage	10/01/91	Drawdown flood flushing
2b	Phalaborwa Barrage	08/02/85	Drawdown flood flushing
2c	Phalaborwa Barrage	21/02/96	Drawdown flood flushing
3a	Elandsdrift	04/12/93	Storage operation during minor flood
4a	De Mistkraal	04/12/93	Storage operation during minor flood
5a	Windsor	05/10//93	Drawdown flushing during low inflows
5b	Windsor	03/02/94	Storage operation during flood
6a	Mbashe	09/93	Empty reservoir with low inflows
6b	Mbashe	25/10/95	Drawdown sluicing with low inflows
6c	Mbashe	12/95-01/96	Drawdown flood flushing
7a	Nagle	24/04/93	Drawdown flushing with low inflows
8a	Gariep	1974	Storage operation during flood

Calibration with the remaining "accurate" selected reliable data gave a correlation coefficient (r^2) of 0,80 using the new transport equation. In a comparable test using input stream power $\left(\frac{vs}{w}\right)$, similar correlation results were found, as indicated in **Table 3.3-2**. This latter equation as calibrated on reservoir data is given as equation 5.3-1 in Chapter 5, where it is used in mathematical modelling.

Table 3.3-2: Calibration of stream power relationships

Sediment transport equation	No of data	Correlation coefficient r^2
Applied stream power (new transport equation)	180	0,80 **(Figure 3.3-4)**
Input stream power (vs/w)	180	0,72 **(Figure 3.3-5)**
Input (vs;w)	180	0,78 **(Figure 3.3-6)**

The best correlation is obtained with the new applied stream power relationship (eg. 3.2-43, but with different coefficients). A relationship for input stream power as a function, with the settling velocity separated, was also used, since it was found in this research and by *Yang (1973)* that w is a dominant variable. Testing of accuracy ranges is indicated in **Table 3.3-3** (using the same data used for calibration).

Table 3.3-3: Accuracy ranges of calibrated new sediment transport equation for reservoir data

Description	$0{,}67 < \frac{Ccalc}{Cobs} < 1{,}5$	$0{,}5 < \frac{Ccalc}{Cobs} < 2$	$0{,}33 < \frac{Ccalc}{Cobs} < 3$	$0{,}25 < \frac{Ccalc}{Cobs} < 4$
New equation	28%	46%	78%	91%
Input (vs/w)	27%	41%	66%	76%
Input = f (vs;w)	29%	49%	76%	86%
New equation calibrated with USA river data (Bagnold)	48%	68%	89%	-

The calibration previously obtained from USA river data is also shown in **Table 3.3-3** for comparison. The variability in predictions of reservoir suspended sediment concentrations is much larger than for river or flume data. The accuracy of laboratory data normally allows a range of 0,5 to 2 of calculated/observed concentrations which includes almost all of the data, while the comparable range for South African reservoirs is at least 0,25 to 4. Nevertheless, the reservoir sediment concentration prediction is better than expected, particularly if the high non-uniformity of flows is considered. (As sediments are trapped where velocities are low, sediment concentrations in reservoirs have to be correlated with minimum upstream vs values.)

In modelling, both a sensitivity analysis and reservoir-specific data should be used as far as possible for the calibration of the sediment transport relationship. It is recommended that the applied stream power relationship (new equation) be used in future modelling,

preferably re-calibrated with local data. This relationship as calibrated here provides a relatively good estimate over a wide range of sediment concentrations and hydraulic conditions for South African reservoir data.

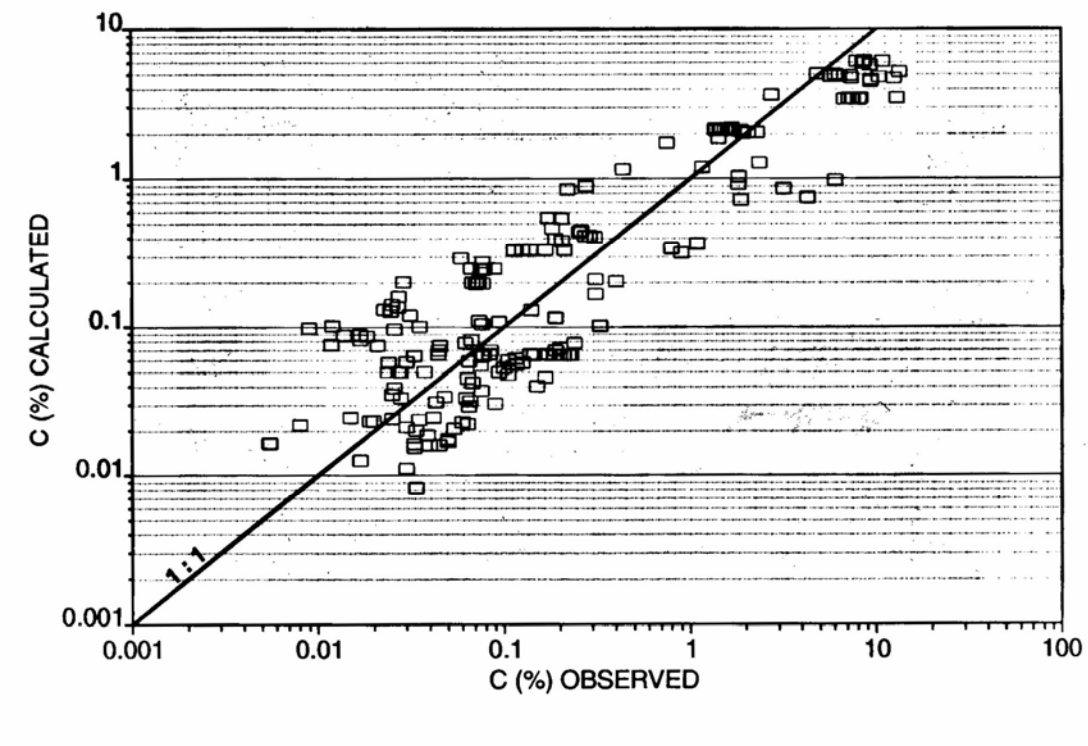

Figure 3.3 - 4 Calibration of new sediment transport equation based on reservoir data

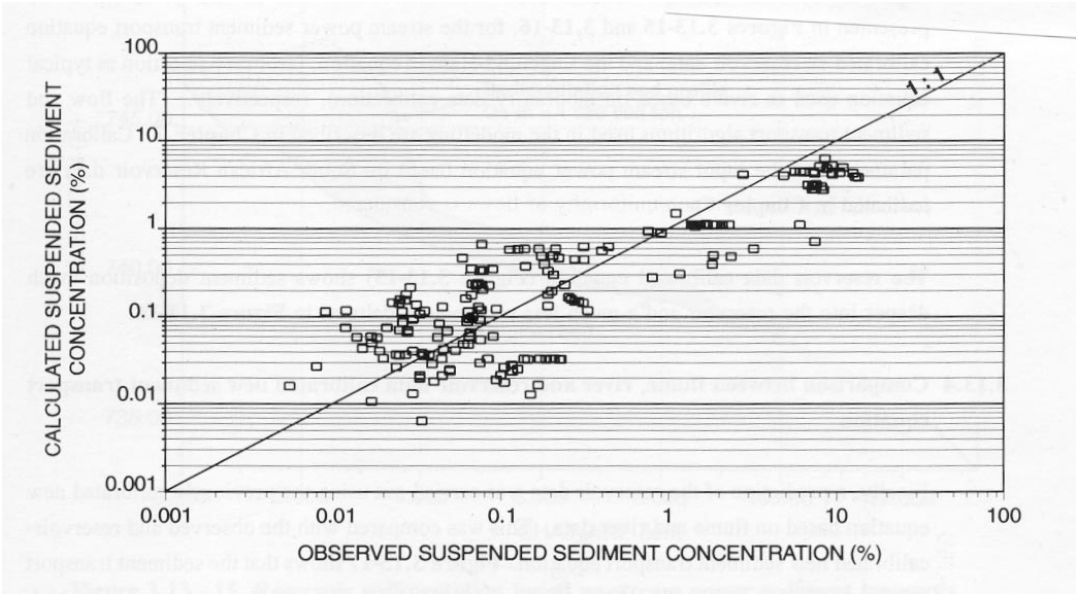

Figure 3.3 - 5 Calibration of input stream power sediment transport equation using reservoir data and not allowing for differences in settling velocity.

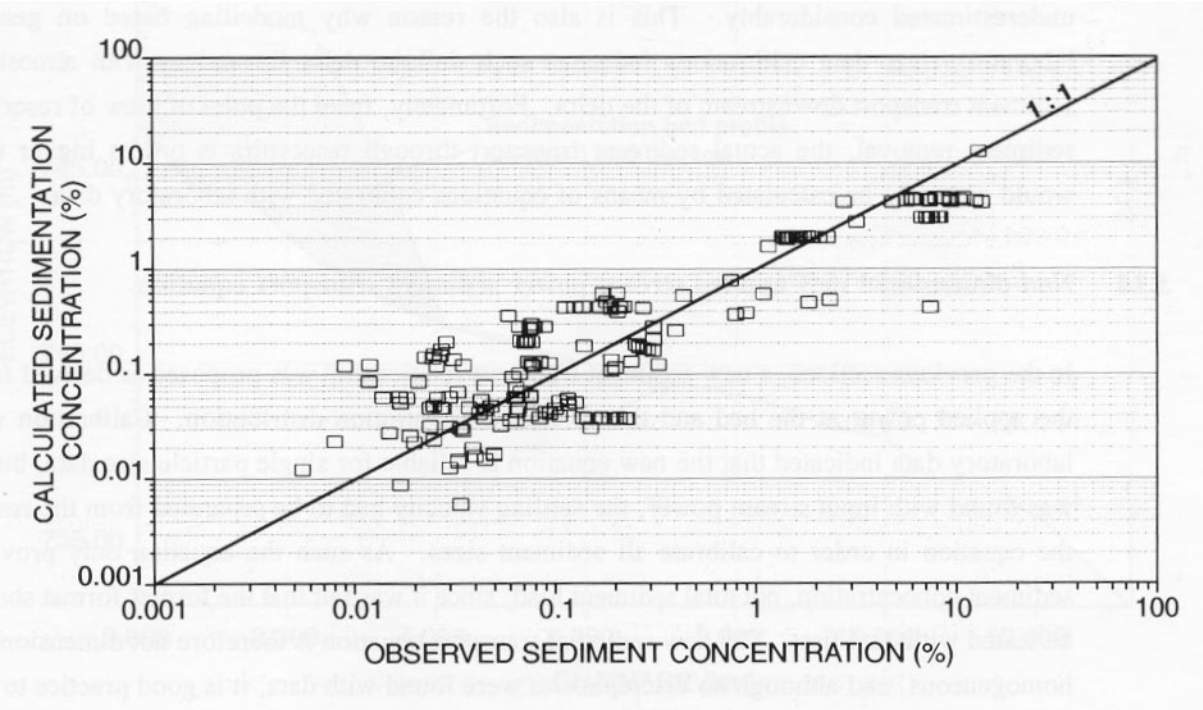

Figure 3.3 - 6 Calibration of input stream power sediment transport equation using reservoir data and allowing for differences in settling velocity.

Mathematical modelling results of reservoir sedimentation (deposition) for the same hypothetical boundary conditions, but with two different sediment transport equations are presented in **Figures 3.3-7** and **3.3-8**, for the stream power sediment transport equation calibrated on reservoir data, and the Engelund-Hansen equation, (arbitrary selection as a typical equation used in rivers based on laboratory data calibration), respectively. (The flow and sediment transport algorithms used in the modelling are described in **Chapter 5**. Calibration parameters of the input stream power equation based on South African Reservoir data are indicated in **Chapter 5**).

The reservoir data calibrated equation (**Figure 3.3-7**) shows sediment deposition much deeper into the reservoir and a much less pronounced delta as in **Figure 3.3-8**.

Finally, a prediction of the reservoir data was carried out using the previously calibrated new equation based on flume and river data. This was compared with the observed and reservoir-calibrated new sediment transport equation. **Figure 3.3-9** shows that sediment transport can be accurately predicted with formulae calibrated on river or flume data only at high concentrations (C> 3 %) and flow conditions approaching those of a river.

At lower flow velocities and sediment concentrations (storage operation), sediment transport can be underestimated considerably. This is also the reason why modelling based on general laboratory/river data calibrations indicates such definite delta formations with almost no sediment transport downstream of the delta. From the point of view of reservoir sediment removal, the actual sediment transport through reservoirs is orders higher than would normally be calculated by means of equations calibrated with laboratory data.

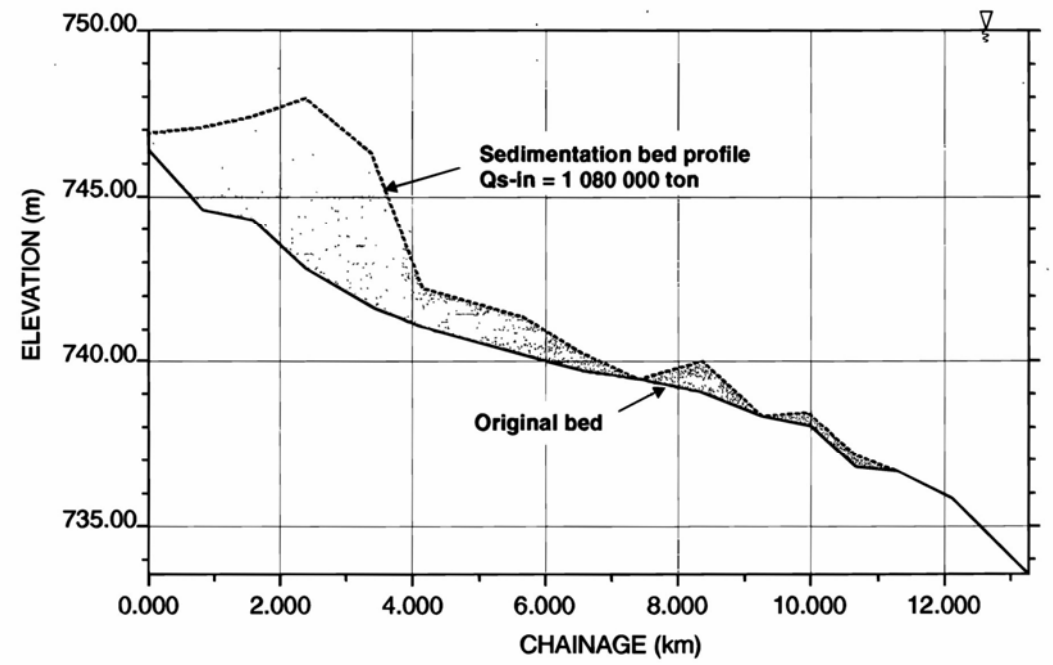

Figure 3.3 - 7 Reservoir sedimentation based on stream power sediment transport equation calibrated with reservoir data

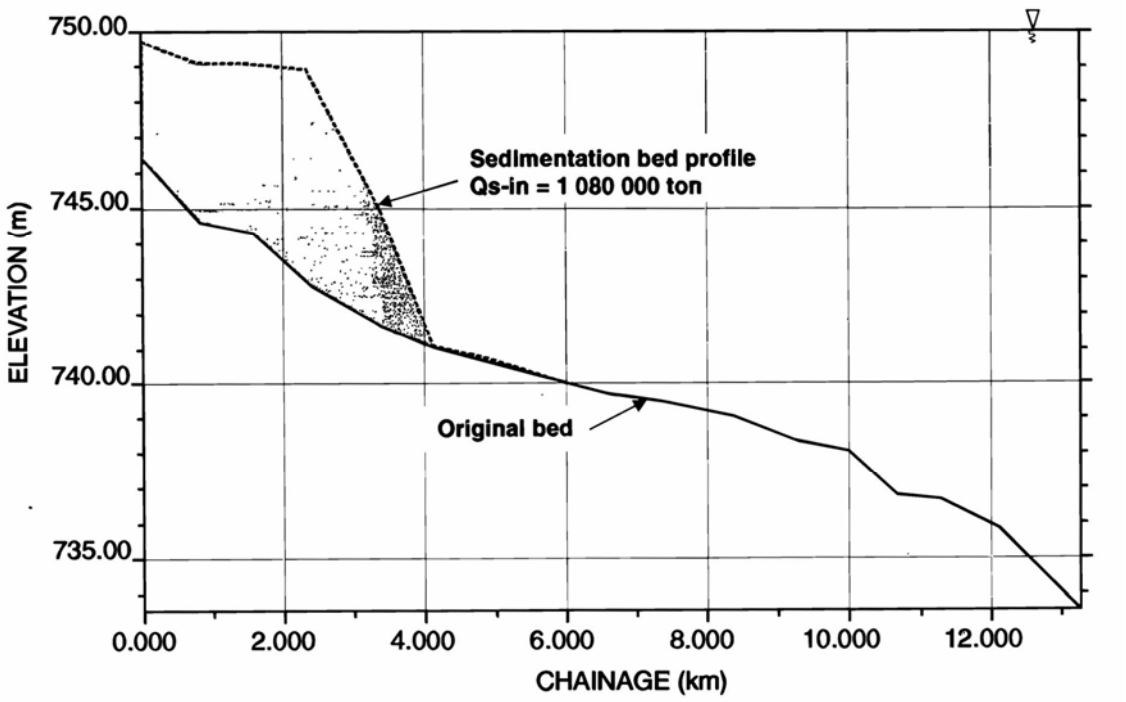

Figure 3.3 - 8 Reservoir sedimentation based on Engelund-Hansen sediment transport equation

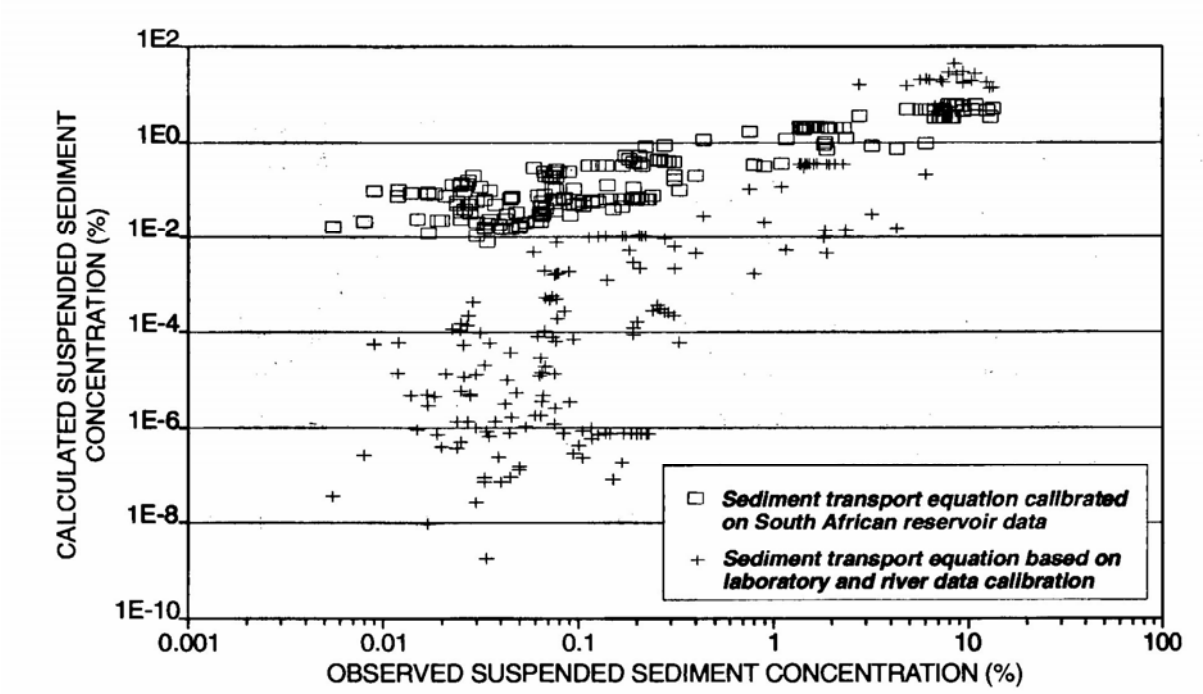

Figure 3.3 - 9 Verification of reservoir sediment transport with new sediment transport equation based on laboratory and river data calibration

The new sediment transport **equation 3.2-43** as calibrated with reservoir data can be used to predict non-uniform sediment transport, but only within the calibrated particle size ranges. Reservoir sedimentation simulation based on the stream power equation (calibrated with reservoir data), has been carried out with uniform and non-uniform sediment particle size distributions (with the same boundary conditions), and the results are shown in **Figures 3.3-10** and **3.3-11**. (Details of the mathematical model flow and sediment transport algorithms are described in **Chapter 5**). The differences in the sedimentation profiles as simulated in **Figures 3.3-10** and **3.3-11** emphasize the importance of accurately predicting the transport of non-uniform sediments. Accurate determination of sediment sizes is also important when considering sediment density, consolidation, critical conditions for mass erosion of non-cohesive or cohesive sediments, etc.

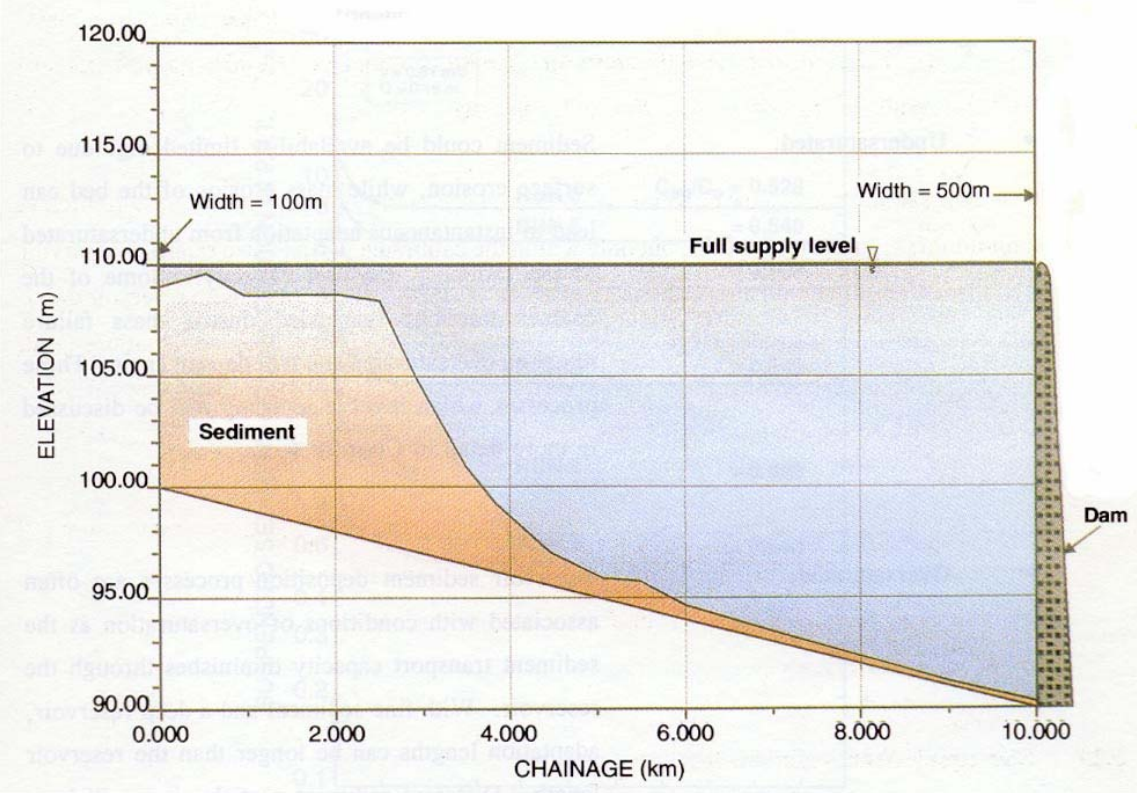

Figure 3.3-10 Reservoir sedimentation profile with uniform sediment size

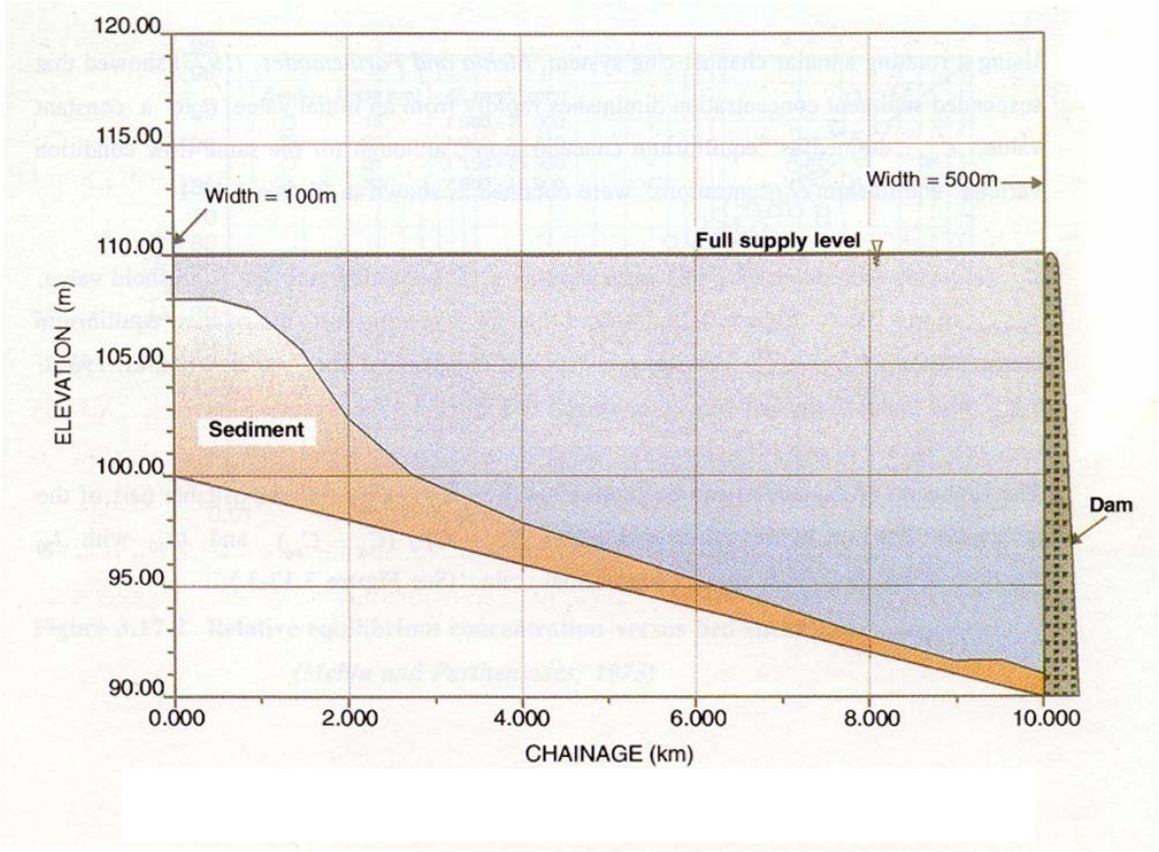

Figure 3.3-11 Reservoir sedimentation profile with non-uniform sediment size

3.4 Non-equilibrium sediment transport

3.4.1 Introduction

Most mathematical models are based on the assumption that the difference in the sediment loads between successive cross-sections is deposited (or eroded) within each reach. A state of sediment equilibrium is therefore reached within each time step of the calculation. Equilibrium in this case refers to the actual sediment transport being equal to the transport capacity at a section.

Instantaneous adjustment of the bed profile is a realistic assumption only when coarse sediments are being transported and without any constraints on sediment availability. With fine sediments, however, adjustment according to the saturated sediment transport capacity is not instantaneous and time and distance lags are found with changes in sediment transport, until equilibrium is reached. This lag, often called "adaptation

length", is due to the low settling velocities of the fine sediments. In this adjustment process the bed roughness, the energy dissipation rate (κ) and the sediment transport capacity change until equilibrium is reached, with minimized stream power.

Two modes of non-equilibrium sediment transport can be identified:

- Undersaturated: Sediment discharge could be availability limited e.g. due to limited surface erosion, while mass erosion of the bed can lead to rapid transition from the under saturated load condition to the full sediment transporting capacity. Some of the coarser fractions suspended during mass failure might be oversaturated and will deposit again. Processes which involve scour are discussed in more detail in Basson and Rooseboom (1997).

- Oversaturated: Reservoir sediment deposition processes are often associated with conditions of over saturation as the sediment transporting capacity diminishes through the reservoir. With fine sediments and a deep reservoir, adaptation lengths can be longer than the reservoir length. Different sediment particle sizes will have different adaptation characteristics.

Using a rotating annular channel-ring system, *Mehta and Partheniades, (1973)* showed that suspended sediment concentration diminishes rapidly from an initial value, C_o to a constant value, C_{eq} defined as the "equilibrium concentration", although for the same flow condition various "equilibrium concentrations" were obtained as T_s shown in **Figure 3.4-1**.

C_{eq} decreases with decreasing bed shear stress, becoming zero for a threshold value, $\tau_{b\min}$, of the latter. **Figure 34-1** shows that for a specific test, the relative equilibrium concentration, $C^*_{eq} = \frac{C_{eq}}{C_o}$, remains constant and independent of C_o *(Partheniades, 1986).* C^*_{eq} was found to depend on τ_b as T_s shown in **Figure 3.4-2**.

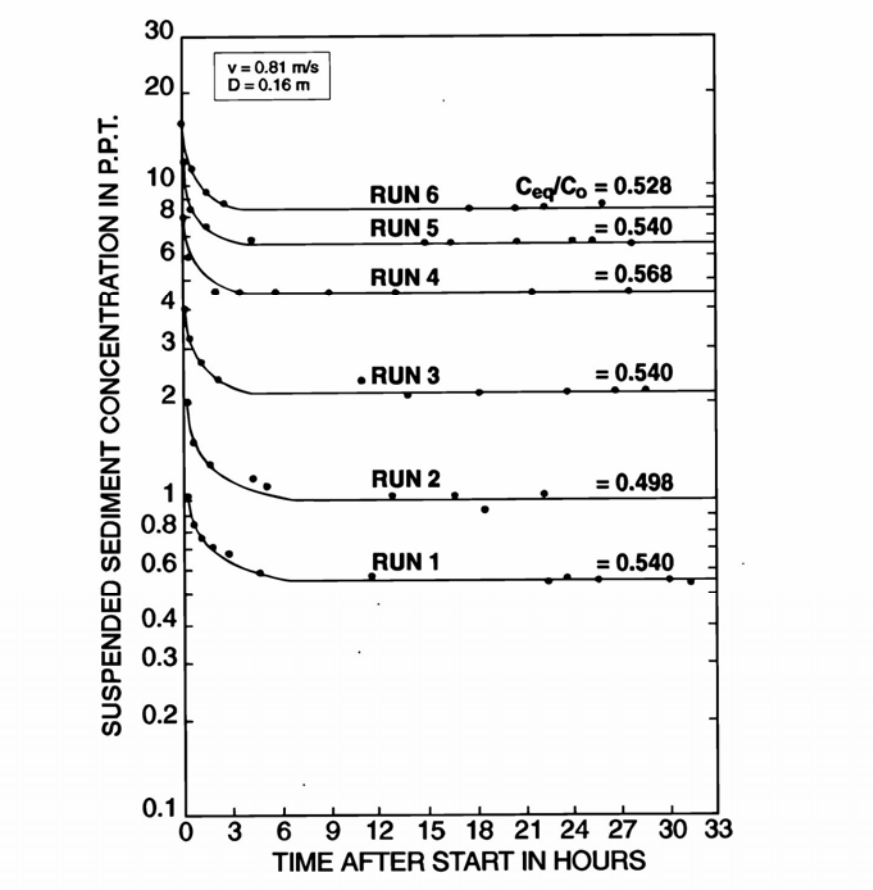

Figure 3.4-1 Variation of suspended sediment concentration with time

(Partheniades, 1986)

The time rate of deposition can be represented by $C_o - C_{eq}$ the depositable part of the sediment load. The best fit was found with $C^* = (C_o - C)/(C_o - C_{eq})$ and t/t_{50} with t_{50} the time at which $C^* = 0.50$ on a log-normal scale. (See **Figure 3.4-3**.)

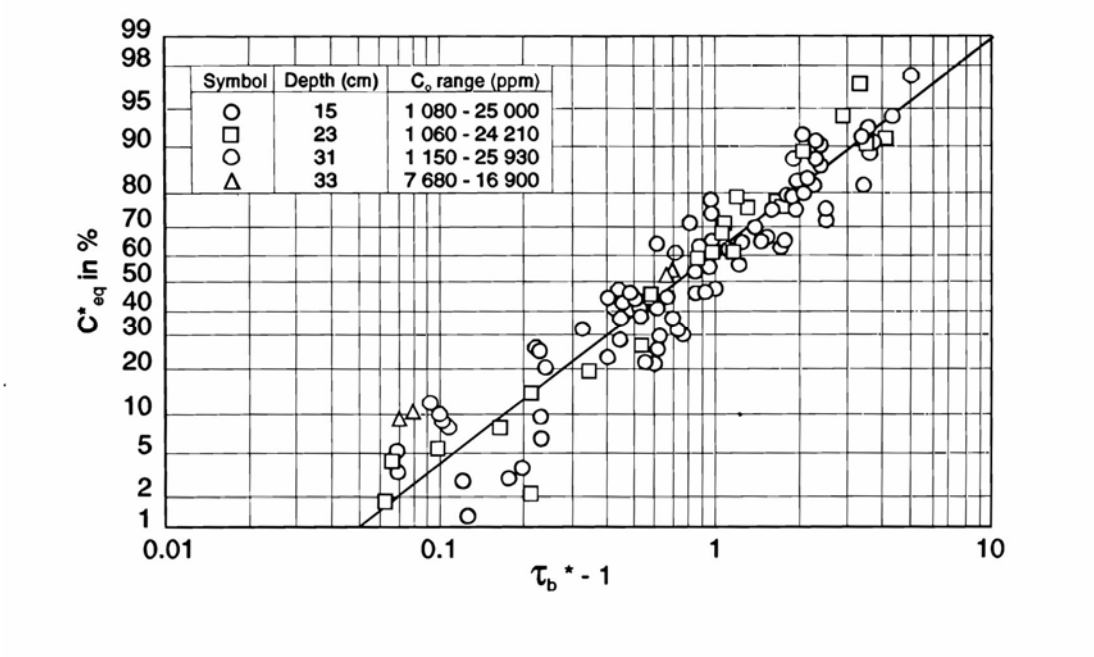

Figure 3.4-2 Relative equilibrium concentration versus bed shear stress parameter

(Mehta and Partheniades, 1973)

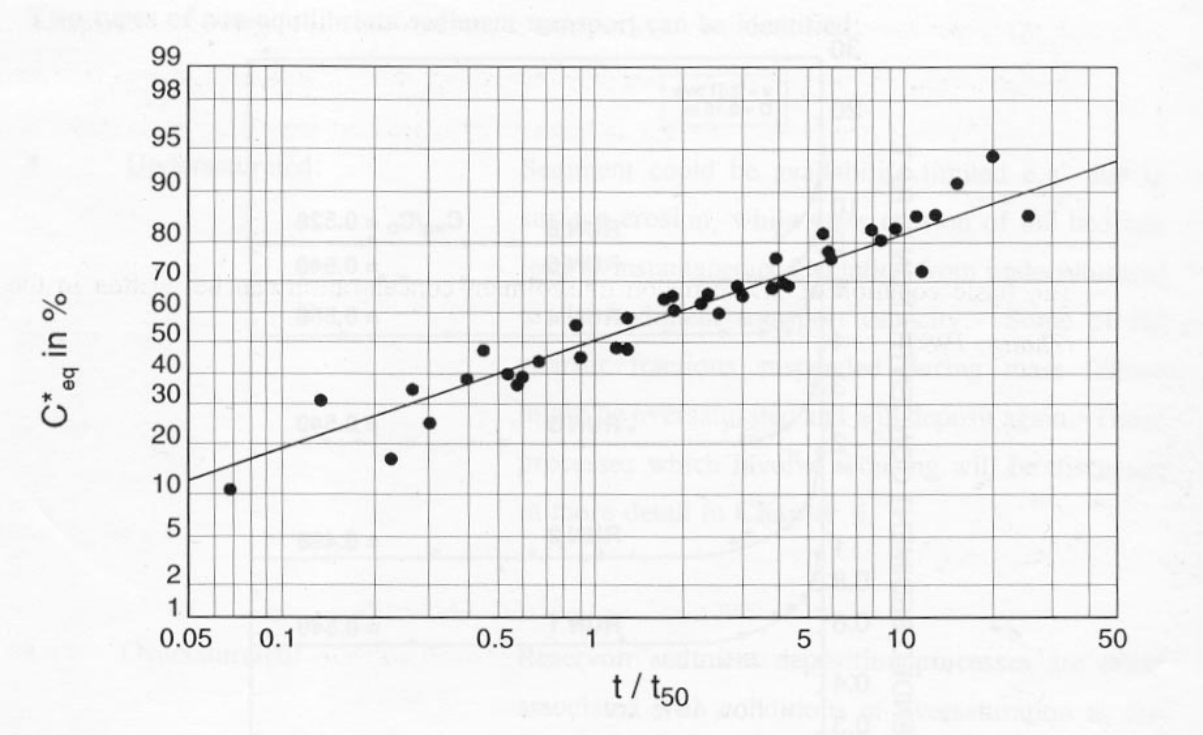

Figure 3.4-3 Deposition rates (*Mehta and Partheniades 1973*)

In terms of sediment transport theory, the adjustment to "equilibrium" sediment transport under the same flow conditions, thereby reducing the suspended sediment load as shown in **Figure 3.4-1**, can be attributed to adjustment of the stream power to minimize energy dissipation. The adjustment is not immediate, due to the relatively low settling velocities of the cohesive sediments. The "equilibrium" condition that is reached does not represent equilibrium sediment transport (or maximum transport), but rather an equilibrium state under conditions of limited sediment availability.

Mathematical descriptions of the non-equilibrium transport process have been given by *Galapatti and Vreugdenhill (1985)* and *Di Silvio (1995)*, but the key variables involved in minimization of stream power were not included. Chinese researchers *(Han and He, 1990)*, have calibrated non-equilibrium equations with field data and have established criteria for non-equilibrium sediment transport calibration coefficients for rivers and reservoirs. Most of these equations are of the same format as the steady advection-dispersion equation.

3.4.2 Review of existing theory

Until recently the "best" equilibrium transport formula was selected among dozens of such equations in the literature. Sediment transport in real life, especially in reservoir storage operation, is often not in equilibrium.

Equilibrium formulae based on uniform flow experiments in hydraulic laboratories are no longer considered as satisfactory components in mobile-bed modelling systems. Time and space lags between actual and equilibrium transported sediment loads should therefore be considered *(Cunge, 1989)*.

The basic equation of 2D diffusion of sediment concentration can be written in the form *(Zhang, 1980)*:

$$v\frac{\delta C}{\delta x} = \varepsilon\frac{\delta^2 C}{\delta z^2} + w\frac{\delta C}{\delta z} \qquad (3.4\text{-}1)$$

with $C(x,t)$ = sediment concentration

$\in$ = coefficient of turbulent exchange

w = settling velocity of sediment particles

v = flow velocity

An analytical solution of **Equation 3.4-1** is possible with the following boundary conditions for the case of deposition:

at the water surface : $z = D,\ \varepsilon \frac{\delta C}{\delta z} + wC = 0$

on the reservoir bed : $z = 0,\ \frac{\delta C}{\delta z} = -\frac{w}{\varepsilon} C_{\kappa,0} = \text{constant}$

at entrance : $x = o,\ C = C_o\, f(z)$

Zhang (1980) derived the analytical solution :

$$C_{cp}(x) = C_{Kp} + (C_o - C_{kpo}) \sum_{n=1}^{\infty} \frac{2 \propto_n^2}{(\propto_n^2 / K_1 + K_1^2/4)(\propto_n^2 + K_1^2/4 + K)} \tag{3.4-2}$$

which, after differentiation and simplification, reads:

$$\frac{dC_{cp}(x)}{dx} = \propto w[C_{Kp} - C_{Cp}(x)]/q \tag{3.4-3}$$

By substituting initial conditions $x = 0,\ C_{cp}(x) = C_0$, the final expression of the rate of change in sediment concentration along the reservoir is:

$$q_s = q_{st} + e^{(-\alpha w x / q)}(q_{so} - q_{st}) \tag{3.4-4}$$

with q_s = sediment discharge per unit width at the exit

q_{st} = sediment-carrying capacity

q_{so} = sediment inflow per unit width at the entrance

If $\zeta = e^{(-\alpha wx/q)}$ denotes sediment transport under non-equilibrium conditions $(0 < \zeta < 1)$, when $x = 0, \zeta = 1{,}0, q_{so} = q_{so}$ no net deposition or scouring occurs and the incoming sediment discharge equals the outflowing discharge. When $x = \infty, \zeta = 0, q = q_s$ it means that outflowing sediment discharge equals the sediment-carrying capacity after self-adjustment along the river course.

Computation of sediment transport under equilibrium conditions is a special case of non-equilibrium conditions. Generally, the equilibrium can only be re-established over a long distance (for fine sediments) *(Zhang, 1980).*

In the case of scouring, similar equations can be derived *(Zhang, 1980)*

The boundary conditions are: $Z = 0, C_{ko} = Const.$

$$Z = D, \in \frac{\delta C}{\delta z} \pm wC = 0$$

$$x = o, C = Const.$$

and the final equation: $q_s = q_{st} - e^{(-\alpha wx/q)}(q_{so} - q_{st})$

In the case of deposition $\alpha_1 = 1 + K_{1/2} \approx 1$ (3.4-5)

and $\zeta_1 = e(-wx/q)$

while with scouring

$\alpha_2 = \pi^2 / K_1 + K_{1/4}$

$= \pi / K_1$

$= K \, v^* \pi^2 / 6 w$

$v^* = \sqrt{gDs}$

$= K^{0,5}\, g^{0,5}\, Q^{0,3}\, s^{0,5}$

Final expressions with the inclusion of empirical coefficients $(K_3, K_4 \text{ and } K_5)$ read:

Deposition: $\zeta_1 = \exp\left(K_3, C^{K4}(0{,}41) - 0{,}77 / gC\right) x / q$ (3.4-6)

Erosion: $\zeta_2 = \exp\left(- K_5 Q^{0,3} s^{0,5} x / q\right)$ (3.4-7)

Soares et al., (1982) derived equations for non-equilibrium suspended sediment transport, similar to those of *Zhang (1980)*.
The mass balance of sediment of a given size d_j is:

$$Q\left(\frac{\delta C^j}{\delta x}\right)\_x = (- q_d^j + q_e^j) T\_x \quad (3.4\text{-}8)$$

with q_d^j, q_e^j = fluxes of deposition and erosion of sediment

Q = flow rate

T = width

$\frac{\delta C}{\delta t}$ is neglected in this equation

Let CT^{*j} = average concentration according to sediment transporting capacity, then:

if $C_i^j > CT_{i+1}^{j*}$ (deposition):

Rate of deposition : $q_d^j = - w_j (C^j - CT^{j*})$ (3.4-9)

and **Equation 3.4-8** becomes = $\frac{\delta C^j}{\delta x} = - w_j (C^j - CT^{j*}) T/Q$ (3.4-10)

Integrating **Equation 3.4-10** between two sections:

$C_{i+1}^j = (C_i^j - CT_{i+1}^*) \exp(- w_j \Delta x T/Q)$ (3.4-11)

if $C_i^j \le CT_{i+l}^{j*}$ (erosion will occur depending on the availability of sediment of the given size class at d_j on the stream bed)

Rate of erosion: $q_e^j = \lambda\left(C_b^j - C^j\right)$ (3.4-12)

The erosion rate is a function of the difference between the availability on the bed and the concentration carried by the flow. Although erosion is dominant, deposition will still occur at a rate $w_j C^j$ and **Equation 3.4-8** becomes:

$$\frac{\delta C^j}{\delta x} = -\left(C^j - \frac{\lambda_j}{\lambda_j + w_j} C_b^j\right)\frac{T}{Q}\left(\lambda_j + w_j\right) \quad (3.4\text{-}13)$$

Integration of **Equation 3.4-13** between sections i and $i+1$ yields:

$$C_{i+1}^j = \left(C_i^j - \frac{\lambda_j}{\lambda_j + w_j} C_b^j\right)\exp\left[-\left(\lambda_j + w_j\right)\frac{T\Delta x}{Q}\right] + \frac{\lambda_j}{\lambda_j + w_j} C_b^j \quad (3.4\text{-}14)$$

When Δx is large, discharge in section $i+1$ will approach the transport capacity

Therefore $CT_{i+1}^{j*} = \frac{\lambda_j}{\lambda_j + w_j} C_b^j$

and the final equation: $C_{i+1}^j = CT_{i+1}^{j*} + \left(C_i^j - CT_{i+1}^{j*}\right)\exp\left[-\frac{T\Delta x}{Q}\left(\lambda_j + w_j\right)\right]$ (3.4-15)

Equation 3.4-16 is similar to the equation presented by *Karanshev (1963)*:

$$C_{i+1}^j = CT_{i+1}^{j*} + \left(C_i^j - CT_{i+1}^{j*}\right)\exp\left[-\frac{T\Delta x}{Q}(1 + K_j)w_j\right] \quad (3.4\text{-}16)$$

and also similar to that of *Zhang (1980)*:

$$q_s = q_{st} - \left(q_{so} - q_{st}\right).\exp\left(-\propto wx/q\right) \quad (3.4\text{-}17)$$

Sundborg (1964) developed another non-equilibrium equation which does not allow for erosion:

$$C_{i+1}^{j} = C_i^{j} \exp\left[-(T\Delta x/Q)\, w\phi(w)\right] \qquad (3.4\text{-}18)$$

Equation 3.4-18 was used by *Hurst and Chao (1975)* in a model for Tarbela Reservoir. The equation implies that if in section i the concentration of sediment of size d_j is zero, the same will be true for all downstream sections, which is clearly an error.

While the transport of coarse sediment depends exclusively on local hydrodynamic conditions, the transport of fine particles also depends on the conditions upstream. *Di Silvio (1995)* proposes the use of the following non-equilibrium transport equation:

$$\frac{\delta C_i}{\delta x} = \frac{1}{L_i^*}\left(\beta_i C_{ci}^* - C_i\right) \qquad (3.4\text{-}19)$$

with C_i = the actual sediment transport per fraction

β_i = the % of i-th fraction in the bed composition

L_i^* = the adaption length for each fraction

C_{ci}^* = the transport capacity of the i-th class

The adaptation length L_i^* can be obtained either experimentally or by an asymptotic solution of the 2D suspended transport equations (*Di Silvio and Armanini, 1981; Galapatti and Vreugdenhil, 1985.*) An evaluation of L_i^* is given by the following approximate formula:

$$\frac{L_i^* w_i}{vD} = \frac{k_s}{D} + \left(1 - \frac{k_s}{D}\right) \exp\left(-1{,}5\left(\frac{k_s}{D}\right)^{-1/6} \cdot \frac{w}{v_*}\right) \qquad (3.4\text{-}20)$$

For fine particles, L_i^* particle falling distance $= \frac{vD}{w_i}$, which means that the adaptation lengths for silt and clay may be even larger than the reservoir length.

For coarse sediment, $L_i^* \to 0$, and C_i *to* $\beta_i\ C_{ci}^*$ and the erosion rate becomes $\frac{\delta \beta_i C_{ci}}{\delta x}$ as with equilibrium transport and instantaneous adaptation.

All the above non-equilibrium sediment transport equations have the same format and were derived for steady flow conditions.

3.4.3 Modelling of non-equilibrium sediment transport processes : Welbedacht Reservoir (Caledon River, South Africa)

In reservoirs, inflows, water levels and inflow sediment concentrations are highly variable and unsteady, and non-uniform flow conditions prevail especially during floods when high sediment loads are being transported into a reservoir. Testing of the proposed non-equilibrium sediment transport approach has been carried out for Welbedacht Reservoir for the period 1973 to 1976. The simulation runs started in August 1973 when the first fill of the reservoir commenced. Observed instantaneous inflows and sediment concentrations, and water levels at the dam have been used as boundary conditions. The simulations continued to October 1976 when the first basin survey was carried out. During this three-year period major floods occurred in the Orange River system and 36 million m^3 of storage capacity was lost in Welbedacht Reservoir due to sedimentation.

Using a typical suspended sediment particle size distribution that has been observed at the upper end of the reservoir, one equilibrium and 2 non-equilibrium fractions have been modelled as indicated in **Table 3.4-1**.

The simulated sedimentation profiles for Welbedacht Reservoir are indicated in **Figure 3.4-4**.

Table 3.4-1: Suspended sediment size distribution of Welbedacht Reservoir inflow

Fraction no	Particle size range (mm)	Percentage in size range
3	0,106 - 0,25	5
2	0,05 - 0,106	19
1	< 0,05	76

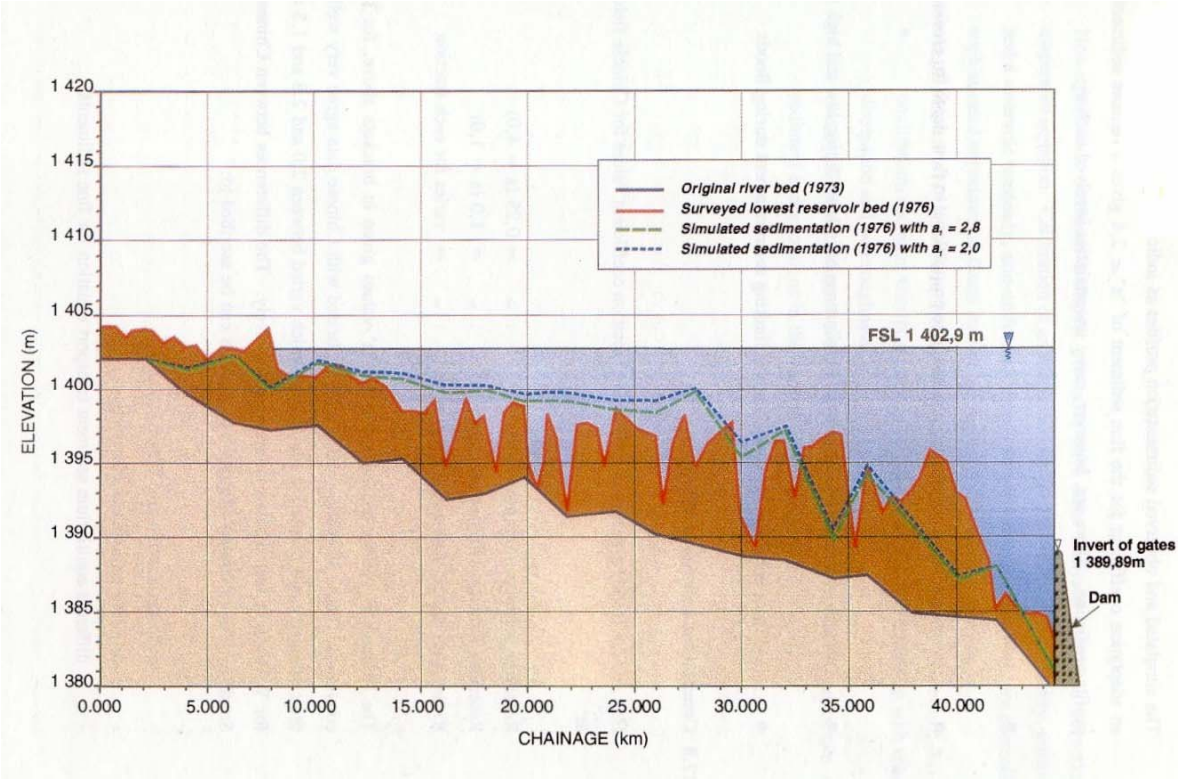

Figure 3.4-4 Non-equilibrium sediment transport calibration: Welbedacht Reservoir, 1973 to 1976

The simulated and observed sedimentation profiles as indicated in **Figure 3.4-4** show that an adaptation coefficient for the fine sediments of "a"≥ 2,8 (a = $\frac{1}{\alpha}$) gives a reliable sedimentation profile prediction (Also refer to equation 5.3-3, Chapter 5). There are, however, many uncertainties involved such as:

- unknown sediment density

- cross-sectional deformation, assumed here proportional to flow depth for erosion and deposition

- changing suspended sediment size distributions of inflows during low and high flows

- sediment cohesion and consolidation, limiting re-entrainment during floods.

3.4.4 Comparison between calibrations

Han and He (1990) give typical calibrated adaptation coefficient values for Chinese field data as:

Reservoir sedimentation (deposition)	:	α	= 0,25
Reservoir flushing with fine sediments	:	α	= 1,0
Rivers with coarse, non-uniform sediments	:	α	= varies for each fraction

These adaptation coefficients calibrated with Chinese reservoir data agree very well with the calibrated flume adaptation coefficients which varied between a = 2,0 and 2,8. The differences between Chinese and South African calibrated adaptation parameters can be ascribed to:

- different fraction size ranges
- different sediment characteristics
- different equilibrium sediment transport equations for fine sediments.

4. DENSITY CURRENTS

4.1 Introduction

Apart from turbulent suspended sediment transport, which is the dominant mechanism by which sediment is transported through most reservoirs, density currents in certain reservoirs provide an additional mechanism for transporting sediments. Density (gravity) currents are flows driven primarily by a difference in density between the current itself and its surroundings. The difference in density can be caused by temperature, chemical species (pollutants) or material phases (sediments).

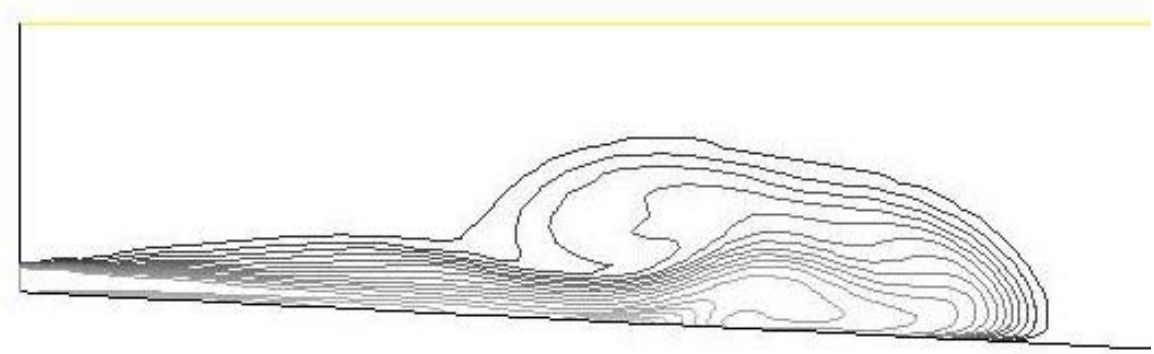

Figure 4.1-1: Density contours of the head of a gravity current entering a reservoir.

Figure 4.1-2: Density contours of the body and head of a gravity current moving

The monograph of Simpson (1997) provides many examples of natural and man-made gravity currents. A river entering a reservoir can often form a density current. The density difference can be created by transporting water that is warmer or cooler, more saline or less saline, more turbid or less turbid than that of the reservoir. A density current is not that different from normal open-channel flow: in the latter case air replaces the overlaying fluid body and the stream can therefore also be seen as a "density current"; only in the case of air above a water stream, the density difference is so large that the inertial effects of the air compared with those of water may be neglected.

Density currents are not only found when liquids of different densities move relative to each other. The movement of moist air in the form of clouds spilling down a mountain valley or dust rolling down a slope are common examples of density currents. When one analysis the behaviour of density currents related to sediment transport through reservoirs (also known as turbidity currents), a number of questions come to mind:

- Why do density currents occur?
- Under what conditions will density currents form?
- How can the density current movement be described mathematically?
- What is the relationship between sediment transport and the hydraulics of a density current?
- Can density currents be utilized effectively as a means of passing sediment through a reservoir without deposition?

4.2 Occurrence of density currents in reservoirs

The formation of density currents was first observed at the beginning of the 20th century in some of the world's large reservoirs. Along the upper reaches of a reservoir, stable, floating debris is observed, indicating the so-called "plunge point" where the inflowing river stream changes into a density current **(Figure 4.2-1)**. The stationary nature of the debris is caused by the slow upstream movement (or near zero velocity) of the overlying water mass, just downstream of the point where the sediment-laden inflow dives below the stored water mass. Apart from the evidence at the plunge point, nothing can be seen of the density current, except when it exits the reservoir through suitable low-level outlets provided that the density current reaches the dam. Under unfavourable boundary conditions, the density current could either be broken up through turbulent mixing in certain parts of the reservoir or through deposition of sediment, whereby the density difference which drives the density current, decreases.

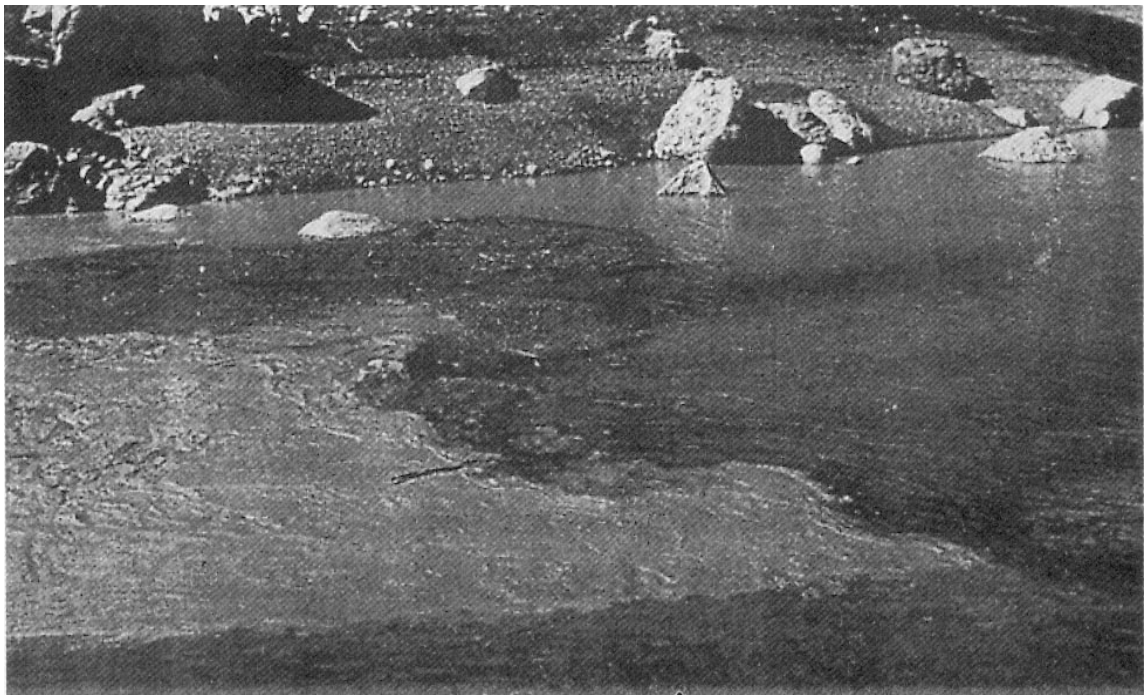

Figure 4.2 - 1 Plunge point at Eril Emda Reservoir

Density currents do not only occur in reservoirs on heavily silt-laden rivers such as the Eril Emda Reservoir in Algeria, Lake Mead in the USA or Sanmenxia Reservoir in China, but also in reservoirs with flows containing low sediment concentrations such as the Sautet Reservoir in France.

Density currents may travel long distances through reservoirs, for example over 100 km in Lake Mead and 80 km (1961) in the Sanmenxia Reservoir.

Typical density current velocity and suspended sediment profiles are shown in **Figure 4.2-2** as observed in Gaunting Reservoir, China and in **Figure 4.2-3** as observed in Sanmenxia Reservoir, China *(Fan, 1986).*

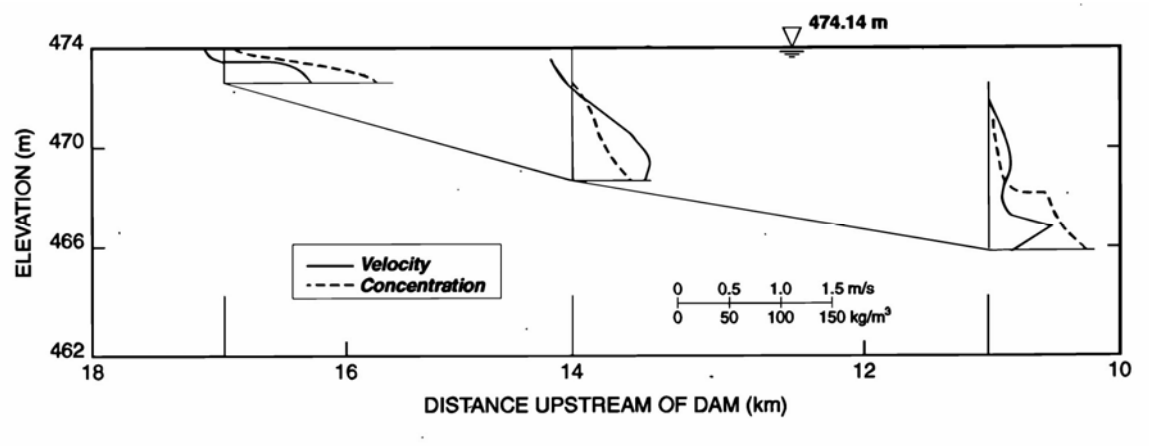

Figure 4.2 - 2 Density current in Guanting Reservoir (*Fan, 1986*)

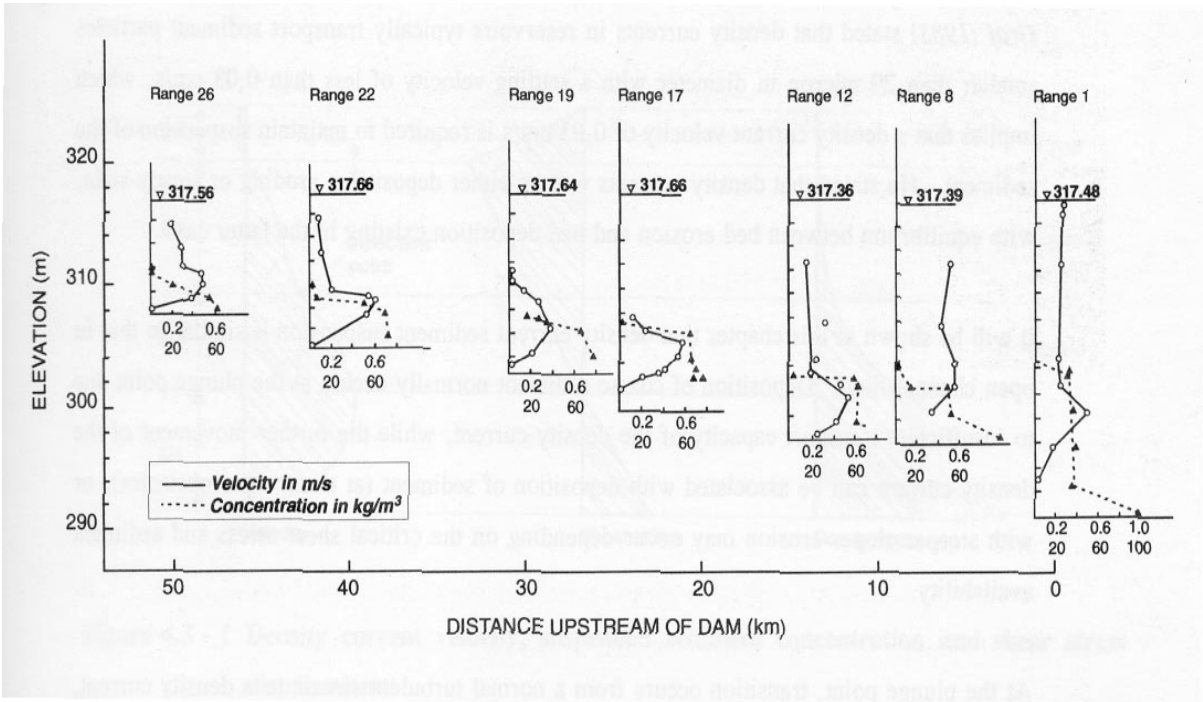

Figure 4.2 - 3 Density current in Sanmenxia Reservoir (*Fan, 1986*)

It was found in practice that a density current moves at a slow speed, typically of the order of 0,1 to 0,3 m/s (higher in some cases), and yet is able to transport high sediment loads for distances of over 100 km through a reservoir. As will be shown later, these low velocities are related to the density difference between the lower denser fluid and the upper "clear" water, which effectively reduces the effective gravitational acceleration by 100 to 1 000 times. The effect of this is that the flow of the density current can be described as if in "slow motion". In flume experiments it was noticed

that a density current can "jump" over obstacles in its path, due to the low relative "gravity" (g). Around bends the surface level increase is often so much that fluid spills out of the main channel and at the downstream outlet the density current can flow vertically upwards provided that the outlet is correctly sized and is at a certain height.

Density currents have often been associated with delta formation in reservoirs. It was and is still believed that a delta provides the ideal boundary conditions for a density current to form. The authors, however, believe that in fact a density current can lead to the formation of a delta. As will be shown later, more favourable conditions for the formation of a density current exist without a delta.

Graf (1983) stated that density currents in reservoirs typically transport sediment particles smaller than 20 micron in diameter with settling velocities of less than 0,03 cm/s, which implies that a density current velocity of 0,03 cm/s is required to maintain suspension of the sediments. He stated that density currents will be either depositing, eroding or steady-state, with equilibrium between rates of bed erosion and bed deposition existing in the latter case.

It will be shown in this chapter that density current sediment suspension is similar to that in open channel flow. Deposition of coarse sediments normally occurs at the plunge point due to insufficient transport capacity of the density current, while the further movement of the density current can be associated with deposition of sediment (at underwater obstacles), or with steeper slopes erosion may occur depending on the critical shear stress and sediment availability.

At the plunge point, transition occurs from a normal turbulent stream to a density current, with continuity in discharge being maintained. Not all incoming sediment is however removed by the density current, as the larger particle sizes are immediately deposited, and invariably in reservoirs all over the world it has been found that only the finest sediment fractions of silt and clay are transported by density currents through the reservoirs. This means that although the settling velocities of the particles are much reduced through the reduction in effective gravity, the transport capacity of a density current is still not sufficient for the transport of all incoming sediments.

Past experimental work on turbidity currents include:

Parker et al. (1987) investigated steady, supercritical turbidity current flow over an erodible bed. One of objectives of the experiments was to create a self-accelerating turbidity current. The flume used was 0.7 m wide, 1.7 m deep, 20 m long having slopes of 0.05 and 0.08. Measurements were made using micro propellers and siphons. Their results include self-similar profiles of mean velocity and concentration, as well as relations for water entrainment, sediment entrainment and bed resistance. These relations are typically required for closing depth-averaged numerical models. They concluded that self-acceleration is possible, even though they were not able to produce such a flow.

Garcia and Parker (1993) also investigated sediment entrainment by a steady supercritical saline underflow. The flume used was 0.3 m wide, 0.78 m deep, 12.8 m long having a slope of 0.08 for the first 5 m. Their results include profiles of mean velocity and concentration, as well as relations for sediment entrainment and boundary shear stress. They concluded that in addition to purely sand-driven currents, currents of silty mud could also entrain substantial amounts of sand and carry it to deep waters.

Garcia (1993) also investigated hydraulic jumps of steady supercritical turbidity and saline currents. The flume used was 0.3 m wide, 0.78 m deep, 12 m long having a slope of 0.08 for the first 5m. Measurements were made using micro propellers and an optical probe for concentration. Results include self-similar profiles of mean velocity and concentration, as well as sediment deposition profiles. The results showed that the vertical structures of saline and fine-grained turbidity currents, having similar inlet conditions, are approximately the same before and after a hydraulic jump. It was also observed that the greatest amount of water entrainment occurred in the supercritical flow region.

Lee and Yu (1997) investigated steady turbidity and saline currents. The flume used was 0.2m wide, 0.6 m deep, 20 m long with a slope of 0.02. Measurements were made using a magnetic current meter and siphons. Their results include self-similar profiles of mean velocity and concentration, as well as criteria for stable plunge point prediction.

Choux (2005) investigated the spatial and temporal evolution of a quasi-steady turbidity current having an initial volumetric concentration of 14%. The density difference of the

turbidity current was 231kg/m^3. The flume used was 0.3 m wide, 0.3 m deep and 10 m long. Measurements were made using ultrasonic doppler velocity profilers and siphons. The current was quasi steady, because a fixed amount of mixture was allowed to drain from an overhead tank into the flume. The results include: the spatial evolution of the mean velocity profile within the head, body and tail; the spatial evolution of the rms velocity profile within the head, body and tail; the spatial evolution of the mean grains size profile within the head, body and tail; the spatial evolution of the mean concentration profile within the head, body and tail. The results suggest that self-similarity holds for turbidity currents having a mean concentration less than 7%. The rms velocity measurements show that the turbulence intensity is greatest within the head and at the base of the flow, while being the weakest at the velocity maximum and tail. It was also found that grain sizes are well mixed within the head, while normal grading occurs within the body and normal to inverse grading occurs within the tail.

4.3 Hydraulics of density currents

4.3.1 General

In the previous sections, density currents and possible reasons/explanations for some of the associated phenomena were given in general terms. It is necessary to obtain a proper mathematical understanding of the movement of a density current and also to review some of the theories proposed by other researchers in the past, as no generally accepted theory exists.

The vertical velocity, suspended sediment concentration and shear stress distribution in density current flow, as indicated in **Figure 4.3-1**, will form the basis of discussions in the following sections.

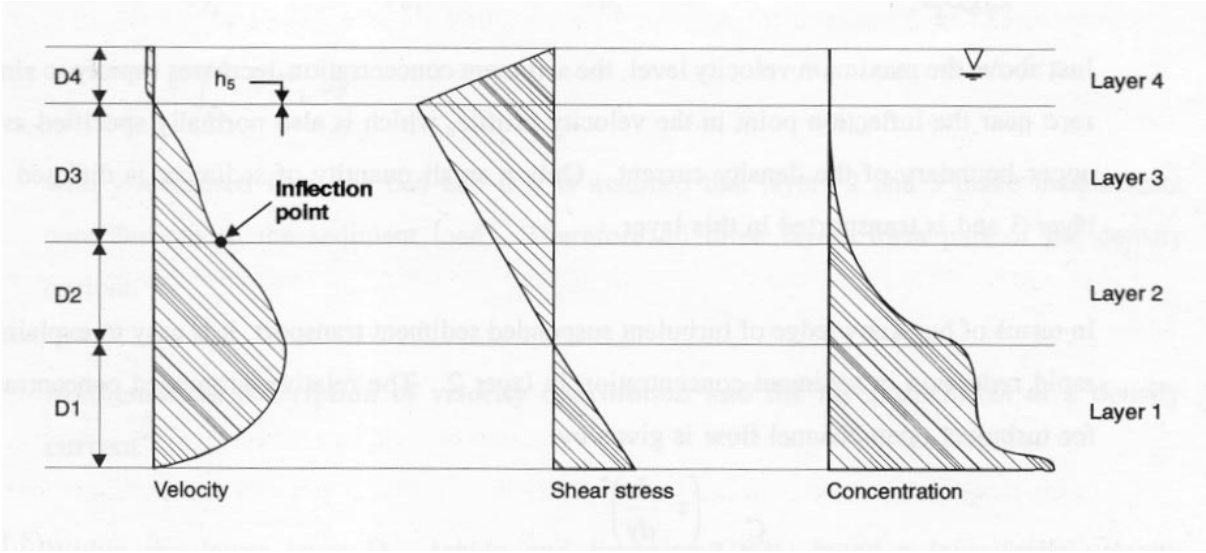

Figure 4.3 - 1 Density current velocity, suspended sediment concentration and shear stress distributions

4.3.2 Velocity distribution

In laboratory and field studies, the vertical velocity distribution has been found to be increasing logarithmically in layer 1 from the bed to the maximum velocity level (between layers 1 and 2) (**Figure 4.3-1**). *(Ashida and Egashira, 1975; Chikita, 1989)* From this point upwards in layer 2, the profile again seems to be decreasing logarithmically until a sudden change in slope at the so-called "inflection point" between layers 2 and 3 is reached. Through layer 3 the velocity decreases upwardly until it reaches zero at the point of contact where the velocity becomes negative due to upstream flow in the upper reservoir layer. In layer 4 the velocity is often zero or slightly negative with a typical open-channel velocity distribution.

4.3.3 Vertical suspended sediment distribution

The sediment distribution should be seen in relationship to the velocity distribution. (**Figure 4.3-1**). In the lower layer 1, the sediment distribution is similar to that found under turbulent flow conditions. Normally the sediment is also uniformly distributed due to the small particle sizes. The reduction in the z value is due to the low settling velocity and related change in distribution as explained in **Chapter 3**, with

$$z = \frac{w}{\kappa\sqrt{gD_1 s}}$$

Just above the maximum velocity level, the sediment concentration decreases rapidly to almost zero near the inflection point in the velocity profile, which is also normally regarded as the upper boundary of the density current. Only a small quantity of sediment is diffused into layer 3 and is transported in this layer.

In terms of our knowledge of turbulent suspended sediment transport, it is easy to explain the rapid reduction in sediment concentration in layer 2. The relative suspended concentration for turbulent open channel flow is given by:

$$\frac{C}{C_o} = \frac{\left(\tau\frac{dv}{dy}\right)^x}{\tau\left(\frac{dv}{dy}\right)_o^z} \qquad (3.8\text{-}1)$$

$$\therefore C\alpha\left(\tau\frac{dv}{dy}\right)^z$$

which means that as the maximum velocity is reached at the top of layer 1, $\frac{dv}{dy} \to 0$ and $\tau \to 0$ and therefore $C \to 0$. It is thus only the turbulence along the boundary of the density current which carries any suspended sediment above layer 1. In theory the suspended sediment transport in layer 2 should be zero, caused by the "barrier" of $\tau\frac{dv}{dy} \to 0$ at v = $v_{maximum}$ between layers 1 and 2.

4.3.4 Shear stress distribution

Within the lower two layers (1 and 2), the shear stress varies linearly (**Figure 4.3-1**) (*Ashida and Egashira, 1975*). In layer 3 a non-linear shear stress distribution is found, while at the top in layer 4, the distribution is linear as in open channel flow.

Although layers 1 and 2 are normally described as the density current, it is believed that at least layers 1, 2 and 3 should be considered in the mathematical description of a density current. From continuity:

$$q = \overline{v_1} D_1 + \overline{v_2} D_2 + \overline{v_3} D_3 \tag{4.3-1}$$

and

$$\begin{aligned} q_c &= \int_{y_o}^{D_1} v_1 C_1 dy + \int_{D_1}^{D_2} v_2 C_2 dy + \int_{D_2}^{D_3} v_3 C_3 dy \\ &= \int_{y_o}^{D_1} v_1 C_1 dy \end{aligned} \tag{4.3-2}$$

with y measured from the bed and if it is assumed that layers 2 and 3 make insignificant contributions to the sediment load. Therefore all three layers form part of the density current.

4.4 Mathematical description of the velocity distribution and the thickness of a density current

Within the lower layer with thickness D_1, *Ashida and Egashira (1975)* have found a logarithmic velocity distribution in laboratory tests (see **Figure 4.4-1**) and therefore adopted a velocity distribution equation of the form:

$$\frac{v}{\sqrt{\frac{\Delta\rho g D_1 s}{\rho}}} = A_r \left(\frac{v^* . k_s}{\nu} \right) + \frac{1}{\kappa_1} \ln \frac{y}{k_s} \tag{4.4-1}$$

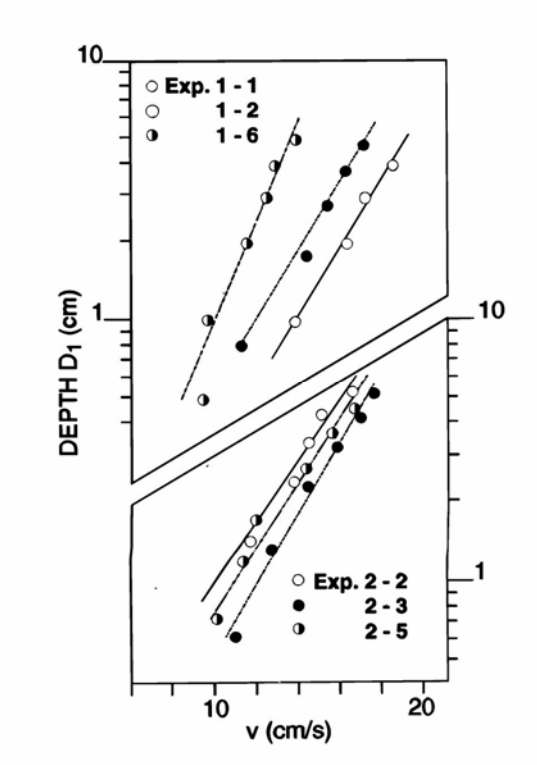

Figure 4.4 - 1 Velocity distribution from channel bed to maximum velocity

(*Ashida and Egashira, 1975*)

In layer two, at the interface, Ashida and Egashira related the mixing length (ℓo) to the layer thickness (D_2) and found the relationship indicated in **Figure 4.4-2**.

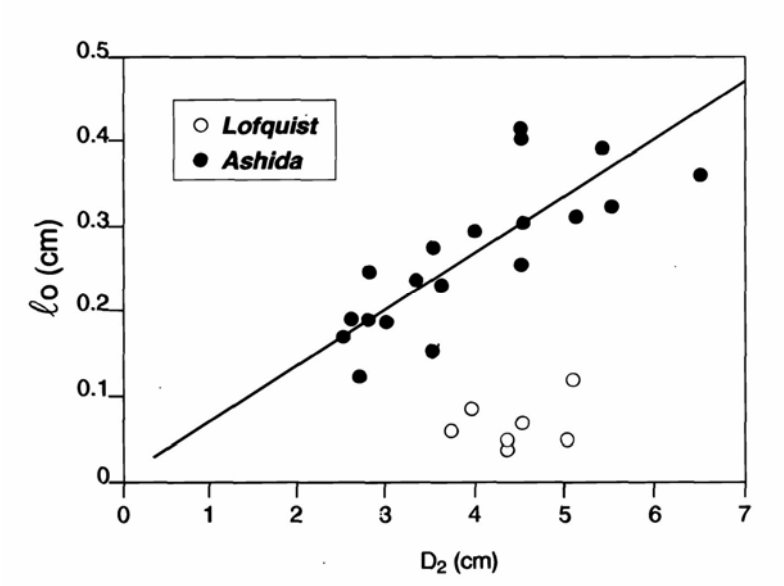

Figure 4.4 - 2 Relationship between mixing length ℓ_o at interface and D_2

(*Ashida and Egashira, 1975*)

With $\ell = \ell o + \kappa_2 (D_1 + D_2 - y)$ at the interface, Ashida and Egashira again assumed a logarithmic velocity distribution for layer 2. By making further assumptions regarding the shear stress distribution in layer 3 (see **Figure 4.4-3**), they derived a velocity distribution relationship for layer 3 and together with assumed sediment concentrations, the discharge and sediment transport continuity equations could be solved mathematically.

Ashida and Egashira were some of the first authors to describe the velocity, shear stress and suspended sediment distribution in a density current. Some of the assumptions made by them can, however, be criticized. The assumed relationship between ℓ o and D_2 is not based on theory and need therefore not be true for all data, as is found with a different data set in **Figure 4.4-2**. The mixing length (or R) at the interface should rather be calculated theoretically by using boundary layer theory as will be shown in the next section.

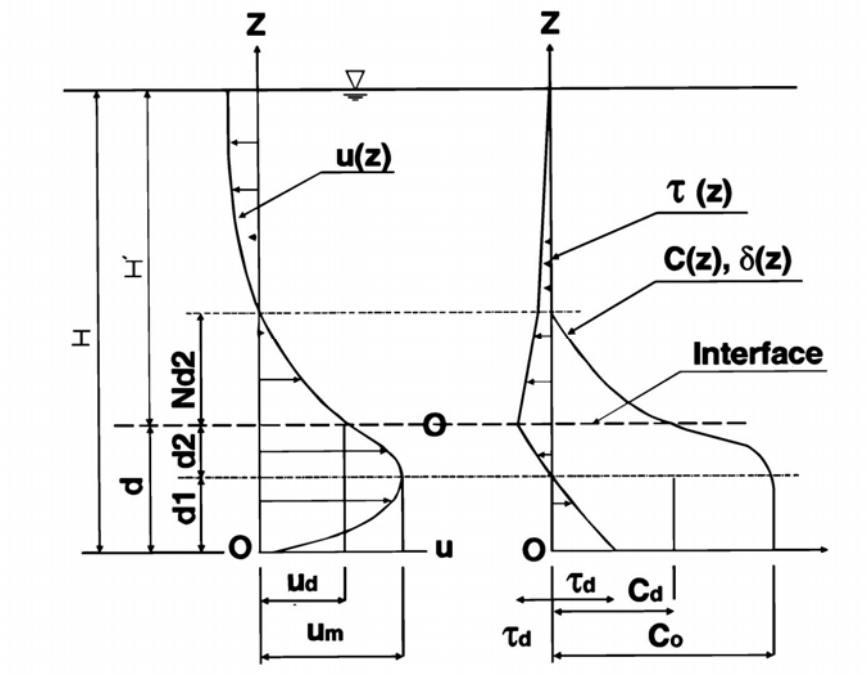

Figure 4.4 - 3 Distribution of velocity, shear stress and sediment concentration

(*Ashida and Egashira, 1975*)

In density current flow, three boundaries can be observed: at the bed, at the top of layer 2 where the suspended sediment concentration $\rightarrow 0$ and at the level where $v \rightarrow 0$.

With certain assumptions, it should be possible to describe the velocity distribution and layer thicknesses in a density current mathematically. The knowledge of laminar and turbulent boundary conditions can be used effectively to describe the mathematical relationships. Unlike the case of flow, the velocity distribution relationship for a density current cannot be established without considering the influence of sediment transport.

The suspended sediment transport in a density current affects the energy dissipation rate as represented by Kappa (κ)as follows: (Refer to **Figure 4.3-1**)

a) At the bed in layer 1, the highest sediment concentration is found with a related reduction in κ to estimated values of as low as 0,2 (typical of that found in open channel flow). A reduction in κ leads to an increased velocity gradient $\left(\frac{dv}{dy}\right)$ in layer 1 near the bed.

b) At the top of layer 3, $v \to 0$ and the suspended sediment concentration approaches zero. Therefore $\kappa \to 0{,}4$, the standard value in turbulent open channel flow with no sediment transport.

c) As the sediment concentration rapidly decreases in layer 2, the inflection point in the velocity distribution (or the interface) is probably caused by the sudden change in the value of κ at the interface.

   The velocity profile of a density current can be described by assuming the following:

   i) A laminar boundary layer at the top of layer 3 where $v \to 0$

   ii) Turbulent flows, corrected for density difference, in layers 3 and 2. Laminar flow above the interface (above layer 2) would at first seem to be more probable, but such an assumption cannot explain the relatively great depth of layer 3 and the velocity distribution. A correction to the

density difference is also required, since some sediment is diffused upward and transported in layer 3.

iii) Turbulent flow, corrected for density difference, in layer 1, derived from the same principles as those applicable to rough bed conditions.

iv) Logarithmic velocity distributions in layers 1, 2, and 3 for turbulent conditions, adjusted with correct κ values as these values change with depth in each layer.

For layers 2 and 3

At the top of layer 3, with y measured downward as in **Figure 4.3-1**, in the laminar layer:

$$\tau = \mu \frac{d\,\mathrm{v}}{\mathrm{dy}} = \Delta\rho\,\mathrm{gs}(\mathrm{D}_{2+3} - \mathrm{y})$$

$$\therefore \frac{d\,\mathrm{v}}{\mathrm{dy}} = \frac{\Delta\rho\,\mathrm{gs}(\mathrm{D}_{2+3} - \mathrm{y})}{\mu} \qquad (4.4\text{-}2)$$

In the rest of layer 3, the flow is turbulent and the shear stress:

$$\tau = \frac{\rho}{2\pi} R^2 \left(\frac{d\,\mathrm{v}}{\mathrm{dy}} \right)^2 = \Delta\rho\,\mathrm{gs}(\mathrm{D}_{2+3} - \mathrm{y}) \qquad (4.4\text{-}3)$$

Following the same derivation as with turbulent open channel flow, it is possible to show that (Basson and Rooseboom, 1997):

$$\therefore \frac{d\,\mathrm{v}}{\mathrm{dy}} = \frac{\sqrt{2\pi\Delta\rho\,\mathrm{g}\,\mathrm{D}_{2+3}\mathrm{s}}}{\rho\,\mathrm{y}} \qquad (4.4\text{-}4)$$

Assuming that at the boundary between the laminar and turbulent density current flow at the top of layer 3, the applied power values are equal i.e.:

$$\tau \frac{d\,\mathrm{v}}{\mathrm{dy}}\,\mathrm{laminar} = \tau \frac{\mathrm{dv}}{\mathrm{dy}}\ _{\text{turbulent}}$$

$\tau_{la\,\mathrm{min}\,ar} = \tau_{turbulent}$, then

$$\frac{d\,\mathrm{v}}{\mathrm{dy}}\,\mathrm{laminar} = \frac{\mathrm{dv}}{\mathrm{dy}}\,\mathrm{turbulent}$$

$$\Delta\rho g s \frac{(D_{2+3} - y)}{\mu} = \frac{\sqrt{2\pi g' D_{2+3} s}}{y}, \text{with } \mathrm{g}' = \frac{\Delta\rho}{\rho}.\mathrm{g} \qquad (4.4\text{-}5)$$

Solving **Equation (4.4-4)** now for $y = h_5$, the thickness of the boundary layer, to be used as integration constant when deriving the velocity:

$$\therefore h_5 = \frac{\sqrt{2\pi g' D_{2+3} s.}\ \mu}{\Delta\rho g s (D_{2+3} - h_5)}$$

$$= \frac{\sqrt{2\pi}\,\mu}{\sqrt{\rho\Delta\rho g (D_{(2+3)} - h_5) s}} \qquad (4.4\text{-}6)$$

Integration of **Equation 4.4-4** yields:

$$\mathrm{v}_{(2+3)} = \sqrt{2\pi\,\mathrm{g}'\,\mathrm{D}_{(2+3)}\ \mathrm{s}}\,\ell\mathrm{n}\ \mathrm{y} + \mathrm{A} \qquad (4.4\text{-}7)$$

with A an integration constant.

At the top of layer 3 at the boundary layer:

$$\mathrm{v}_{(2+3)} = \frac{\Delta\rho\,\mathrm{gs}}{2\mu}(2\,\mathrm{Dy} - \mathrm{y}^2.\mathrm{h}_5) = \sqrt{2\pi\,\mathrm{g}'\mathrm{Ds}}\ \ell\mathrm{n}\ \mathrm{h}_5 + \mathrm{A} \qquad (4.4\text{-}8)$$

$$\therefore A = \frac{\Delta\rho g s\, D h_5}{\mu} - \sqrt{2\pi g\_Ds}\,\ell n\, h_5$$

and **Equation 4.4-7** becomes:

$$v_{(2+3)} = \sqrt{2\pi g' D_{(2+3)} s\ell n}\left(\frac{y}{h_5}\right) + \frac{\Delta\rho g s D_{2+3} h_5}{\mu}\Bigg|_{h_5}^{D_{2+3}} \qquad (4.4\text{-}9)$$

Substituting **Equation 4.4-6** in **Equation 4.4-9** gives:

$$v_{2+3} = \sqrt{2\pi\, g' D_{(2+3)}}\, s\ell n\left(\frac{y\sqrt{gsD}\sqrt{\rho\Delta\rho}}{\sqrt{2\pi}\mu}\right) + \frac{\Delta\rho\, gsD\sqrt{2\pi}.\mu}{\mu.\sqrt{gsD}\sqrt{\rho\Delta\rho}}$$

$$= \sqrt{2\pi g' D_{(2+3)}}\, s\ell n\left(\frac{y\sqrt{gsD}\sqrt{\rho\Delta\rho}}{\sqrt{2\pi}\mu}\right) + \sqrt{\frac{\Delta\rho}{\rho}}\sqrt{2\pi}\sqrt{gsD} \qquad (4.4\text{-}10)$$

In layer 1, the velocity at any level can be derived, but with the density difference adjustment.

Therefore

$$v_1 = \sqrt{2\pi\, g' D_1}\, s\ell n\left(\frac{D_1}{y_o}\right) \qquad (4.4\text{-}11)$$

Equations 4.4-10 and **4.4-11** can now be solved together by using the fact that the maximum velocities in both equations are common:

Equation 4.4-10 becomes

$$v_{(2+3)}(\max) = \sqrt{2\pi\, g' D_{(2+3)}}\, s\ell n\left(\frac{D\sqrt{gD_{(2+3)}}\sqrt{\rho\Delta\rho}}{\sqrt{2\pi}\mu}\right) + \sqrt{2\pi}\sqrt{gsD_{(2+3)}}\sqrt{\frac{\Delta\rho}{\rho}} \qquad (4.4\text{-}12)$$

and **Equation 4.4-11**:

$$v_{(1)}\max = \sqrt{2\pi\, g' D_1}\, s\ell n\left(\frac{D_1}{y_o}\right) \qquad (4.4\text{-}13)$$

with $y_o = \frac{k_s}{30}$

Equations 4.4-12 and **4.4-13**, however, contain 3 unknowns: D_1, D_{2+3} and v_{max}. A third equation is therefore required which expresses D_1 in terms of D_{2+3}. This third equation is found when combined translation and rotation in turbulent flows are considered. Turbulent flow translates at relative velocity $v_0 = y_o \frac{dv}{dy}$. In a density current the same principle applies near the bed as well as at the top of layer 3, so that the translation velocity at the top and bottom of the density current velocity profile should be equivalent:

$$y_1 \frac{d\,v}{dy_{10}} = y_3 \frac{dv}{dy_{30}} \qquad = \text{constant if acceleration} = 0 \tag{4.4-14}$$

$$\therefore \frac{\sqrt{g' D_1 s}}{\kappa_1} = \frac{\sqrt{g' D_{(2+3)} s}}{\kappa_{2+3}} \tag{4.4-15}$$

$$\therefore \frac{D_1}{D_{(2+3)}} = \frac{\kappa_1^2}{\kappa_{(2+3)}^2}$$

with typical expected values of $\kappa_1 \rightarrow 0{,}2 \;\; to \;\; 0{,}3 \;\; and \;\; \kappa_{(2+3)} = 0{,}3 \;\; to \;\; 0{,}4$

Equations 4.4-12, **4.4-13** and **4.4-15** can now be applied simultaneously to solve for D_1 and D_{2+3} (Basson and Rooseboom, 1997).

4.5 Verification of theory to predict the velocity profile and depth of a density current with laboratory and field data

Using the data of *Ashida and Egashira (1975)* and *Chikita (1989)* as sources of laboratory and field data respectively, it is possible to calculate the upper layer depths D_{2+3} from observed D_1-values as a first check on the validity of **Equations 4.4-12** and

4.4-13. Predicted $D_{(2+3)}$ values can, however, only be determined accurately if correct values of κ_1 and $\kappa_{(2+3)}$ are used. Although κ_1 values have been determined by Ashida and Chikita, no data for κ_{2+3} -values are available, and realistic values had to be assumed.

Assuming $\kappa_{(2+3)} = 0{,}4$ (as for no sediment transport) and $\kappa_1 = 0{,}2$ at the bed, the predicted D_{2+3} versus observed D_{2+3} data are indicated in **Figure 4.5-1**. It is clear that the assumptions made in the derivation of **Equations 4.4-12** and **4.4-13** give consistent upper layer depths for both laboratory and field data. Predicted versus observed $D_{(2+3)}$ depths however still need to be compared using real Kappa values.

Unfortunately D_3 data were not published by Ashida, and for only 3 experiments were the ratios of $D_{(2+3)}/\ D_2$ being indicated as varying from 2,1 to 2,5. Using $\kappa_1 = 0{,}25$ and $\kappa_{2+3} = 0{,}32$ provides realistic observed κ_1 data as well as solutions in terms of **Equation 4.4-15** for assumed D_1 and D_{2+3} = 2,5 x D_2 values for Ashida's data. With κ_1, κ_{2+3} and D_1 known, D_{2+3} can be calculated from **Equations 4.4-12** and **4.4-13** and compared with "observed" $D_{(2+3)}$ data = 2,5 x D_2 as shown in **Figure 4.5-1**. Using the same approach, reservoir data of *Chikita (1989)*, are also used to verify the mathematical assumptions, as shown in **Figure 4.5-1**. In this case $D_{(2+3)}$ = 3 x D_2 had to be used, as inferred from the data of Chikita. Although a number of assumptions had to be made owing to the lack of certain observed variables in the laboratory and field data, it is believed that the basis of the theory used in deriving **Equations 4.4-12, 4.4-13** and **4.4-15** is sound, as was provisionally proven in **Figure 4.5-1**. Future detailed laboratory tests will be required to establish $\kappa_1, \kappa_2, \kappa_3$, D_1, D_2 and D_3 values with different channel slopes, discharges, sediment loads and bed roughnesses.

4.6 Movement of a density current : flow resistance and velocity

It is possible to derive theoretically, from equations of sediment transport and discharge continuity, a relationship for the average velocity of a density current by integrating the velocity distribution with depth and by using the theory as derived in the previous

sections. The many unknowns in such a relationship make it difficult to apply in practice and therefore most researchers have resorted to Chezy type equations with all the unknowns incorporated into a single empirical constant C_H in the equation:

$$\bar{v} = C_H . \sqrt{g' D s} \qquad (4.6\text{-}1)$$

with $s = s_o$, the bed slope, assuming a uniform density current
and D = depth of layers 1 and 2.

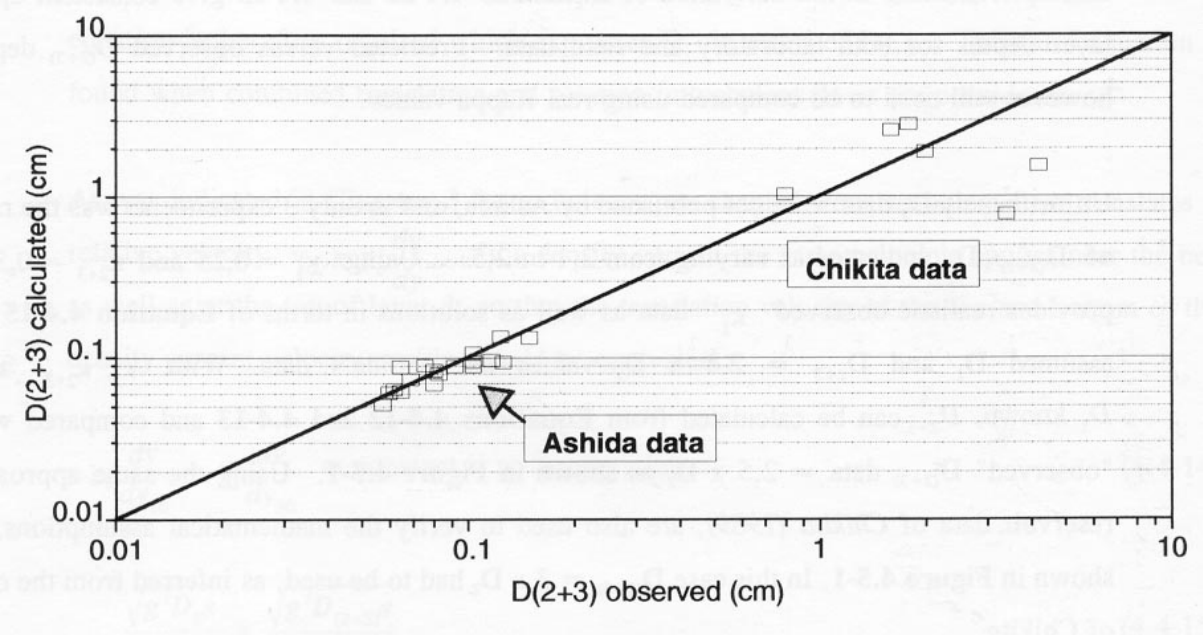

Figure 4.5 - 1 Observed versus calculated density current layer depths

Studies have been undertaken by *Raynaud (1951), Bata and Knezevich, (1953), Blancket (1954), Michon et al. (1955),* and *Levy (1958)* on the value of C_H in laminar and turbulent regimes.

Fan (1960) described the movement of a density current in terms of the equation of motion. Consider a fluid element in a density current:

$$\frac{1}{\gamma'}\frac{dp}{dx} + \frac{dy}{dx} + \frac{1}{\gamma'}\frac{d\tau}{dy} + \frac{v}{g}\frac{dv}{dx} + \frac{1}{g}\frac{dv}{dt} = 0 \qquad (4.6\text{-}2)$$

with p = total pressure = p_1 (due to lighter fluid) + Δp (due to density difference)

γ' = specific weight of the density current

y = distance from horizontal reference line

If the depth of the density current is h´ and the depth of the overlying water h, then the total depth is H = h + h[1] (see **Figure 4.6-1**).

Assuming homogeneous fluids, above and below the interface

$$p + \gamma' y = \gamma H + (\gamma' - \gamma) h' + \gamma y_o \tag{4.6-3}$$

and $\frac{dp}{dx} + y\frac{dy}{dx} = \frac{dH}{dx} + y\frac{d^1h}{dx} + y^1\frac{dy_0}{dx}$

with γ = specific weight of overlying water

Fan further assumed that τ_o, the mean bed shear stress, and τ_i, the shear resistance at the interface, are proportional to the square of the mean velocity:

$$\tau_o = \frac{\lambda_o}{4}\rho'\frac{v^2}{2}; \tau_1 = \frac{\lambda_i}{4}\rho\frac{v^2}{2} \tag{4.6-4}$$

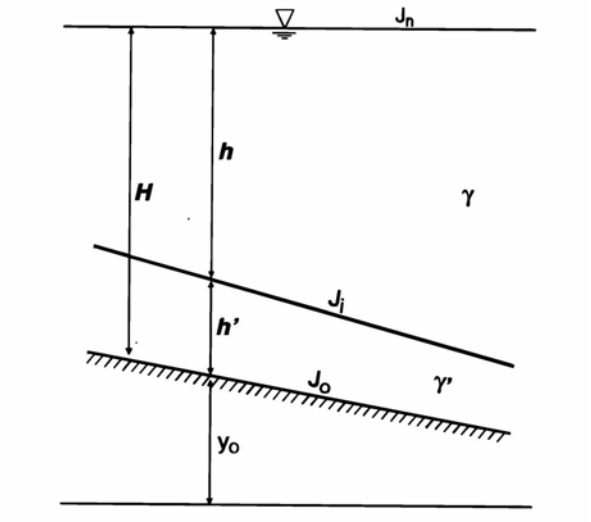

Figure 4.6 - 1 Schematic diagram of a density current

Where λ_o and λ_i are the corresponding coefficients of friction.

Considering a segment of the density current with width b, bed slope J_o and interface slope J_i, the equation of mean motion of the density current reads:

$$\frac{1}{\gamma'}\frac{dH}{dx} + \frac{\_\gamma}{\gamma'}\frac{dh\_}{dx} + \frac{dy_o}{dx} + \left(\frac{\lambda_o \, v^2}{8\,gh^1} + \frac{\lambda_i \, v^2}{8\,gh^1}\right) + \left(\frac{v}{g}\frac{dv}{dx} + \frac{1}{g}\frac{dv}{dt}\right) = 0 \qquad (4.6\text{-}5)$$

in which:

$$\frac{dH}{dx} = J_0 - J_n$$

$$\frac{dy_o}{dx} = J_0$$

$$\Delta\gamma = \gamma' - \gamma$$

and J_n = negative slope at water surface.

The frictional stress exerted along the interface is

$$\tau_i = \frac{\lambda_i}{4} p' \frac{v^2}{2} = -\gamma \frac{bh}{b + 2h} \cdot J_n$$

Substituting the above equations into **Equation 4.6-4** yields:

$$\frac{y}{y'}\left(J_0 - \frac{dh_1}{dx}\right) + \frac{v^2}{g'h}\frac{d'h}{dx} - \frac{\lambda m v^2}{8gR} - \frac{1}{g} = 0 \qquad (4.6\text{-}6)$$

with λ_m = mean friction coefficient of the underflow

$$= \lambda_o + \lambda_i \left[\frac{b}{2h' + b} + \frac{h'(b + 2h)}{h(b + 2h')}\right] \qquad (4.6\text{-}7)$$

For <u>unsteady, non-uniform</u> density currents, Fan used **Equation 4.6-5** to predict depths. For steady density currents $\lambda_m = 0{,}02$ to 0,03, but Fan used λ_m = 0,05 for unsteady conditions.

For <u>steady, non-uniform</u> density currents:

$$\frac{d'h}{dx} = \frac{J_o - \left(\frac{\lambda_m v^2}{8 \frac{-\gamma}{\gamma'} gR} \right)}{1 - \left(\frac{v^2}{\frac{-\gamma}{\gamma} g'h} \right)} \qquad (4.6\text{-}8)$$

with R = hydraulic radius $= b'h/(2h' + b)$

and for <u>uniform flow</u> $\frac{dh'}{dx} = 0$ then

$$\bar{v} = \sqrt{\frac{8}{\lambda_m} \cdot \frac{\Delta\gamma}{\gamma'} \cdot gRJ_o} \qquad (4.6\text{-}9)$$

$$= \sqrt{\frac{8}{\lambda_m}} \cdot \sqrt{g' RJ_0}$$

which is similar to a Chezy type equation for uniform open channel flow.

Fan found the mean friction factor λ_m **(Equation 4.6-6)** from flume studies to be independent of the Reynolds number and to remain almost constant as shown in **Figure 4.6-2**, when the flow is turbulent.

For a bed friction factor of $\lambda_o = 0{,}02$, Fan found the interfacial friction factor $\lambda_i = 0{,}005$ as shown in **Table 4.6-1**.

Table 4.6-1: Interfacial friction factor

J_o	*Average h′ (cm)*	*Average* λ_i
0,0005	14,4	0,0047
0,005	17,8	0,0051

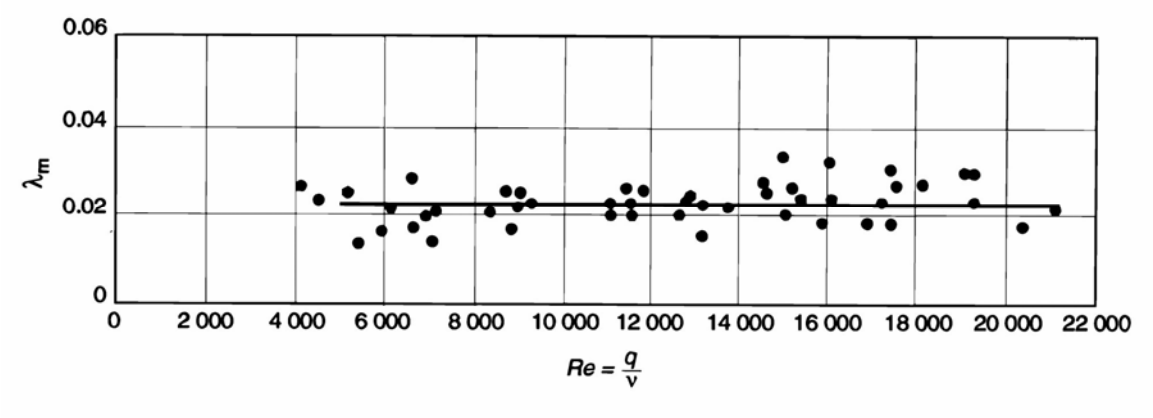

Figure 4.6 - 2 Friction factor λ_m from flume studies *(Fan, 1960)*

In the Guanting Reservoir, China, Fan found the same constant mean friction factor as in the flume tests (with the same sediment), with λ_m = 0,02 to 0,03 as shown in **Figure 4.6-3**.

Fan (1960) also found that supercritical and subcritical conditions can prevail in the density current, and that the transition from one condition to another is possible in the plunging phase, with submerged hydraulic jumps being formed.

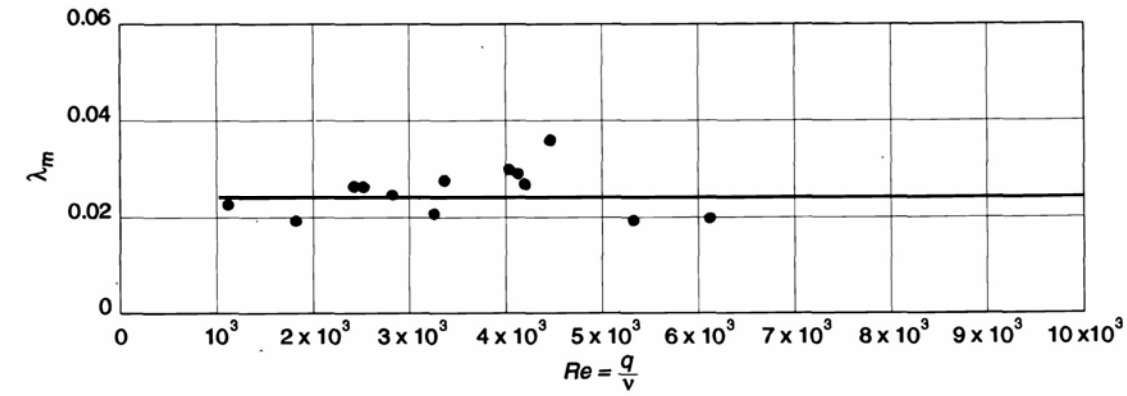

Figure 4.6 - 3 Friction factor for Guanting Reservoir *(Fan, 1960)*

A relationship between typical depths of flow and density current thicknesses for the Guanting Reservoir as well as flume data is shown in **Figure 4.6-4**.

Such a relationship will be site-specific and will depend on a number of specific boundary conditions such as bed slopes, discharge, sediment characteristics, etc.

So far, only one-dimensional density currents have been considered. The influence of flow width on a density current is, however, also important in order to quantify total sediment transport.

4.7 Cross-sectional variation in velocity and sediment concentration across a density current in a reservoir

At the early stages of impoundment, a density current usually moves along the original river channel. Later, as the main channel is filled through sedimentation, the topographical width exceeds the width of the density current. Examples of observed lateral and vertical velocity and concentration distributions in Sanmenxia Reservoir, 1961, are depicted in **Figure 4.7-1** *(Fan, 1986)*.

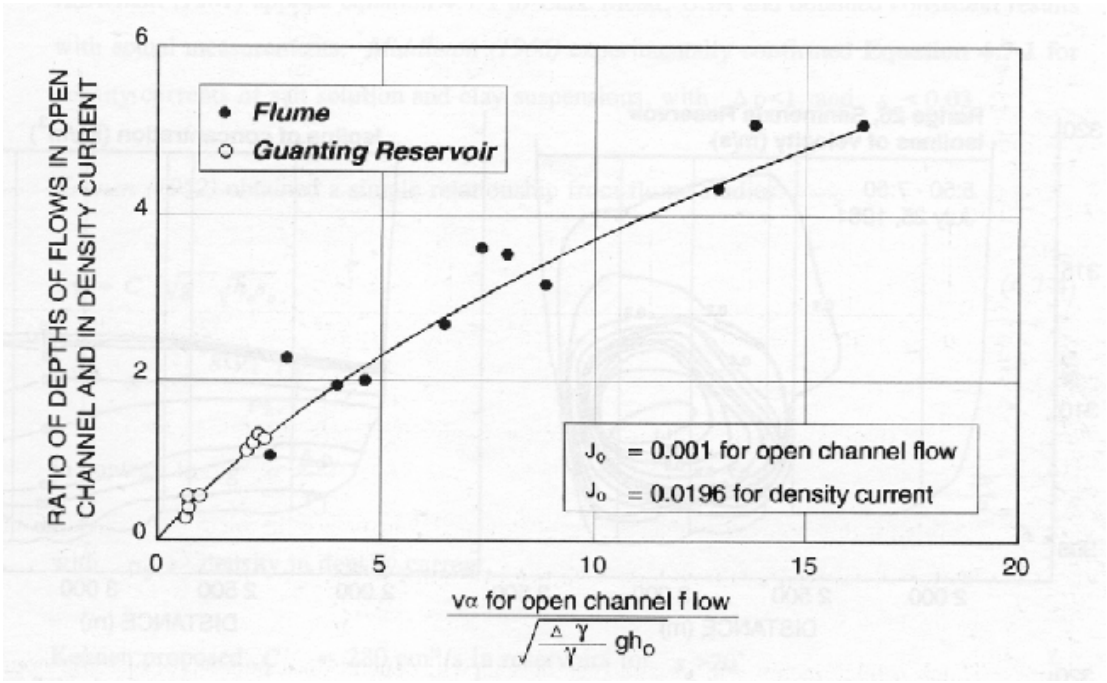

Figure 4.6 - 4 Ratio of density current depth to open channel flow depth in Guanting Reservoir *(Fan, 1960)*

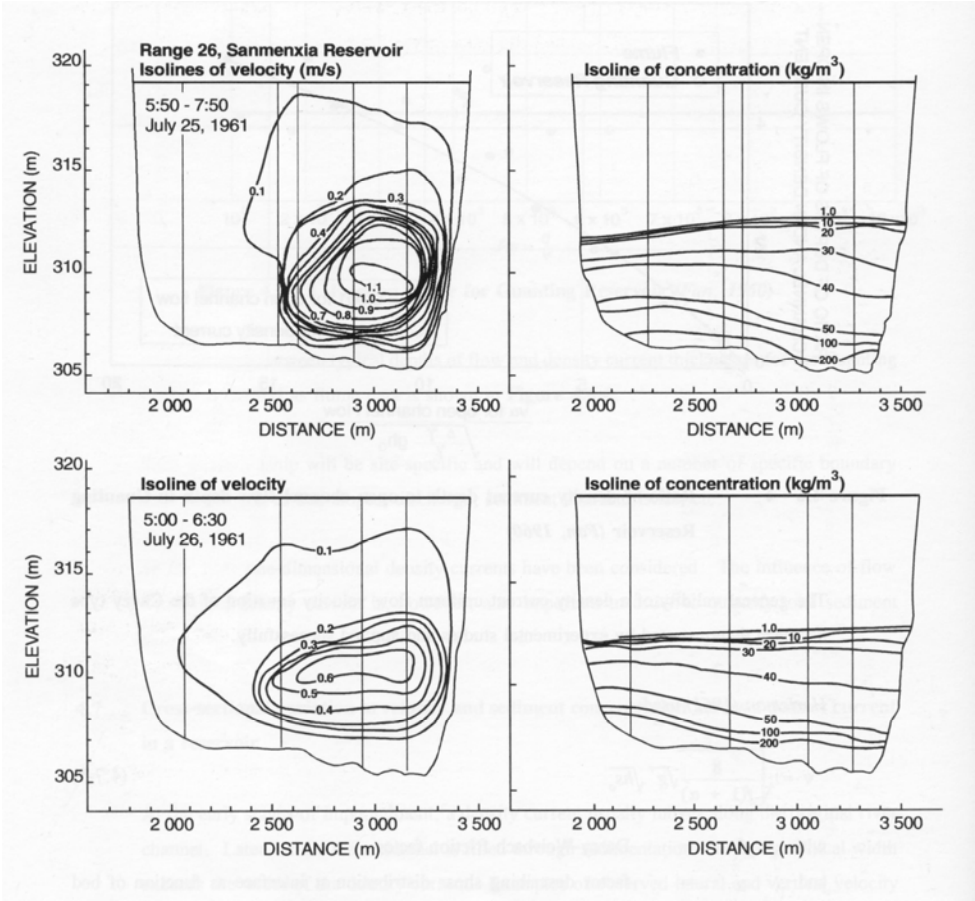

Figure 4.7-1 Density current lateral velocity and concentration distribution in Sanmenxia Reservoir *(Fan, 1986)*

The general validity of a density current uniform flow velocity equation of the Chézy type has been demonstrated by experimental studies and also through successful application.

Harleman (1961) used:

$$v = \sqrt{\frac{8}{f(1+\alpha)}}\sqrt{g'}\sqrt{hs_o} \qquad \textbf{(4.7-1)}$$

with f = Darcy-Weisbach friction factor

and α = factor describing shear distribution at interface as function of bed shear, with $\tau_i = \alpha \tau_o$ (4.7-2)

Harleman proposed the use of $\alpha = 0{,}43$ for turbulent density current flow and f-values from the Moody diagram for pipe flow.

For laminar flow (Re < 1000), Harleman proposed

$$v = 0{,}375\sqrt{Re}\sqrt{g'}\sqrt{hs_o} \tag{4.7-3}$$

which was determined theoretically.

Harleman (1961) applied equation 4.7-1 to Lake Mead, USA and obtained consistent results with actual measurements. *Middleton (1966)* experimentally confirmed **Equation 4.7-1** for density currents of salt solutions and clay suspensions, with $\Delta\rho < 1$ and $s_o < 0{,}03$.

Keunen (1952) obtained a simple relationship from flume studies:

$$v = C''\sqrt{g''}\sqrt{h_o s_o} \tag{4.7-4}$$

with $g'' = \dfrac{g(\rho_1 - \rho_2)}{\rho_2}$

in contrast to $g' = \dfrac{\Delta\rho}{\rho_1}$

with ρ_2 density in density current,

Keunen proposed $C'' = 280\, cm^{1/2}/s$ in reservoirs for $s_o > 20°$

Hinze (1960) showed that the empirical relationship used by *Keunen (1952)* can be derived theoretically. Using boundary layer theory, Hinze obtained **Equation 4.7-4** with *C"=f*(suspension density distribution, friction coefficient at interface) with $280<C"<560 cm^{1/2}/s$.

Bagnold (1962) proposed an auto-suspension model as the criterion for the continued self-maintenance of a density current, which can be rewritten in the form:

$$v = C\sqrt{g'}\sqrt{h \sin\theta} \tag{4.7-5}$$

but the term $\sin\theta$ is replaced by $\left(\sin\theta - \frac{w}{v}\right)$, with *w* = settling velocity of particles.

Bagnold used an energy balance principle:

Layer integrated turbulent energy production = work done against negative buoyancy force + turbulent energy dissipation.

$$\int_o^H (\overline{u'v'})\frac{\delta u}{\delta y}.dy = \int_o^H bv\cos\theta\, dy + \int_o^H E dy \tag{4.7-6}$$

$$\therefore s_2 BHU(\sin\theta - v_f \cos\theta) = \int_o^H E dy$$

The energy dissipation term cannot be evaluated properly without velocity and density profiles. It is therefore difficult to verify Bagnold's concept *(Middleton, 1966)*.

4.8 Motion of the head of a density current

Every uniform flow region of a density current is preceded by an initial head also known as the nose. *Hinze (1960)* referred to it as the spreading-out phenomenon, during which the density current displaces the fluid which it enters. *Altinakar et al. (1990)* plotted the shape of the head non-dimensionally as shown in **Figure 4.8-1**.

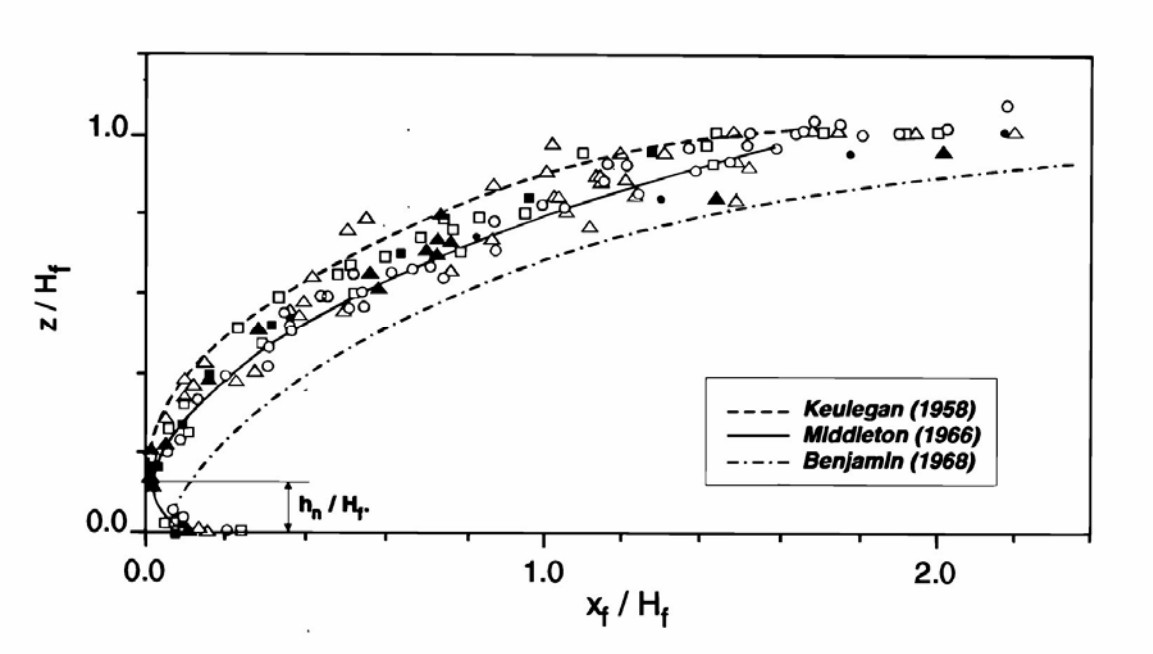

Figure 4.8-1 Non dimensional density current head shape *(Altinakar et al., 1990)*

Middleton (1966) observed that the head had a well-defined shape, with a depth twice the uniform flow depth, while the velocity is less than that of the uniform flow. It is also a region of intensive erosion. He found from flume studies that the motion of the head in the density current was closely described by the laws developed by *Keulegan (1958)* for saline surges. It was found that the velocity of the density current head on slopes up to 4% is adequately expressed by Keulegan's formula:

$$v_n = 0{,}75\sqrt{g'h_n} \qquad (4.8\text{-}1)$$

with h_n = thickness of the head.

Turner (1973, 1979) proposed **Equation 4.8-2** for the velocity of the head:

$$v_n = \sqrt{2}\sqrt{g'h_n} \qquad (4.8\text{-}2)$$

with h_n = depth of uniform density current flow.

When considering the three-dimensional motion and slope influence, Turner proposed:

$$v_n = 0{,}75\sqrt{g'h_n} \qquad (4.8\text{-}3)$$

which is the same equation as proposed by *Keulegan (1958).*

Density currents are characterized by a distinctive raised head, followed by a quasi-uniform flow region called the body. **(Figure 4.8-2)**

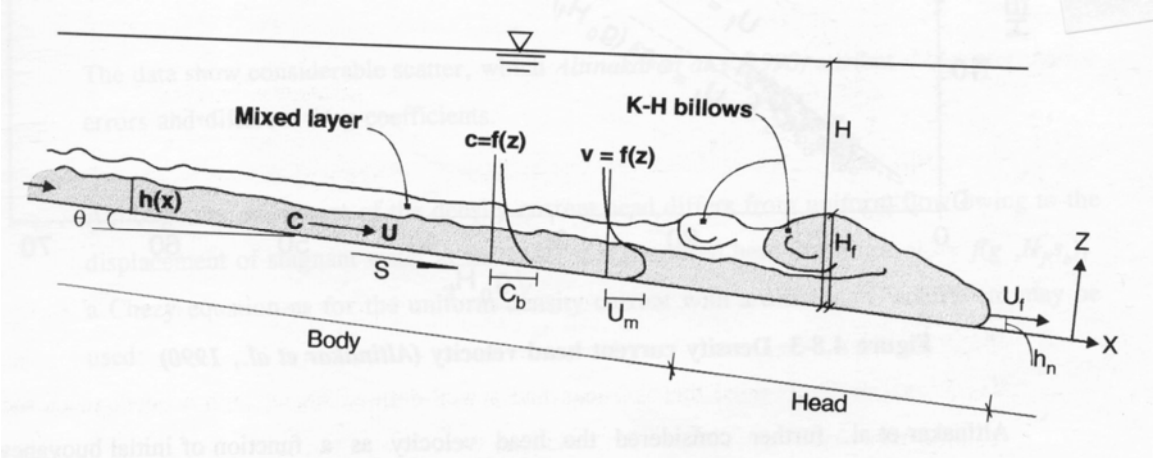

Figure 4.8-2 Density current head *(Altinakar et al., 1990)*

The head constitutes a region of intense mixing and wave breaking, with a highly irregular front.

Altinakar et al. (1990) compared his flume data with those of Middleton and Turner and proposed a smaller "Chezy" coefficient value of 0,63 in the equation:

$$v_n = 0{,}63\sqrt{g' h_n} \qquad (4.8\text{-}4)$$

which is shown graphically in **Figure 4.8-3**.

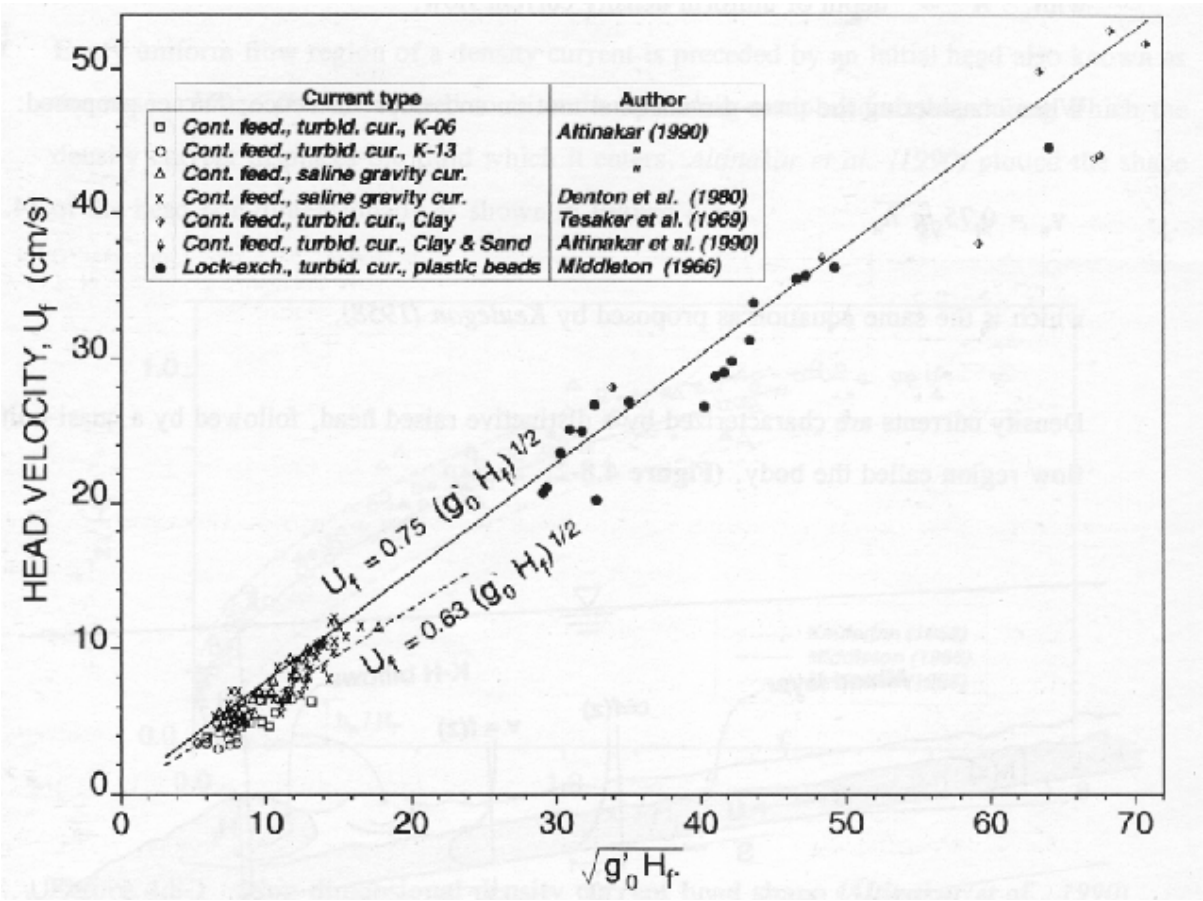

Figure 4.8-3 Density current head velocity *(Altinakar et al., 1990)*

The data used in **Figure 4.8-3** show considerable scatter, but this is understandable since the channel slope was not considered. The data in the Altinakar experiments were derived from bed slopes < 3%.

Altinakar et al. further considered the head velocity as a function of initial buoyancy flux $B_o = +g_o q_o$ and slope (s_0):

$$Uf = (g_0 q)^{1/2} f(s_0) \tag{4.8-5}$$

as is shown graphically in **Figure 4.8-4**.

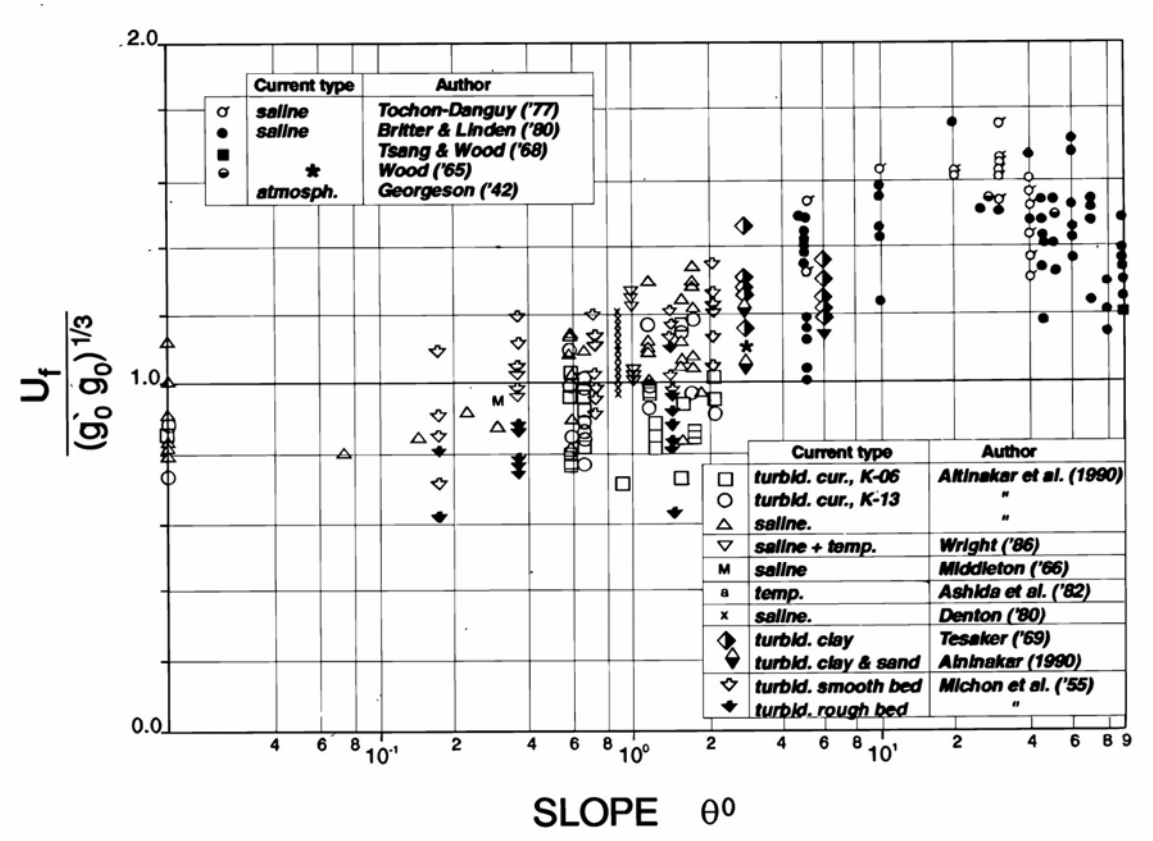

Figure 4.8-4 Dimensionless head velocity as function of bed slope *(Altinakar et al., 1990)*

The data show considerable scatter, which *Altinakar et al., (1990)* attributed to experimental errors and different drag coefficients.

Although the movement of the density current head differs from uniform flow owing to the displacement of stagnant water at the nose, it is proposed here that since $v_a = f\left(g, H_f s_o\right)$ a Chezy equation as for the uniform density current with a different C coefficient may be used:

$$v_n = C_n \sqrt{g' H_f s_o} \tag{4.8-6}$$

The data of Altinakar are shown in **Figure 4.8-5** and it is clear that **Equation 4.8-6** does indeed provide an accurate predictor of the density current head velocity.

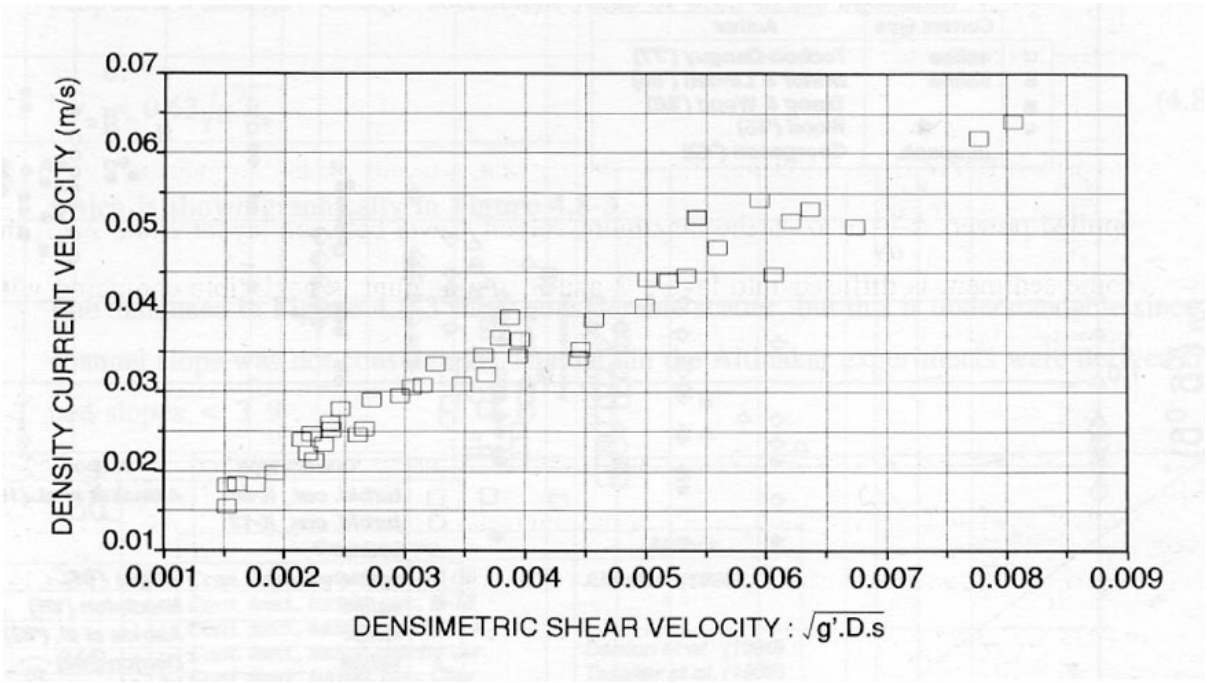

Figure 4.8-5 Velocity of density current head using Chezy type equation

4.9 Sediment transport by density currents

Bell (1940) expresses a very interesting view on density currents: "In ordinary streams, water propels suspended sediment. In turbid density currents, sediment propels water. Once the significance of this paradox has been grasped, a deal of mystery that surrounds density currents is stripped away".

From our current knowledge of hydraulics, we know that the density difference associated with sediment transport is required for density current movement. Both open channel flows and density current flows will however transport sediment (if available), since the sediment provides the mechanism through which the bed can be deformed and whereby the applied energy can be minimized. It is therefore not the water that propels the suspended sediment or vice versa in streams or density currents, but rather an intricate interrelationship between sediment and clear-water transport in a process of minimization of energy.

When a density current develops from turbulent inflow into a reservoir, coarser sediment is immediately deposited (in the delta area) while the fine sediments, up to the

sediment transport capacity of the density current, can be carried through the reservoir. The physics involved in the sediment transport process is almost the same as with turbulent open channel flow.

The vertical suspension of sediment is limited by the applied power $\tau \frac{dv}{dy} \to o$ at the maximum velocity level between layers 1 and 2. Although some sediment is diffused into layers 2 and 3, the amount is negligible compared with the load in layer 1.

The sediment being transported in a density current consists of the silt and clay fractions, with typical particle sizes and concentration distributions shown in **Figures 4.9-1**. It is clear that in layer 1 a constant suspended sediment concentration and density can be assumed in most cases, and therefore the sediment transport can be given by:

$$q_c = \int_{y_o}^{D_1} Cv\, dy = \overline{C}\,\overline{v} \tag{4.9-1}$$

with

$$\overline{C} = C_o \int_{y_o}^{D_1} \frac{\left(\tau \frac{d\,\mathrm{v}}{\mathrm{dy}}\right)^{\mathrm{z}}}{\left(\tau \frac{\mathrm{dv}}{\mathrm{dy}}\right)_{\mathrm{o}}^{\mathrm{z}}} \mathrm{dy}$$

Density current movement is unsteady due to the nature of floods, especially in arid areas. Measurements at the Guanting Reservoir clearly illustrate the characteristic of an unsteady density current with a reduction in sediment transport and with finer sediment being transported by the density current than by the inflow **(Figure 4.9-1)**.

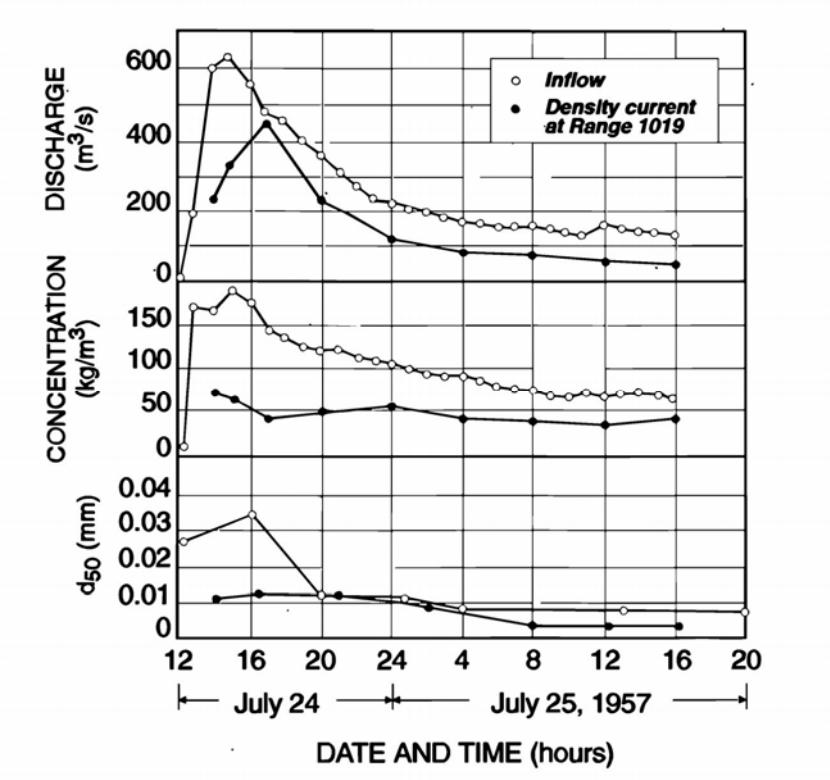

Figure 4.9-1 Unsteady density current measured in Guanting Reservoir *(Wu, 1994b)*

Fan (1960) investigated the sediment transport capacity of density currents in terms of the limiting particle size being transported. From flume tests he established that coarse sediment settles almost immediately while finer particles are transported at a constant gradation d_{90} = 0,008 to 0,018 mm and d_{50} = 0,002 to 0,003 mm, with plunge point velocities of 40-80 mm/s.

In the Guanting Reservoir the suspended sediment in the density current was found to be much coarser with d_{90} = 0,01 to 0,13 mm and d_{50} = 0,002 to 0,003 mm, with a plunge point velocity of 0,2 m/s resulting in greater transport capacity and the related larger particles that were transported compared to flume studies.

4.10 Density current formation following flushing

While *Lewis (1936)* stated that density currents had been observed in Lake Arthur, no quantitative data or information was published. No other density currents (turbidity driven) had been reported in the country until recently. Although the sediment loads in many local rivers are high enough to create density currents, and suspended sediment

loads include enough fine particles, the main limiting factor must be the small bed slopes of reservoirs, especially after some time of deposition, which prevent the progression of density currents through reservoirs.

During recent research density currents were observed after each flushing of Welbedacht Reservoir during filling of the reservoir. While the 5 gates in the dam were closed to cause filling of the empty reservoir, river outlets remained open which allowed venting of sediment transported towards the dam.

While suspended sediment samples taken near the surface upstream of the dam indicated low concentrations, the suspended concentrations of outflows sampled just downstream of the dam continued to be high for many hours after closure of the main gates, as shown in **Figure 4.10-1**.

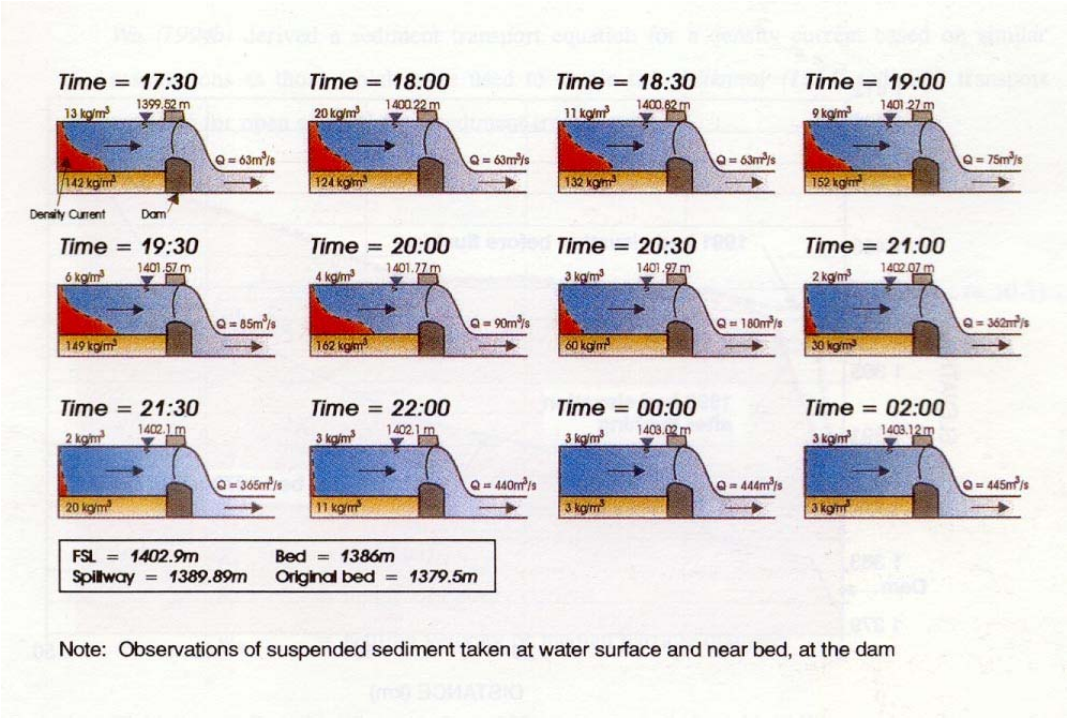

Figure 4.10-1 Density current venting at Welbedacht Reservoir

The streampower relationship proved that the high observed concentrations cannot be related to turbulent suspended sediment transport in the reservoir and that some other transport mechanism, which could only be density currents, had to be responsible for the high concentrations being vented from the reservoir. Flushing with water level draw-down of course provided high turbulent sediment transport capacity and related high

concentrations. Once the main outlets were closed, however, the coarse sediments were immediately deposited, whereas high concentrations of fines created density differences, resulting in density currents moving along the bed as the reservoir filled. The steep front set slope of the sediment deposit within Welbedacht Reservoir provided enough streampower for the density current to move through the reservoir down to the dam **(Figure 4.10-2)**. The duration of density current flow is limited, however, by the limited availability of sediment after turbulent scouring action had taken place during the flushing process. After some time, the outflow concentration decreased to become equal to the inflow sediment concentration.

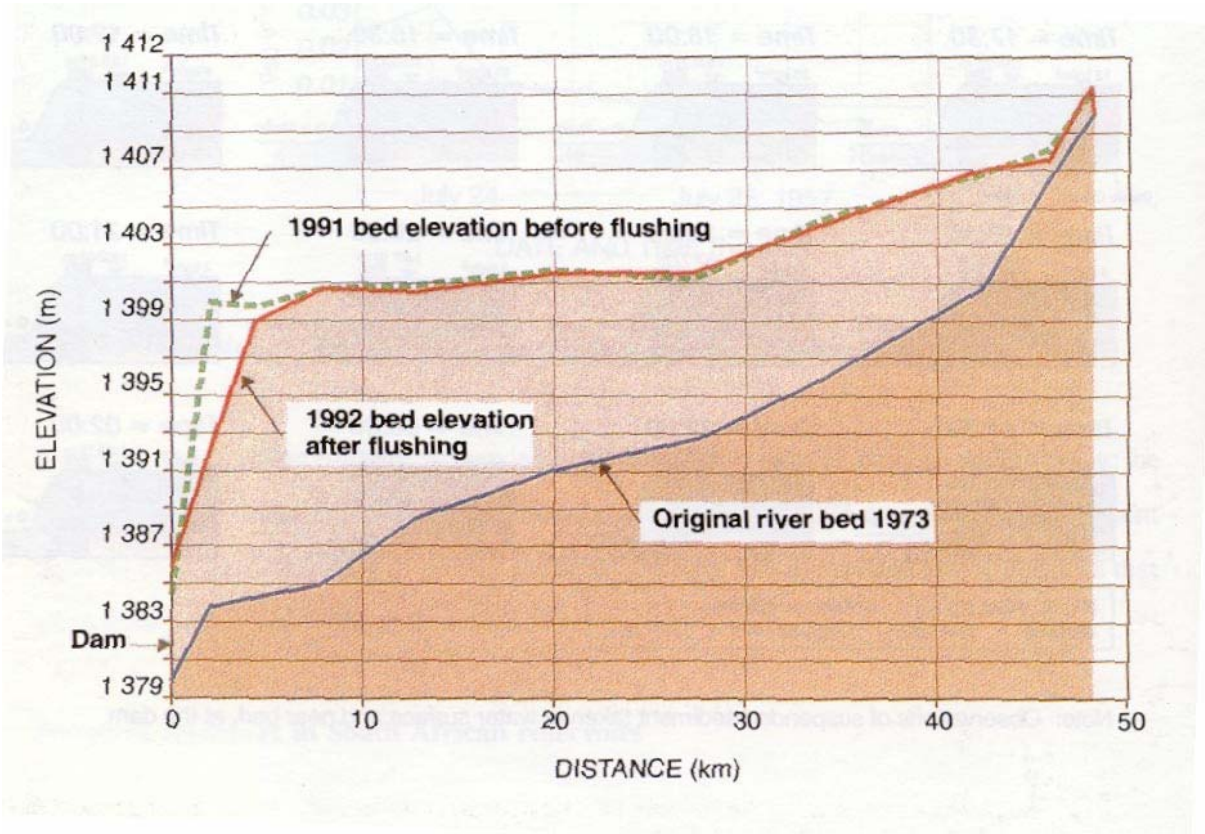

Figure 4.10-2 Longitudinal profile of Welbedacht Reservoir bed

Using the scoured profile of the main channel, it is possible to calculate the mean velocity of the density current observed in Welbedacht Reservoir. Suspended sediment concentration can then be related to the input streampower function for the density current and compared with similar reservoir data from China.

Unfortunately only the averaged suspended sediment particle size distribution was determined for the 1994 flushings at Welbedacht Dam, and information on the sediment

size transported by the density current as compared to turbulent transport is not available. During 1995, however, the reservoir was flushed again under similar flow conditions as in 1994 and this time more detailed sampling and grading analyses were carried out. **Figure 4.10-3** shows the effective settling velocity changes from the full reservoir before flushing, during flushing and during filling with density current venting.

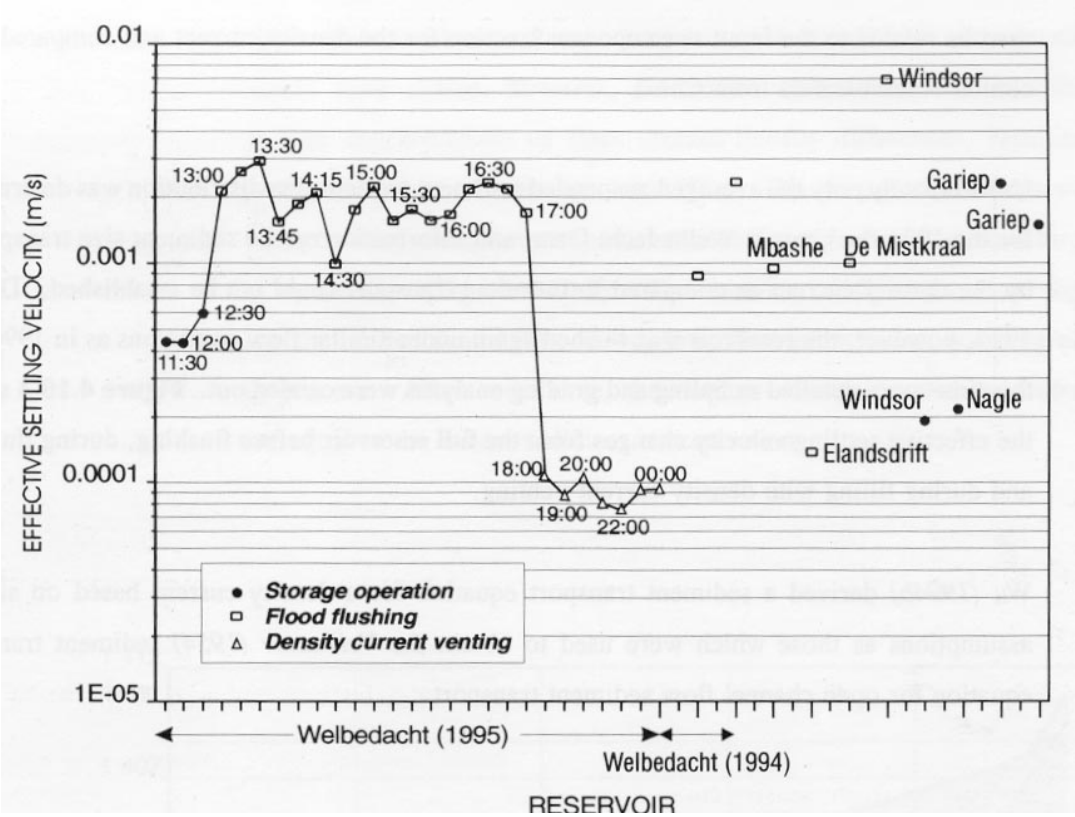

Figure 4.10-3 Reservoir operation and settling velocity based on observed sediment characteristics

Wu (1994b) derived a sediment transport equation for a density current based on similar assumptions as those which were used to obtain the *Velikanov (1954)* sediment transport equation for open channel flow sediment transport:

$$\overline{C} = K_1 \frac{\overline{v^3}}{gh\, w_{50}} \qquad (4.10\text{-}1)$$

with $\bar{v} = K_2 \sqrt{\frac{\Delta\lambda}{\gamma} gh}$

and K_1 , K_2 = constants

h = height of density current

w_{50} = settling velocity of median particle diameter

Field data of Guanting, Sanmenxia and Hongshan reservoirs with sediment concentrations < 100 kg/m^3 were used to calibrate **Equation 4.10-1** as indicated in **Figure 4.10-4** and **Equation 4.10-2**.

$$C = 12{,}75\left(\frac{v^3}{ghw_{50}}\right)^{0{,}285} \qquad (4.10\text{-}2)$$

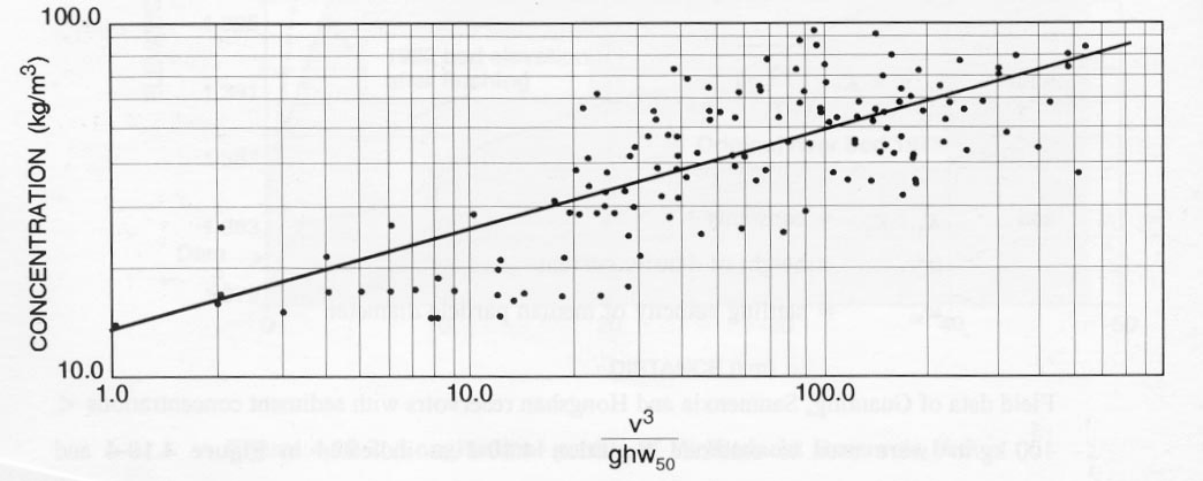

Figure 4.10-4 Chinese reservoir density current sediment transport relationship *(Wu, 1994b)*

Calculation of the input streampower versus sediment transport of the Welbedacht Reservoir density current shows a direct relationship **(Figure 4.10-5)** and also agrees with Chinese reservoir data **(Figure 4.10-4)**.

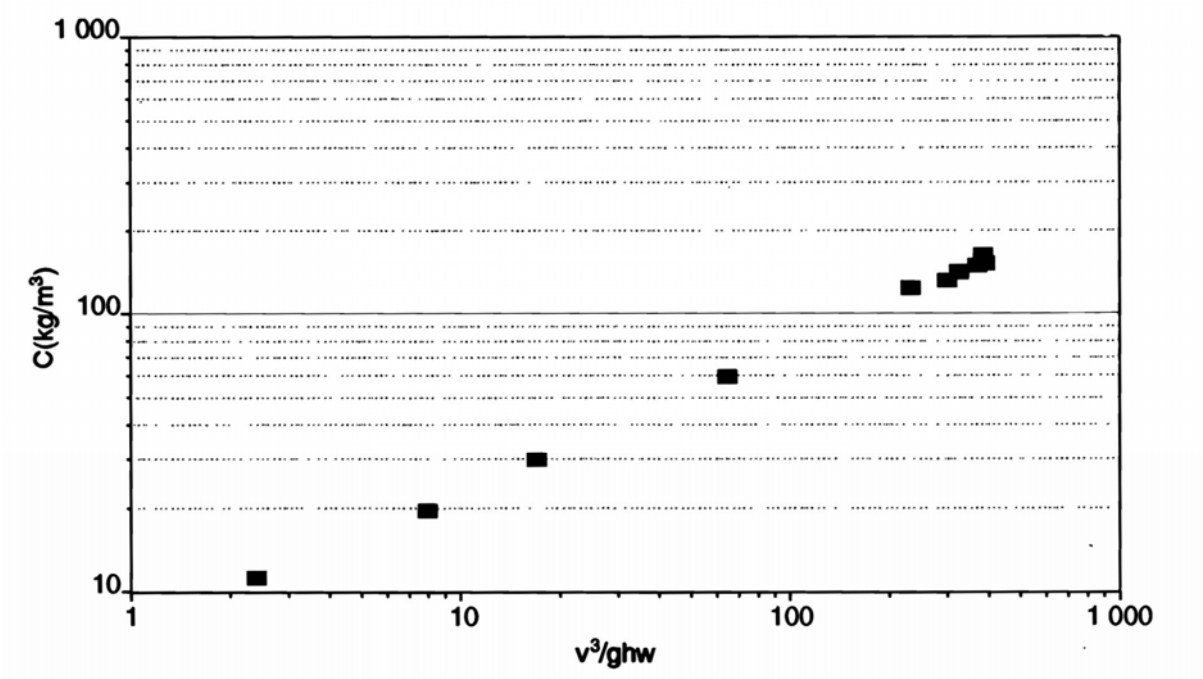

Figure 4.10-5 Welbedacht Reservoir density current sediment transport relationship

4.11 Non-equilibrium density current sediment transport

Wu (1994b) proposed the use of a non-equilibrium relationship in predicting/modelling sediment transport by density current through a reservoir, similar to the approach followed for turbulent fine sediment transport in reservoirs in China and also proposed in this study:

$$\frac{dC}{dx} = \frac{-\propto w}{vh}(C - C^{*}) \qquad (4.11\text{-}1)$$

with α = coefficient

C^{*} = equilibrium sediment concentration

v = density current velocity

h = density current depth

Equation 4.11-1 which has been calibrated for turbulent open channel flow conditions in this study (**Chapter 3**), will probably also be applicable in the case of density current sediment transport. Much more data collection and analyses of equilibrium sediment

transport in density currents need to be carried out, however, before a proper theoretical understanding of non-equilibrium sediment transport would be possible.

4.12 Graded sediment transport by density currents and the sorting process

Field data from China have been used to establish an empirical relationship between sediment size and transport:

$$\frac{C_x}{C_o}\ \% = 1{,}1.\ \frac{dx_{90}}{dD_{90}}\ \% - 12 \qquad (4.12\text{-}1)$$

with C_o = mean suspended sediment concentration at entrance (plunge point),
D_{90} = size of particles for which 90% of the material is finer, from the frequency distribution curve for the appropriate sample.

This relationship is shown graphically in **Figure 4.12-1** *(Wu, 1994b)*.

Non-uniform sediment transport in a density current can be predicted as for homogeneous open channel flow when the equilibrium sediment transport equation is calibrated for various particle sizes suspended in the density current.

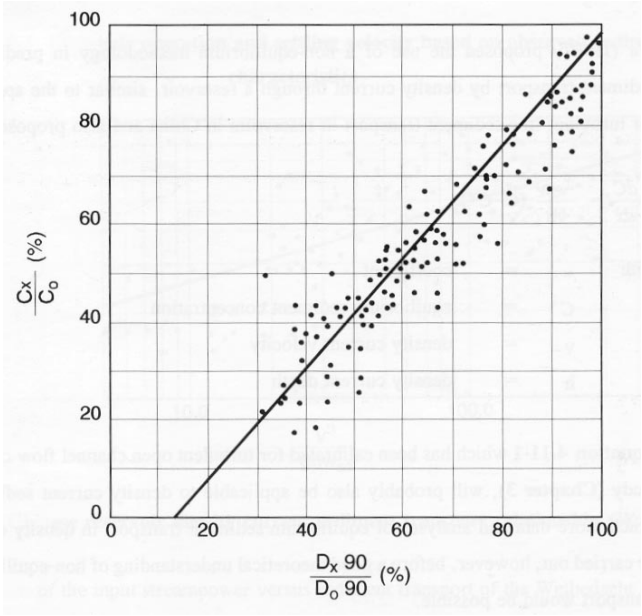

Figure 4.12-1 Graded sediment transport in a density current (*Wu, 1994b*)

4.13 Formation of a density current

4.13.1 Review of theory

Many attempts have been made to predict the formation of a density current:

Dequennois (1956) suggested $(\gamma' - 1)q$ as a criterion for the turbulent flow to form a density current.

Levy (1958) analysed the minimum silt concentration below which a density current will not occur.

Fan (1960) concluded that in the transition from open channel flow to density current flow, increases rapidly at the interface, and $\frac{dh'}{dx} \to \infty$. **Equation 4.6-9** can therefore be rewritten with

$$\frac{v^2}{\frac{\Delta\gamma}{\gamma'} gh'} = 1 \qquad (4.13\text{-}1)$$

From **Figure 4.13-1**, it is evident that the velocity decreases as the depth increases in the transition zone and that the velocity reaches a minimum value and the water depth a maximum value at the plunge point. Fan therefore proposed that the specific energy

$$E = h' + \frac{\mathrm{v}^2}{2\frac{\Delta\gamma}{\gamma}\mathrm{g'h}}$$

reached a minimum value at the plunge point, or

$$\frac{dE}{d'h} = 1 - \frac{q^2}{\frac{\Delta\gamma}{\gamma} gh_o^3} = 0$$

$$\frac{v_0}{\sqrt{\frac{\Delta\gamma}{\gamma'} g h_o}} = 1$$

This parameter is known as the densimetric Froude number (Fr_D).

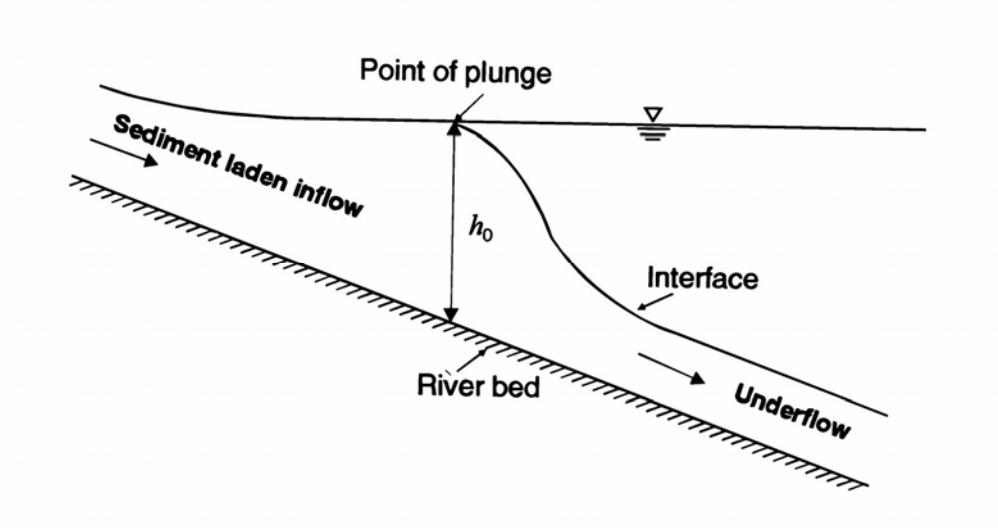

Figure 4.13-1 Schematic diagram of density current formation *(Fan, 1960)*

By conducting flume tests, *Fan* established a relationship for the densimetric Fr_D as given in **Figure 4.13-2**.

with (4.13-2)

$$\frac{v_o}{\sqrt{\frac{\Delta\gamma}{\gamma} g h_o}} = 0{,}78 (< 1)$$

Fan gave the reason for the experimental Fr_D value being < 1 as "a point of inflection in the streamlines at the interface, which is located downstream of the plunge point, where $Fr_D = 1$."

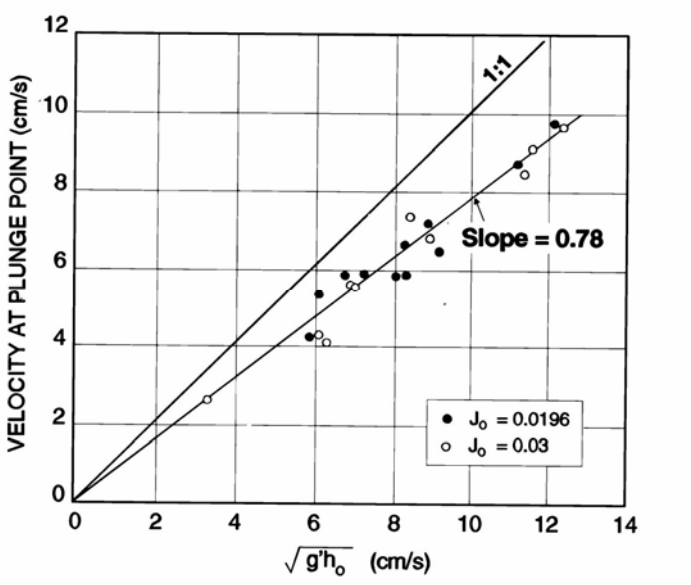

Figure 4.13-2 Densimetric Froude number and density current formation *(Fan, 1960)*

Fan (1986) found that the formation of density currents can be forecast by means of **Equation (4.13-2)** for concentrations < 100 kg/m^3. It was, however, found that the densimetric Froude number also depends on the inflow sediment concentration and decreases with increasing concentration. This explains why different researchers have found such a wide range of densimetric Froude numbers which predict density current formation from their experiments.

Cao (1992) published a relationship between Fr_D and the density difference **(Figure 4.13-3)**. It appears that when sediment concentrations are < 40 kg/m^3, $Fr_D \approx 0{,}78$. As the sediment concentration increases the density current changes from turbulent to transitional to laminar with hyperconcentrations.

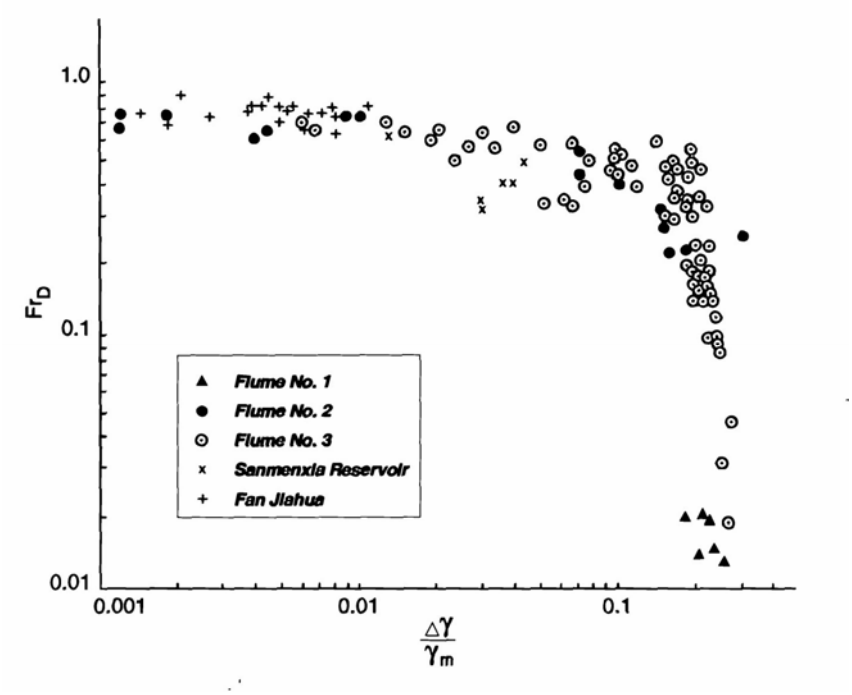

Figure 4.13-3 Densimetric Froude number and density difference ratio *(Cao, 1992)*

Akiyama et al., (1987) found an approximate average densimetric Froude number of 0,68 at plunging. The Fr_D was only weakly related to the inflow densimetric Froude number (F_o) and the angle of channel divergence as shown in **Figure 4.13-4**.

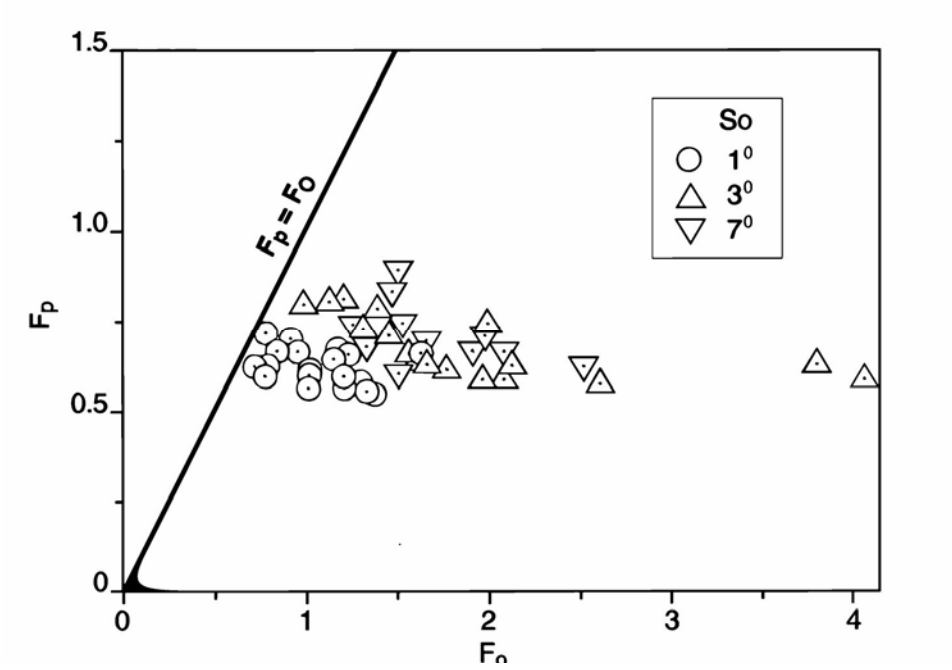

Figure 4.13-4 Densimetric Froude number *(Akiyama et al., 1987)*

Savage and Brimberg (1975) considered the plunging phenomenon in terms of equations of motion for gradually varying two-layer flow. The pressure distribution was considered to be hydrostatic and mixing was neglected. Different solutions for the interface profile were obtained depending on the bed slope and the relative importance of the two boundary shear stresses.

Denton et al. (1981) carried out experiments on temperature-induced density currents and found that for mild bed slopes, interfacial and bed shear stresses are important, but for steep slopes $(S_o > 0{,}02)$, momentum balance conditions at the plunge point dictate a maximum densimetric Froude number criterion of 0,67.

Singh and Shah (1971) and *Philpott (1978)*also conducted flume studies and obtained $Fr_D \approx 0{,}7$ for the plunge point, although a range of $0{,}3 < Fr_D < 0{,}7$ was observed.

The criteria for plunging used by the above researchers indicate a general variation of observed values $0{,}1 < Fr_D < 0{,}7$, which shows the unreliability of prediction of density current formation.

Previous studies have dealt with sloping channels, rectangular cross-sections of constant width, or triangular shapes that represent reservoir geometry. Investigations of the formation of a density current based on the densimetric Froude number show considerable variation, as is shown in **Table 4.13-1**.

Table 4.13-1: Densimetric Froude number (Fp) at plunging

Reference	Fp
Ford and Johnson (1980)	0,1 to 0,7
Itakura and Kishi (1979)	0,54 to 0,69
Singh and Shah (1971)	0,30 to 0,80
Kan and Tamai (1981)	0,45 to 0,92
Fukuoka and Fukushima (1980)	0,40 to 0,72
Farrell and Stefan (1986)	0,66 to 0,70
Akiyama et al. (1987)	0,56 to 0,89

Akiyama et al. (1987) showed that the angle of divergence also plays a role in estimating $\boldsymbol{F_p}$, but the scatter of data is still considerable.

Rooseboom (1975) also proposed a method to predict the formation of a density current. Consider a fluid element with density $\rho + \Delta\rho$ underneath a non-uniform fluid layer of density ρ. Under normal turbulent flow conditions, the element with length Δ_x is pushed forward owing to a pressure difference which exists across the element:

$$\Delta p = \rho g s_s . \Delta x \qquad (4.13\text{-}3)$$

with s_s = slope of surface line

ρ = mass density of upper fluid

In situations where density currents are important, the value of $\boldsymbol{s_s}$ is small and $\approx s_f$, the energy slope.

Due to the existing density difference, an additional pressure difference is generated across the element $= \Delta\rho g s_o \Delta x$ ($\boldsymbol{s_o}$ = reservoir bed slope).

The ratio

$$\frac{"density"\ pressure}{"turbulent"\ pressure} = \frac{\Delta\rho . s_o}{\rho . s_f} > 1 \qquad (4.13\text{-}4)$$

indicates the relative importance of density differences in the forward propulsion of sediments through reservoirs.

Using the Chezy equation, **Equation 4.13-4** can be rewritten:

$$\frac{\Delta\rho\, s_o C^2 R}{\rho\, v^2} \qquad (4.13\text{-}5)$$

with R = hydraulic radius, $\boldsymbol{C}$ = Chezy coefficient.

Density difference will therefore play an important role relative to turbulent suspension if the value of **Equation 4.13-5** is high, i.e. in cases of :

- large flow depths
- large density differences
- steep reservoir bed slopes
- low flow velocities.

Assuming $\frac{\Delta\rho}{\rho} \approx$ constant in all reservoirs, R = average water depth at full supply level, and taking the cross-sectional area as D^2,
the following dimensionless parameter was obtained:

$$\frac{s_o \cdot C^2 \cdot D^5}{Q^2} \qquad (4.13\text{-}6)$$

with Q = discharge, with sufficient sediment transport capacity through reservoir.
The data in **Table 4.13-2** were used to calibrate **Equation 4.13-6**

With the limited data it is difficult to obtain a definite relationship. Conditions in Treska Reservoir represent a poorly developed density current and therefore a value of > 10000 for the dimensionless parameter was assumed *(Rooseboom, 1975)*.

Table 4.13-2 Density current formation *(Rooseboom, 1975)*

Reservoir	**s_o**	**D(m)**	**Q(m^3/s)**	**C($m^{1/2}$/s)**	$\left(\frac{So.C^2 \cdot D^5}{Q^2}\right)$ **2**
Lake Mead	0,00074	82	500	70	54 000
Sautet	0,018	50	200	63	56 000
Treska	0,004	10	9,5	55	13 000
Sengari	0,0049	16	1	59	18 000 000

4.13.2 Prediction by means of minimum stream power principle

A flowing stream of water with a movable bed will always try to change the boundary conditions imposed on it until equilibrium conditions are reached. At equilibrium the energy dissipation per unit volume is minimized. In terms of applied stream power, this means that the flow can adjust the values of κ, k_2 D and s_f in **Equation 4.13-7**.

$$\tau \frac{d\,\mathrm{v}}{\mathrm{dy}} = 30\,\rho\,\mathrm{g}\,\mathrm{s_f}\,\mathrm{D}\,\frac{\sqrt{\mathrm{gD\,s_f}}}{\kappa.\mathrm{k_s}} \qquad (4.13\text{-}7)$$

Minimization of streampower will also be the reason why a turbulent stream dives to the reservoir bed to progress as density current through the reservoir. At the plunge point (as indicated in **Figure 4.13-5**) input streampower for the density current should therefore become equal to or less than that of the turbulent inflow, assuming that the streampower in the upper layer is approximately zero as $v \to o$ in the upper layer.

At the plunge point from streampower continuity:
Streampower of turbulent inflow = streampower of density current

$$\int_{y_o}^{D} \rho g \bar{v} s_f = \int_{y_o}^{d} \Delta\rho g \bar{v} s_o \qquad (4.13\text{-}8)$$

Therefore, for a density current to form it is expected that:

$$\frac{\Delta\rho g Q\, s_o}{\rho g Q\, s_f} \le 1 \qquad \text{and from continuity this simplifies to} \qquad (4.13\text{-}9)$$

$$\frac{\Delta\rho s_o}{\rho s_f} \le 1 \qquad (4.13\text{-}10)$$

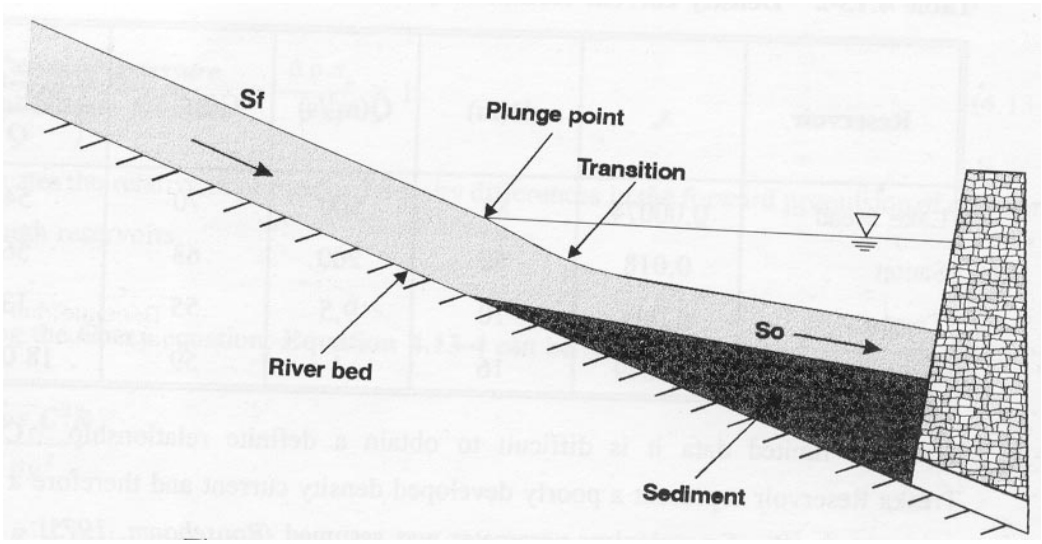

Figure 4.13-5 Plunge point characteristics

Laboratory data on the plunge phenomenon are rather scarce since most experiments have concentrated on uniform density current movement. As a preliminary test of **Equation (4.13-10)**, laboratory data of *Akiyama et al. (1987)*, in which the density difference was created by temperature differences, was used **(Figure 4.13-6)**.

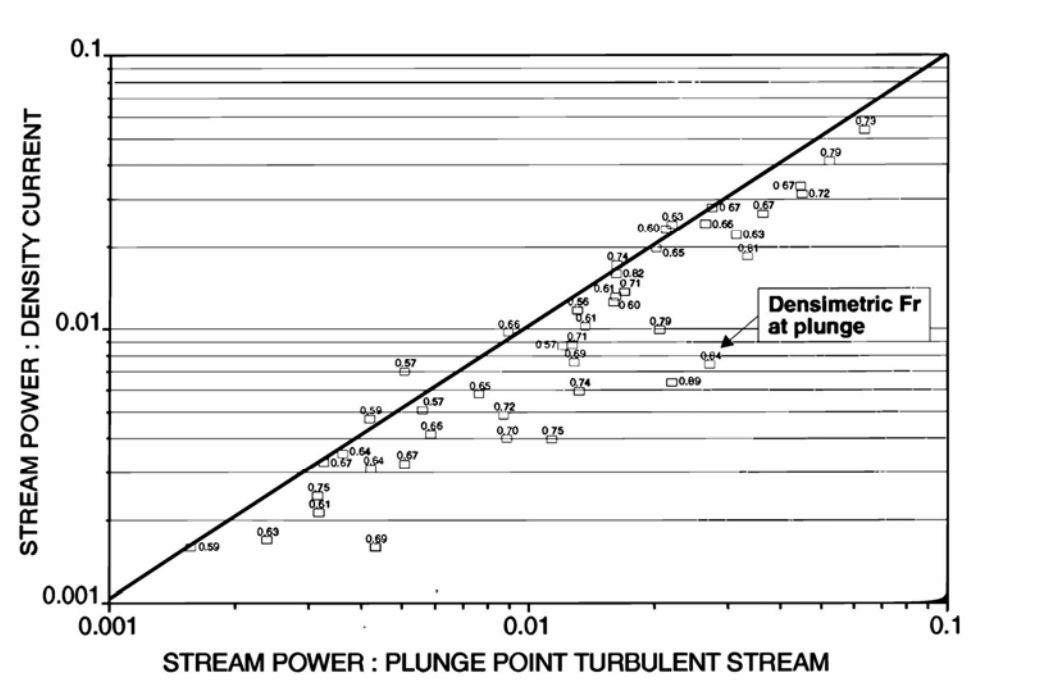

Figure 4.13-6 Density current formation and minimum stream power

Verification of **Equation 4.13-10** to test for density current formation does indeed show that less streampower is used by the density current than by turbulent open channel inflow. Furthermore, **Figure 4.13-5** shows that the densimetric Froude number does not provide an accurate means of predicting density current formation due to the large scatter in values. The general trend indicates a lower density current stream power value as the densimetric Froude number increases.

Even if the stream power in the layer above the density current is added to that of the density current streampower, the difference will be negligible due to the small slope (due to the reservoir depth) and low velocity in the upper layer.

Equation 4.13-10 seemingly contradicts the **Equation 4.13-4** proposed by *Rooseboom (1975)*, who stated that larger density differences, larger slope s_o, and smaller slope s_f (of reservoir) will provide better conditions for density current formation. A steep bed slope in the reservoir and large density difference will indeed help to ensure the continuous movement of the density current through a reservoir, but what **Equation 4.13-10** in fact says is that at the plunge point a steeper approaching turbulent flow slope s_f will create favourable conditions for density current formation as the river meets the water mass in the reservoir. The high momentum of the inflowing river enables it to dive underneath the water mass, and once near the bed the density difference creates the density current flow and prevents a "hydraulic jump" of the submerged flow, with consequent turbulent suspended sediment transport through the reservoir. This is shown schematically in **Figure 4.13-5**.

Field and laboratory studies indicate that the density differences between riverflow/density current and reservoir water can be very small. The dominant variables therefore in the formation of a density current (given that there is some density difference), are the river and density current slope differences. On the other hand, the bed slope in the reservoir still needs to be steep enough for the propagation of the density current after formation.

Equation 4.13-10 also shows that for a given inflow river slope, the reservoir bed slope at the plunge point has an upper limit at which turbulent mixing can prevent a density current from forming.

4.14 Laminar density currents associated with hyperconcentrated sediment transport

So far only the characteristics of turbulent density currents have been addressed. Laminar density currents also occur and are associated with hyperconcentrated sediment transport.

First, consider the differences between vertical velocity distribution in laminar and turbulent density currents as shown in **Figure 4.14-1** *(Cao, 1992).*

Figures 4.14-1a and **4.14-1b** show typical laminar conditions in the density current. At Reynolds number (Re_n) < 43 (**Figure 4.14-1a**), the boundary condition at the interface is laminar, the resistance at the interface is relatively small, and the profile of velocity distribution of the density current is similar to that of open channel flow. The resistance at the interface is, however, not negligible as in homogeneous flow.

From flume studies, *Cao (1992)* established three types of plunging patterns **(Figure 4.14-2)**:

Type A: Supercritical open channel flow with hydraulic jump transition at the plunge point.

Type B: Subcritical open channel flow with mild undulation transition to density current.

Type C: Hyperconcentrated homogeneous laminar open channel flow with still transition to density current. Two types C can be further observed: $J_m = J_o$ **(Figure 4.14-2C)** and $J_m > J_o$ (**Figure 4.14-2C[1]**). In the latter the plunging point is not stationary but keeps progressing until reaching the point where a non-uniform density current forms with the stable gradient $J_m = J_o$ when the plunging point becomes stationary.

The flow velocity, sediment transport and prediction of formation of laminar density currents can be derived following similar approaches as with turbulent density current flow in the previous sections.

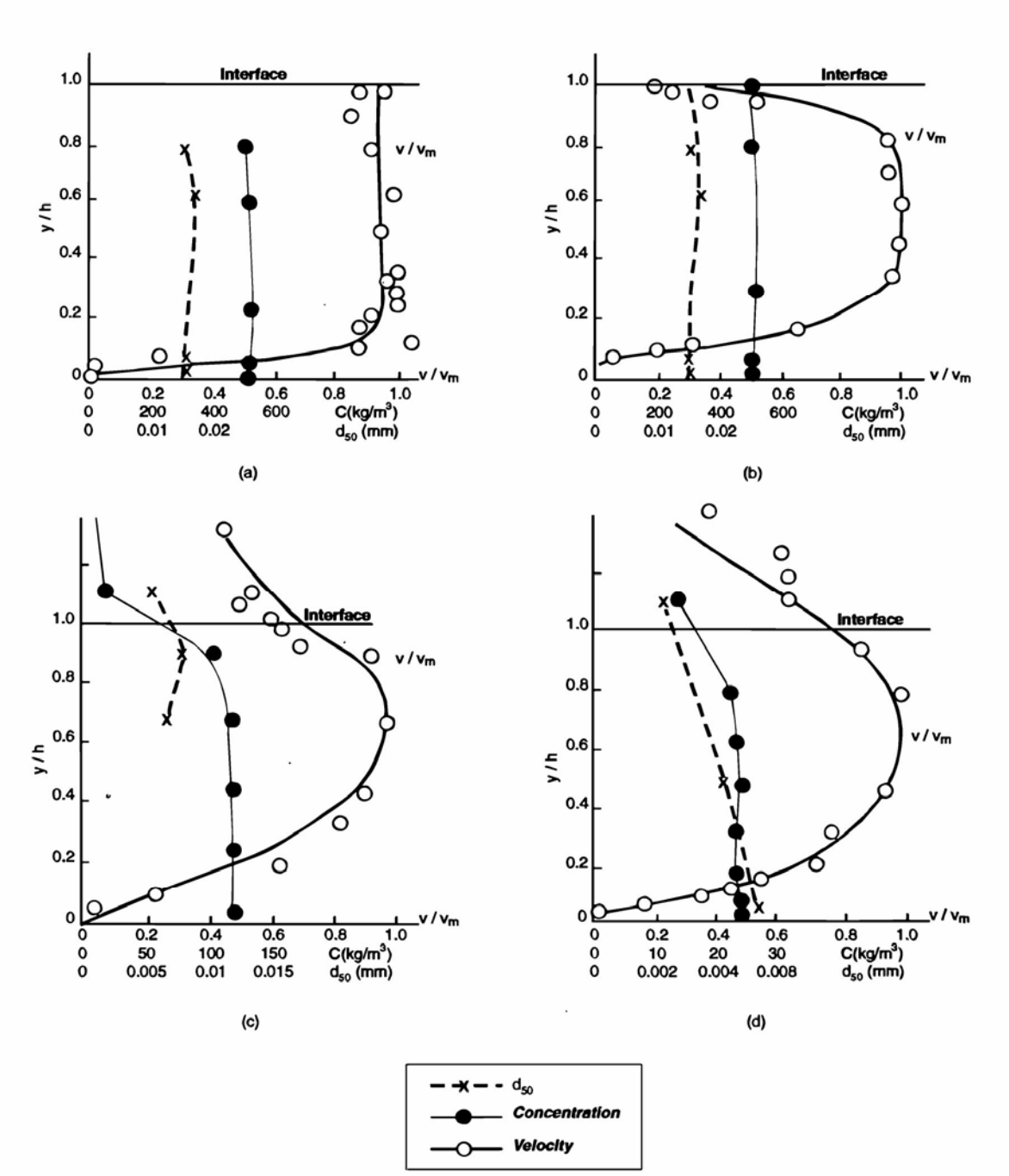

Graph	Q(ℓ/s)	S(kg/m³)	Re_m	$\bullet_m$	K
(a)	2.5	520	11.6	9.26	107
(b)	2.5	410	70	1.71	120
(c)	2.5	124	1 250	0.15	188
(d)	2.5	24	38 300	0.041	

Figure 4.14 - 1 Typical density current velocity distribution *(Cao, 1992)*

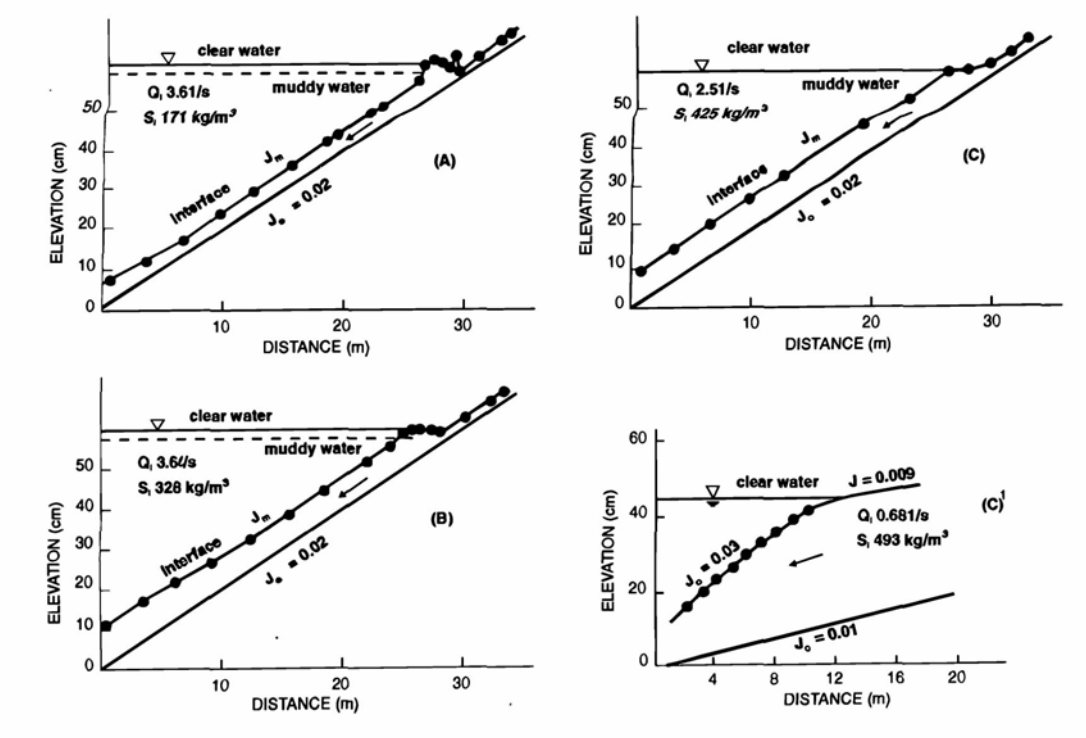

Figure 4.14 - 2 Profile of interface of density current *(Cao, 1992)*

4.15 Venting of density currents through reservoirs

When a density current reaches the dam, it can either be vented through bottom outlets or will "climb" up the dam and fall back to form a muddy pool. The climbing nature of the density current can be utilized to vent the density current at a high level. By either providing a siphon type outlet or curtain at the dam, the density current can be aided to flow out at even higher levels above the bed. This approach will be especially useful at existing reservoirs without bottom outlets and where density current flows are experienced.

Bell (1942) indicated the possibility of using a curtain near the dam in flume studies as shown in **Figure 4.15-1**.

Fan (1960) investigated the maximum height up to which a density current can "climb" to be vented and found that openings directly in the path of a density current were the most efficient.

Laboratory results indicated that the maximum height (h_L) to which a density current can climb to be vented through a circular outlet *(Wu, 1994b)*:

$$h_L = \left(\frac{0{,}154 \lambda Q^2}{\Delta \gamma g} \right)^{1/5} + \left(\frac{\gamma_o q^2}{2 \Delta \gamma g h^2} \right) \qquad (4.15\text{-}1)$$

with q = unit width density current discharge (m^2/s)

h = height of density current (m)

Q = outlet capacity (m^3/s)

γ = specific weight of clear-water (kg/m^3)

γ_o = specific weight of turbid water

The discharge capacity of outlets should equal the density current flow for maximal discharge of transported suspended sediments. Secondly the outlets should not be too high above the bed, but at a maximum elevation given by the potential energy of the density current, represented in the last term of **Equation 4.15-1**.

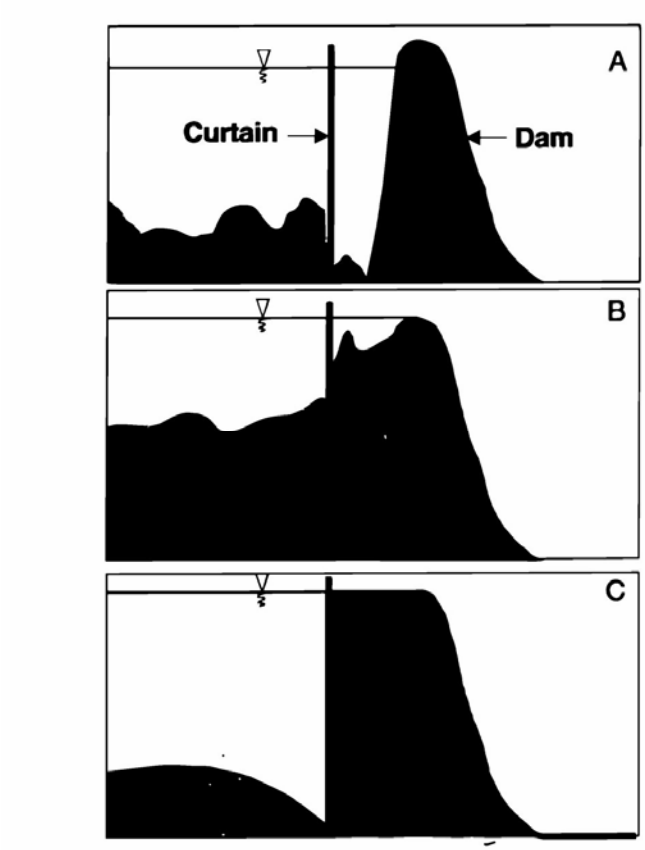

Figure 4.15-1 Density current climbing *(Bell, 1942)*

5. MATHEMATICAL MODELS AND CASE STUDIES

5.1 One dimensional mathematical models

5.1.1 Introduction

The theory derived and discussed in previously chapters can now be used to predict long-term equilibrium reservoir sedimentation. Not only sediment deposition during storage operation, but also flood flushing with retrogressive erosion have to be evaluated in order to make accurate predictions of long-term sedimentation. In this chapter one dimensional and state-of-the-art two dimensional (2D plan) models are described with representative case studies of turbulent (1D) sediment transport. Mathematical modelling of density current sediment transport is also described in 2D and 3D models.

It is not the idea to promote specific models in this Chapter, but rather to indicate the key characteristics such a model should have. The following turbulent sediment transport models and case studies are presented in this chapter:

- Mike 11 – Reservoir Flushing Model (1D) – Welbedacht Dam, South Africa. Deposition and erosion model designed to simulate deposition and flushing in cohesive and non-cohesive sediments.
- GSTARS – Tarbela Dam, Pakistan. Quasi 2D using stream tubes and equilibrium non-uniform sediment transport equation.
- RESSASS (1D) – Tarbela Dam, Pakistan. Coarse and fine sediment fractions.
- Mike 11 (1D) – Roxburgh Dam, New Zealand River model used on reservoir. Non-cohesive sediments.
- Mike 21 (2D) (quasi 3D) – Welbedacht Dam, South Africa.
  Modified river model to be applicable to shallow reservoirs with fine cohesive sediment transport.
- 3D model with Three Gorges project case study, China.

5.1.2 Reservoir sedimentation model (1D): Mike 11-RFM: Welbedacht Reservoir

5.1.2.1 Model description

Several mathematical models have been developed in the past to simulate reservoir sedimentation deposition processes, but only a handful have been designed to simulate sluicing/flushing with reservoir water level drawdown *(Han, et al., 1973, 1990; Thomas and Prasuhn, 1977; Chollet and Cunge, 1980; Sanchez, 1982; Zhang, et al., 1983; Pitt and Thompson, 1984; Holly and Rahuel, 1990; Yang, 1992; Vasiliev et al., 1993; Wang, 1993;, etc)*. Although most "river" mathematical models can simulate the latter condition, which are close to river flow conditions, there are factors such as fine sediment transport, cohesive sediment deposits, consolidation of the bed, as well as different modes of re-entrainment of sediment which also need to be accounted for.

For modelling of reservoir sedimentation processes, a model should be able to simulate both short-term (flushing) and long-term deposition events, with non-cohesive and cohesive sediments. It should be borne in mind that the "ideal" mathematical model is only as good as the theory it is based on.

The mathematical model MIKE 11 of DHI Water and Environment has been modified to incorporate the theory for reservoir sedimentation processes, which has subsequently been calibrated and verified with reservoir data. The reservoir flushing model which has been developed has the following characteristics:

a) **One-dimensional (1D) Model**

One-dimensional models are mostly used in river and reservoir applications around the world, although computationally "heavy", two-dimensional (2D) and even 3D models have been developed. The main constraints in using a 2D model with sediment transport is often a lack of data for calibration of the model and the long simulation run times required. For flushing application, a 1D model could be adequate due to the river-like flow conditions which prevail in the narrow channel which is formed when reservoir flushing is practised.

Two-dimensional models can be of specific benefit when considering:

- deposition outside the main channel across the wide-open reservoir basins often encountered;

- sediment build-up at a specific position in a reservoir, such as at a tunnel or hydropower intake; and

- modelling of flushing when sediment transport conditions vary across the main channel.

b) **St Venant equations for hydrodynamic simulation**

A fully hydrodynamic approach is required to describe the rapidly changing flow and bed level conditions during flushing. The model must also be able to simulate the supercritical flow conditions which can be encountered during drawdown flushing. Typical outflow conditions during flood flushing are indicated in **Figure 5.1.2-1** as observed at Phalaborwa Barrage, 1996.

Figure 5.1.2-1 Phalaborwa Barrage flood flushing (900 m^3/s, February 1996)

c) **Sediment transport**

The unit (input) stream power equation *(Yang, 1973)* was implemented in the MIKE 11 model by using user-defined input parameters M and N in **Equation 5.3-1**:

$$\log(C) = M + N \log\left(\frac{vs}{w_i}\right) \qquad (5.3\text{-}1)$$

with C = sediment concentration (ppm)
M,N = values defined by user
v = flow velocity
s = energy slope
w_i = settling velocity of fraction i.

Equation 5.3-1 has been calibrated with data from a number of South African reservoirs for flood flushing and storage operation conditions as described in Chapter 3, with M = 4,31 and N = 0,343.

Several other well-known sediment transport equations are also available in the MIKE 11 model to simulate transport of coarse fractions.

d) **Coupled solution of flow and sediment equations, with sediment continuity**

A coupled solution is required due to the rapidly changing hydrodynamic and sediment transport conditions during flushing and during floods when sediment is deposited.

e) **Non-uniform sediment modelling**

It is essential in reservoir modelling that sediment transport calculations are carried out per size fraction in order to model the sorting process and related non-cohesive and cohesive deposits through the reservoir.

f) **Non-equilibrium transport of fine sediments**

Non-equilibrium transport of fine sediments occurs, which means that transition to saturated sediment transport capacity conditions is not instantaneous as for coarser fractions, but a time and distance lag is involved. The multifraction model (MIKE 11) can operate with a traditional equilibrium transport equation for some fractions and a non-equilibrium formula for others.

The non-equilibrium modelling is based on solution of the unsteady advection-dispersion equation, with a source/sink term ***(ss)*** describing erosion and deposition:

$$\frac{\delta C}{\delta t} + u\frac{\delta C}{\delta x} - D\frac{\delta^2 C}{\delta x^2} = ss \qquad (5.3\text{-}2)$$

with D = the dispersion coefficient,
u = flow velocity
t = time
x = distance in direction of flow

In the case of non-cohesive sediments the source/sink term (ss) is represented by:

$$ss = \frac{\left(C^* - C\right)}{aT} \qquad (5.3\text{-}3)$$

with C^* = the equilibrium sediment transport calculated with a sediment transport formula,
"T" = the time scale defined as settling time (water depth divided by settling velocity),
"a" = a calibration parameter as described in **Chapter 3** and can be interpreted as a mean (relative) settling depth. In the model implementation, the coefficient "a" is different for various given size fractions, for erosion and deposition.

For non-cohesive sediments, incipient motion is determined according to the sediment transport model used. For cohesive sediment (fractions) the source/sink term should be represented by:

$$ss = 0 \qquad ; \tau < \tau_{ce} \qquad \text{(No erosion)} \tag{5.3-4}$$

$$ss = E(\tau - \tau_{ce}) \quad ; \tau_{ce} < \tau < \tau_{cme} \quad \text{(Surface erosion)} \tag{5.3-5}$$

$$ss = \frac{\left(C^{*} - C\right)}{\Delta t} \; ; \; \tau > \tau_{cme} \qquad \text{(Mass erosion, no lag)} \tag{5.3-6}$$

with τ = bed shear stress,
τ_{ce} = critical shear stress for surface erosion,
τ_{cme} = critical shear stress for mass erosion,
E = erosion rate.

g) **Calculation of erosion**

The model combines theory for non-cohesive and cohesive sediment to model three cases of erosion: cohesive sediment, non-cohesive sediment and a mixture of the two. In the latter case, a linear combination of the cohesive and non-cohesive relationship is used. The erosion rate, assuming both cohesive and non-cohesive sediments, is calculated, and the actual rate determined via linear interpolation.

For surface erosion, the erosion rate is checked against sediment transporting capacity in order not to exceed the capacity. Mass erosion modelling is based on the assumption that (instantaneous) erosion will take place to satisfy the sediment transporting capacity.

The availability of sediment for erosion is checked. If the calculated erosion rate exceeds the available sediment supply, the rate is reduced to reflect the amount of available sediment.

h) **Cross-section deformation**

Solution of the bed continuity equation determines whether erosion or deposition will occur.
When deposition occurs it is assumed that:

$$dz = aD^b \qquad (5.3\text{-}7)$$

with *dz* the change in bed level, *a* and *b* input calibration parameters and *D* the flow depth.

During erosion phases it is assumed that the cross-section will be of a trapezoidal shape described by regime type equations (relating width and depth to the discharge). Bank slopes of the trapezoid are required as input parameters. The difference between the actual bed level and that of the trapezoidal section is integrated to determine what changes are required.

The following special cases have been identified:

- The trapezoidal section is "smaller" than the actual section: **Equation 5.3-7** is used for changing the bed level

- Erosion goes below the original (bedrock) section : increase width if bed is non-erodible and lower bed if sides are non-erodible; otherwise erosion is limited.

Typical surveyed cross-sections of Welbedacht Reservoir are shown in **Figure 5.1.2-2.**

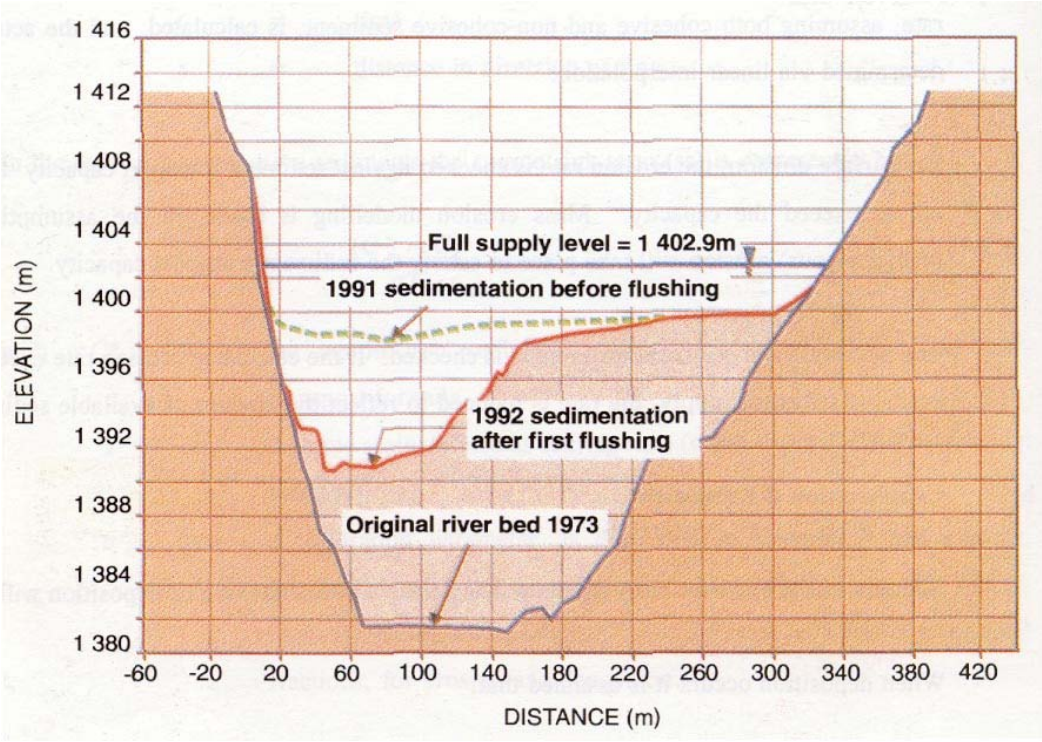

Figure 5.1.2-2 Welbedacht Reservoir flushing channel deformation

i) **Consolidation of sediments**

Modelling of consolidation is important when critical conditions for mass erosion are linked to sediment characteristics and density. A consolidation methodology as proposed by *Miller (1953)* which relates sediment density changes with time to reservoir operation and sediment characteristics was incorporated in the model, with certain changes:

- The consolidation constant used by *Miller (1953)* was calibrated with South African reservoir data based on reservoir basin surveys. This was necessary because it was found that sedimentation and changing water demands lead to changes in reservoir operation patterns in time.
- Erosion and deposition rates are not constant with time, and the integration method adopted by Miller had to be changed by incorporating an effective time approach which accounts for previous deposits as well as recent changes in the bed surface.

5.1.2.2 Calibration and verification of the 1D model (RFM) with South African reservoir data

a) General

A number of South African reservoirs have been monitored during flood flushing events since 1993. The data for Welbedacht Reservoir are used here to calibrate the 1D model. Welbedacht Dam **(Figure 5.1.2-3)** was completed in 1973 on the Caledon River and is located in a high sediment yield region. During the first three years of operation, it had lost 36 million m^3 of its original 114 million m^3 capacity due to sedimentation. By 1991 the full supply capacity was only 17 million m^3.

Figure 5.1.2-3 Welbedacht Dam

During 1991 it was decided to use flood flushing in order to regain some of the storage capacity. The dam is equipped with five gates, but their elevation is 15 m above the original river bed. Two flushings during October 1991 managed to scour a channel with a bed width of approximately 50 m, and a longitudinal bed profile as indicated in **Figure 5.1.2-4**. During subsequent flood flushings during the rainy seasons of 1994 and 1995, additional field data were gathered with which the 1D model was calibrated and verified.

5.1.2.3 Calibration of the 1D model

The bed shear stress required for mass erosion was determined for two flood flushings during October 1991, using a trapezoidal flushing channel profile in the model and the 1991 sedimentation levels. The scoured bed profile as surveyed in 1992 after the flushings was compared with simulated profiles and a critical mass erosion bed shear stress at the end of flushing was determined.

Unfortunately, sediment transport loads were not measured during the 1991 flushings and the model could therefore only be calibrated in terms of bed shear stress to achieve the observed scoured bed profile. A sediment transport equation calibrated in this bulletin using existing data from a number of South African reservoirs (with flushing and storage operation) was used. The observed and calibrated bed profiles are shown in **Figure 5.1.2-4**. Observed inflows and water levels at the dam, with inflow suspended sediment concentrations based on a sediment load-discharge rating curve were used as boundary conditions in the model. The surveyed 1991 reservoir bed was used as the starting condition, and calibration was based on the surveyed 1992 reservoir bed profile.

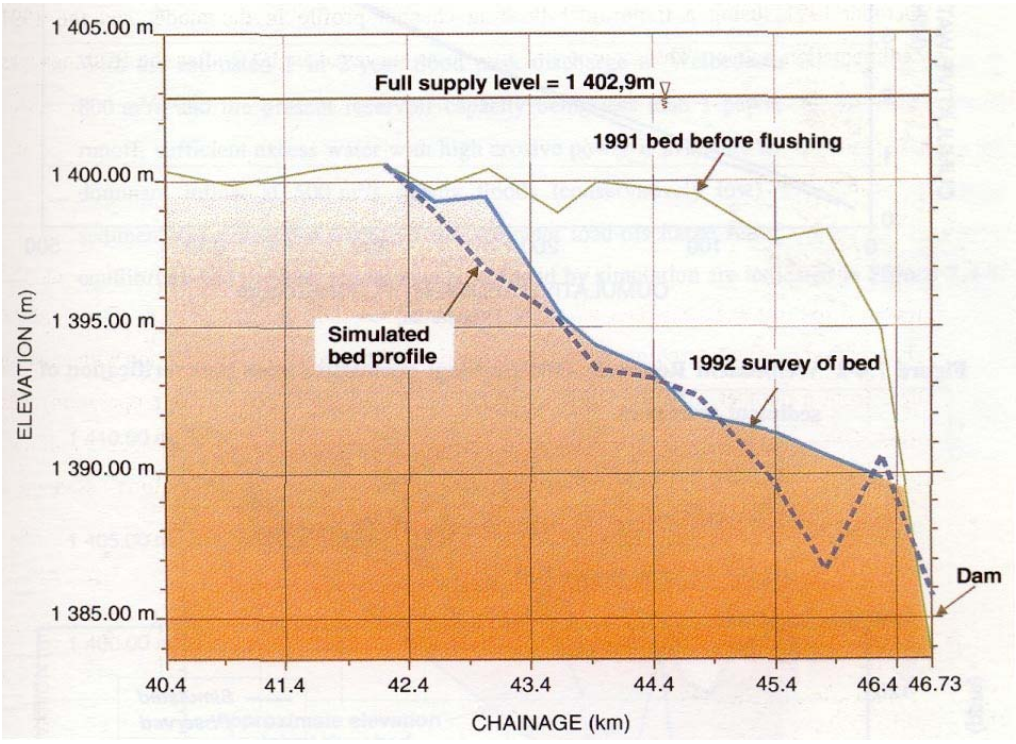

Figure 5.1.2-4 Calibrated and observed flushing channel bed profiles at Welbedacht Reservoir

5.1.2.4 Verification of the 1D model

Using exactly the same model setup which had been used to determine shear stresses (1991 flushings), it was possible to simulate a 1995 flushing at Welbedacht Dam while using as input the stream power relationship which had been calibrated with South African reservoir data. The simulated curve of cumulative water discharge versus cumulative flushed sediment is shown in **Figure 5.1.2-5**, and excellent agreement with observed data was obtained. The observed and predicted sediment transport versus time relationship is shown in **Figure 5.1.2-6**. The 1D model prediction reliability has therefore been proven by the 1995 flushing event.

Although not calibrated for a wide range of flood events, the calibrated model for Welbedacht Reservoir might be used to investigate changes in the outlet configuration and operation to improve sluicing/flushing efficiency and to predict sustainable long-term equilibrium reservoir storage capacities.

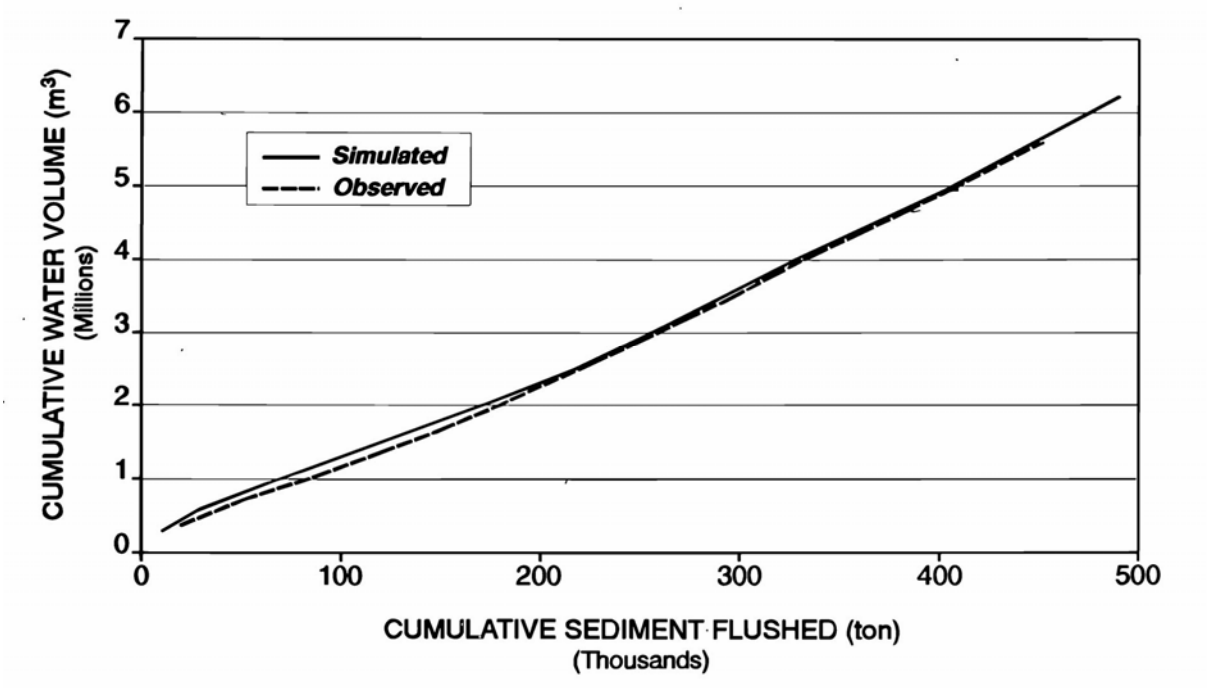

Figure 5.1.2-5 Welbedacht Reservoir 1995 flushing; cumulative double mass plot verification of sediment transport

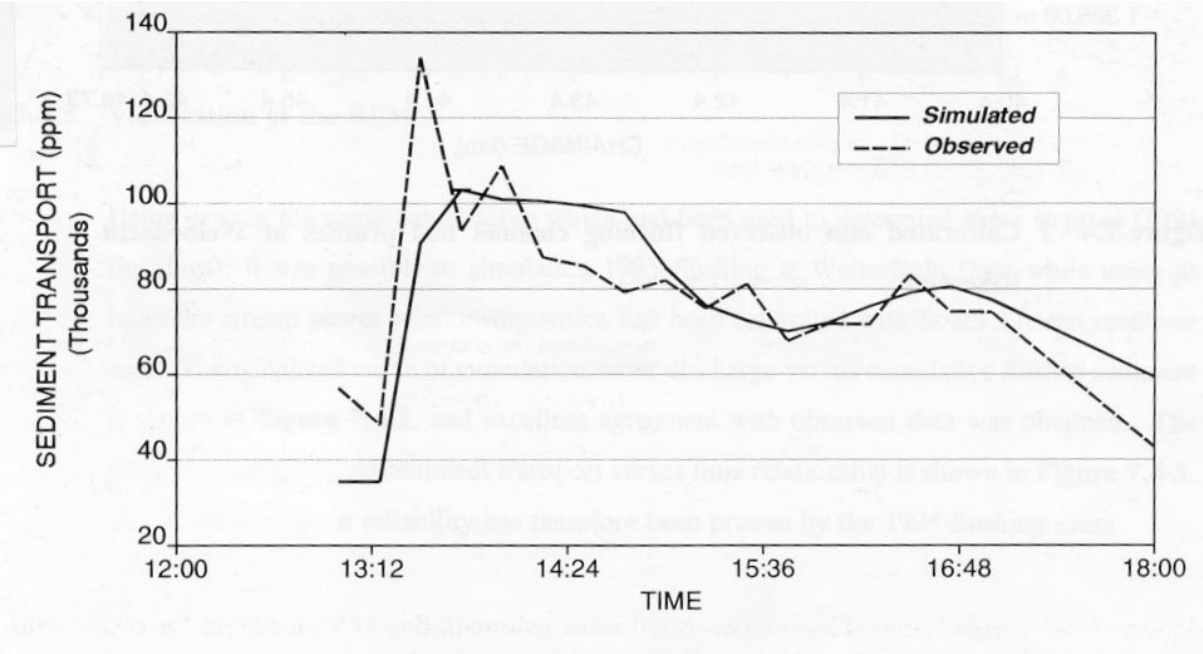

Figure 5.1.2-6 Welbedacht Reservoir 1995 flushing; verification of sediment transport modelling

5.1.2.5 Simulation of long-term Welbedacht Reservoir capacity

Using the same model configuration as calibrated and verified in the previous sections, simulation of the long-term reservoir capacity which could be achieved through flood flushing was carried out with the current outlets (at a high elevation), but also a scenario with hypothetical gates located at the original river bed.

With the estimated 1 in 2-year flood peak discharge at Welbedacht Dam being equal to 800 m^3/s and the present reservoir capacity being less than 1 percent of the mean annual runoff, sufficient excess water with high erosive power is available for flushing. Taking the dominant inflow at 500 m^3/s during floods (conservatively low) and inflow suspended sediment concentrations based on the sediment load-discharge rating curve, the long-term equilibrium bed profiles which have been found by simulation are indicated in **Figure 5.1.2-7**.

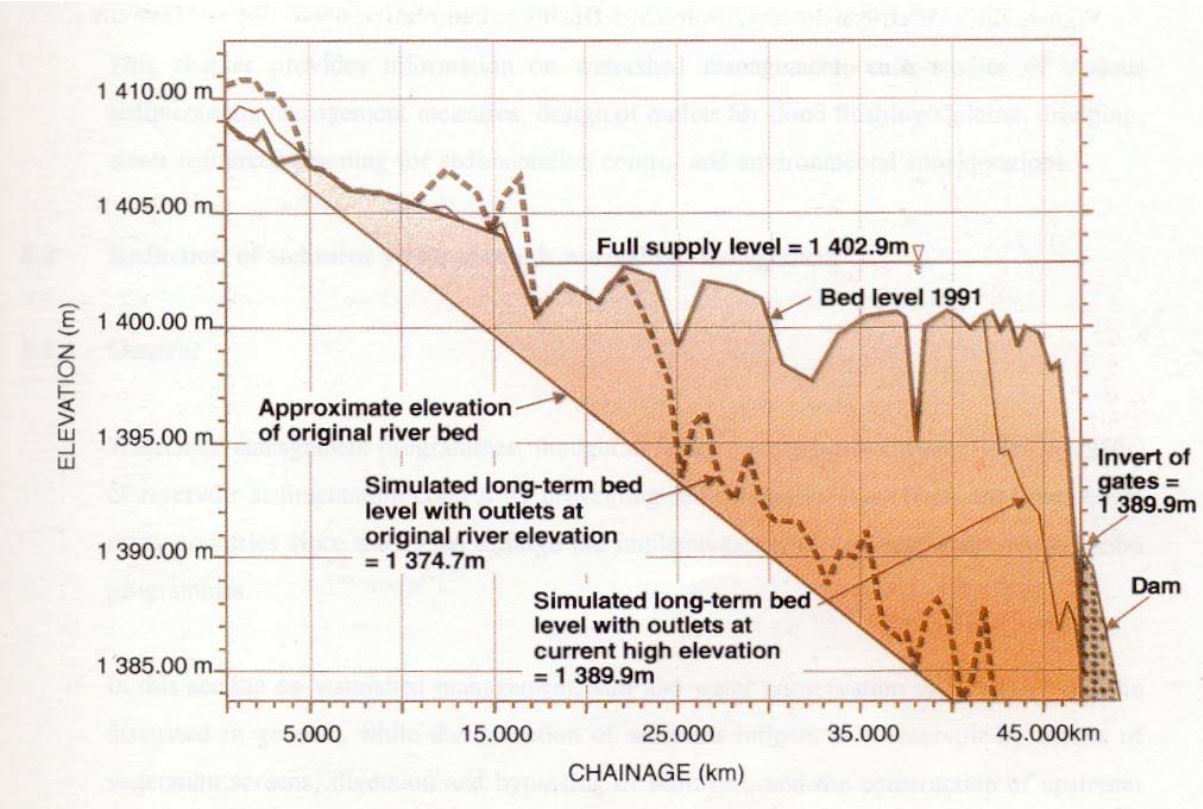

Figure 5.1.2-7 Simulation of long-term equilibrium sedimentation at Welbedacht Reservoir with flood flushing and different outlet configurations

The current high elevation of the outlets prevents retrogressive erosion far upstream from the dam. In the scenario with bottom outlets and water level drawdown, flushing will be much more efficient. According to **Figure 5.1.2-7** it looks as if a major part of the original 114 million m^3 reservoir capacity can be restored, but only the flushing channel will be scoured down to the original bed level with bottom outlets provided. The flushing channel shape determines the long-term storage capacity of the reservoir, and overbank sediment deposits will not be resuspended during flushing (unless flushing duration is long and meandering of the flushing channel develops). The long-term equilibrium storage capacities that can be maintained, simulated with high outlet (current) and bottom outlets, are 10 million m^3 and 30 million m^3, respectively.

The Mike 11 – RFM considers deposition and erosion processes. Simulation results with this model for a 1973-1976 deposition period (used for calibration) is presented in Chapter 3.

5.1.3 Reservoir Sedimentation Model: GSTARS: Tarbela Dam, Pakistan (Yang and Simoes, 2003)

5.1.3.1 Background

Tarbela Dam, located in northern Pakistan along the Indus River, is the largest earth-fill dam in the world. The reservoir, with a gross storage capacity of 14340 million m^3, is a 38 km long run of the river type of reservoir with two major tributaries, the Siran and the Brandu. Tarbela's main function is provision of water for irrigation. Additionally, the hydropower capacity of the power station totals 3478 MW and produces 32% of Pakistan's needs. The reservoir's storage capacity has been continuously depleted since the dam has been built in 1974, with an annual inflow rate of 265 million tons of sediment, most of which in the silt and clay range. This loss in capacity threatens the resources and revenue associated with the dam and reservoir.

5.1.3.2 Mathematical model description

GSTARS3 (Generalized Sediment Transport model for Alluvial River Simulation is the most recent version of a series of numerical models for simulating the flow of water and sediment transport in alluvial rivers developed at the Sedimentation and River Hydraulics Group of the Technical Service Center, U.S. Bureau of Reclamation, Denver.

GSTARS consists of four major parts. The first part uses both the energy and the momentum equations for the backwater computations. This feature allows the program to compute the water surface profiles through combinations of subcritical and supercritical flows. In these computations, GSTARS3 can handle irregular cross sections regardless of whether single channel or multiple channels are separated by small islands or sand bars.

The second part is the use of the stream tube concept, which is used in the sediment routing computations. Hydraulic parameters and sediment routing are computed for each stream tube, thereby providing a transverse variation in the cross section in a semi-two-dimensional manner. Although no flow can be transported across the boundary of a stream tube, transverse bed slope and secondary flows are phenomena accounted for in

GSTARS3 that contribute to the exchange of sediments between stream tubes. The position and width of each stream tube may change after each step of computation. The scour or deposition computed in each stream tube give the variation of channel geometry in the vertical (or lateral) direction. The water surface profiles are computed first. The channel is then divided into a selected number of stream tubes with the following characteristics: (1) the total discharge carried by the channel is distributed equally among the stream tubes; (2) stream tubes are bounded by channel boundaries and by imaginary vertical walls; (3) the discharge along a stream tube is constant (i.e., there is no exchange of water through stream tube boundaries).

The third part is the use of the theory of minimum energy dissipation rate (Yang, 1971, 1976; Yang and Song, 1979, 1986) in its simplified version of minimum total stream power to compute channel width and depth adjustments. The use of this theory allows the channel width to be treated as an unknown variable, which is one of the most important capabilities of GSTARS3. Whether a channel width or depth is adjusted at a given cross section and at a given time step depends on which condition results in less total stream power.

The fourth part is the inclusion of a channel bank side stability criteria based on the angle of repose of bank materials and sediment continuity.

GSTARS3 is a general numerical model developed for a personal computer to simulate and predict river and reservoir morphological changes caused by natural and engineering events. Although GSTARS3 is intended to be used as a general engineering tool for solving fluvial hydraulic problems, it does have the following limitations from a theoretical point of view (Yang and Simoes, 2003):

a) GSTARS3 is a quasi-steady flow model. Water discharge hydrographs are approximated by bursts of constant discharges. Consequently, GSTARS3 should not be applied to rapid, varied, unsteady flow conditions.

b) GSTARS3 is a semi-two-dimensional model for flow simulation and a semi-three-dimensional model for simulation of channel geometry change. It should not be applied

to situations where a truly two-dimensional or truly three-dimensional model is needed for detailed simulation of local conditions

c) GSTARS3 is based on the stream tube concept. Secondary currents are empirically accounted for. The phenomena of diffusion, and superelevation are ignored.

d) Many of the methods and concepts used in GSTARS3 are simplified approximations of real phenomena. Those approximations and their limits of validity are, therefore, embedded in the model.

5.1.3.3 Model setup

In this example, GSTARS3 is used to simulate 22 years of reservoir sedimentation (from 1974 through 1996) for a reach that spans nearly 93 km upstream from the Tarbela Dam (see **figure 5.1.3-1**). The hydrology of the system is given in **figure 5.1.3-2**, together with the dam operation. The tributaries have a relatively small contribution when compared with the main stem discharge, therefore they are not included in **figure 5.1.3-2** (but they are included in the computations).

There is a large percentage of silt and clay in the sediments in transport, but there is no data to simulate them using the Krone/Ariathurai methods. Secondly, analysis of the 1996 cross-sectional data suggests that deposition occurs in the form of a horizontal fill as can be observed in **figure 5.1.3-3** below. Finally, there exists a rating curve but during the calibration runs it was observed that the amount of deposition was severely underpredicted. That rating curve was adjusted to correctly reproduce the reservoir deposition volume. The distribution of the incoming sediment load was also a subject of calibration.

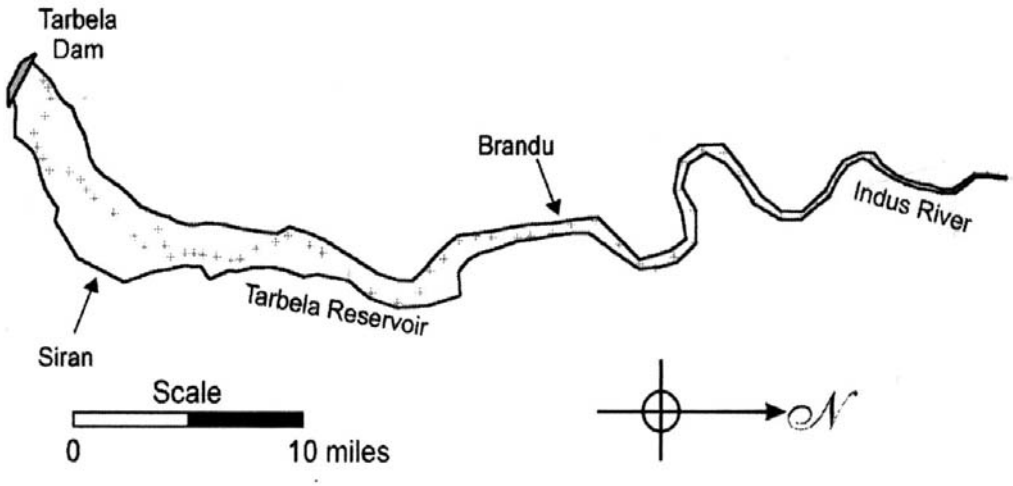

Figure 5.1.3-1 Tarbela dam and reservoir. The points (+) mark the thalweg and the locations of the cross sections used in this study (Yang and Simoes, 2003)

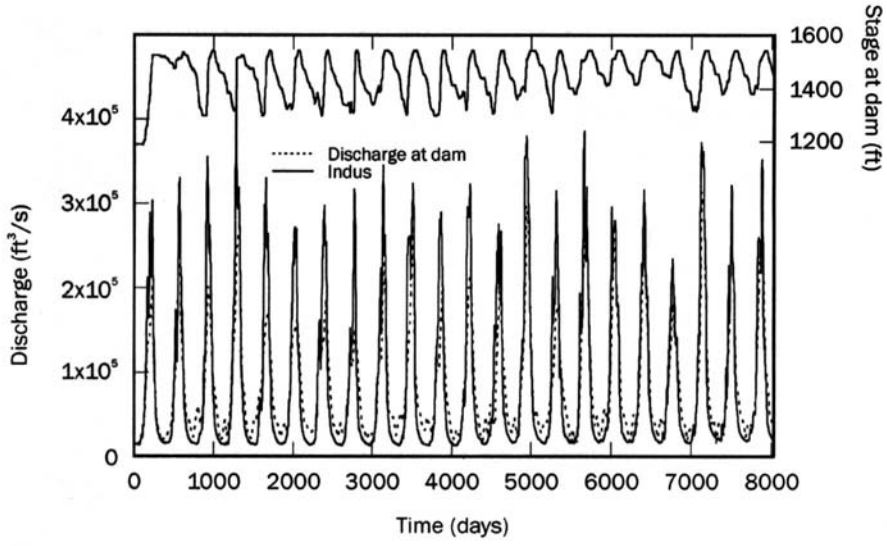

Figure 5.1.3-2 Hydrology and dam operation for Tarbela Reservoir (1974 to 1996) (Yang and Simoes, 2003)

The Tarbela Reservoir's bathymetry was discretized using existing surveyed cross sections, which are marked in **figure 5.1.3-1**. The horizontal sediment deposition observed in **figure 5.1.3-3** indicates that there is not much transverse variation in the sedimentation processes, therefore GSTARS3 simulations were carried out using one stream tube.

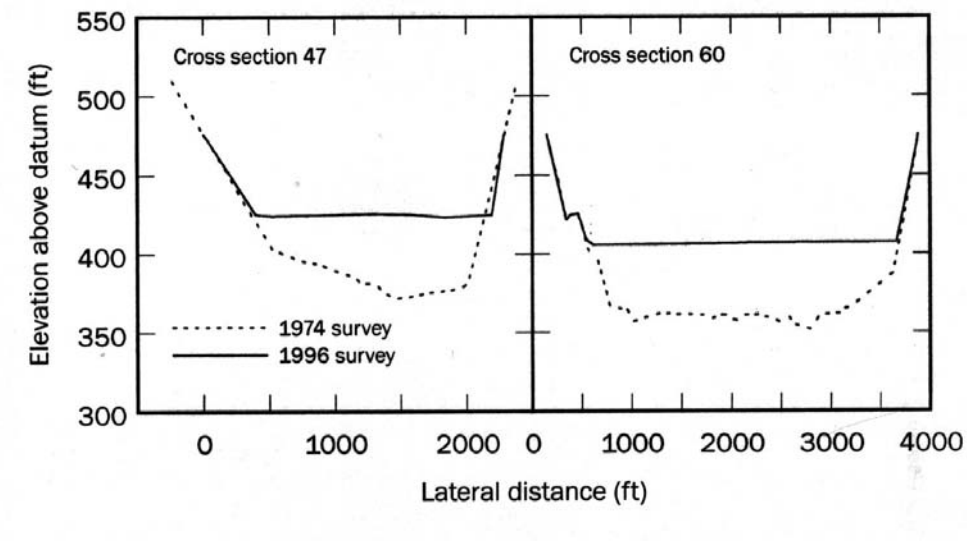

Figure 5.1.3-3 Two reservoir cross sections showing uniform sedimentation (Yang and Simoes, 2003)

Yang's (1973) equation was used for this study. Because there is no information concerning the deposition characteristics of the silt and clay fractions, it is difficult to use the Krone/Ariathurai methods effectively. Instead, the Yang (1973) was extrapolated for these size ranges. (The particle size distributions are in the range of 0.002 to 2.0 mm). This approach can sometimes yield good results, especially in mainly depositional processes such as those occurring in large reservoirs. However, care should be exercised, and the results of the simulations should always be confirmed by careful validation using field data.

Daily time steps for the hydraulic computations and 4.8 hours for sediment routing computations (8 040 time steps for hydraulics, 40 200 times steps for sediment) were used.

5.1.3.4 Simulation results

The results of a 1996 survey carried out in Tarbela Reservoir, corresponding to the end of the period of the simulation, are used here. Note that this example does not constitute an exhaustive and definitive study of the sedimentation processes in Tarbela reservoir for the 1974-1996 period.

The simulation results for the thalwegs are shown in **figure 5.1.3-4**. They are in good agreement with measurements, especially as in what concerns the location of the frontset of the delta and its slope. This is important to determine capacity loss, the useful life of the reservoir, and the impact that dam operations have on the reservoir's deposition pattern.

Cross-sectional geometries were better predicted in the downstream reservoir region than in the upstream region. That is because the upstream part has mostly riverine characteristics, and horizontal deposition is not the most appropriate technique for this circumstance. However, this region is limited to the first 21 cross sections, which represents less than one fourth of the entire simulated reach. Even then, deposition volumes are in general well predicted, even if thalweg elevations are not very accurate. Two representative cross section in this region are shown in **figure 5.1.3-5** for comparison purposes.

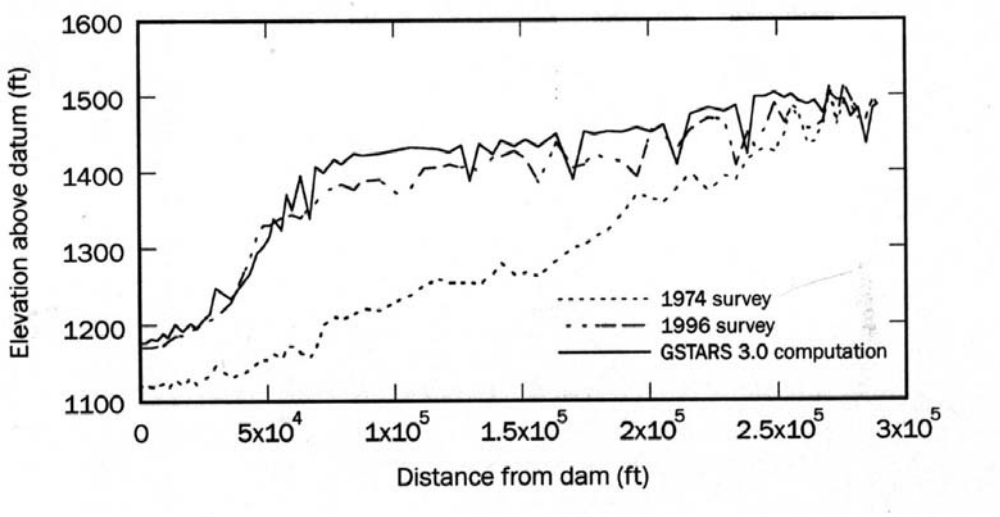

Figure 5.1.3-4 Results of the simulation of the Tarbela delta advancement over a period of 22 years (Yang and Simoes, 2003)

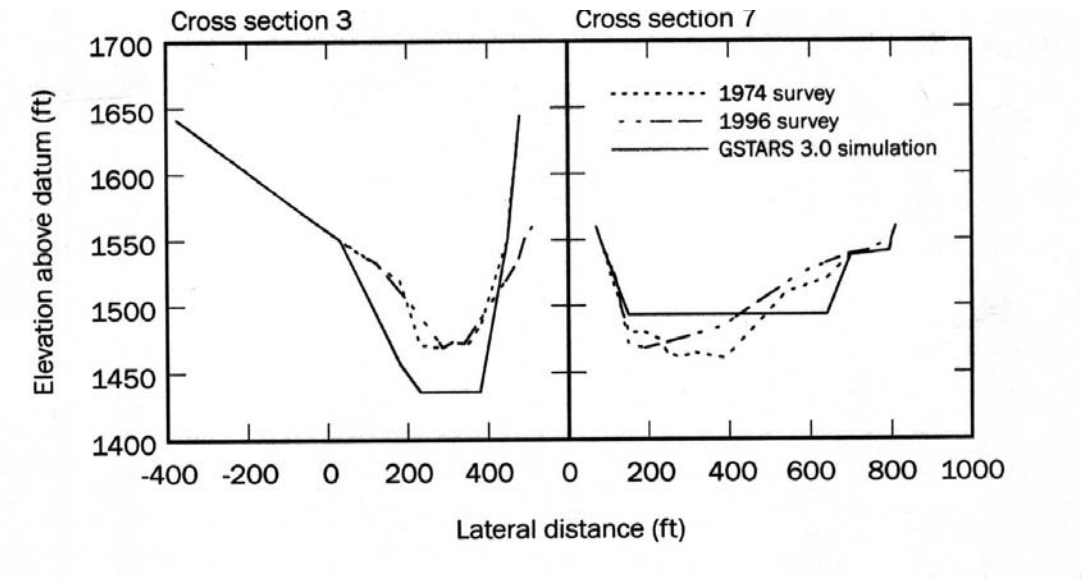

Figure 5.1.3-5 Comparison of measurements and GSTARS3 computation for two cross sections in the upstream region of Tarbela reservoir (Yang and Simoes, 2003)

In the reservoir region, which constitutes the focus of the study, deposition volumes are well predicted, in spite of a small tendency to overpredict the thalweg elevations. Four representative cross sections are shown in **figure 5.1.3-6**. These cross sections were taken from the full width of the reservoir region.

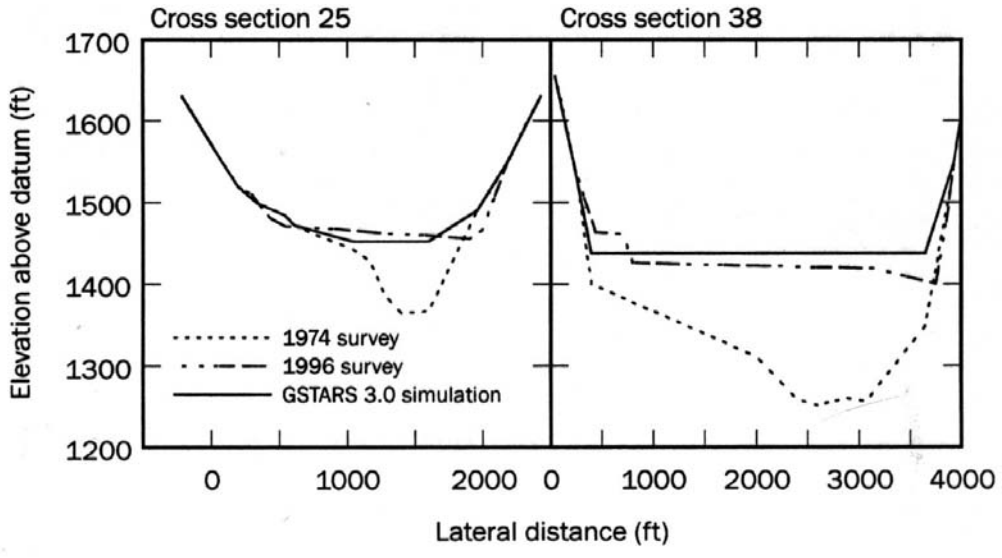

Figure 5.1.3-6 Comparison of measurements and GSTARS3 computation for two cross sections in the reservoir region of the study reach

The error associated with the predicted thalwegs is shown in **figure 5.1.3-7**. Most data are inside the 20% error band, which is a very good result for this type of simulation (22 years of sedimentation spanning a 36 km reach). However, this study could easily be improved with the use of little additional data. Such data would comprise more accurate bed-sediment size distributions, as well as more information about the inflowing sediment sizes traveling through the Indus. Further improvements would be attained from a study of the cohesive-sediment fraction properties within the reach (Yang and Simoes, 2003).

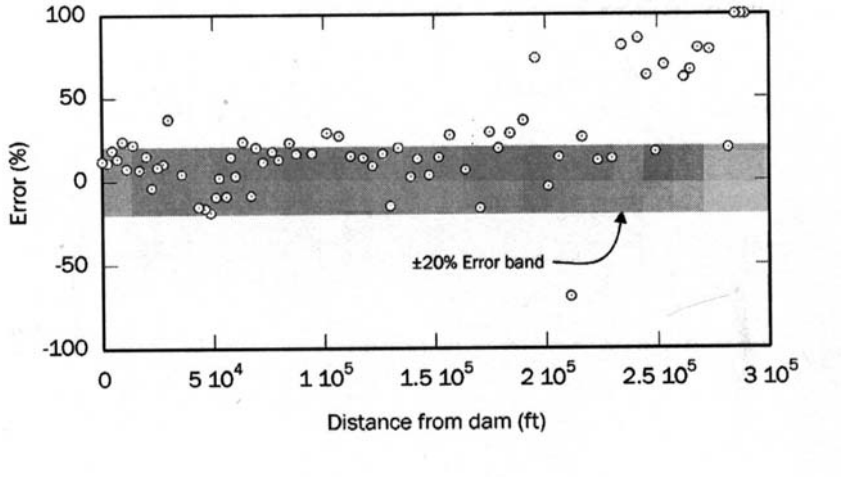

Figure 5.1.3-7 Relative error of the thalweg elevation predictions

5.1.4 Reservoir Sedimentation Model RESSASS: Tarbela Dam (TAMS, 1998)

a) Background

Tarbela Dam was built between 1970 and 1975 and is located on the Indus. The dam is vital to Pakistan's economy as it provides 40 per cent of the country's water storage, crucially important for irrigation during the dry season, and 35 per cent of the country's energy requirements from hydroelectric generation. About 25% of the original live storage had been lost and the sediment delta was approaching the dam by 1997.

b) Description of the model

The numerical model RESSASS of HR Wallingford was used to simulate reservoir sedimentation in Tarbela Reservoir. The model is one-dimensional in the sense that all hydraulic variables are considered constant at any cross-section at any particular

time. The model is based on the equations that describe flow and sediment movement. Within the model, sediment transport calculations are carried out for a range of different sediment sizes. The model is a time-stepping one, that is, initial conditions are input to equations which predict water levels and bed levels a short time later, typically one day. These predictions then provide the input conditions for the next time step. The process is repeated many times to make predictions over the required time period. Cross-sections are used to specify the geometry of the reservoir. The inflow of water and sediment at the upstream end of the reservoir are described using a discharge-time sequence and a discharge-sediment concentration relationship. The model then predicts revised bed levels and the location and composition of sediment deposits.

The model runs on a 60 year sequence of sediment and water inflows. The sequence consists of the 1967 to 1996 inflows to Tarbela repeated once to give the required 60 year sequence. The inflows are based on the flow records at Besham Qila. The sediment inflows were calculated using the sediment rating equation on these inflows together with the Ackers and White equation. For the model verification runs, the model water levels were matched to the observed levels since the first impoundment of the reservoir.

The model operates with the following boundary conditions:

- Variations of incoming flow with time;
- Corresponding variations of incoming sediments with time;
- Variations of water level at the dam as defined by the operating policy.

This means that, at any particular time, the model computes the outflow through the dam (the model does not take account of where that outflow occurs or whether the infrastructure at Tarbela is capable of delivering that discharge). It also computes the outflow of sediments at any particular time based on flow conditions immediately upstream of the dam.

c) Verification of the model performance

The model was verified by simulating the observed sediment deposition from the date of impoundment to 1996. The observed flow sequence at Besham Qila from 1975 was used together with the appropriate sediment rating curve. Observed historic reservoir water levels were used for the downstream boundary conditions. Based on field observations, the model was set up with two sand sizes, 0.155 mm and 0.200 mm, and five silt sizes giving a range of settling velocities between 0.002 mm/s and 3.6 mm/s. With these realistic parameters the model gave good agreement between observed and predicted bed levels and volumes of deposition. **Figure 5.1.4-1** and **Figure 5.1.4-2** show the predicted and observed longitudinal profiles and the predicted and observed stage-storage curves for 1996, respectively. It can be seen that the agreement between the model and the observed values is good. The agreement between the observations and predictions is particularly good in the neighborhood of the pivot point and immediately in front of the dam. One can thus have confidence that the model is representing accurately the processes of sediment deposition within Tarbela reservoir.

Figure 5.1.4-1Tarbela Dam spillway

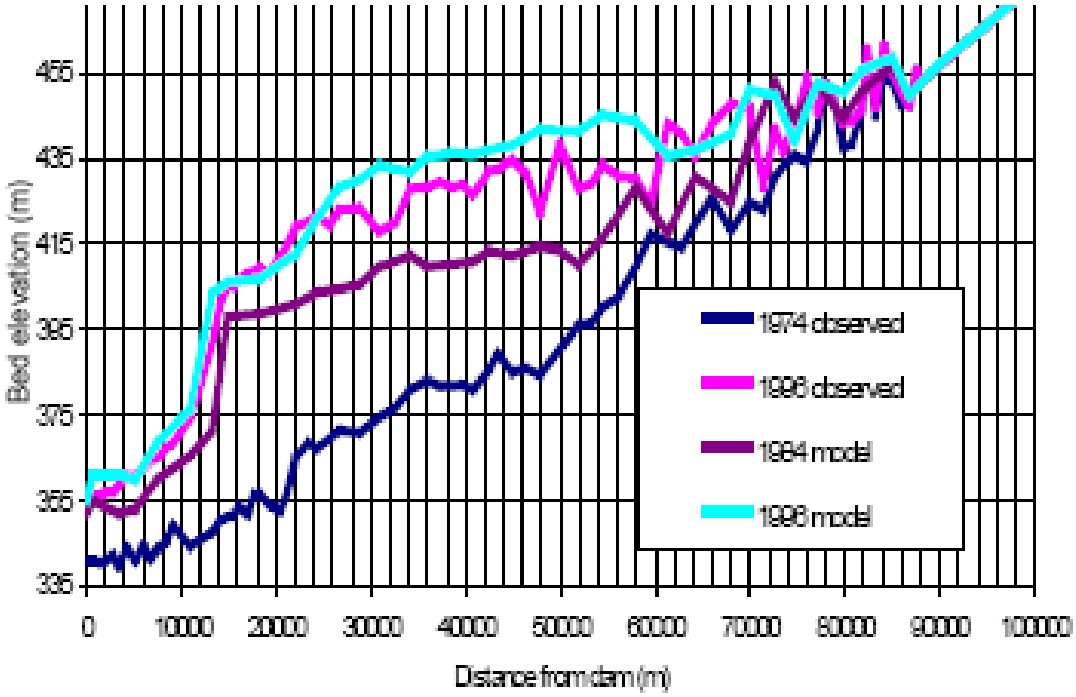

Figure 5.1.4-2 Simulated and surveyed longitudinal profile of Tarbela Reservoir

5.1.5 River model Mike 11: Lake Roxburgh, New Zealand (Mackay et al., 2000)

In this study particular attention was given to determining the effect on Alexandra of sediment redistribution in Lake Roxburgh, New Zealand. The relationship between water level and flow at Alexandra for given headwater level conditions at Roxburgh Dam was determined based on the latest cross-section survey data. The latest rating curve was also compared to previous curves.

The sediment redistribution which has occurred in Lake Roxburgh and the practice of lowering the reservoir in advance of a flood event have combined to reduce flood levels at Alexandra by 1.7 m from January 1994 to December 1999.

Overall a total of 11.5 million m^3 of sediment has been eroded from the middle and upper reaches of Lake Roxburgh since the January 1994 flood event. The total sediment moved since the full bed surveys completed in February 1994 and December 1999 is about 10 million m^3. An additional 1.5 million m^3 of material was moved between the partial bed survey in January 1994 and the February 1994 bed survey.

Water levels at Alexandra during the November 1999 flood would have peaked at about 143.8 m if there had been no sediment redistribution in the lake since 1994, and the lake had not been drawn down at the flood peak. This level is 1.5 m higher than the measured peak water level of 142.3 m in November 1999.

A sediment transport model was calibrated that gave a good comparison between actual measured and computed sediment volume changes in Lake Roxburgh. The key aspects of the model (Mike 11) selected were:

- Ackers and White sediment transport equation used since reservoir sediment is sand and gravel.
- One-dimensional since the reservoir is long and narrow.

The model was calibrated by adjusting the sediment grain size from upstream to downstream until a satisfactory match in bed volume changes was achieved. Calibration using sediment grain size implicitly allows for the reduced erodibility of fine cohesive sediments without having to be concerned with the details of the erosion process.

This calibrated model was used to simulate the effects of continuing the flood drawdown strategy (to promote sediment redistribution within Lake Roxburgh) using either 850 m^3/s or 1100 m^3/s as the threshold flow for drawing the lake down.

For a flood drawdown threshold of 850 m^3/s, the model predicted further erosion of 1.3 million m^3 of bed material over 5 years and 2.1 million m^3 over 10 years. For flows between 2400 and 3600 m^3/s, this would reduce water levels at Alexandra Bridge for a given headwater level at Roxburgh Dam by a further 0.7 – 0.8 m in 5 years time and by 1.1 m in 10 years time (**Figure 5.1.5-1**).

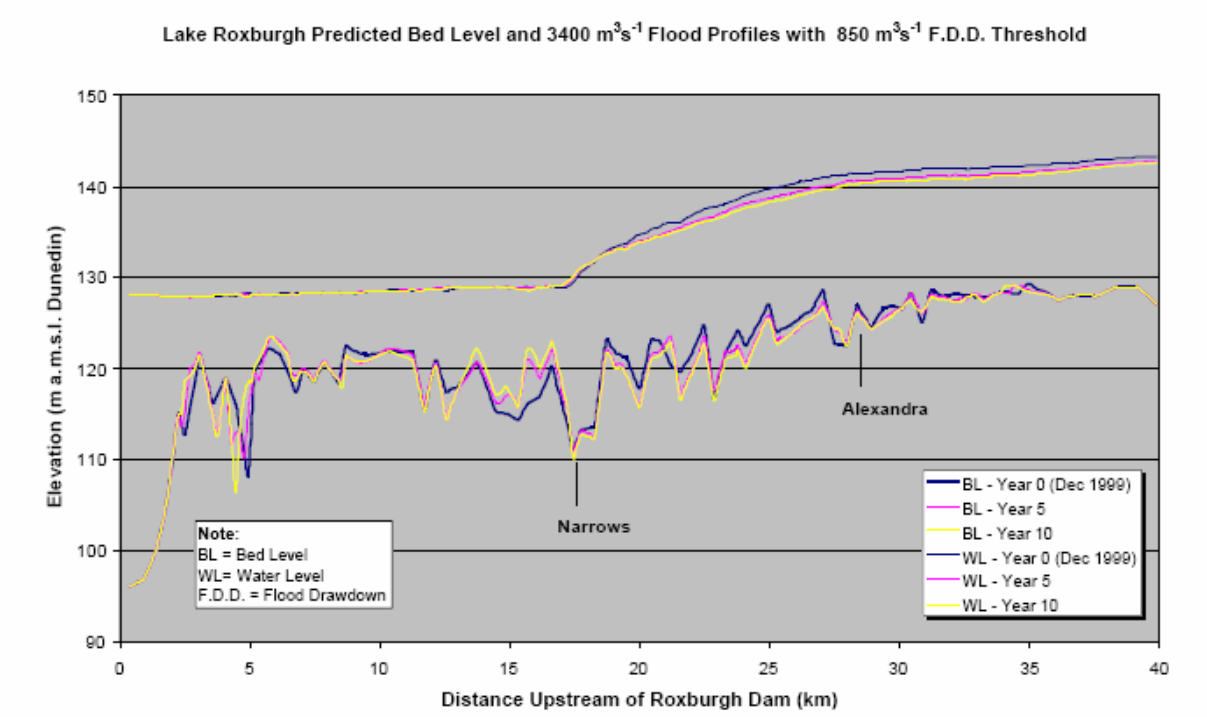

Figure 5.1.5-1 Predicted Future Bed Level and 3400 m^3/s^{-1} Flood Profiles at Year 0.5 and 10 (850 m^3/s^{-1} F.D.D. threshold)

5.2 Computational modelling of reservoir sedimentation and flushing with a two-dimensional model

5.2.1 Background

This section of the paper describes a mathematical model, which is applicable to shallow reservoirs, and its application to the Welbedacht Reservoir in South Africa. The mathematical model is an adaptation of an existing river morphological model, which has been used in numerous studies throughout the world. The key characteristics of the model are:

- Solution of the fully dynamic 2D St. Venant equations
- Parameterised description of the vertical distribution of main flow, helical flow and
- Suspended sediment transport
- Representation of time and space lag of suspended sediment
- Simulation of dynamic development of bed level, alluvial resistance and bank erosion.

Computational river models can be used to simulate reservoir sediment flushing, but with special consideration of the following:

- Sediment transport into the reservoir has to consider the total load, including the fine washload
- Deposited sediment in the reservoir is often cohesive and critical conditions for re-entrainment should be incorporated
- During flushing retrogressive erosion is dominant, but both erosion and deposition processes are active
- During flushing near supercritical flow conditions can be reached

The research and application have been carried out as a joint effort between University of Stellenbosch, South Africa, and DHI Water & Environment, Denmark. The Mike 21C model was used.

The Welbedacht Dam was completed in 1973 on the Caledon River, South Africa, which is located in a high sediment yield region with a sediment yield of about 3000 t/km^2.a. During the first three years of operation the reservoir had lost 36 million m^3 of its original 114 million m^3 storage capacity due to sedimentation (**Figure 5.2-1**). A longitudinal profile of the

reservoir sedimentation is shown in **Figure 5.2-2**. As a verification case the model was used to simulate this three year period (1973 to 1976). Subsequently, alternative operation strategies were tested in the model with the objective to sluice the sediment through the reservoir and flush out accumulated sediment.

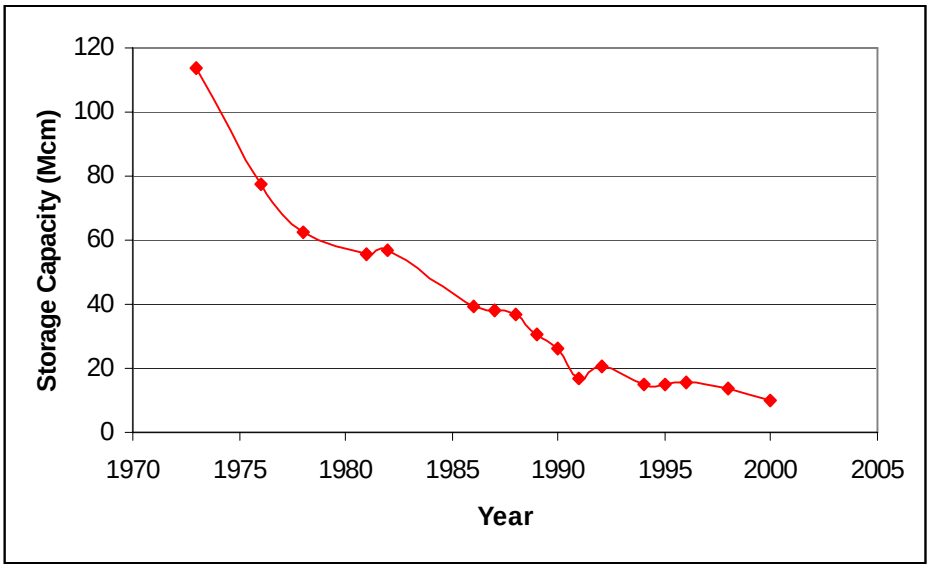

Figure 5.2-1. Observed loss in storage capacity due to sedimentation at Welbedacht Dam

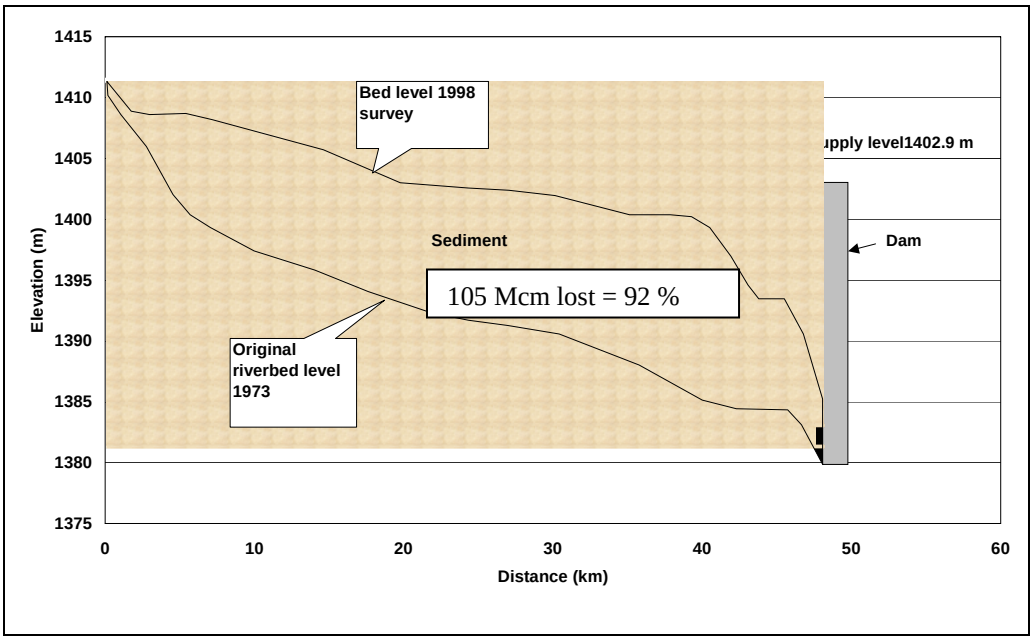

Figure 5.2-2. Longitudinal profile of the Welbedacht Reservoir sedimentation

5.2.2 Data

The geometry of the reservoir was taken from aerial photography (**Figure 5.2-3**), and mapped with a curvilinear grid, as shown in **Figure 5.2-4**. The grid contains 250 cells in the longitudinal direction, and 15 points across, totaling 3750 grid cells fully flooded. The model was formulated with an upstream inflow and a downstream reservoir water level. Time-series were available for 1973-76 both for inflow discharge and reservoir level, indicated in **Figures 5.2-5 and 5.2-6.**

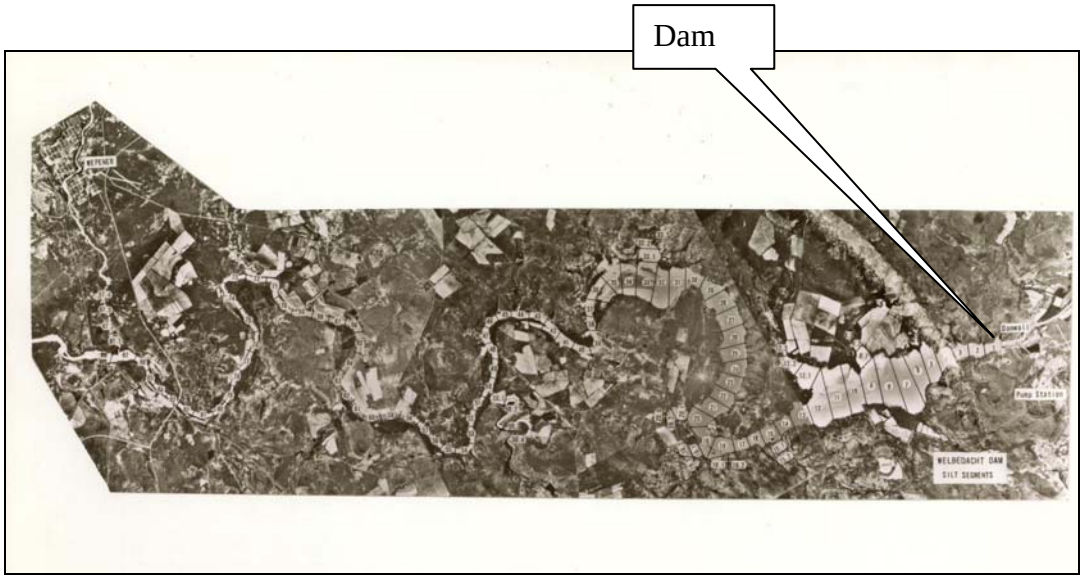

Figure 5.2-3. Aerial photograph of Welbedacht Reservoir

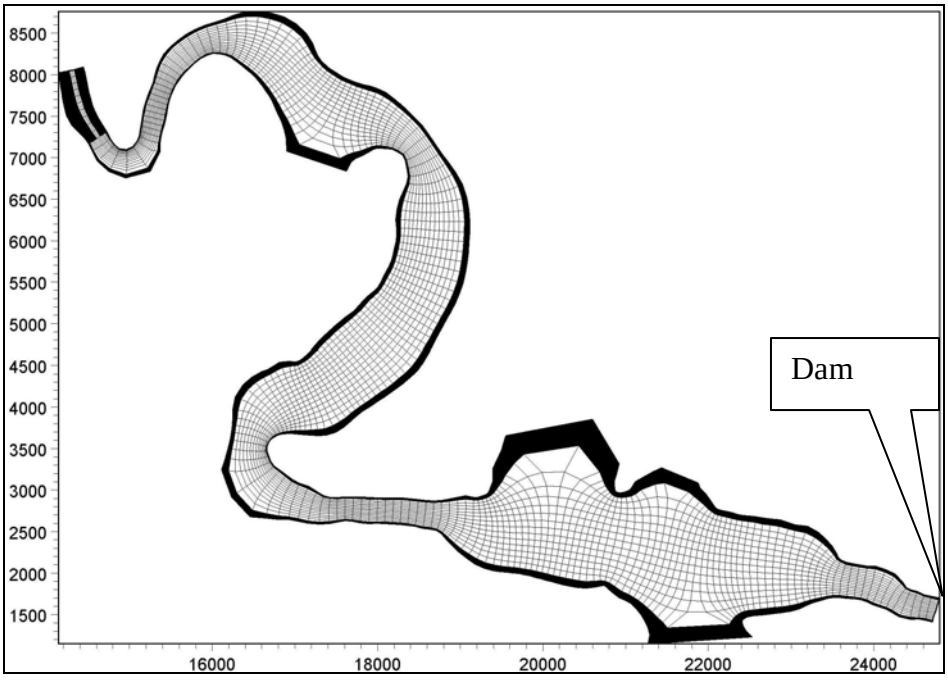

Figure 5.2-4 . Curvilinear grid used for the 2D model, 250x15 cells

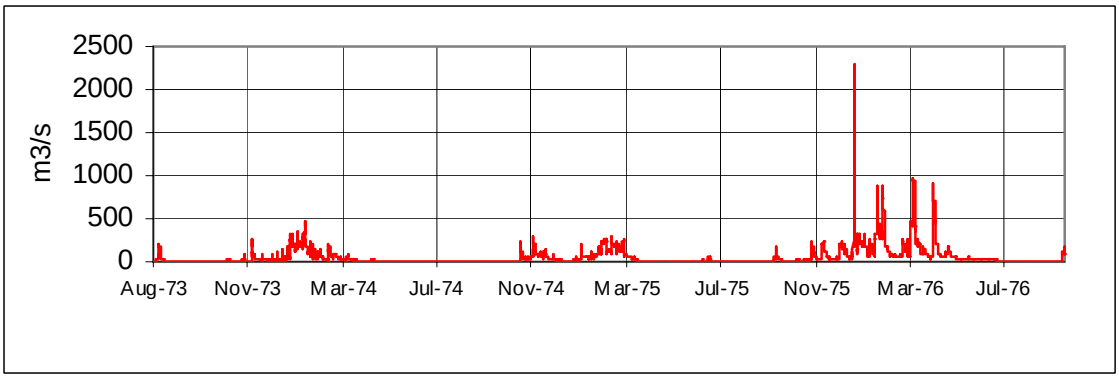

Figure 5.2-5. Time series of observed reservoir inflow

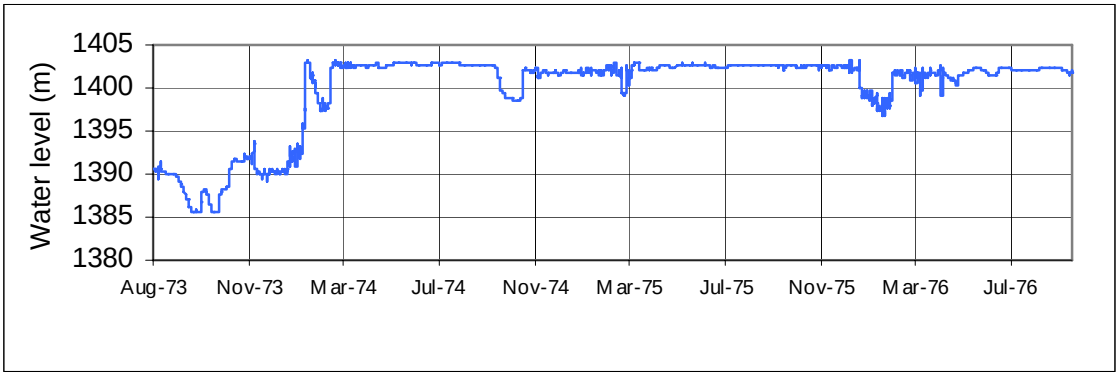

Figure 5.2-6. Time series of observed reservoir water level at dam

Basson and Rooseboom, (1997) gives the following sediment characteristics for the Welbedacht inflow:

- Fraction 1: d_{50}<0.05 mm, 76% (mud)
- Fraction 2: 0.05<d_{50}<0.106, 19% (silt)
- Fraction 3: 0.106<d_{50}<0.25 mm, 5% (fine sand)

For this study the following relationship between concentration and discharge was found from observed data:

$$C = 793.32Q^{0.664} \qquad 5.2\text{-}1$$

Where C is in g/m^3 and Q in m^3/s. All the sediment is basically taken as being the same cohesive type.
The relationship between discharge and concentration is however poor due to sediment availability limitation from the catchment.

The settling velocity seems to be in the order of magnitude 1 mm/s. It is noted that this parameter does not play a completely decisive role in the cohesive sediment transport model. The settling velocity only influences the rate of deposition, which may sound critical. However, the system tends to stabilise itself because a lower settling velocity will cause slower deposition, which causes the sediment concentration to rise, again causing higher deposition. The sensitivity towards the settling velocity was tested and a change of about 10% was found by doubling the value.

By using the hydrograph from 1 August 1973 to 30 September 1976 it was found that the total inflow to the reservoir was 4925 million m^3 of water. The sediment concentration expression yields that along with the water, 53 million m^3 of sediment entered the reservoir (assuming 2650 kg/m^3 density for the sediment). According to Basson et al (1996), the sedimentation during the period was 36 mill m^3. This suggests an average trapping efficiency of 68% for the Welbedacht reservoir.

5.2.3 Theoretical Background

The modelling tool is described in the following, including grid generation, hydrodynamic, cohesive sediment transport and bathymetry development.

5.2.4 Grid Generation

MIKE 21C is designed to function on any orthogonal curvilinear grid. Here we employ a grid generated with an anisotropic conformal mapping method, which is much more flexible than conformal mapping, as there is no constraint on the cell aspect ratio. It is often preferable to use cells that are elongated in the flow direction for this type of models. Anisotropic conformal mapping is described by the anisotropic Laplace equations:

$$(gx_\xi)_\xi + (g^{-1}x_\eta)_\eta = 0$$
$$(gy_\xi)_\xi + (g^{-1}y_\eta)_\eta = 0 \qquad \text{5.2-2}$$

Where:

g	Grid weight
x,y	Horizontal coordinates (m)
ξ,η	Transformed integer coordinate system

The grid weight, equal to the aspect ratio of the grid, is given by:

$$g = \sqrt{\frac{x_\xi^2 + y_\xi^2}{x_\eta^2 + y_\eta^2}} \qquad \text{5.2-3}$$

Orthogonality is enforced in all boundary points through the non-linear condition:

$$x_\xi x_\eta + y_\xi y_\eta = 0$$
$$f(x,y) = 0 \qquad \text{5.2-4}$$

Which is stating that the grid line is orthogonal to the boundary (zero dot product) and that the grid line follows the boundary line (second condition). The elliptic equations are solved implicitly with continuous update of the boundary condition that is handled by Newton iteration. Stone's Strongly Implicit Procedure (Stone, 1968) is applied for the elliptic equations.

5.2.5 Hydrodynamics

The hydrodynamics are described by the 2-dimensional Saint-Venant equations:

$$\frac{\partial p}{\partial t} + \frac{\partial (p^2/h)}{\partial x} + \frac{\partial (pq/h)}{\partial y} + \frac{gp\sqrt{p^2+q^2}}{C^2h^2} + gh\frac{\partial s}{\partial x} = h\frac{\partial}{\partial x}\left(E\frac{\partial (p/h)}{\partial x}\right) + h\frac{\partial}{\partial y}\left(E\frac{\partial (p/h)}{\partial y}\right)$$
$$\frac{\partial q}{\partial t} + \frac{\partial (pq/h)}{\partial x} + \frac{\partial (q^2/h)}{\partial y} + \frac{gq\sqrt{p^2+q^2}}{C^2h^2} + gh\frac{\partial s}{\partial y} = h\frac{\partial}{\partial x}\left(E\frac{\partial (q/h)}{\partial x}\right) + h\frac{\partial}{\partial y}\left(E\frac{\partial (q/h)}{\partial y}\right) \qquad \text{5.2-5}$$
$$\frac{\partial h}{\partial t} + \frac{\partial p}{\partial x} + \frac{\partial q}{\partial y} = 0$$

Where:

p,q Flux field (m^2/s)
h Water depth (m)
t Time (s)
g Acceleration of gravity (9.81 m/s^2)
C Chezy number ($m^{1/2}/s$)
s Surface elevation (m)
E Eddy viscosity (m^2/s)

The Saint-Venant equations are solved on the curvilinear grid with a finite-volume scheme. State-of-the-art methods from CFD are applied for the solution, which incorporates the use of a Cartesian base for the velocity field, non-staggered allocation with momentum interpolation (Majumdar et al, 1992). The SIMPLER method (Patankar, 1980) is applied for the continuity equation.

5.2.6 Cohesive sediment transport model

The transport of the cohesive sediment is described by an advection-dispersion equation:

$$\frac{\partial hc}{\partial t} + \frac{\partial p'c}{\partial x} + \frac{\partial q'c}{\partial y} = \frac{\partial}{\partial x}\left(hD_{xx}\frac{\partial c}{\partial x}\right) + \frac{\partial}{\partial y}\left(hD_{yy}\frac{\partial c}{\partial y}\right) + E - D \qquad 5.2\text{-}6$$

Where:

p',q' Modified flux field (m^2/s)
c Concentration (g/m^3)
D_{xx} Dispersion in the x-direction (m^2/s)
D_{yy} Dispersion in the y-direction (m^2/s)
E Erosion function
D Deposition function

The modified flux field that transport the suspended sediment is derived from the depth integrated flux field in the manner:

$$\begin{pmatrix} p' \\ q' \end{pmatrix} = \alpha_{01} \begin{pmatrix} p \\ q \end{pmatrix} + \alpha_{02} \frac{h}{R} \begin{pmatrix} -q \\ p \end{pmatrix} \qquad 5.2\text{-}7$$

Where a_{01} and a_{02} are functions of the distribution of momentum and sediment over the water column. The term h/R is the water depth divided by the streamline radius of curvature; the latter derived from the flow field. The modified flux field arises from the 3-dimensional character of the problem.

α_{01} modifies the streamwise convection, and represents the fact that the sediment concentration rises towards the bed, while the velocity rises towards the surface. The streamwise convection of the sediment is hence not as effective, as $\alpha_{01}=1$ would imply. A value of $\alpha_{01}=1$ is found for uniformly distributed sediment, i.e. very fine material. α_{01} is calculated from the logarithmic velocity profile and the distribution of sediment.

α_{02} represents the impact of secondary flow, and produces convection across the streamlines. α_{02} is calculated from the helical flow taken from standard theory (see e.g. Rozowskii, 1957), and the distribution of sediment.

The α_{01} and α_{02} parameters are calculated from local values of the flow velocity, flow resistance and settling velocity. The calculation is done on each morphological time-step in describing the change in sediment concentration and sedimentation in time.

An implicit scheme is applied for the AD equation in which the local availability of sediment is accounted for by limiting the erosion to not surpass the available mud in the cell. The implicit solution of the AD equation furthermore allows for implicit updating of the local mud layer thickness, which is done through the source/sink terms of the equation (sediment entering the water column comes from the bed, and vice versa). The implicit AD scheme is unconditionally stable for any choice of the time-step.

The dispersion in the equation originates from the profile functions, while additional dispersion can be added. Refer to DHI (2003) for details about the dispersion terms. Herein only the dispersion associated with the profile functions were applied (particularly important across streamlines). No additional dispersion has been added.

A standard cohesive model gives the erosion and deposition functions (E and D):

$$E = E_0\left(\frac{\tau}{\tau_{ce}} - 1\right)^m, \quad \tau > t_{ce}$$
$$D = w_s c\left(1 - \frac{\tau}{\tau_{cd}}\right), \quad \tau < t_{cd} \qquad \text{5.2-8}$$

Where:

w_s Settling velocity, w_s ~ 1 mm/s

τ_{ce} Critical shear stress for erosion, τ_{ce} ~0.2 N/m^2 for fluid mud and ~0.6 N/m^2 for mud

τ_{ce} Critical shear stress for deposition, τ_{ce} ~ 0.05 N/m^2

E_0 Erosion constant, E_0 ~0.1 g/m^2/s

m Exponent (non-linearity) of the erosion, m ~ 1-3

The mentioned value ranges are standard, though the variation from situation to situation can be substantial.

5.2.7 Calibration of sedimentation during 1973-76

Calibration/validation is carried out by comparing observed and simulated sedimentation rates for the initial three years of operation from 1973-76.

The present model has 82 million m^3 of initial water storage calculated by assuming 1402.9 m (full supply level) water level everywhere in the model. According to Basson et al (1996) the initial storage capacity was 114 mill m^3, which is substantially higher. The reason for this is that the present model does not cover the total area counted in the 114 mill m^3, e.g. tributaries etc.

The initial bathymetry from 1973 (based on cross section data) and the simulated bathymetry in 1976 are shown in **Figure 5.2-7.** The following cohesive model parameters were used in the simulation:

w_s	Settling velocity	1 mm/s
τ_{ce}	Critical shear stress for erosion	0.6 N/m^2
τ_{ce}	Critical shear stress for deposition	0.05 N/m^2
E_0	Erosion constant	0.1 g/m^2/s
m	Exponent (non-linearity) of the erosion	2
n	Porosity	0.5
ρ	Density	2650 kg/m^3

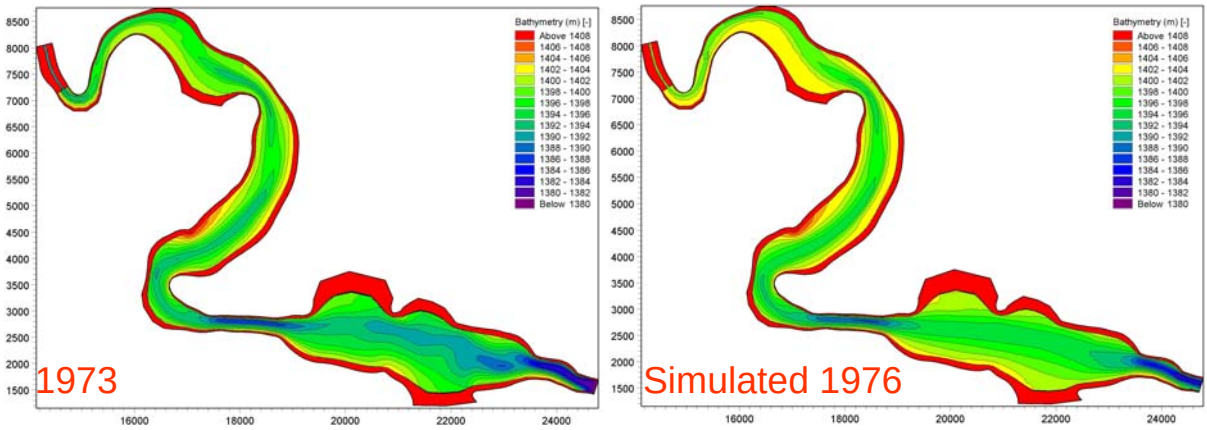

Figure. 5.2-7. Initial bathymetry from 1973 (left) and simulated bathymetry in 1976 (right).

The simulated bathymetry development from 1973-1976 was integrated into volumes, as shown in **Figure 5.2-7**. The simulated sedimentation was 25 million m^3, while the observed was 36 mill m^3. The reason for this is that the model does not cover the whole reservoir. The ratio between the simulated and observed sedimentation matches the ratio between the full initial reservoir volume and the volume in the model.

The simulated sedimentation is fairly sensitive to the model parameters. Of particular importance is the critical erosion shear stress. In the present simulations there is actually some erosion during the flood peaks, which can be seen also from **Figure 5.2-8**.

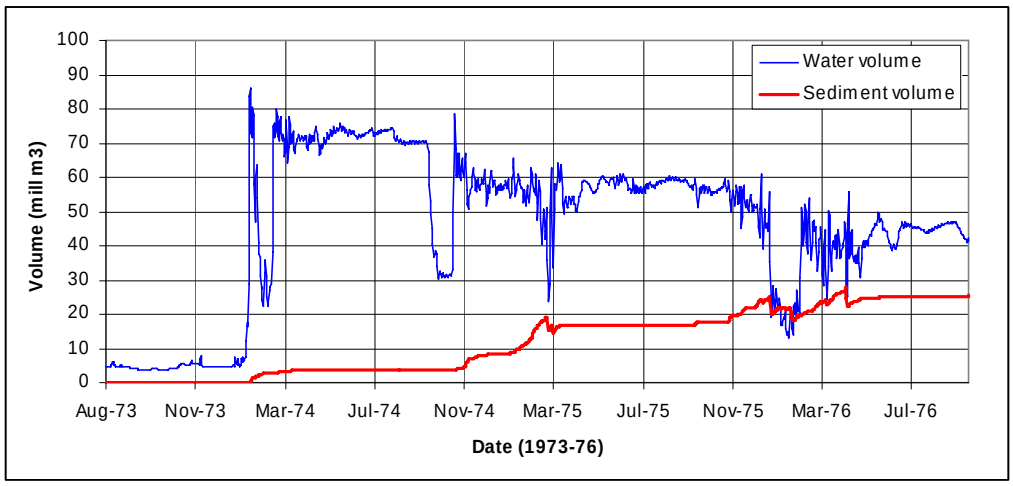

Figure. 5.2-8. Simulated sedimentation development from 1973-76, sediment volume and water volume in the reservoir.

5.2.8 Flushing during 1991

Flushing during floods has been carried out since 1991 at Welbedacht Dam. A typical flushing viewed from the right bank at the dam looking upstream is shown in **Figure 5.2-9**.

According to Basson et al. (1996) the reservoir full supply capacity volume had dropped to 17 million m^3 by 1991. The flushing operation was simulated in the model by linearly decreasing the reservoir water level from full supply level to 1392 m during a period of 5 hours.

Figure 5.2-9. Welbedacht Reservoir during flushing

The simulations yielded an incised channel being cut into the reservoir. The channel was cut from downstream moving upstream. As the erosion migrates upstream into a wider section, it will start dividing into more channels, as shown in **Figure 5.2-10**. A comparison with observed minimum bed levels is given in **Figure 5.2-11**. The agreement is satisfactory, considering that the survey was not carried out immediately after the flushing.

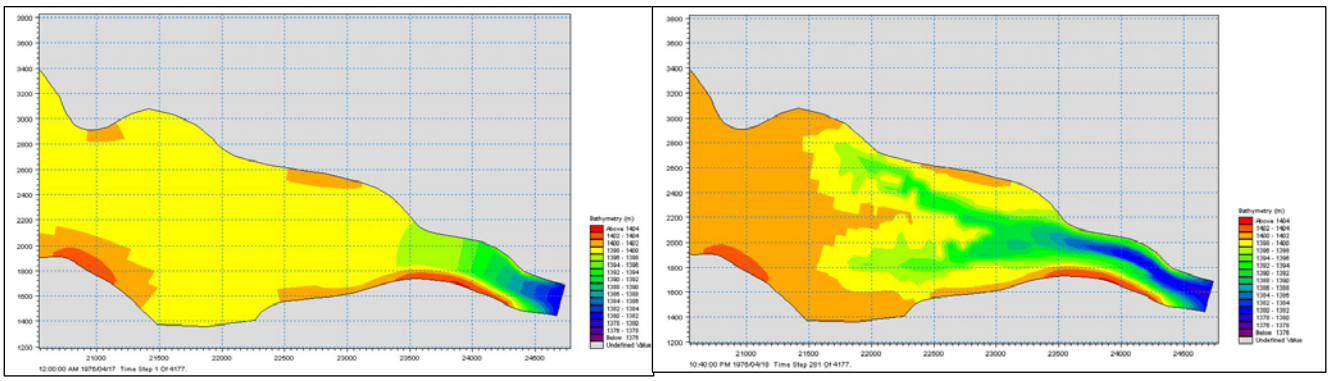

Figure 5.2-10. Bathymetry before (left) and simulated after (right) flushing in 1991.

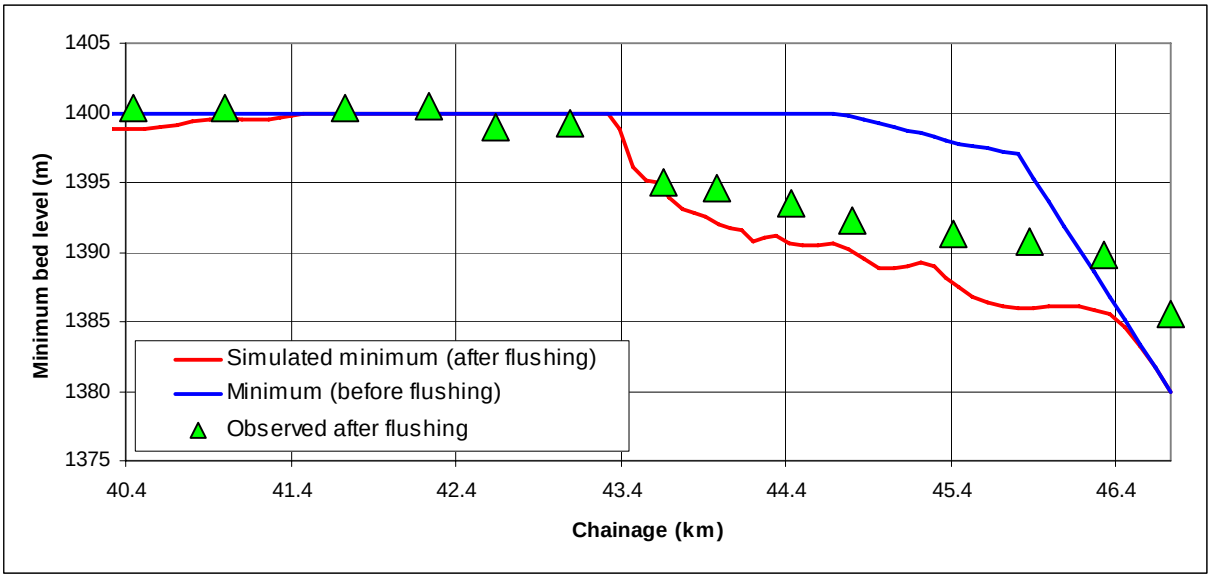

Figure 5.2-11. Observed and simulated minimum bed level as function of chainage before and after flushing in 1991.

5.2.9 Flushing with Low Level Outlets

The gates at Welbedacht Dam are not placed at the original river bed level, but 15 m above the bed. If the gates were located at the bed level, flushing should be more effective. This scenario was simulated with the model for a one month duration flushing at 600 m^3/s (**Figure 5.2-12**) and it is clear it has a significant impact on the long-term storage capacity.

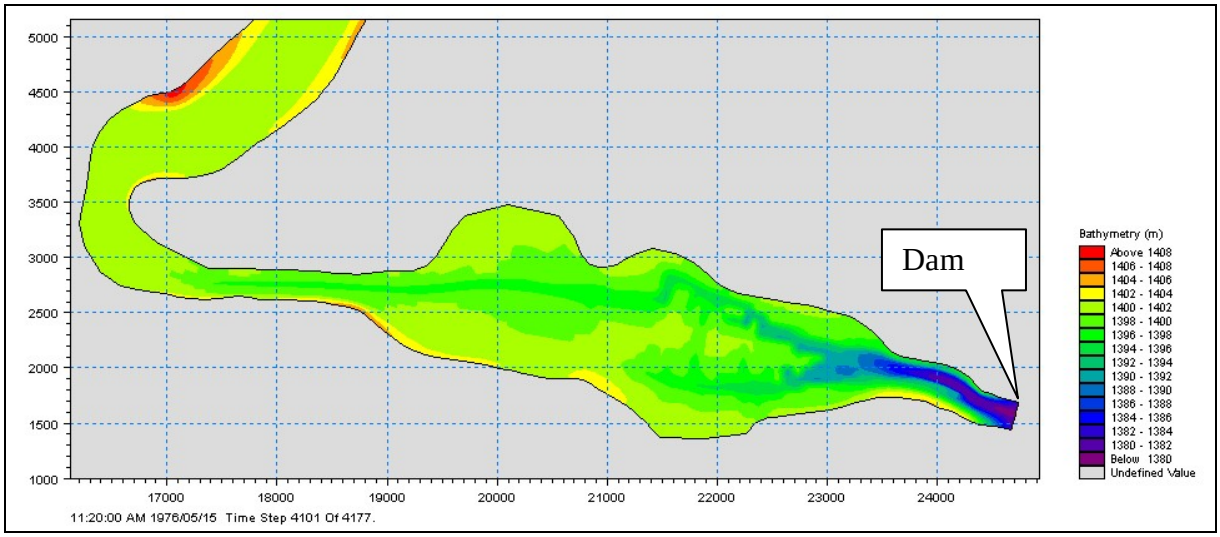

Figure 5.2-12. Flushing simulation with gate invert level at the bed at 1380 m

5.2.10 Conclusions

Flushing of sediment from a reservoir requires: excess water, suitable large low level outlets, a steep and narrow reservoir basin and judicious operation. Flushing could be carried out on a seasonal basis, or during specific flood events (usually in semi-and conditions).

A basic cohesive transport model was incorporated into a 2D curvilinear modelling system. This model was originally developed for sand transport, and has a pseudo 3D description included accounting for the 3-dimensionality of the flow and sediment. The model solves the Saint-Venant equations on any orthogonal grid combined with an advection-dispersion equation that includes the 3-dimensionality through profile functions. The inclusion of the 3D effects results in the transporting flux field being different from the depth-integrated flux field. In the streamwise direction the

convection is reduced due to the fact that most of the sediment is located in the lower part of the water column. The 3-dimensionality also results in depth-integrated convection across the main streamline due to streamline curvature driven secondary flow.

A calibration of the model was carried out for the Welbedacht reservoir. The default parameters for the cohesive model gave satisfactory results, though there is room for improvement. The model was then applied for simulation of flushing of the same reservoir in 1991. It was demonstrated that the model is capable of capturing the incised channel that is cut into the reservoir bed during such flushing operations, and that the model can also handle the 2-dimensionality of the channel formation. The model can be used as management tool to determine the effectiveness of flushing operation under various flood and outlet conditions.

5.3 Three-dimensional Mathematical Modelling (turbulent sediment transport)

5.3.1 3D Model Equations

Generally, the 3D flow field is determined by the following Reynolds-averaged continuity and Navier-Stokes equations (Wang and Wu, 2004):

$$\frac{\partial u_i}{\partial x_i} = 0 \qquad (5.3\text{-}1)$$

$$\frac{\partial u_i}{\partial t} + \frac{\partial (u_i u_j)}{\partial x_j} = F_i - \frac{1}{\rho}\frac{\partial p_i}{\partial x_i} + \frac{1}{\rho}\frac{\partial \tau_{ij}}{\partial x_j} \qquad (5.3\text{-}2)$$

where:

u_{i}- = Velocity components (i = 1, 2, 3)
F_i = External forces including gravity per unit volume
p = Pressure
τ_{ij} = Turbulent stresses determined by a turbulence model

For shallow water flow, the pressure can be assumed to be hydrostatic and all the vertical components of fluid acceleration can be ignored, thus yielding the quasi-3D governing equation as (Wang and Wu, 2004):

$$\frac{\partial u}{\partial x}+\frac{\partial v}{\partial y}+\frac{\partial w}{\partial z}=0 \tag{5.3-3}$$

$$\frac{\partial u}{\partial t}+\frac{\partial (uu)}{\partial x}+\frac{\partial (vu)}{\partial y}+\frac{\partial (wu)}{\partial z}=-g\frac{\partial z_s}{\partial x}+\frac{1}{\rho}\frac{\partial \tau_{xx}}{\partial x}+\frac{1}{\rho}\frac{\partial \tau_{xy}}{\partial y}+\frac{1}{\rho}\frac{\partial \tau_{xz}}{\partial z}+fv \tag{5.3-4}$$

$$\frac{\partial v}{\partial t}+\frac{\partial (uv)}{\partial x}+\frac{\partial (vv)}{\partial y}+\frac{\partial (wv)}{\partial z}=-g\frac{\partial z_s}{\partial y}+\frac{1}{\rho}\frac{\partial \tau_{yx}}{\partial x}+\frac{1}{\rho}\frac{\partial \tau_{yy}}{\partial y}+\frac{1}{\rho}\frac{\partial \tau_{yz}}{\partial z}-fu \tag{5.3-5}$$

where f is the Coriolis coefficient.

The hydrostatic pressure assumption brings significant simplification to the full 3D problem of equations 5.3-1 and 5.3-2. However, this assumption is valid only for the gradually varying open-channel flows. A full 3D model without this assumption should be used in regions of rapidly varying flows.

Sediment transport is divided into suspended load and bed load and hence the flow domain is divided into a bed-load layer with a thickness δ and the suspended load layer above it with a thickness of h -δ. The exchange of sediment between the two layers is through deposition (downward sediment flux) at a rate of D_{bk} and the entrainment from the bed load layer (upward flux) at a rate of E_{bk}. The distribution of the sediment concentration in the upper layer is governed by the following advection-dispersion equation:

$$\frac{\partial c_k}{\partial t}+\frac{\partial [(u_j-w_{sk}\delta_{j3})c_k]}{\partial x_j}=\frac{\partial}{\partial x_j}\left(\frac{\nu_t}{\sigma_c}\frac{\partial c_k}{\partial x_j}\right) \tag{5.3-6}$$

where c_k is the local concentration of the k-th size class of suspended sediment load; δ_{j3} is the Kronecker delta with j=3 indicating the vertical direction. At the free surface, the vertical sediment flux is zero and hence the condition applied is:

$$\frac{\nu_t}{\sigma_c}\frac{\partial c_k}{\partial z}+w_{sk}c_k=0 \tag{5.3-7}$$

At the lower boundary of the suspended sediment layer, the deposition rate is $D_{bk}=w_{sk}c_{bk}$, while the entrainment rate, E_{bk} is:

$$E_{bk} = -\frac{\nu_t}{\sigma_c}\frac{\partial c_k}{\partial z} = w_{sk} c_{b*k} \qquad (5.3\text{-}8)$$

where c_{b*k} is the equilibrium concentration at the reference level $z = z_b + \delta$, which needs to be determined using an empirical relation. In the 3D model, the bed load transport is simulated by using the equation:

$$\frac{\partial(\delta_b \overline{c}_{bk})}{\partial t} + \frac{\partial(\alpha_{bx} q_{bk})}{\partial x} + \frac{\partial(\alpha_{by} q_{bk})}{\partial y} + \frac{1}{L}(q_{bk} - q_{b*k}) = 0 \quad (k = 1, 2, ..., N) \qquad (5.3\text{-}9)$$

where $\overline{c}_{bk}$ is the average concentration of bed load at the bed load zone, q_{bk} is the bed load transport rate of the *k*-th size class and q_{b*k} is the corresponding bed load transport capacity. α_{bx} and α_{by} are the direction cosines of the bed shear stresses, known from the flow calculation.

The bed change can be determined by either the exchange equation:

$$(1 - p'_m)\left(\frac{\partial z_b}{\partial t}\right)_k = D_{bk} - E_{bk} + \frac{1}{L_s}(q_{bk} - q_{b*k}) \qquad (5.3\text{-}10)$$

or the overall sediment mass-balance equation integrated over the water depth *h*:

$$(1 - p'_m)\left(\frac{\partial z_b}{\partial t}\right)_k = \frac{\partial(hC_{tk})}{\partial t} + \frac{\partial q_{tkx}}{\partial x} + \frac{\partial q_{tky}}{\partial y} = 0 \qquad (5.3\text{-}11)$$

where C_{tk} is the depth-averaged sediment concentration and q_{tkx} and q_{tky} are the components of the total load sediment transport in the *x*- and *y*- directions:

$$q_{tkx} = \alpha_{bx} q_{bk} + \int_{\delta}^{h}\left(u c_k - \frac{\nu_t}{\sigma_c}\frac{\partial c_k}{\partial x}\right)\partial z; \qquad q_{tky} = \alpha_{by} q_{bk} + \int_{\delta}^{h}\left(v c_k - \frac{\nu_t}{\sigma_c}\frac{\partial c_k}{\partial x}\right)\partial z \qquad (5.3\text{-}12)$$

5.3-2 Three-dimensional Model (case study): Three Gorges Reservoir Project, China (Dou et al., 2004)

This study applies a 3D mathematical model for suspended load motion in turbulent flows, which is based on the following new methods:

- A new stress model based on the stochastic theory of turbulent flows by Dou (1980)
- Refined wall function for treatment of solid walls
- Introduction of traditional equations of suspended load motion and sorting of bed material into a 3D model
- Orthogonal curvilinear grid system, with horizontal layers employed over the water depth

The equation system is solved by using the SIMPLE–C algorithmic. The above model is first validated using hydrological data collected before and after the construction of the existing Gezhouba Dam. The model is then applied to the sedimentation problem of the much larger Three Gorges Project (located upstream of the Gezhouba Dam) and predictions are made of the sediment deposition pattern, the size distribution of the deposits and the flow fields.

a) Background

The dam area of the Three Gorges Project is located within Xiling Gorge on the Yangtze River. A 16km long river reach was simulated between Miaohe and the dam axis at Sandouping, a deep valley of heavily weathered anticline diorite and granite, with low mountains and hills on both sides. The width of the river in this section is usually 600m to 700m during a flooding period. The maximum width of 1 400m is found near Sandouping. The river reach under investigation is slightly curved. The inlet is Miaohe with a width of only about 500m. Figure 5.3-1 shows the river regime in the dam area. The riverbed consists of gravel and cobble. The slope is steep with rapid flows. The water surface gradient during dry and flooding periods varies between 0.375% and 0.506%. This reach is amongst the worst in terms of navigation conditions in the Sichuan province. After the impoundment of Gezhouba Reservoir, the present reach belongs to the perennial backwater area: during dry periods the water level rises 15m to 20m, during flooding periods it rises 2m to 4m, and the gradient becomes 0.016% to 0.297%.

The Yangtze River has a high runoff volume, and the sediment discharge is also large. The average annual runoff is $4.39 \times 10^{12} m^3$, and the average annual suspended load discharge is 526 million tons.

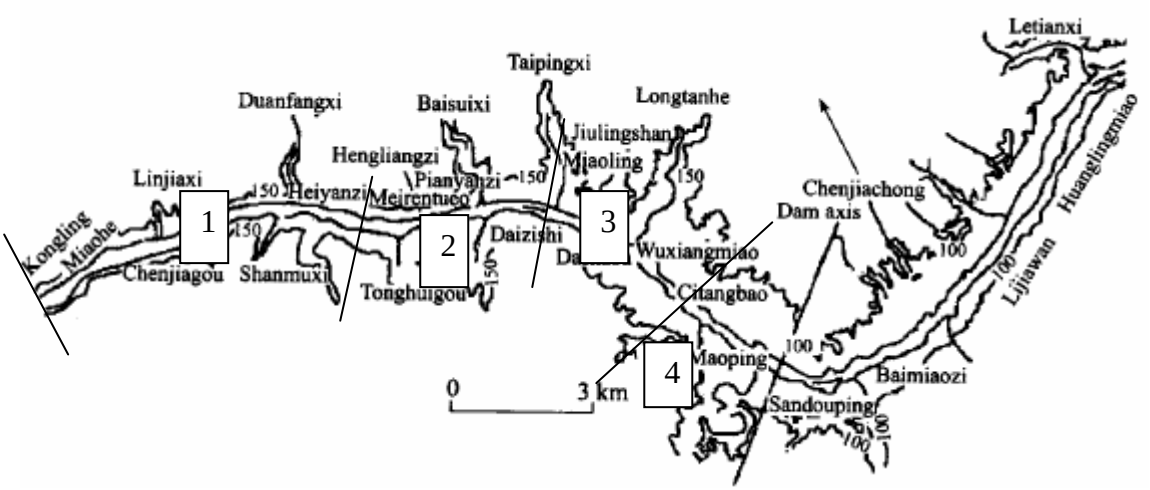

Figure 5.3-1: River Regime in the Dam Area of Three Gorges Project (Dou et al., 2004)

b) Generation of Computational Grids

A total of 163 layers of mesh were arranged along the longitudinal direction, and 81 layers across the river width. At the maximum water depth there were 15 layers in the vertical direction. Orthogonal curve grids were generated numerically and the total number of grid points is 163 x 81 x 15.

c) Verification of Deposition in the Three Gorges Dam Site Area Due to Gezhouba Reservoir

A period of three years was selected for the reservoir sedimentation verification (from June 1981, after the impoundment of the existing Gezhouba Reservoir to December 1984) Calculation time step was 3 to 4 days on average. Calculation of sediment concentration of suspended load was conducted for 7 grain size groups, and the average values during 1981 to 1984 were used regarding the percentage of each grain size.

Table 5.3-1 is a comparison between the calculated and measured amounts of deposition for the reaches numbered 1 to 4 on **Figure 5.3-1**. It can be seen from **Table 5.3-1** that the predictions were quite close to the measured values.

Table 5.3-1: Comparison between the calculated and measured deposition amount for various reaches (10^4 m^3) (Dou et al., 2004)

Reach	**1**	**2**	**3**	**4**	**Total**
Calculated	271.2	231.9	300.4	432.6	1236.1
Measured	310.5	224.6	240.4	418	1193.5
Error (%)	-12.7	3.2	25	3.5	3.6

a) Calculation Conditions for Predictions of the Three Gorges Project

The incoming hydrographs of runoff and graded suspended load into the Three Gorges Project dam area are provided by the Yangtze River Scientific Research Institute by use of a 1D model calculation.

During the initial operation of the reservoir both the amount of suspended load and their grain sizes will be small. After 90 year of operation, most suspended load will enter the dam area and the median diameter will be increased to 0.027mm, close to the average annual median diameter of natural suspended load, i.e. 0.031mm, For large discharges, the median diameter could be larger than 0.031mm.

Though the grain size distribution of suspended sediment entering the dam area may vary with time and discharges, it is assumed that the size distribution is related to d_{50}. In this model study, the following equation by Zhou (1997) was used. It is based on statistical analysis of data from Yangtze River Scientific Research Institute:

$$P_L = 1 - e^{-0.639\left(\frac{D_L}{d_{50}}\right)} \qquad (5.3\text{-}13)$$

where D_L is the grain size of sediment group (mm), P_L the percentage by weight of the sediment group in question. The above equation is used for the size distribution of suspended load. A total of 7 size groups for suspended load were used in the calculation.

e) Hydrological Series in the Simulation

The hydrological series adopted for the calculation is a 10-year series, based on observed data during 1961 to 1970. The average incoming water and sediment loads during the 10 years is close to the annual averaged amounts, and is considered highly representative. In order to take into consideration the impact of extra-large flood and sediment years during long-term simulation, it has been suggested that after 30 years of operation of the reservoir an extra high-flood-high-sediment year, 1954, be inserted into the hydrological series. In total, a period of 76 years was simulated.

f) Sediment Deposition at the Upper Reach of the Dam Area

Figure 5.3-2 shows deposition development results of the entire 16 km reach compared to that of the 6.8 km near dam reach.

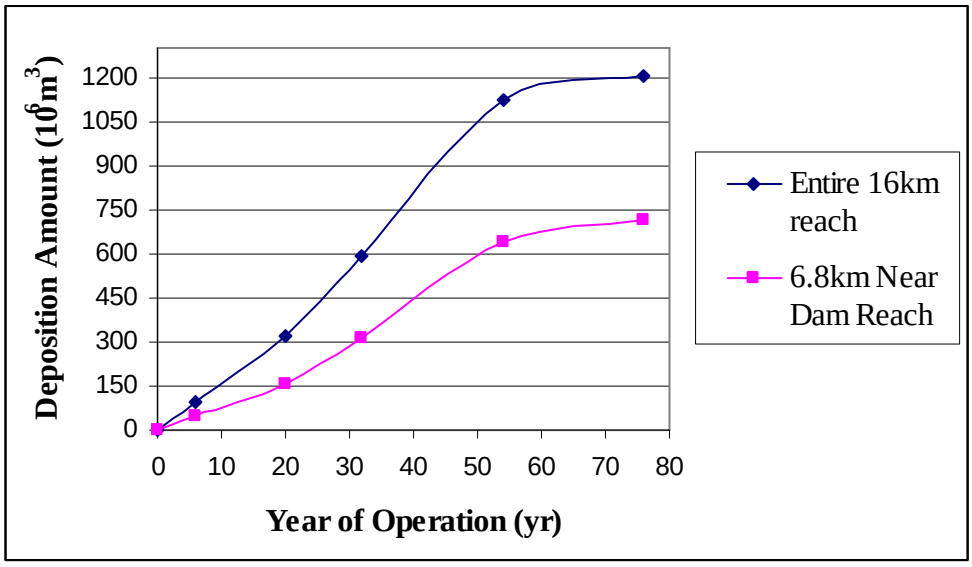

Figure 5.3-2: Development of the deposition of the entire and near dam reaches (Dou et al., 2004)

The simulated results indicate that during the initial 32 year period, the regime is mainly characterised by a large cross-sectional area and small flow velocity. Though sediment concentration is small and the grain size is fine at the inlet reach of the dam area, it still maintains a saturated state. The entire river reach appears to have uniform and unidirectional deposition. The accumulated deposition in the entire river reach and near-dam reach will be 589

million m^3 and 312 million m^3 respectively. The average thickness in the upper reach will be 33.3m and that of the near-dam reach is 24.3m.

After 60 to 70 years of operation, the upper reach of the dam area will reach a state of equilibrium, i.e. both erosion and deposition will occur in the dam area without unidirectional deposition. After 76 years , the accumulated amount of deposition in the entire reach will be a steady 1.208 million m^3 and that of the near dam reach will be 714 million m^3, with the average thickness in the upper reach 56.3 m and that in the near-dam reach 56.0m, which are very close to one another.

The results of the Three Gorges model demonstrate that within 30 years' reservoir operation, the cumulative sediment deposition will have no serious impact on the project's normal operation both in the dam area and in the fluctuating backwater region. But several decades later, sediment deposition in the fluctuating backwater region might affect the navigation and harbour operation during extremely dry years when the reservoir's water level drops down to the lowest level.

g) Sediment Concentration Field

The largest difference between 3D and 2D models is that 2D models can only simulate depth-averaged flow fields and sediment concentration fields, while 3D models can predict flow fields and sediment concentration fields at different water depths or elevations. The 3D simulated results however show that the distribution of sediment concentrations over the depth is relatively uniform. Sediment concentration at the riverbed is slightly larger than that in the middle and near the surface.

5.4 Models of density currents

5.4.1 Introduction

Numerical models used in simulating turbidity currents can be divided into two groups: Depth-averaged models and 2D vertical mixture Navier-Stokes models. Both these models have their advantages and disadvantages. In order to practically solve the Navier-Stokes model, some sort of turbulence model has to be assumed (with the k-ε turbulence model being the most widely used). However, unlike depth-averaged models the Navier-Stokes models are able to provide information on the vertical structure of a turbidity current.

5.4.1.1 2D vertical mixture models

2D vertical mixture models make no assumptions about the vertical profiles of the flow (temperature, salinity, concentration and velocity) and are therefore quite general. The main challenges with these models are computational cost (a 2D mesh is required) and the selection of a proper turbulence model.

A turbulence model is required to describe the turbulent transport of momentum and mass. However, turbulence model selection is complicated by the fact that most turbulence models and wall functions are based on shear flows that do not account for buoyancy effects. It is well known that stable stratification attenuates turbulence, while unstable stratification enhances turbulence.

Choi and Garcia (2002) modeled a gravity current by using a 2D vertical mixture model, together with an extended k-epsilon turbulence model. Their results were compared with that of a depth-averaged mixture model. They concluded that the self-similarity assumption used in depth-averaged models is justified.

Huang and Imran (2005) used a 2D vertical mixture model, together with an extended k-epsilon turbulence model to simulate a turbidity current. The model allowed the bed boundary to dynamically evolve by sediment deposition and entrainment. Their results compared well with experimental data and they recommended using a turbulent Schmidt number of 1.3 for the turbulent flux of sediment.

Brors and Eidsvik (1992) used a 2D vertical mixture model, together with a Reynolds stress turbulence model to simulate a turbidity current. They argue that k-epsilon models underpredict the turbulence level at the current's maximum velocity. Their Reynolds stress model gave a higher turbulence level at the current's velocity maximum.

5.4.1.2 Depth-averaged mixture models

In contrast to 2D vertical mixture models, depth averaged models assume some sort of self-similar vertical profile (temperature, salinity, concentration and velocity) and is therefore less general, but computationally less expensive (a 1D mesh is required). The main challenge with these models are selecting empirical relations for water entrainment and shear velocity to close the governing equations.

Parker et al. (1986) used a three and a four equation depth-averaged mixture model to investigate the possibility of self-acceleration of turbidity currents. Self-acceleration occurs when a turbidity current reaches a critical speed whereon sediment entrainment increases, the concentration and density difference increases and subsequently the current velocity increases. This leads to even more sediment entrainment. A self-reinforcing cycle of sediment entrainment and increasing velocity develops. Their numerical results showed that self-acceleration is possible.

Winslow (2001) investigated the sensitivity of a turbidity current (depth-averaged mixture model) to various initial conditions, channel properties, closure relationships and fluid mixture properties. The results showed that initial conditions (current height, velocity and sediment concentration) only have a short lived effect on model predictions. However, channel properties (slope and bed friction) and fluid mixture properties (kinematic viscosity and sediment grain size) control the long-term evolution of turbidity currents.

5.4.1.3 Proposed density current model

It is important to note that density differences can occur due to temperature, material phases with different densities or chemical species with different densities. Hence, in order to properly model gravity currents the mechanism responsible for the difference in density has to be identified. In the case of turbidity currents, the density difference is created by the multiphase mixture of sediments and water.

Manninen (1996) recommends different models for multiphase flows, depending on the strength of the coupling between the different phases.

a) For drag dominated flows in which the phases are strongly coupled (their velocities equalize over short length scales) a homogeneous flow model is recommended.
b) For flows where gravity or centrifugal forces create velocity differences (e.g. sedimentation of sand in water), but the velocities of the phases also equalize over short length scales, the mixture model is recommended. Most liquid-particle mixtures fall within this category.
c) The phases of gas-particle mixtures are generally weakly coupled (their velocities do not equalize over short length scales) and therefore a full multiphase model is recommended.

For turbidity currents the mixture model is should be used. It consists of the following equations:

Density equation:

$$\rho = c\rho_s + (1-c)\rho_w$$

where ρ is the density of the mixture; c is the volume fraction of sediment; ρ_s is the density of the sediment and ρ_w is the density of water.

Mixture continuity equation:

$$\frac{\partial \rho}{\partial t} + \frac{\partial \rho u_i}{\partial x_i} = 0$$

where t is time; x_i corresponds to the i'th spatial coordinate axis and u_i is the Reynolds averaged velocity of the mixture.

Mixture momentum equation:

$$\frac{\partial \rho u_i}{\partial t} + \frac{\partial \rho u_i u_j}{\partial x_j} = -\frac{\partial P}{\partial x_i} + \frac{\partial}{\partial x_j}\left(\mu \frac{\partial u_i}{\partial x_j} - \rho \overline{u_i' u_j'}\right) + (\rho_s - \rho_w) c g_i$$

where P is the Reynolds averaged pressure; μ is the dynamic viscosity of the mixture; $\rho \overline{u_i' u_j'}$ is the Reynolds stress and g_i is the gravity acceleration in the i'th direction.

Sediment continuity equation:

$$\frac{\partial \rho c}{\partial t} + \frac{\partial \rho c\left(u_j - w_s \delta_{j2}\right)}{\partial x_j} = \frac{\partial}{\partial x_j}\left(\frac{\mu_t}{Sc_t}\frac{\partial c}{\partial x_j}\right)$$

where w_s is the settling velocity of sediment (calculated from an algebraic force equilibrium equation); δ_{i2} is the kronecker delta (for the vertical direction); μ_t is the turbulent viscosity and Sc_t is the turbulent Schmidt number.

In addition to the above equations a turbulence model is required to model the Reynolds stresses occurring in the mixture momentum equation.

5.4.2 Case study 1: Laboratory flume and field data, Canada

5.4.2.1 Background

Kassem and Imran (2001) have used a Navier-Stokes model (2D vertical) to simulate a turbidity current. Their results compare favourably with the laboratory observations of Lee and Yu (1997), as well as Garcia and Parker (1989).

The governing equations used in their model are the Reynolds-averaged, incompressible Navier-Stokes equations for fluid and momentum conservation along with a sediment-conservation equation for each grain size. Furthermore, in order to close the turbulent stress terms in the Navier-Stokes equations a k-ε turbulence model was introduced. Although the turbidity current can be viewed as incompressible, its density varies due to the continual change in mixture composition of the grain sizes. To properly model this behaviour the conservation form of the governing equations were used.

An implicit finite volume method was used to discretize the above mentioned differential equations in space and time. The resulting non-linear, coupled algebraic equations were then linearized and solved iteratively using a scheme such as Newton-Raphson.

Kassem and Imran's Navier-Stokes model was used to simulate a turbidity current in a laboratory flume, as well as a turbidity current in the Saguenay fjord, Canada. The

results compared favourable and indicated that the Navier-Stokes model can be successfully applied to small scale and field scale problems.

5.4.2.2 Laboratory scale application

The numerical model was used to simulate the turbidity current movement for the flume experiments of Lee and Yu. The flume dimensions was as follows: 20 m long, 0.2 m wide and 0.6 m deep. The suspended material was kaolin. The computational grid consisted of 10000 grid points (10 x 1000), with a time-step of 0.1 s.

Figure 5.4-1: A-E shows that the numerical model computes the detail of the plunging movement. This confirms Lee and Yu's observation that the plunge point location is time dependent.

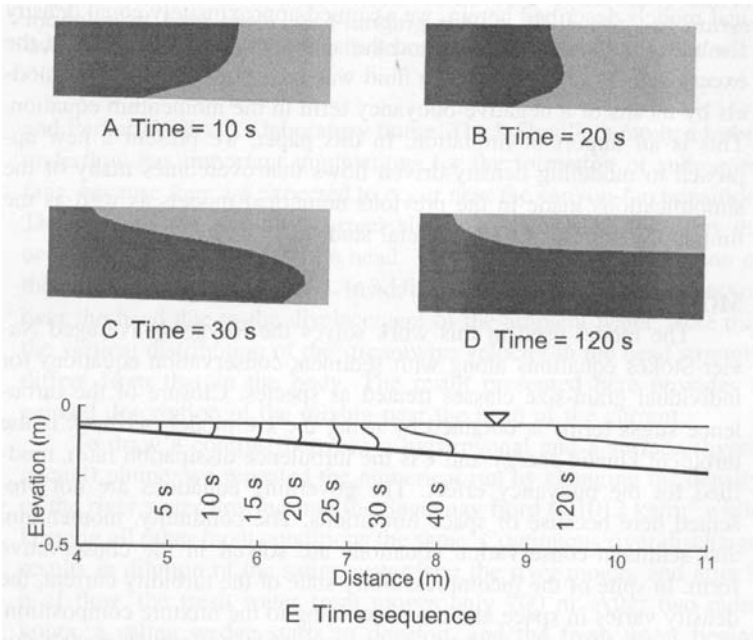

Figure 5.4-1: Evolution from open channel flow to underflow, with stable plunge point

Figure 5.4-2 shows that the typical vertical structure of the turbidity current agrees well with the experimental observations of Lee and Yu.

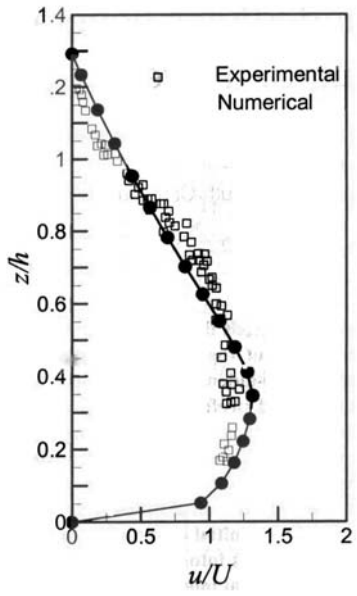

Figure 5.4-2: Comparison between computed and measured non-dimensional velocity distributions

5.4.2.3 Field scale application

The numerical model was also used to simulate the movement of a turbidity current along a 40 km section in the Saguenay fjord, Canada. The fjord has an approximately constant width. Using the data synthesized by Mulder (1998) for the 1663 flood, caused by a massive land-slide a computational grid with 100 000 grid points (4000 x 25) was selected with a time-step of 10 to 40 s.

Figure 5.4-3 shows that after 9 hours the turbidity current has traveled nearly 30 km. It shows how the thickness of the turbidity current increases, due to the entrainment of the ambient water surrounding the current. It also reveals the formation of an internal hydraulic jump where the slope changes at 20 km. This is in qualitative agreement with the laboratory flume observations made by Garcia and Parker (1989).

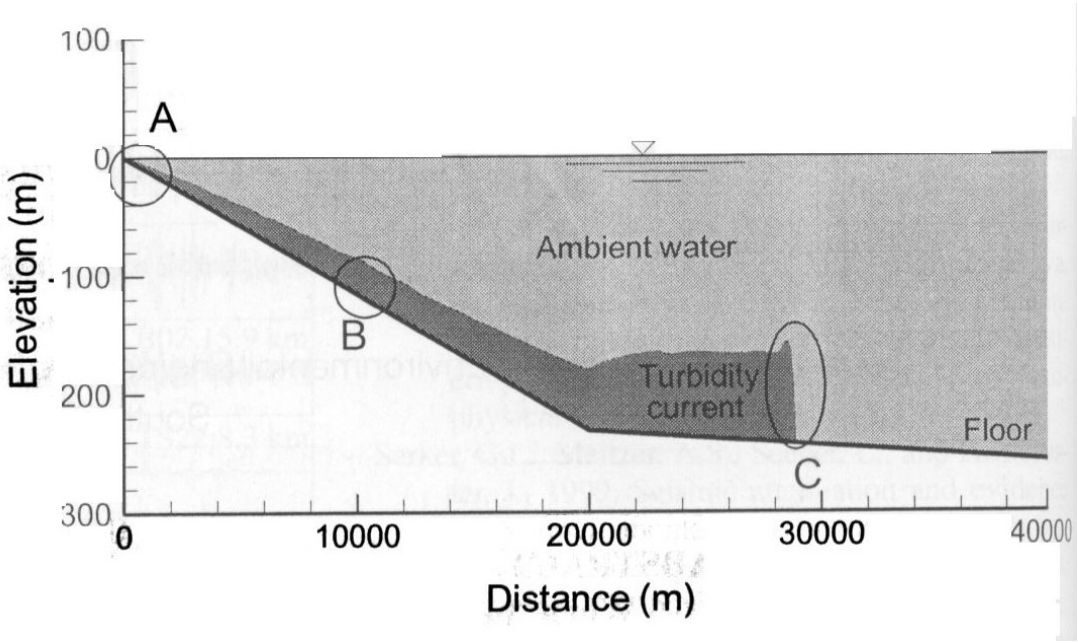

Figure 5.4-3: Simulated turbidity current in Sauenay fjord

Figure 5.4-4 A, B and C are the vertical structure views corresponding to locations A, B, C in **Figure 5.4-3**. **Figure 5.4-4** A shows the plunge point, whose location and depth agrees closely with the semi-empirical formula described by Akiyama and Stefan (1984). **Figure 5.4-4** B reveals how the thickness increases due to entrainment of the ambient water. It shows how this entrainment increases the discharge of the turbidity current and correspondingly decreases the sediment concentration. **Figure 5.4-4** C reveals the backward flow over the head due to the displacement of the ambient water.

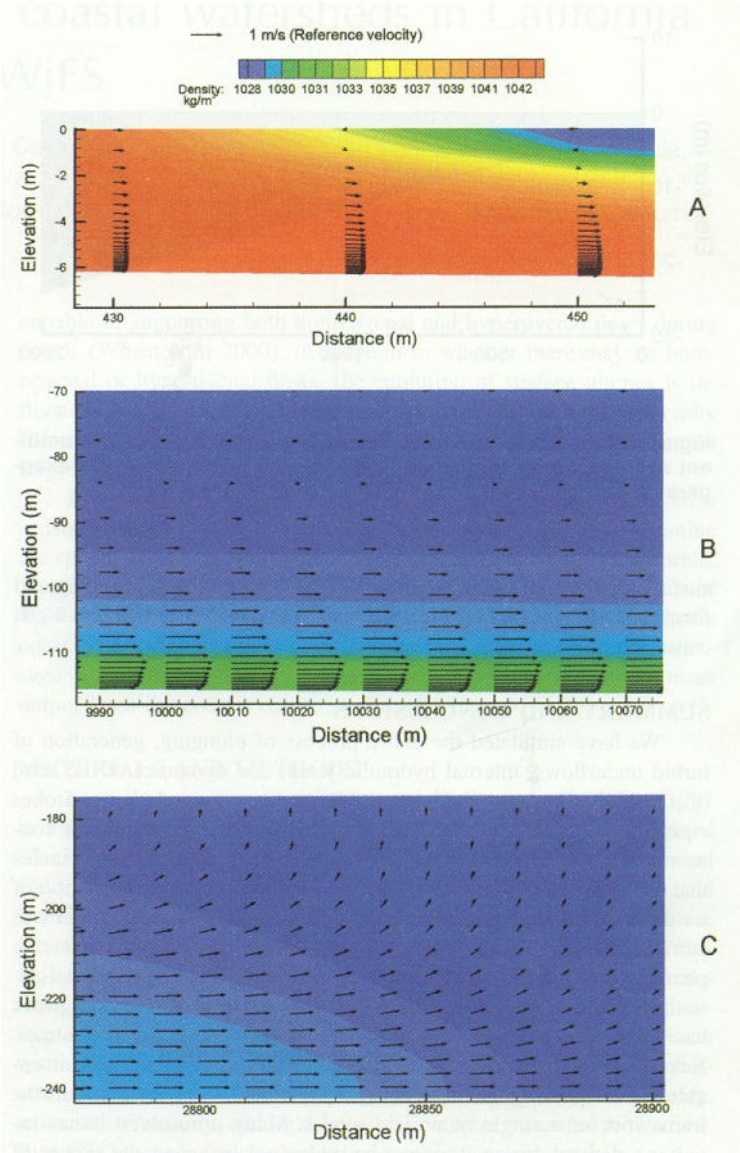

Figure 5.4-4: Computed flow and concentration fields for turbidity current in Saguenay fjord at locations A, B, C

5.4.3 Case study 2: Luzzone Reservoir, Switzerland

De Cesare et al. (2001) have also used a Reynolds-averaged Navier-Stokes model (3D) to simulate the movement of a turbidity current in the Luzzone Reservoir in the Swiss Alps.

5.4.3.1 Governing equations

The incompressible Navier-Stokes equations used by De Cesare et al. are:

Fluid conservation:

$$\frac{\partial u_i}{\partial x_i} = 0 \tag{5.4-1}$$

Momentum conservation:

$$\frac{\partial u_i}{\partial t} + \frac{\partial \left(u_i u_j\right)}{\partial x_j} = \frac{\Delta \rho}{\rho} g_i + \frac{\partial \sigma_{ij}}{\partial x_j} \tag{5.4-2}$$

where

$$\sigma_{ij} = \frac{-p}{\rho}\delta_{ij} + \nu_{eff}\left(\frac{\partial u_i}{\partial x_i} + \frac{\partial u_j}{\partial x_i}\right) \tag{5.4-3}$$

Sediment conservation with allowance for depositional behaviour:

$$\frac{\partial c_s}{\partial t} + \frac{\partial \left(c_s \cdot u_i\right)}{\partial x_i} = \frac{\nu_{eff}}{\sigma_c} c_s \left(\frac{\partial u_i}{\partial x_j} + \frac{\partial u_j}{\partial x_i}\right) - v_{si}\frac{\partial}{\partial x_i}\left(c_s \frac{\rho_f}{\rho}\right)$$

where:

- u_i is the velocity vector component
- x_i is the spatial vector component
- t is time
- $\Delta\rho$ is the density difference between the particle and the fluid
- g is the gravity acceleration constant
- σ_{ij} is the stress tensor component on plane i in direction j
- p is pressure
- ν_{eff} is the effective kinematic viscosity
- c_s is the sediment concentration
- v_{si} is the particle sinking velocity
- ρ is the mixture density
- ρ_f is the fluid density

Furthermore, a k-ε turbulence model (modified to account for the buoyancy effect) was used to provide closure for the stress terms appearing in the momentum equation. A current-bed interaction model was also added to account for sediment deposition and erosion. This current-bed interaction model is based on the ideas of Parker et al.

(1986,1987). The above mentioned differential equations are then discretized in space and time using the finite volume method.

5.4.3.2 Model application

a) Field measurements

During the summers of 1995 and 1996 measuring campaigns took place in the Luzzone reservoir to quantify the variations in discharge, temperature and turbidity. A 1000 yr flood was synthesized from the obtained data and used as input for the numerical model. The 1000 yr flood had a peak discharge of 137 m^3/s and the maximum sediment concentration (d_{50}= 0.02 mm), based on in situ measurements, was set at 265 g/l.

b) Numerical model

Figure 5.4-5 shows the computational grid used to represent the topography of the reservoir. The topography was obtained from bathymetric measurements done in 1994. The computational grid consisted of 36 000 cells (100 along the main reservoir axis, 20 laterally and 18 vertically), with a typical bottom-center cell representing the physical dimensions of 25x5x2 m^3. Although a current-bed interaction model was used alongside the Navier-Stokes equations, the computational grid (and hence the reservoir topography) was not allowed to evolve with time.

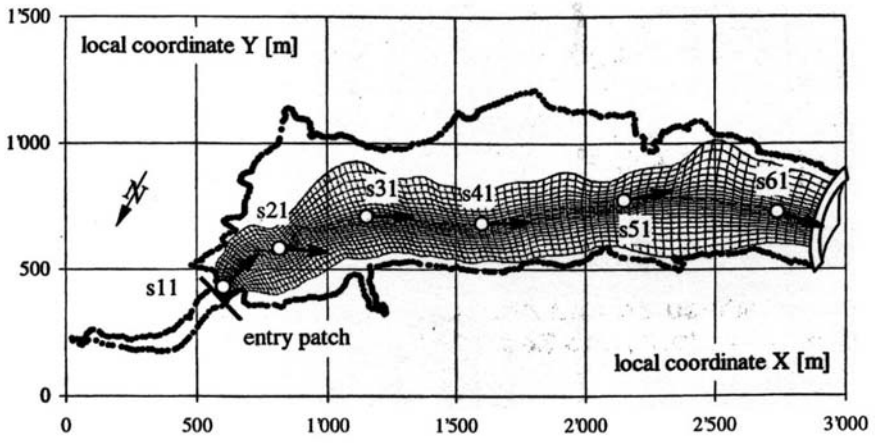

Figure 5.4-5: Station locations and computational grid superimposed on reservoir bottom

c) Results

Figure 5.4-5 indicates the locations of six stations where the flow details were extracted from the numerical model. **Figure 5.4-6** gives the time variation of the flow-velocities for the six stations. The mean river inflow velocity is only 0.09 m/s for the design flood. The turbidity current however attains a maximum of 2.5 m/s in the narrow canyon just below the inlet of station s11 and maintains a velocity in excess of 1.5 m/s in the larger part of the reservoir, from stations s31 to s61. After about 40 minutes, the turbidity current head arrives at the dam wall. It is reflected and returns upstream, interacting with the still downstream moving body of the turbidity current. This returning current travels upstream over a distance of about two-thirds of the total reservoir length. It reaches a velocity of 0.3 m/s. The global motion inside the lake becomes insignificant after approximately four hours, while the sediment inflow stopped already after 1.5 hours. A sediment laden underwater "muddy lake" is formed, which will then settle its granular material over several hours or even days.

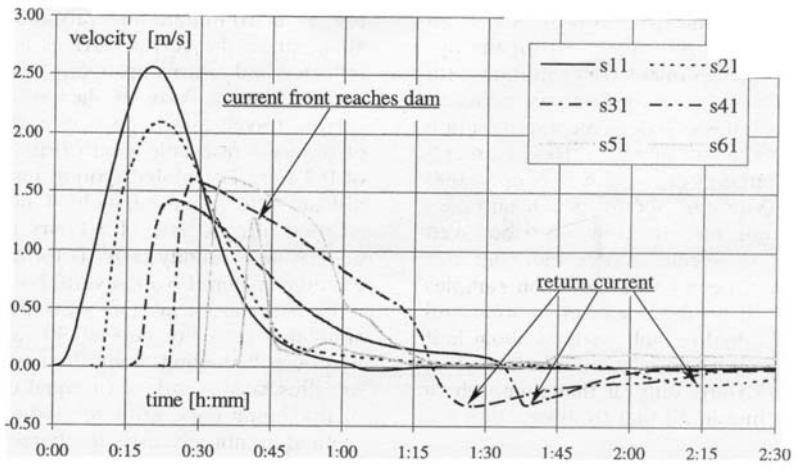

Figure 5.4-6: Velocity variation for stations s11 to s61

5.4.4 Conclusion

The results of the Navier-Stokes model indicates that the plunge point location and depth, as well as the vertical structure of a density current event can be successfully simulated. However, further research is still needed on combining the model with bed-current interaction models, as well as investigating the behavior of the model in flow conditions which are not conducive to density current formation.

6. CONCLUSIONS AND RECOMMENDATIONS

A great deal of information is available on sediment transport, deposition and erosion in reservoirs. Mathematical modelling however needs to be undertaken with great care as sediment transport in reservoirs tends to vary greatly both in time and in space. As sedimentation problems in reservoirs are very difficult and costly to remedy afterwards, dam designers need to use a conservative approach in making allowance for sedimentation problems in dam designs.

Suitable mathematical models developed for reservoir sedimentation, describing the physical processes involved as accurately as possible, should be used for reliable simulations. Accurate prediction of the long-term sedimentation yield is however as important as modeling of sediment deposition patterns in a reservoir. Where turbulence is the main sediment transporting mechanism, one-dimensional mathematical models are still often used for long-term sediment deposition predictions, but for detailed studies two dimensional or quasi-3D models are recommended for use in future, incorporating a fully hydrodynamic approach (quasi-steady for long-term simulations), modules for erosion and deposition in cohesive and non-cohesive sediments, to be able to simulate storage, sluicing or flushing reservoir operation.

Where density currents form in a reservoir, Navier-Stokes 2D vertical or 3D models should be used to describe the formation, movement and sediment transport of the density current.

These models are calibrated on local reservoir field data, especially when dealing with cohesive sediments.

7. REFERENCES

Ackers, P. and White, W.R. (1973). Sediment Transport: New Approach and Analysis. JHD, *Proc. Am. Soc. Civ. Engrs*, 99 (HY-11).

Akiyama and Stephan, J. and Stefan, H.G.(1987). Onset of Underflow in Slightly Diverging Channels. *J. Hydr. Engrg., Am. Soc. Civ. Engs*, 113 (7), pp. 825-844.

Altinakar, M.S., Graf, W.H. and Hopfinger, E.J. (1990). Weakly Depositing Turbidity Current on Small Slopes. *J. Hydr. Res*., 28 (1), NL.

Annandale, G.W. (1984). *Deposition of Sediment in Reservoir Basins*. (In Afrikaans). D. Eng. Thesis, University of Pretoria, South Africa.

Ashida, K. and Egashira, S. (1975). Basic Study on Turbidity Currents. *Japan Soc. of Civil Engrg*., 237, pp 37-50.

Bagnold, R.A. (1962). Auto-suspension of Transported Sediment: Turbidity Currents. *Proc. Royal Soc. of London,* Ser. A., 265 pp. 315-319.

Bagnold, R.A. (1966). An Approach to the Sediment Transport Problem from General Physics. *Geol. Survey professional paper 422-1.*

Basson, G.R. (1997). *Development of a New Sediment Transport equation based on applied stream power ICHE, Hong Kong.*

Basson, G.R. and Rooseboom, A (1997). Dealing with Reservoir Sedimentation. South African Water Research Commission Publication.

Basson, G.R., Rooseboom, A., Olesen, K.W. (1996). "Mathematical Modelling of Reservoir Flushing", *Proceedings of the International Conference on Reservoir Sedimentation*, Fort Collins, USA, pp 559-570, 1996

Basson, G.R. and Rooseboom, A. (1997). Dealing with Reservoir Sedimentation. South African Water Research Commission publication.

Bata, G. and Knezevich, B (1953). Some Observations on Density Currents in the Laboratory and in the Field. *Proc. Minnesota Int. Hydraul. Convtn.*

Bell, H.S. (1040). Density Currents as Agents for Transporting Sediments. J. Geol. L.5.

Bell, H.S. (1942). Stratified Flow in Reservoirs and its Use in Prevention of Silting. Misc. Publication No 491, US Dep of Agriculture.

Blancket (1954). In Delft Hydraulics, 1992.

Brors, B. and Eidsvik, K. (1992). “Dynamic Reynolds modeling of turbidity currents.” Journal of Geophysical Research.

Bruk, S. (ed) (1985). Methods of Computing Sedimentation in Lakes and Reservoirs. Unesco, Paris, IHP-11 Project.

Brune, G.M. (1953). Trap efficiency of reservoirs. Trans. Am. Geoph. Union, 34 (3).

Cao, R. (192). Experimental Study on Density Current with Hyper concentration of Sediment. Int. J Research, 8 (1).

Chikita, K. (1989). A Field Study on Turbidity Currents Initiated from Spring Runoffs. *Wat. Resour. Res.*, 25 pp. 257-271.

Chollet, J.P. and Cunge J.A. (1980). Simulation of Unsteady Flow in Alluvial Streams. *Appl. Mathematical Modelling*, 4.

Choi, S. and Garcia, M. H. (2002). “k-_ turbulence model of density currents developing two-dimensionally on a slope.” Journal of Hydraulic Engineering.

Choux, C., Baas, J., Mccaffrey, W., and Haughton, P. (2005). “Comparison of spatio-temporal evolution of experimental particulate gravity flows at two different initial concentrations, based on velocity, grain size and density data.” Sedimentary Geology.

Churchill, M.A. (1948). Analysis and use of reservoir sedimentation data. Discussion by L.C. Gottschalk, Proc. Federal Inter-Agency Sedimentation Conference, Washington DC., Jan. 1948, pp.139-140.

Cunge (1989). In Delft Hydraulics, 1992.

De Cesare G, Schleiss, A, and Hermann, F. (2001). ASCE Journal of Hydraulic Engineering V127 No. 1; pp. 6-16.

Delft Hydraulics (192). *The Control of Reservoir Sedimentation – A Literature Review*. Ministry of Development Co-operation, Government of the Netherlands, Delft Hydraulics.

Delft Hydraulics (1992). The Control of Reservoir Sedimentation- A Literature review. Ministry of Development Co-operation, Government of the Netherlands, Delft Hydraulics.

Denton, R.A., Faust, K.M. and Plate, E.J. (1981). Aspects of Stratified Flow in Man-made Reservoirs. Research Report ET-203, Sonderforschungs-bereich 80, Univ. of Karlsrühe, Germany.

Dequennois, H. (1956). New Methods of Sediment Control in Reservoirs. *Water Power*, pp. 174-180.

DHI. (2003). "MIKE 21C River Hydrodynamics and Morphology", User Guide, *DHI Water & Environment*, 2003

Di Silvio, G. and Armanini, A. (1981). Influence of the Upstream Boundary Conditions of the Erosion-Deposition Processes in Open Channel. XIX Int. Ass. Hyd. Res. Congress, Paper 22, sub. A(a), New Delhi, India, 1981.

Di Silcion, G. (1995). River modelling. UNESCO IHP-IV Project H-1-2, Working Group on Erosion, Riverbed Deformation and Sediment Transport in River Basins as related to National and Manmade changes.

Dou, G. (1974). Similarity Theory and its Application to the Design of Total Sediment Transport Model. Research Bulletin of Nanjing Hydraulic Research Inst., Nanjing, China.

Engelund, F. and Hanse, E. (1967). A Monograph on Sediment Transport in Alluvial Streams. Teknisk Forlag, Denmark.

Fan, J. (1960). Experimental Studies on Density Currents. *Scientia Sinica*, 9(2), pp 275-303.

Fan, J. (1986). Turbid Density Currents in Reservoirs. *Wat. Int.* 11(3), pp. 107 – 116.

Fernandez, R. and Imberger, J. (2006). “Bed roughness induced entrainment in a high Richardson number underflow.” Journal of Hydraulic Research.

Galapatti, G. and Vreugdenhil, C.B. (1985). A Depth-integrated Model for Suspended Sediment Transport. *J. Hydr. Res., Int. Ass. Hyd. Res.*, 23 (4), pp. 359 – 377.

Garcia, M and Parker, G. (1989). Experiments on hydraulic jumps in turbidity currents near a canyon-fan transition: Science V245, pp. 393-396.

Garcia, M. and Parker, G. (1993). “Experiments on the entrainment of sediment into suspension by a dense bottom current.” Journal of Geophysical Research.

Garcia, M. (1993). “Hydraulic jumps in sediment-driven bottom currents.” J. Hydraul. Res.

Gilbert, G.K. (1914). The Transportation of Debris by Running Water, Based on Experiments made with the Assistance of E.C. Murphy. U.S. Geol. Survey Prof. Paper 86,263 p.

Graf, W.H. (1971) *Hydraulics of Sediment Transport.* McGraw-Hill.

Graf, W.H. (1983). The Hydraulics of Reservoir Sedimentation. *Int. Water Power and Dam Construction.* 35, (4), pp. 45 – 52, April.

Guan, Y., Rong, F., Wang, J., Yin, L. and Wang, H. (1991). A Numerical Model for Sedimentation in Fenhe Reservoir and the Adjoining Reaches. *Int. Journal of Sediment Research*, 6 (1), IRTCES.

Guy, H.P., Simons, D.B. and Richardson, E.V. (1966). Summary of Alluvial Channel Data from Flume Experiments, 1956 to 1961. Sediment Transport in alluvial channels. *Geological Survey Professional Paper 462 – 1.*

Han, Q., et al. (1973). *Non-equilibrium Transportation of Sediment in Reservoirs.* Collection of Reports on Reservoir Sedimentation, Yellow River Conservancy Commission (in Chinese).

Han, Q and He, M. (1990). A Mathematical Model for Reservoir Sedimentation and Fluvial Porcesses. *Int. J. Sed. Res.,* IRTCES, 5 (9), April, pp. 43-84.

Harleman, D. (1961). Stratified flow. In: *Handbook of Fluid Dynamics*, Ed. V. Streeter, McGraw Hill, New York, USA.

Hinze, J.O. (1960). *Turbulence.* McGraw-Hill Book Company, Inc., New York, N.Y.

Holly, F.M. and Rahuel, J.L. (190). New Numerical/Physical Framework for Mobile-bed Modelling.: *J. Hydr. Res., Int. Ass. Hyd. Res.*, 28 (4-5).

Huang, H., Imran, J., and Pirmez, C. (2005) “Numerical modeling of turbidity currents with a deforming bottom boundary.” Journal of Hydraulic Engineering.

Hurst and Chao (1975). In Delft Hydraulics, 1992.

ICOLD (2000). Dealing with Reservoir Sedimentation, ICOLD Bulletin 115.

Kassem, A and Imran, J. (2001). Geology; V29 No. 7, pp. 655-658.

Keunen, P.H. (1952). Estimated Size of the Grand Banks Turbidity Current. *An. J. Sci.*

Lee, H and Yu, W. (1997). ASCE Journal of Hydraulic Engineering V123 No. 6, pp. 520-528.

Lee, H. and Yu, W.(1997). "Experimental study of reservoir turbidity current." Journal of Hydraulic Engineering.

Levi, I.I. (1958). Injenernaia Ghidrologhia. Moscow.

Lewis, A.D. (1936). Silting of Four Large Reservoirs in South Africa. Communication No 5, 2nd Congress on Large Dams, Washington.

Mackay, G.A. Webby, M.G., and Walsh, J.M. (2000). Lake Roxburgh Hydraulic Modelling. Contact Energy Study Brief CLU#5, New Zealand.

Mahmood, K. (1987). Reservoir Sedimentation: Impact, Extent and Mitigation. World Bank Technical Paper, No. 71, The World Bank, Washington D.C.

Majumdar, S., Rodi, W., Zhu, J. "Three-dimensional finite-volume method for incompressible flows with complex boundaries", *Journal of Fluids Engineering*, Vol. 114, pp 496-503, 1992

Manninen, M. and Taivassalo, V.(1996). On the mixture model for multiphase flow. VTT Publications.

Mehta, A.J. and Partheniades, E.(1973). Effects if Ohysico-chemical Properties of Fine Suspended Sediment on the Degree of Deposition. *Proc. Of the International Symp. On River Mechanics, Bangkok,* 1, Paper A – 41, pp. 465-476.

Michon, X., Goddet, J. and Bonnefille, R. (1955). Etude Thèorique et Experimentale de Courants de Densite. Tome 1 et 2, Lab. Nat. d'Hydraulique, Chatou, France.

Middleton, G.V. (1966). Experiments on Density and Turbidity Currents. *Can. J. Earth Sci.,* 3 (4).

Miller, C.R., (1953). Determination of the Unit Weight of Sediment for use in Sediment Volume Computations. Memorandum, Bureau of Reclamation, U.S. Dep. of the Interior, Denver, Colorado.

Mulder, T, Syvitski, J and Skene, K. (1998). Modelling of erosion and deposition by turbidity currents generated at river months. Journal of Sedimentary Research V68, pp. 124-137.

Palmieri, A. (2003). Social and economic aspects of reservoir conservation. World Water Forum, Kyoto, Japan.

Parker, G, Fukushima, Y and Pantin, H. (1986). Self accelerating turbidity currents. Journal of Fluid Mechanics V. 171, pp. 145-181.

Parker, G et al. (1987). Experiments on turbidity currents over an erodilde bed. Journal of Hydraulic Research, Delft, The Netherlands, V25(1), pp. 123-147.

Partheniades, E (1986). The Present State of Knowledge and Needs for Future Research on Cohesive Sediment Dynamics. In: Wang, S.Y., Shen, H.W. and Ding, L.Z. (ed) *River Sedimentation* III, *Proc. Third Int. Symp. On River Sedimentation,* Univ. if Mississippi, Mississippi, USA, pp. 3 – 25.

Patankar, S.V. "Numerical Heat Transfer and Fluid Flow", *McGraw-Hill*, 1980

Philpott, W. (1978). The Plunging of Density Currents. Research Report, Dept. of Civil Eng., Univ. of Canterbury, Christchurch, New Zealand.

Pitt, J.P. and Thompson, G. (1984). The Impact of Sedimentation on Reservoir Life. *Proc. Symp. On Challenges in African Hydrology and Water Resources,* IAHS, Harare, Zimbabwe, Publ. No 144.

Raynaud (1951). In Delft Hydraulics, 1992.

Rooseboom, A. (1975). Sediment Transport in River and Reservoirs. D.Eng dissertation, University of Pretoria, (In Afrikaans). (Later published by Water Research Commission, South Africa, Report No 297/1/92, 1992 English).

Rooseboom, A and Mulke, F.J. (1982). Erosion Initiation. Proc. Symp. On recent developments in the explanation and prediction of erosion and sediment yield, IAHS Publication No. 137.

Rooseboom, A, et al. 1986. Welbedacht Reservoir – The Effect of Different Operating Rules on the Sedimentation Rate and Reservoir Yield with Reference to Off-channel Storage in the Proposed Knelpoort Reservoir. South African Department of Water Affairs and Forestry.

Rooseboom, A. (1992). *Sediment Transport in Rivers and Reservoirs – A South African perspective.* South African Water Research Commission, Report No 297/1/29, South Africa.

Rooseboom, A and Le Grange, A. (2000). *The Hydraulic Resistance of Sand Streambeds under Steady Flow Conditions.* Journ. Hydr. Research Vol. 38, 2000 No 1.

Rozowskii, I.L. "Flow of water in bends of open channels", English translation: *Israel Progr. For Scientific Transl. Jerusalem*, 1961

Sanchez, J.C. (1982). Mathematical Model for Simulation of Delta Formation and Erosion Downstream of a Reservoir. *Proc. 14th Int. Congress on Large Dams,* ICOLD, Rio de Janeiro, Brasil, III (Q54, R8), pp. 117-129.

Savage, S.B. and Brimberg, J. (1975). Analysis of Plunging Phenomena in Water Reservoirs. *J. Hydr. Res., Int. Ass. Hyd. Res.,* 13 (2) pp. 187-204.

Simpson, J. (1997). Gravity currents in the environment and the laboratory. Cambridge University Press.

Singh, B. and Shah, C.R. (1971). Plunging Phenomenon of Density Currents in Reservoirs. *La Houille Blanceh,* 26 (1) pp. 59 –64.

Soares et al. (1982). In Delft Hydraulics, 1992.

Stein, R.A. (1965). Laboratory Studies of Total Load and Apparent Bed-load. *J. of Geoph. Res.,* 70 (8), pp. 1831 – 1842.

Stone, H.L. " Iterative solution of implicit approximations of multidimensional partial differential equations", *SIAM Journal Num. Analysis*, Vol. 5, No 3, pp 530-559, 1968

Sundborg, A. (1964). The Importance of the Sediment Problem in the Technical and Economic Development of River Basins. *Ann. Acac. Reg. Sci.* Uppsala, 8, pp. 3 –52.

TAMS. (1998). Tarbela Dam Sediment Management Study. Pakistan Water and Power Development Authority.

Tan, Y. (1994). Reservoir Design and Management to Control Sediment. Topic VI, Russia.

Thomas, W.A. and Prashuhn, A.L. (1977). Mathematical Modelling of Sediment Transport, Scour and Deposition in River Channels. 17th Congress Int. Ass. Hyd. Res., Germany.

Turner, J.S. (1973) *Buoyancy Effects in Fluids.* Cambridge University Press, Cambridge, England.

Turner, J.S. (1979). *Buoyancy Effects in Fluids.* Cambridge Univ. Press, London, England.

Van Rijn, L.C. (1984a). Sediment Transport, Part I: Bed Load Transport, *J. Hyd. Engrg.*, 110 (10).

Van Rijn, L.C. (1984b). Sediment Transport, Part II: Suspended Sediment Load Transport, *J. Hydr. Engrg.*, 110 (11).

Vasiliev, O.F., et al. (193). Mathematical Modelling of Sedimentation in Deept Reservoir. Proc. Of 1st ICHE, I, Part A, USA.

Velikanov, M.A. (1954). Principle of the Gravitational Theory of the Movement of Sediments. Acad. Of Sci. Bul., USSR, Geophy Series, No. 4, pp. 349 – 359.

Wang, S.S.Y. (193). Advances in Hydro-Science and Engineering. *Proc. Ist ICHE,* USA.

White et al. (1975). Sediment Transport Equation Accuracies. In: Raudkivi, A.J. *Loose Boundary Hydraulics,* 1992, Publisher R Maxwell.

Winslow, K.(2001). PhD Dissertation: Sediment transport by turbidity currents. UMI Dissertation Services.

Wu, D. (1994a). Personal Communications, IRTCES, China.

Wu, D (ed.) (1994b). Movement of Density Current in Reservoir. International Research and Training Center on Erosion and Sedimentation.

Yang, C.T. (1972). Unit Stream Power and Sediment Transport. *Proc. Am. Soc. Civ. Engrs.*, 98 (10).

Yang, C.T. (1973). Incipient Motion and Sediment Transport. *Proc. Am. Soc. Engrs.,* 99 (HY10).

Yang, C.T. (1979). Unit Stream Power Equations for Total Load. *J. Hydr.,* 40, pp. 123 – 138.

Yang, C.T. and Molinas, A. (1982). Sediment Transport and Unit Stream Power Function. *J. Hydr. Div. Am. Soc. Civ. Engrs.*, 108 (HY6), June, pp. 774 – 793.

Yang, C.T. (1984). Unit Stream Power Equation for Gravel. *J. Hydraul. Div. Am. Soc. Civ. Engrs.*, 110 (HY12).

Yang, C.T. and Kong, X. (1991), Energy Dissipation Rate and Sediment Transport. *J. Hydraul. Res.* , 29 (4).

Yang, G. (1992). Mathematical Modelling of Alluvial Rivers. (in Chinese)

Yang, C.T., and Simoes. (2000)

Yang, C.T., and Simoes. (2003). GSTARS3 Reference Manual.

Zhang, Q and Long, Y. (1980). Sediment Problems of Sanmenxia Reservoir, *Proc. Intern. Symp. On River Sedimentation,* 2 China.

Zhang, Q., et al (1983). A Mathematical Model for the Prediction of the Sedimentation Process in Rivers. *Proc. 2nd ISRS, China.*

Zhang, R (1959). A Study of the Sediment Transport Capacity of the Middle and lower Yangtze River, *J, Sediment Research,* 4 (2), Beijing, China (In Chinese).

Zhou, Z (1995). Preservation of Reservoir Storage Capacity – Experience of China. *Proc. 195 Int. Workshop on Reservoir Sedimentation,* San Francisco, California.